VNiVERSiDAD
D SALAMANCA

# Cambios climáticos a escala orbital y milenaria en el Atlántico norte entre 800.000 y 400.000 años

Montserrat Alonso García

TESIS DOCTORAL

Salamanca, 2010

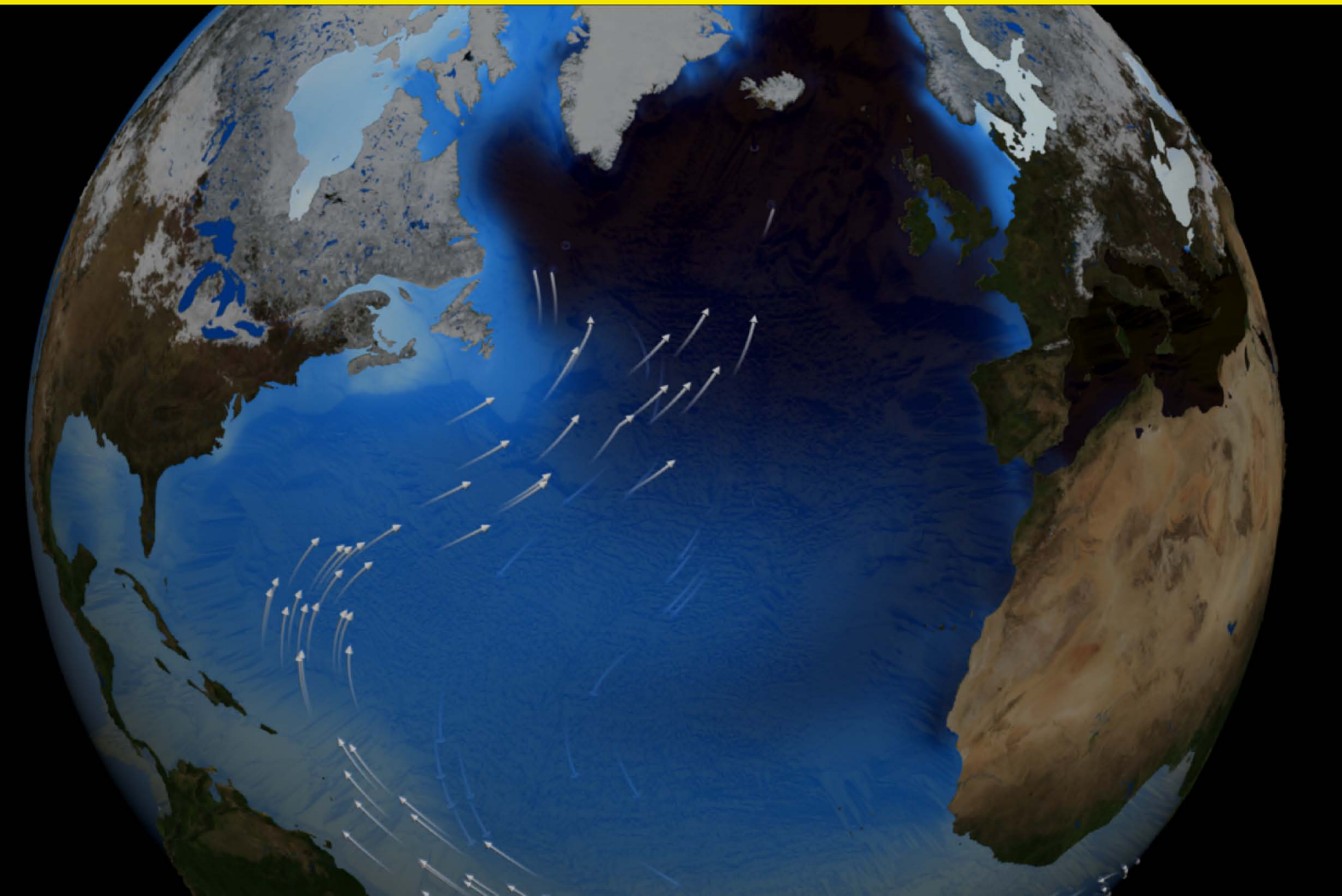

VNiVERSiDAD
D SALAMANCA

Facultad de Ciencias
Departamento de Geología-Área de Paleontología

# Cambios climáticos a escala orbital y milenaria en el Atlántico norte entre 800.000 y 400.000 años

**Memoria presentada por Montserrat Alonso García para optar al Grado de Doctor en Geología por la Universidad de Salamanca con Mención "Doctor Europeus"**

**Esta Tesis Doctoral se ha realizado bajo la dirección de los profesores:**

**Dr. D. Francisco Javier Sierro Sánchez**

**Dr. D. José Abel Flores Villarejo**

**D. Francisco Javier Sierro Sánchez** y **D. José Abel Flores Villarejo** profesores del Área de Paleontología del Departamento de Geología de la Facultad de Ciencias (Universidad de Salamanca)

CERTIFICAN que,

**Dña. Montserrat Alonso García** ha realizado en el Departamento de Geología y bajo nuestra supervisión el trabajo:

**Cambios climáticos a escala orbital y milenaria en el Atlántico norte entre 800.000 y 400.000 años**

y para que conste, firmamos el presente certificado en Salamanca en Noviembre de 2010

Los directores

Francisco J. Sierro Sánchez José A. Flores Villarejo

La doctoranda

Montserrat Alonso García

Este trabajo ha sido realizado gracias a la financiación de los proyectos CGL2005-00642/BTE, CGL2006 – 10593, CGL2008-05560, así como al proyecto del Ministerio de Ciencia e Innovación GRACCIE (CONSOLIDER-INGENIO CSD 2007-00067), a los fondos de la Junta de Castilla y León (Grupo de excelencia GR34) y al Ministerio de Educación mediante la beca predoctoral FPU (AP-2005-2805) otorgada a la autora. Gracias a la Universidad de Tübingen por poner a nuestra disposición su microscopio electrónico. Gracias a *Integrated Ocean Drilling Program* por suministrarnos las muestras estudiadas en esta tesis doctoral. También agradecemos al proyecto EPICA (*European Project for Ice coring in Antarctica*) y a las personas que han trabajado en el Site ODP 980 (principalemte B. P. Flower, A. K. Wright y J. F. McManus) y a E. S. Kandiano por poner sus datos disponibles, que han sido utilizados como complemento a esta Tesis Doctoral.

# AGRADECIMIENTOS

Cuando comencé la Tesis parecía que cuatro años era muchísimo tiempo, pero la verdad es que el tiempo vuela y aquí estoy, poniendo punto y final a mi etapa predoctoral. Desde que terminé la carrera tenía claro que quería dedicarme a la investigación por eso agradezco enormemente a mis directores de Tesis (Paco y José Abel) que me apoyasen a la hora de solicitar las becas predoctorales y me integrasen en su grupo de investigación. Estos años trabajando en vuestro grupo he aprendido mucho y además he tenido la oportunidad de conocer diferentes aspectos del mundo de la investigación en congresos y estancias. Gracias por permitirme participar en todo ello.

Por supuesto gracias también a todos los del grupo, empezando por Lines y Elena que siempre se han preocupado por nuestra "precaria" situación, y continuando con todos los becarios (algunos ya doctores) Mariem, Iván, Andrés, Débora, Alejandra, Carmen, Beatriz, Rubén, Margarita, Mieke, Aleix, Eloy, Miguel Ángel, Manuel y José Ignacio. Espero no haberme dejado a nadie, somos tantos… Beatriz, gracias por todos tus consejos en mis inicios y por tu interés aunque ya no estuvieras en Salamanca. Elena, gracias también por tus consejos y por tu disponibilidad para ayudarnos, es una pena que ya no estés en Salamanca, pero me alegro mucho por ti, no es fácil conseguir algo estable en este mundillo. Mariem, gracias por tu ayuda en el día a día, con el *Surfer*, con el papeleo, las preguntas sobre la tesis, en fin siempre has estado ahí para lo que fuera, ¡mucha suerte con tu postdoc! Margarita gracias por alimentarnos con tu zancocho, tu ajiaco, tus pastas… y por estar ahí cuando uno necesita hablar. Iván gracias por ayudarme cuando empezaba y por nuestras charlas científicas sobre el Atlántico norte, que espero no terminen con las tesis. Y a todos los demás, ha sido un placer trabajar con todos vosotros aunque a veces nos faltase el oxígeno, jeje.

No me gustaría olvidarme de dar las gracias también a Juan Ramón Colmenero por confiar en mi como investigadora desde incluso antes de terminar la carrera. También quiero dar las gracias a la gente del Área de Paleontología, en especial a Maruja y a Jorge, y a la gente del Área de Geodinámica interna por su interés por mi trabajo, en especial a Baby, Toña, Juan y Puy. Tampoco quiero olvidarme del resto de becarios y exbecarios del departamento, Diego, Óscar, Pedro Huerta, Mila, Colo, John Jairo, Natalia, Luismi, Tere, Daniel y Ana. Colo y Nata, gracias por introducirme al mundo colombiano y por vuestra amistad. Y hablando de amigos, Tere y Luismi, gracias por todos estos años (que ya son muchos desde que empezamos la carrera).

Durante las estancias breves he tenido la suerte de contar con gente maravillosa que ha hecho que el estar sólo y lejos de casa fuera menos duro. Thanks to Michal Kucera, Isabel Cacho and Heiko Pälike for supervising my work there and for including me in your working groups. Working in Tübingen, Barcelona and Southampton was a great experience for me. Thanks to Lea, Gabi, Siccha, Ulrike, Roman and Hartmut for your kindness. También gracias a mis erasmus favoritas Cris, Maite, Sonia, Ali y Guio, que pena no poder estar allí todo el año con vosotras. Gracias también al grupo de Barcelona, en especial a Leo, Gemma, Patri, Mireya y Mayte, y también a Montse Guart y a mi cubano favorito, Israel. Patri y Mireya, nunca olvidaré nuestras sobremesas con ositos, jaja. And thanks as well to Patrizia Ferretti for all your help and advices while I was in Barcelona. And last but

not least thanks to the PhD and MSc students of Southampton, Mike, Ed, David, Jeff, Clara, Maike, Diederick, Anna, Anya, Daria, Chris, Joe, Alex, Romain, and of course to my Spanish Team (Moni, Sonia, María, Eva, Marcos y Antonio I miss you!!). And I can't forget my officemates Katharine and Steve, thanks for solving everything I needed.

Y ahora fuera de lo académico me gustaría dar las gracias a todas mis amigas que aunque no sabéis de qué va esto de la investigación siempre estáis ahí, para apoyarme, para relajarme y olvidarme por unas horas del trabajo, y para lo que haga falta, y siempre lo habéis estado, desde el instituto (Yesi, Mir, Vane, Laura y Elena) y desde Palm Beach (Marta, Isa, María, Elena, Raquel, Blanca y Julita). Por supuesto gracias también a esos novios/maridos maravillosos que tenéis, porque es un placer ampliar esta segunda familia con vosotros y con tus pequeñinas Juli.

A mis padres y a toda mi familia, simplemente porque me queréis tal y como soy y yo a vosotros. Y también por seguirme allá donde voy, ¿cuál será el próximo viaje? Que quede claro que también incluyo a mis tíos y primos que son los mejores y que cada año nos traen más alegrías a la familia en forma de princesitas, a ver cuando llegan los príncipes…

Bueno cari, parecía que nunca iba a llegar este día, eh? pero si, todo llega en esta vida sólo hay que tener paciencia, gracias por la tuya y por todos estos años y los que nos quedan, que no te vas a librar de mí : P

Seguramente me olvide de alguien, porque ya sabemos que el despiste lo llevo en los genes, así que muchas gracias a todos los que de una manera u otra habéis pasado por mi vida, especialmente estos últimos años.

*A toda mi familia,*
*especialmente a mi abuela Asun*

# ÍNDICE

# RESUMEN

El Atlántico norte es una zona muy sensible a los cambios climáticos y oceanográficos puesto que las principales zonas de formación de aguas profundas, que son el motor de la circulación termohalina, se encuentran en el Mar del Labrador y el Mar de Noruega-Groenlandia. Por tanto los cambios en la circulación oceánica del Atlántico norte tienen una gran influencia en la circulación global. En esta Tesis Doctoral se ha estudiado un testigo de sedimento oceánico que está ubicado en un lugar clave dentro del Atlántico subpolar. El área de estudio nos ha permitido analizar tanto cambios superficiales, en especial variaciones en la corriente Noratlántica (NAC) y eventos de descarga de icebergs, como cambios en la intensidad de la circulación profunda.

En esta Tesis Doctoral se ha elaborado un registro de isótopos estables de oxígeno y carbono en foraminíferos bentónicos (principalmente *C. wuellerstorfi*), un registro de isótopos estables de oxígeno y carbono en dos especies de foraminíferos planctónicos, *N. pachyderma* sin y dex, un registro de acumulación de IRD, un registro de cambios en las asociaciones de foraminíferos planctónicos y un registro de la proporción de elementos traza en las conchas de *N. pachyderma* sin. Además se ha realizado un análisis espectral de los registros anteriormente mencionados y de otros como los del testigo de hielo antártico EDC.

Uno de los objetivos prioritarios de esta Tesis ha sido establecer el modelo de edad para el intervalo estudiado. Para ello se ha correlacionado el registro de $\delta^{18}O$ de foraminíferos bentónicos con el registro de temperatura obtenido a partir del testigo de hielo antártico EDC. El intervalo de estudio comprende desde el MIS 19 al 11, que corresponde a un intervalo desde hace 800 a 400 mil años (ka) aproximadamente.

En base a las herramientas paleoceanográficas y paleoclimáticas utilizadas en este trabajo hemos identificado una serie de patrones que nos ha permitido establecer una división de los ciclos climáticos en cinco fases:

1) Fase inicial de los periodos interglaciales. Durante esta fase los frentes Ártico y Polar estaban situados en una posición similar a la que presentan hoy en día. La circulación termohalina era muy activa y la NAC llegaba al Mar de Noruega-Groenlandia y al Mar del Labrador donde se hundía para formar aguas profundas, como ocurre en el presente.

2) Fase tardía de los periodos interglaciales. En esta fase el frente Ártico empezó a migrar hacia el sureste cerca del Site U1314. Sin embargo, los valores de $\delta^{18}O$ de foraminíferos bentónicos indican que los casquetes de hielo aún no habían empezado a crecer. La formación de aguas profundas en el Mar del Labrador se redujo y las aguas del giro subpolar disminuyeron su salinidad por la reducción de la llegada de aguas de la NAC. En cambio, en el Mar de Noruega-Groenlandia la

formación de aguas profundas era muy activa.

3) Primera fase de los periodos glaciales. El inicio de los periodos glaciales se ha establecido como el punto de inflexión de los valores de $\delta^{18}O$ de foraminíferos bentónicos, es decir cuando comenzó a aumentar el volumen de hielo. Durante esta fase la circulación termohalina continuó activa en el Mar de Noruega-Groenlandia porque los frentes Ártico y Polar aún no habían migrado hacia el sur en esa zona. Este hecho favoreció el transporte de vapor de agua hacia altas latitudes y por ende la acumulación de hielo en los continentes. Sin embargo, una banquisa de hielo perenne cubría gran parte del Mar del Labrador, por lo que la convección dejó de producirse en esta área. El frente Ártico se situaba entre el Site U1314 y el Site 980 de ODP, de modo que la NAC fluía por el este del Atlántico pero aún llegaba al Mar de Noruega-Groenlandia. Las aguas profundas probablemente fueron enfriándose durante esta fase y ese enfriamiento se transmitió al hemisferio sur, y a todo el océano, a través de la circulación termohalina.

4) Segunda fase de los periodos glaciales. Esta fase comienza con la primera descarga de IRD, y se caracteriza por un crecimiento progresivo de los mantos de hielo que fue interrumpido por varios eventos de escala milenaria, que hemos denominado *ice sheet collapse events* (ISCE). La primera descarga de icebergs da comienzo a la ralentización de la circulación termohalina y a la generación de aguas intermedias (GNAIW) en vez de profundas (NADW). Los ISCE comienzan con una descarga de IRD hacia el Atlántico norte que ralentiza la formación de GNAIW y produce un calentamiento en el hemisferio sur por el efecto *see-saw*, que a su vez da lugar a la liberación de $CO_2$ del océano a la atmósfera. A esta primera etapa de enfriamiento extremo en el hemisferio norte le sucede un calentamiento brusco del agua superficial que incrementa la ablación de las grandes masas de hielo en el hemisferio norte. La estructura de los ISCE es similar a la de un evento Heinrich y su posterior interestadial, descritos para el último periodo glacial. Durante las etapas de acumulación de hielo el frente Ártico estaba a unos 55º N con una dirección casi E-W, las aguas de la NAC solamente llegaban al Site 980 y la GNAIW se generaba probablemente al sur de los 60º N. En cambio, durante los periodos cálidos de los ISCE el frente Ártico migró hacia el norte, la NAC llegaba más al norte y la GNAIW se formaba también más al norte.

5) Fase final de los periodos glaciales y Terminación. Durante esta fase el frente Ártico comenzó a retroceder lentamente hasta que durante la Terminación se produce una brusca migración hacia el noroeste mientras se reduce el volumen de hielo. La NAC va penetrando hacia el norte y reactiva la formación de aguas profundas tanto en el Mar de Noruega-Groenlandia como en el Mar del Labrador.

Las asociaciones de foraminíferos planctónicos nos muestran cambios muy bruscos entre la asociación predominante en los periodos cálidos, donde dominan las especies transicionales-subpolares *N. pachyderma* dex, *G. inflata* y *G. bulloides*, y la asociación prácticamente monoespecífica de *N. pachyderma* sin que predomina durante los periodos fríos. Estos cambios bruscos se deben a la posición del frente Ártico, que determina la presencia de aguas de la corriente

noratlántica o aguas Árticas en la zona del testigo. Cuando el frente estaba cerca del área de estudio se registran altos porcentajes de *T. quinqueloba*.

Los cálculos de paleotemperaturas a partir de la relación Mg/Ca y de las asociaciones de foraminíferos planctónicos nos muestran que las temperaturas de Mg/Ca en latitudes altas son fiables durante los periodos interglaciales, cuando el frente Ártico estaba al norte del Site U1314, mientras que la presencia de las aguas árticas interfiere en la relación del Mg/Ca con la temperatura, corroborando estudios previos. El análisis de las temperaturas junto a los análisis del $\delta^{18}O$ en las conchas de los foraminíferos planctónicos *N. pachyderma* sin y dex nos muestra que durante los periodos interglaciales la diferencia entre ambas especies indica estacionalidad y mezcla en la columna de agua. Los MIS 15 y 11 presentaron una mayor estacionalidad con veranos más cálidos e inviernos más fríos que los MIS 17 y 13, en parte como consecuencia de una mayor estratificación de la columna de agua durante el verano. Estas diferencias en la estratificación pudieron estar relacionadas con un aumento en la fuerza de los vientos durante los veranos de los MIS 17 y 13. Durante los periodos glaciales la presencia de banquisa de hielo durante la mayor parte del año favoreció que ambas especies vivieran en la misma estación y en la misma masa de agua dentro de la columna dado que es posible que el deshielo de la banquisa produjera una gran estratificación. Las descargas de icebergs no produjeron cambios significativos en el $\delta^{18}O$ del agua excepto en las Terminaciones.

El análisis de la ciclicidad de los diferentes registros elaborados en esta Tesis y su comparación con los registros de EDC, nos ha permitido observar un progresivo aumento en la importancia de la precesión en los ciclos climáticos. Desde el establecimiento casquete de hielo del este de la Antártida sobre la plataforma marina el hemisferio Sur ha alternado entre estar en fase o desfasado respecto al hemisferio norte hasta que en el MIS 12 se establece en fase. Este periodo de adaptación provocó un desplazamiento en la ITCZ hacia el norte que aumentó el transporte de vapor de agua al hemisferio norte contribuyendo a la formación de grandes masas de hielo que alcanzaron su máximo desarrollo en el MIS 16. Desde el MIS 16 al 12 la insolación sobre altas latitudes del hemisferio norte controlaba los cambios climáticos globales y la concentración de $CO_2$, pero el clima estaba aún estaba influido por la oblicuidad. A partir del MIS 12 la ITCZ se situó más cerca del ecuador, las temperaturas durante los interglaciales aumentaron en el hemisferio sur y los cambios de volumen de hielo se produjeron en fase en ambos hemisferios.

# ABSTRACT

From a climatic and oceanographic point of view, the North Atlantic is a very important area because the main sources of deep water formation, which drive thermohaline circulation, are in the Norwegian-Greenland Sea and the Labrador Sea. Hence, changes in North Atlantic circulation have a great impact on global circulation. In this Thesis a section of the North Atlantic sediment core IODP Site U1314 was studied. This core was recovered in a key area for studying North Atlantic current variations and IRD discharges as well as changes in the strength of the Atlantic Meridional Overturning circulation (AMOC).

Several records were obtained from micropaleontological and geochemical analysis on foraminifers: stable oxygen and carbon isotopes from benthic foraminifers (mainly *C. wuellerstorfi*), stable oxygen and carbon isotopes from two planktic foraminifer species *N. pachyderma* sin y dex, IRD fluxes, planktic foraminifer assemblages and trace elements from the planktic foraminifer *N. pachyderma* sin. Additionally, time series analyses were performed on all the records above mentioned and on the records from the Antarctic ice core EDC.

The first aim of this Thesis was establishing the chronological framework for the studied interval. We tuned our benthic $\delta^{18}O$ with the Antarctic temperatures from EDC ice core. The studied interval encompasses from MIS 19 to 11, which means from 800 to 400 thousand years (ka) approximately.

Using the paleoceanographic and paleoclimatic proxies above mentioned, we propose that glacial-interglacial cycles can be divided in five stages:

1) Early interglacial stage. During this stage the Arctic and Polar fronts were located in a position similar to their present day position. The AMOC was very active and the NAC reached the Norwegian-Greenland Sea and the Labrador Sea where it sank to generate deep waters, like it happens nowadays.

2) Late interglacial stage. During this stage the Arctic front started to migrate southeastwards reaching a position near Site U1314. However, the low benthic $\delta^{18}O$ values indicated that the ice sheets did not started to grow. Deep water formation in the Labrador Sea was reduced lowering the input of NAC waters in the subpolar gyre and hence the salinity of the gyre. Conversely in the Norwegian-Greenland Sea deep water formation was very strong.

3) First stage of glacial periods. The beginning of glacial periods was established at the inflection of benthic $\delta^{18}O$ record, in other word when the ice volume began to grow. During this stage the AMOC was active in the Norwegian-Greenland Sea because the Arctic and Polar fronts were rather north in this area. That favoured the fresh water transport towards high latitudes and the accumulation of snow in the continents. In the Labrador Sea a perennial sea ice cover prevented

convection and deep waters were not produced at this area. The Arctic front was located between Site U1314 and ODP Site 980, whereby the NAC flowed through the East Atlantic and still reached the Norwegian-Greenland Sea. It is likely that deep waters progressively cooled and that cooling was transmitted through the AMOC to the Southern Hemisphere, and the whole ocean.

4) Second stage of glacial periods. This stage began with the first ice-rafting event and it is characterised by a progressive ice sheet growth that was interrupted by several millennial-scale events that we denominated ice sheet collapse events (ISCE). As a consequence of the first iceberg discharges the AMOC was disturbed and intermediate water (GNAIW) was generated instead of deep water (NADW). The ISCE present two phases, first iceberg discharges dampened the formation of GNAIW and because of the see-saw effect, the Southern Hemisphere warmed and $CO_2$ was outgased from the ocean to the atmosphere. Subsequently an abrupt warming occurred in the Northern Hemisphere melting part of the ice sheets. The ISCE present a similar sequence of events as the Heinrich events and the subsequent interstadial that where described for the last glacial period. During the progressive ice sheet growth the Arctic front was at approximately E-W and was located at 55 º N. The NAC reached Site 980 and GNAIW was likely generated south of 60º N. Conversely, during the warm phase of the ISCE the Arctic front migrated northwards, the NAC reached northernmost positions and the GNAIW was generated northernmost too.

5) Late glacial periods-termination. At the end of glacial periods the Arctic front began to retreat slowly and then at the Termination the Arctic front migrated northwestwards abruptly as the ice volume was reduced. The NAC entered in the Norwegian-Greenland Sea and the Labrador Sea where it resume the deep water formation, and hence, the AMOC.

Planktic foraminifer assemblages showed abrupt shifts between cold and warm assemblages. *N. pachyderma* dex, *G. inflata* y *G. bulloides* were dominant during the warm periods whereas during cold periods the assemblage was almost monospecific and *N. pachyderma* sin dominated. The abrupt shifts were related to the position of the Arctic front respect to the studied area, which determined the presence of NAC waters or Arctic waters. When the Arctic front was near Site U1314 high percentages of *T. quinqueloba* were recorded.

Paleotemperature reconstructions performed with transfer functions for planktic foraminifers and Mg/Ca paleothermometry showed that Mg/Ca paleothermometry is reliable when the Arctic front was north of Site U1314 whereas the presence of the Arctic waters interfered in the Mg/Ca-temperature relationship, supporting previous works. Additionally the analysis of temperatures and $\delta^{18}O$ records on planktic foraminifer tests of *N. pachyderma* sin and dex suggests that during interglacial periods the difference between both species is related to seasonality and stratification of the water column. During MIS 15 and 11 seasonality was higher, with cooler winters and warmer summers than during MIS 17 and 13 summer stratification of the water column was higher than during MIS 17 and 13. The differences in seasonality might be related with the strength of summer winds. During interglacial periods the presence of sea ice during most of the year favoured that

both species lived during the same season and in the same water mass because the sea ice melting might have produced a low salinity lid that prevented water mixing. The iceberg discharges did not produce significant changes in the seawater $\delta^{18}O$ except at the Terminations.

Time series analyses performed on the different records of the Thesis and their comparison with the spectral analyses of EDC records, showed a progressive importance of the precession band in the climatic cycles. From the marine-establishment of the East Antarctic Ice Sheet the Southern Hemisphere fluctuated between in and out phase responses respect to the Northern hemisphere until MIS 12. This change produced a northward shift in the ITCZ increasing moisture transport to higher latitudes and contributing to the snow accumulation and the large ice sheet growth of MIS 16. From MIS 16 to 12 high latitude northern hemisphere insolation controlled global climate changes and the $CO_2$ concentration, but the climate was still highly influenced by obliquity. After MIS 12 the ITCZ migrated near the equator, sea surface temperatures in the Southern Hemisphere increased and ice volume changes occurred in phase.

# PRESENTACIÓN DE LA TESIS

El interés por el clima de la Tierra y sus variaciones está en auge puesto que se prevé que el creciente efecto invernadero, derivado del aumento de las emisiones de $CO_2$ y otros gases invernadero, podría hacer variar el clima hacia un calentamiento global. Entender cómo y por qué ocurrieron los cambios climáticos del pasado nos puede ayudar a predecir futuros escenarios relacionados con cambios climáticos. En esta tesis se aportan nuevos datos y enfoques sobre los cambios climáticos y oceanográficos que se registraron entre aproximadamente 800 y 400 mil años (ka) en las latitudes altas del Atlántico Norte y que se relacionan con el clima y la circulación oceánica global.

El Atlántico norte es una zona sensible a cambios en el clima puesto que los cambios en sus masas de agua repercuten en la circulación termohalina y se propagan por todo el planeta. Esta zona es una región muy estudiada debido a que en esta área tienen lugar los procesos de producción de aguas profundas que alimentan la circulación profunda. El análisis de las asociaciones de foraminíferos planctónicos y los estudios geoquímicos tanto en foraminíferos planctónicos como en bentónicos nos han permitido realizar una reconstrucción de los procesos climáticos que se manifestaron a lo largo de los distintos ciclos glaciales e interglaciales que ocurrieron entre 800 y 400 ka. Además el intervalo de estudio, incluido en el Pleistoceno medio, es muy interesante debido a los cambios a nivel global que tuvieron lugar en la ciclicidad glacial-interglacial. A comienzos del intervalo de estudio los ciclos de ~100 ky que habían surgido aproximadamente hace 950-900 ka muestran un aumento progresivo en la intensidad de los periodos glaciales produciéndose grandes acumulaciones de hielo en el hemisferio norte. Sin embargo, no es hasta aproximadamente 400 ka cuando los ciclos de ~100 ka adquieren su mayor amplitud, con periodos glaciales muy fríos e interglaciales muy cálidos. Por lo tanto durante este intervalo podemos estudiar cómo evolucionaron las pautas y patrones de los ciclos climáticos de ~100 ky desde 900 a 400 ka.

Esta Tesis Doctoral opta al grado de "*Doctor Europeus*" y por tanto tiene capítulos escritos en castellano y en inglés. Además, como la ciencia hoy en día se escribe mayoritariamente en inglés, muchas palabras de difícil traducción se han dejado en inglés en el texto en castellano pero en cursiva para indicarlo. En la medida de lo posible se ha intentado que las figuras en los capítulos en castellano estuvieran en castellano, pero al ser figuras tomadas de otros autores esto no siempre fue posible, por lo que en el pie de figura se han traducido las partes más relevantes. La Tesis está organizada en diferentes capítulos que se exponen a continuación.

Primero se ha realizado una introducción a la zona de estudio, a los patrones que controlan las variaciones climáticas en la Tierra, al periodo temporal estudiado y a los foraminíferos como herramienta paleoceanográfica y paleoclimática.

El capítulo 2 constituye una descripción detallada de los materiales utilizados para la realización de la tesis y las metodologías empleadas en la misma.

Los capítulos 3, 4 y 5, en inglés, son los artículos científicos derivados de la Tesis. En ellos se exponen los resultados y las conclusiones obtenidas a partir del análisis de los diferentes datos obtenidos durante la realización de la Tesis. En el primer artículo (capítulo 3) se establece el modelo de edad utilizado en esta Tesis Doctoral. Este artículo destaca el desarrollo y las características de los periodos glaciales mediante el uso de isótopos estables de foraminíferos planctónicos y bentónicos, de las temperaturas obtenidas a partir de las asociaciones de foraminíferos planctónicos y de la comparación con los datos de los testigos de hielo de EPICA.

En el segundo artículo (capítulo 4) se han utilizado las asociaciones de foraminíferos planctónicos como *proxy* para la evaluación de la posición del Frente Ártico en el Atlántico Norte y su migración durante los ciclos glacial-interglacial. Esto junto a los datos obtenidos en el primer artículo nos ha llevado a dividir los ciclos climáticos en cinco fases.

En el tercer artículo (capítulo 5) se han evaluado los factores que afectan a los cálculos de temperaturas comparando cálculos realizados con funciones de transferencia para las asociaciones de foraminíferos planctónicos, cálculos realizados a partir de la relación Mg/Ca en las conchas del foraminífero planctónico *Neogloboquadrina pachyderma* sin, y análisis de los isótopos de oxígeno en *N. pachyderma* sin y *N. pachyderma* dex.

En el capítulo 6, también en inglés, se exponen y discuten los resultados obtenidos a partir de los análisis de la ciclicidad de las series estudiadas, realizados mediante diversas técnicas (Blackman-Tuckey, filtros Gaussianos y *cross wavelet analysis*) y su posible significado relacionado con los cambios climáticos que acontecieron durante el Pleistoceno medio.

El capítulo 7 resume las conclusiones principales obtenidas en los capítulos anteriores. Este capítulo presenta una versión en castellano y otra en inglés. Y finalmente se han elaborado una serie de anexos que complementan la Tesis y facilitan su lectura y comprensión.

# OBJETIVOS

El objetivo fundamental de esta Tesis Doctoral es **estudiar las variaciones climáticas y oceanográficas así como los cambios en la ciclicidad que tuvieron lugar en el Atlántico norte entre 800 y 400 ka, y su relación con el clima global**. Para desarrollar este objetivo principal se han llevado a cabo varios objetivos secundarios que se detallan a continuación.

- Elaborar un registro de las variaciones en las asociaciones de foraminíferos planctónicos.
- Reconstruir las paleotemperaturas utilizando funciones de transferencia con las asociaciones de foraminíferos planctónicos.
- Elaborar un registro de isótopos estables de oxígeno y carbono en foraminíferos bentónicos.
- Elaborar un registro de isótopos estables de oxígeno y carbono en dos especies de foraminíferos planctónicos (*N. pachyderma* sin y dex).
- Elaborar un registro de elementos traza en las conchas de *N. pachyderma* sin para obtener paleotemperaturas a partir de la relación Mg/Ca y analizar sus posibles complicaciones.
- Elaborar un modelo de edad para el intervalo estudiado.
- Evaluar cambios en el volumen de hielo y en la circulación termohalina a lo largo de los ciclos climáticos comprendidos en el intervalo de estudio.
- Identificar los principales eventos de descarga de IRD al Atlántico y analizar su relación con otros proxies de circulación, temperatura y salinidad.
- Comparar los registros obtenidos a partir del Site U1314 con los registros de temperatura y gases invernadero de los testigos de hielo de la Antártida.
- Analizar las condiciones de las masas de agua superficiales a lo largo de los ciclos climáticos, combinando los registros de paleotemperaturas, isótopos estables y las propias asociaciones de foraminíferos planctónicos.
- Realizar análisis espectrales de las series temporales obtenidas, utilizando el método de Blackman-Tuckey, filtros Gaussianos, y análisis espectral de tipo *wavelet* y *cross wavelet*.
- Estudiar los cambios en la ciclicidad a lo largo del intervalo de estudio y sus posibles causas.

# CAPÍTULO 1.

# INTRODUCCIÓN

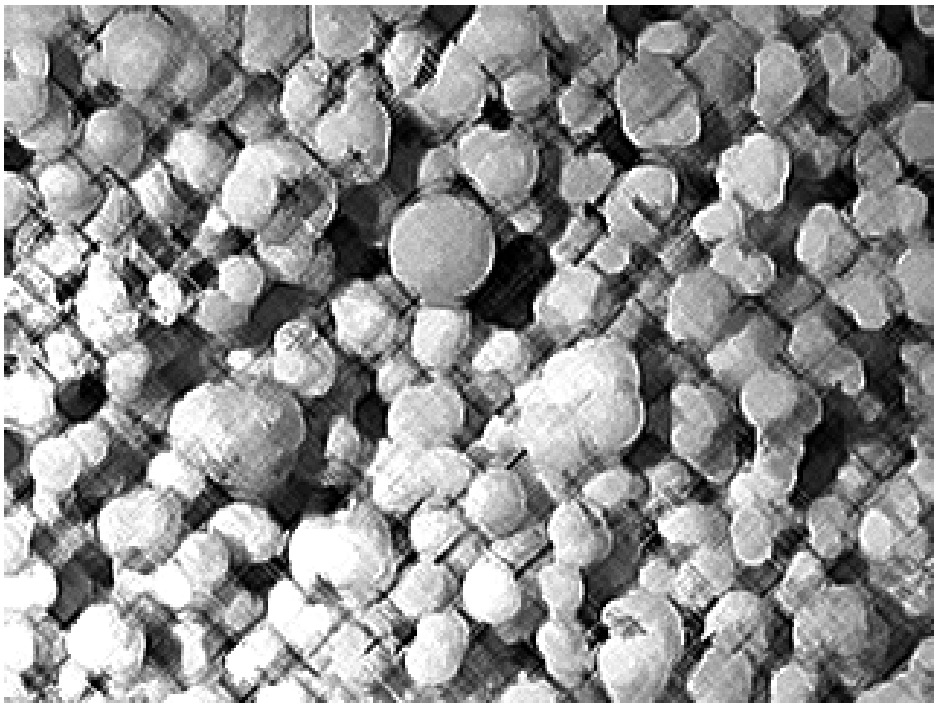

# 1. INTRODUCCIÓN

## 1.1. CIRCULACIÓN OCÉANICA Y ATMOSFÉRICA EN EL ATLÁNTICO NORTE

El Atlántico norte es uno de los océanos mejor conocidos. Son muy numerosos los estudios que se han realizado sobre él y que se siguen realizando debido a la relación existente entre su circulación y los cambios climáticos a nivel global. Aunque el testigo estudiado en este trabajo esté situado en el Atlántico norte, es preciso explicar brevemente la dinámica atmosférica y oceánica tanto del Atlántico norte como del Mar de Noruega-Groenlandia (*Norwegian-Greenland Sea*, NGS), ya que los procesos que tienen lugar en el mar de Noruega-Groenlandia también afectan al área del testigo.

### 1.1.1. Circulación atmosférica

El polo norte se caracteriza por tener altas presiones atmosféricas durante todo el año (fig. 1.1), alcanzando sus máximos en invierno cuando forman una cadena de altas presiones que va desde la cuenca de Canadá hasta el norte de Groenlandia (Tomczak and Godfrey, 1994, y referencias citadas por estos autores). Estas altas presiones generan vientos del este (*easterlies*) y estos a su vez dan lugar a una circulación oceánica superficial anticiclónica (hacia el oeste).

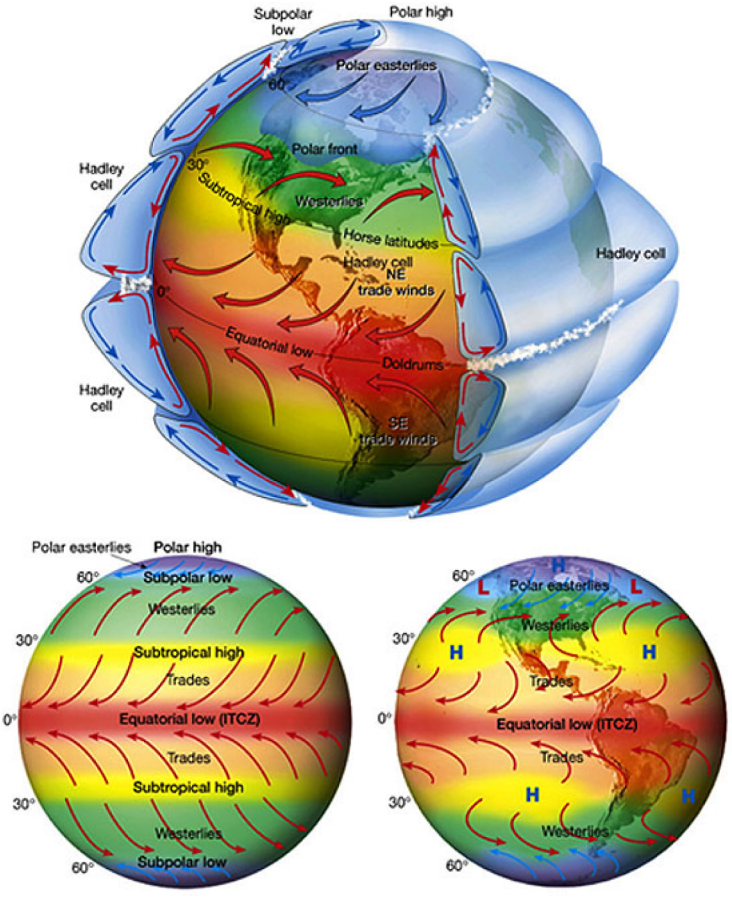


Fig. 1.1. Circulación atmosférica global en la que se muestran los principales sistemas de vientos y células de presiones. En las figura de abajo a la izquierda se muestran los cinturones de vientos y presiones teóricos, mientras que en la de abajo a la derecha se muestran los reales, que se ven influidos por la presencia /ausencia de continentes. En el Atlántico norte podemos observar la célula de altas presiones de las Azores en torno a 30º N (en amarillo), la célula de bajas presiones de Islandia (en azul) y la célula de altas presiones en el polo norte (en morado). Esta figura fue tomada de la página web de la NASA (http://rst.gsfc.nasa.gov/Sect14/Sect14_1c.html).

Sin embargo en el NGS el sistema de vientos está dominado por las bajas presiones situadas sobre Islandia que producen vientos del oeste (*westerlies*). Las precipitaciones son mucho mas abundantes en la zona subpolar que en la polar, debido a la presencia de los vientos del oeste, que generan fuertes tormentas.

La circulación atmosférica del Atlántico varía mucho en función de la estación. Durante los inviernos el cinturón subtropical de altas presiones en el Atlántico norte va desde Florida-Bermuda a las islas Canarias, las Azores, y continúa por el Sahara y el mar Mediterráneo (Tomczak and Godfrey, 1994). En esta estación el Atlántico norte está dominado por las bajas presiones de Islandia que llevan asociados fuertes vientos del oeste, responsables de traer precipitaciones a Europa. En cambio, durante los veranos el cinturón de altas presiones del Atlántico norte se debilita quedando reducido a una célula de alta presión situada sobre las Azores que genera vientos moderados y tiempo anticiclónico en Europa. Sin embargo, esta configuración atmosférica varía ligeramente dependiendo de la diferencia entre las altas presiones de las Azores y las bajas de Islandia, lo que se conoce como oscilación del Atlántico Norte (e.g. Wanner et al., 2001).

### 1.1.2. Circulación oceánica

En la figura 1.2a se muestra como el mar de Noruega-Groenlandia está separado del océano Atlántico por una cordillera submarina que va desde Groenlandia hasta Escocia pasando por Islandia y las Islas Feroe (*Greenland-Iceland-Faroe-Scotland Ridge*, GIFSR) y del océano Ártico por el estrecho de Fram (*Fram Strait*) (Hansen and Østerhus, 2000). En él se distinguen varios mares, el somero mar de Barents (*Barents Sea*), el mar de Groenlandia (*Greenland Sea*), el mar de Islandia (*Iceland Sea*) y el mar de Noruega (*Norwegian Sea*). Dentro del Atlántico subpolar también se distinguen tres cuencas, la cuenca de Irminger *(Irminger Basin*), separada de la cuenca de Islandia (*Iceland Basin*) por la dorsal oceánica (también conocida en esta zona como la cordillera de Reykjanes o *Reykjanes Ridge*), y ésta, a su vez, esta separada del canal de Rockall (*Rockall Channel*) por la meseta submarina de Rockall-Hatton (*Rockall-Hatton Plateau*).

La corriente Noratlántica (*North Atlantic Current*, NAC) transporta las aguas cálidas y salinas del trópico hacia el noreste cruzando el Atlántico hasta llegar al mar de Noruega (fig. 1.2) donde se convierte en la corriente de Noruega (*Norwegian Current*, NC). Durante el trayecto desde el Golfo de México hasta el mar de Noruega la corriente va cediendo su calor a los vientos del oeste, que se encargan de traspasar ese calor al continente europeo (Hansen and Østerhus, 2000). Esto hace que en Europa la temperatura sea más alta que en otras partes del mundo con una latitud similar. La NAC separa el giro subtropical del giro subpolar (Tomczak and Godfrey, 1994). El primero, de sentido anticiclónico recircula las aguas cálidas de la NAC hacia el sur mezclándolas con las de la corriente de Portugal-Canarias (*Portugal-Canary Current*, PCC). El giro subpolar, de sentido ciclónico, recircula las aguas cálidas a través de la corriente de Irminger (*Irminger Current*, IC) por las costas de Groenlandia y Canadá mezclándose con las aguas frías de

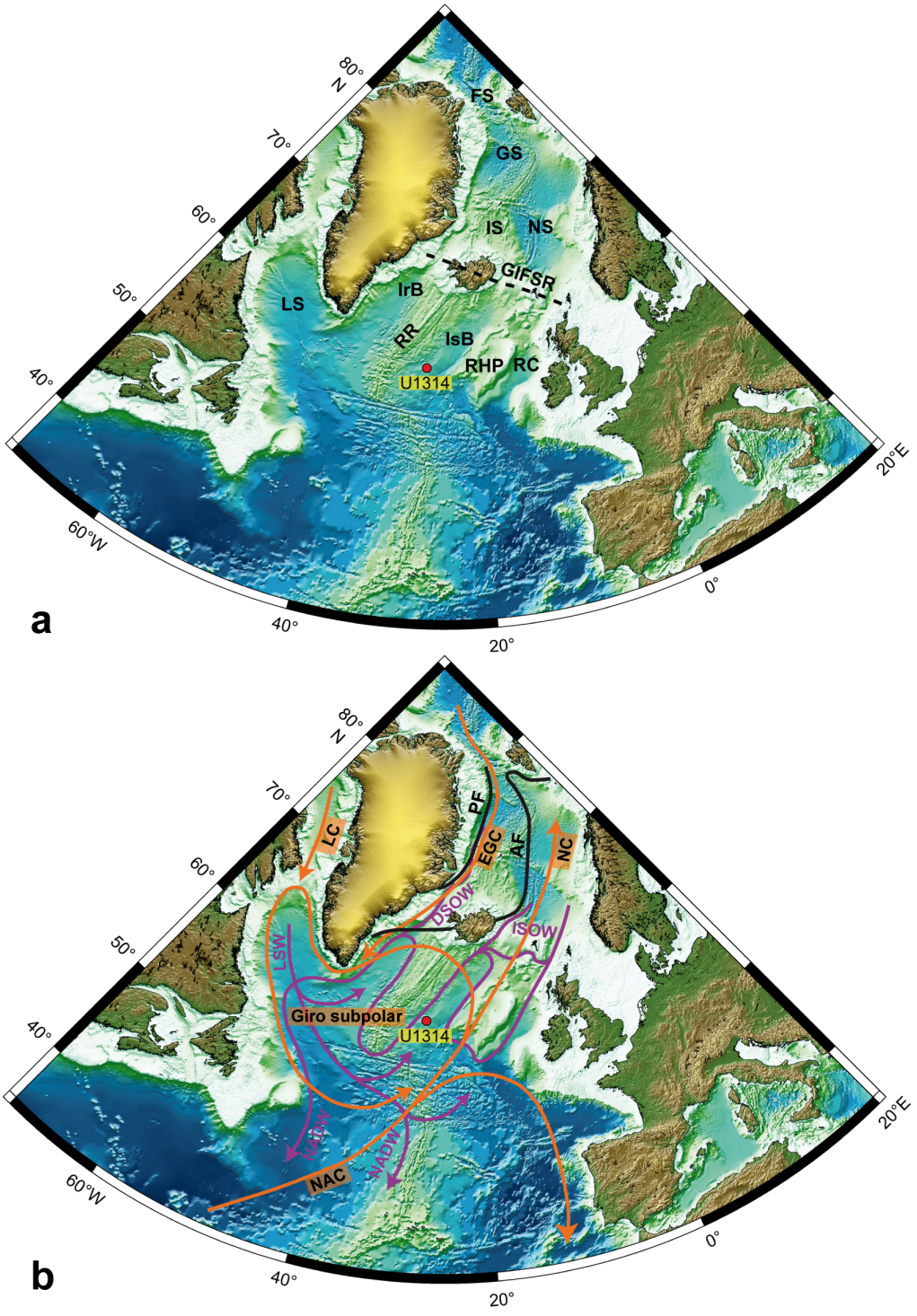


Fig. 1.2. Localización de la zona de estudio. a) Principales cuencas en las que se dividen el Atlántico subpolar y el Mar de Noruega-Groenlandia. También se indica la situación de los promontorios más importantes, la situación del testigo estudiado en esta tesis doctoral y las principales corrientes superficiales con flechas naranjas (Schmitz and McCartney, 1993). b) Circulación superficial (flechas naranjas) y profunda (flechas moradas) según Schmitz and McCartney (1993) y Dickson et al. (1990). También se muestra la posición actual de los frentes Ártico y Polar descritos en el Mar de Noruega-Groenlandia por Swift (1986). El mapa de base ha sido facilitado por IODP.

la corriente del este de Groenlandia (*East Greenland Current*, EGC) y la del Labrador (*Labrador Current*, LC).

Entender la dinámica de masas de agua existente en el mar de Noruega-Groenlandia hoy en día es fundamental para poder hacer reconstrucciones de cómo pudieron ser las masas de agua en el Atlántico norte durante los periodos glaciales. Según Hurdle (1986), actualmente en el mar de Noruega-Groenlandia se pueden distinguir tres tipos de masas de agua superficiales (aguas polares, árticas y atlánticas) separadas entre sí por dos frentes (fig. 1.2b). Las aguas polares, frías y de baja salinidad (< -1 ºC, 30-33, según Tomczak and Godfrey, 1994), que corresponden con las aguas de la EGC, están separadas de las aguas árticas, también frías pero de mayor salinidad, por el Frente Polar (Polar front, PF). El Frente Ártico (Arctic front, AF) separa las aguas árticas de las atlánticas, cálidas y salinas (6-8 ºC, 34-35) que corresponden a la corriente de Noruega. Éste frente está situado ligeramente al oeste de la máxima extensión de la banquisa de hielo (la de invierno), mientras que el Frente Polar está situado ligeramente al oeste de la mínima extensión de la banquisa (la de verano). Por tanto las aguas árticas están estacionalmente cubiertas por hielo y en ellas se produce convección profunda durante el invierno principalmente.

La formación de aguas profundas se produce al hundirse las aguas superficiales debido a que sufren un aumento de densidad. Esto puede producirse por aumentos en la salinidad, disminución de la temperatura o más frecuentemente una combinación de ambas. Las aguas árticas profundas (*Arctic Bottom Waters*, ABW) provienen de dos fuentes, el mar de Groenlandia y las plataformas árticas. Las aguas profundas del mar de Groenlandia se forman por convección debido al fuerte enfriamiento que sufren en invierno y al enriquecimiento en sal que tiene lugar en las aguas superficiales al formarse la banquisa de hielo (ver revisión de Tomczak and Godfrey, 1994). La salinidad de las aguas profundas del Mar de Noruega-Groenlandia alcanza 34,95 y la temperatura puede ser menor de -1,5º C. Sin embargo, en las plataformas árticas, la baja salinidad de las aguas procedentes de los ríos facilita la formación de hielo, y en este proceso la sal es expulsada incrementando la salinidad de las aguas que están por debajo del hielo y con ello su densidad. Estas masas de agua formadas en la plataforma tienen características diferentes a las formadas en el Mar de Noruega-Groenlandia.

Las aguas profundas generadas en el Mar de Noruega-Groenlandia fluyen al Atlántico subpolar a través de los canales existentes en la cordillera submarina que va desde Groenlandia hasta Escocia (ver fig. 1.2b y 1.3a). Las masas de agua más importantes son las aguas que salen por el estrecho de Dinamarca (*Denmark Strait Overflow Water*, DSOW) y las que salen por los canales que hay entre Islandia y Escocia (*Iceland Scotland Overflow Water*, ISOW). Ambas constituyen una de las fuentes principales de las aguas Noratlánticas de fondo (*North Atlantic Deep Water*, NADW) junto a las aguas profundas que se forman en el Mar del Labrador (*Labrador Sea Water*, LSW). A menudo se distingue a las masas de agua formadas en el Labrador como las aguas superiores de la NADW (*upper NADW*, UNADW) y las del NGS como las aguas inferiores de la

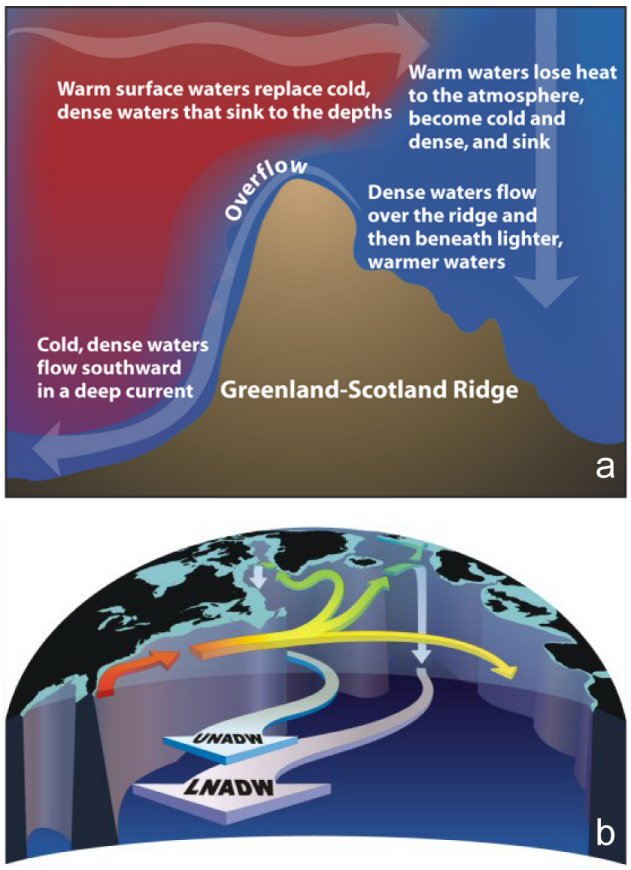


Fig. 1.3. a) Esquema del hundimiento de aguas en el NGS y su posterior flujo al Atlántico a través de los canales del promontorio que va desde Groenlandia a Escocia. Imagen de E. Paul Oberlander, Woods Hole Oceanographic Institution (http:// www.whoi.edu/oceanus/ viewImage.do?id=47152&aid=20727). b) Esquema de la formación de aguas profundas tanto en el NGS donde se forman las aguas inferiores de la NADW como en el Mar del Labrador donde se forman las aguas superiores de la NADW. Imagen del proyecto RAPiD (http://www.noc.soton.ac.uk/rapid/images/ thc_nadw.jpg).

NADW (*lower NADW*, LNADW) (fig. 1.3b).

La NADW es el motor principal de la circulación termohalina global. Durante los periodos interglaciales, como en el presente, la NAC transporta aguas cálidas y salinas desde la zona tropical hasta latitudes altas, donde se enfrían, cediendo su calor a la atmósfera, y se hunden para formar la NADW. El volumen de hundimiento de aguas tanto en el Mar del Labrador como en el NGS es muy alto y genera una fuerte corriente de aguas profundas que se desplazan hacia el hemisferio sur (fig. 1.4 panel superior). En cambio, durante los periodos glaciales (fig. 1.4 panel inferior) la circulación termohalina estaba debilitada y, en consecuencia, la NAC transportaba menor cantidad de agua hacia altas latitudes. Las aguas que llegaban al Atlántico subpolar se hundían generando una corriente menos profunda, las aguas noratlánticas intermedias glaciales (*Glacial North Atlantic intermediate Water*, GNAIW) y las aguas antárticas de fondo (*Antarctic Bottom Water*, AABW) reemplazaron a la NADW en el fondo del Atlántico (e.g. Hodell and Venz-Curtis, 2006). Ambas masas de agua tienen unas características intrínsecas muy diferentes y por tanto se creó un gradiente muy fuerte entre 2000 y 2300 m de profundidad, donde se encontraba el límite entre las aguas de la GNAIW y la AABW (Oppo et al., 1995; Raymo et al., 1997; Venz et al., 1999; Venz and Hodell, 2002; Hodell et al., 2003; Kleiven et al., 2003; Raymo et al., 2004; Curry and Oppo, 2005). Este modo de circulación produjo que el fondo oceánico estuviera menos ventilado, puesto que la AABW es una masa de agua que se forma bajo la banquisa de hielo antártica y por tanto presenta menor ventilación.

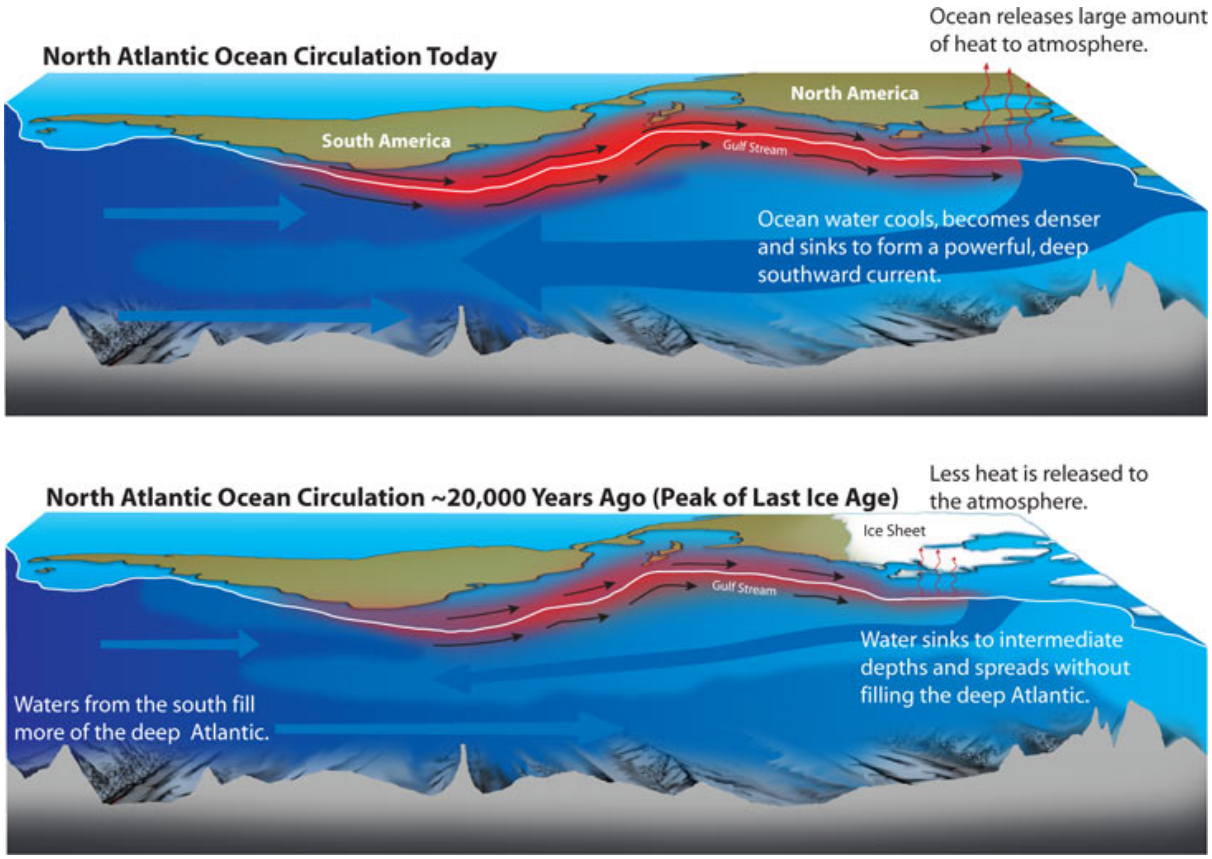


Fig. 1.4. Esquema del funcionamiento de la circulación termohalina y el transporte de calor asociado a ella para el presente (imagen superior) y el último máximo glacial (imagen inferior) hace unos 20 mil años. Ilustración de E. Paul Oberlander, Woods Hole Oceanographic Institution (http://www.whoi.edu/page.do?pid=12455&tid=441&cid =33957&ct=61&article=17906).

## 1.2. EL CLIMA EN LA TIERRA Y LOS CICLOS DE MILANKOVITCH

Milankovitch (1941) descubrió que lejos de ser un sistema caótico, la variabilidad climática terrestre estaba controlada en parte por los parámetros orbitales: excentricidad, oblicuidad y precesión.

La **precesión** puede descomponerse en dos factores: (a) la inclinación del eje de la Tierra en relación a las estrellas; y (b) la orientación de la orbita excéntrica respecto a las estrellas (ver revisiones de Weedon, 2003; Maslin and Ridgwell, 2005). Debido también a que se produce una rotación sinistrógira del eje de excentricidad de la órbita la Tierra se sitúa en el punto de mayor proximidad al sol (perihelio) durante el verano del hemisferio norte una vez cada 21000 años. Esta periodicidad es opuesta en fase en los dos hemisferios (fig. 1.5). Un ciclo completo incluye que cada hemisferio pase por varias etapas: (1) verano intermedio/invierno intermedio; (2) verano corto y muy cálido/invierno largo y frío; (3) verano intermedio/invierno intermedio; y (4) verano largo y cálido/invierno corto y muy frío. Estas cuatro fases conforman un ciclo de precesión

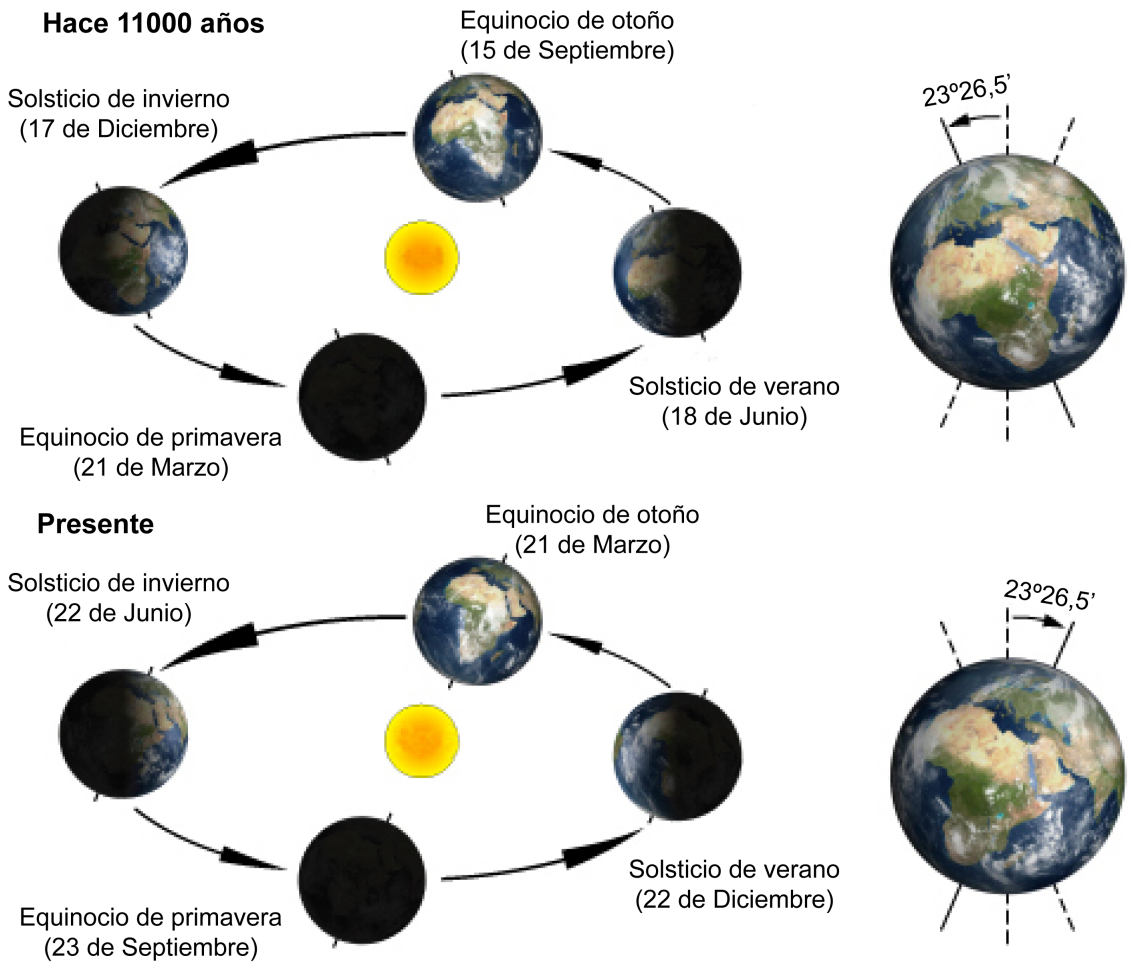


Fig. 1.5. Las variaciones en la precesión de los equinoccios hacen que las estaciones vayan rotando, de modo que la época de mayor proximidad al sol (perihelio) coincide con el verano en cada hemisferio cada 11000 años. Un ciclo completo de precesión dura aproximadamente 21 kyr. Ilustración extraída de http://hyperion57.free.fr/IMG/jpg/ Milankovitch.jpg.

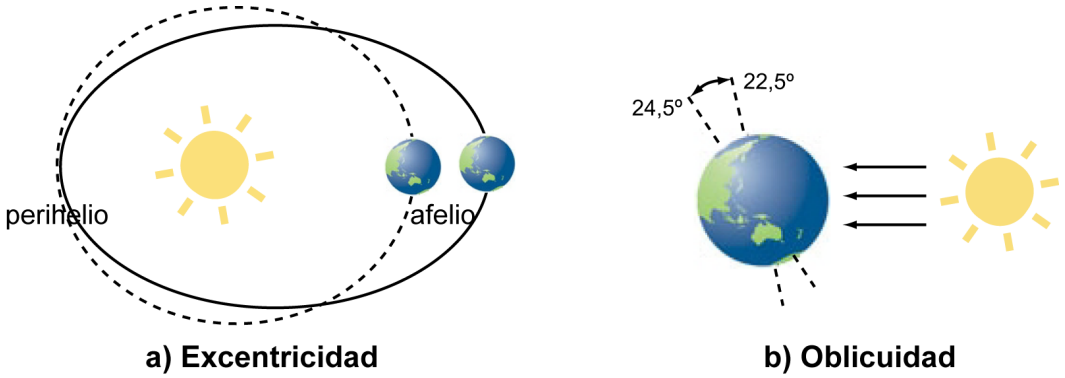


Fig. 1.6. a) Las variaciones en la excentricidad de la órbita se producen cada ~100 kyr ~400 kyr. Sus variaciones modulan la precesión. b) La oblicuidad o inclinación del eje de la Tierra varía de 24,5 a 22,5º y produce ciclos de ~41 kyr. Cuanto mayor es la oblicuidad, más perpendiculares pueden incidir los rayos solares en las latitudes altas aumentando la estacionalidad.

completo de aproximadamente 21 kyr. El efecto de la precesión es mayor en los trópicos, no obstante en altas latitudes también es el parámetro que más influye en la insolación recibida (Berger and Loutre, 1991).

El control de la excentricidad de la órbita (fig. 1.6) se hace notable a través de la modulación que produce en la amplitud de la precesión (ver Weedon, 2003; Maslin and Ridgwell, 2005). La excentricidad varía en ciclos de aproximadamente 100 kyr (generalmente entre 95 y 125 kyr) y 400 kyr. Sin embargo, los cambios en la excentricidad son tan sutiles que su efecto en la insolación anual total que recibe la Tierra es menor al 0,2 % (Berger, 1988; Imbrie et al., 1993). Por este motivo, desde hace unos años se han venido realizando muchas investigaciones sobre la ciclicidad de los últimos ciclos climáticos, que aparentemente siguen un patrón de ~100 kyr, y sobre cómo y por qué se produjo ese cambio en la ciclicidad climática, pasando de ser dominantes los ciclos de ~41 kyr a los de ~100 kyr (Imbrie et al., 1992; Imbrie et al., 1993; Raymo, 1997; Raymo and Nisancioglu, 2003; Ruddiman, 2006, entre otros; Huybers, 2007).

Debido al efecto estabilizador de la Luna, la inclinación u **oblicuidad** del eje terrestre (fig.1.6) oscila dentro de un rango relativamente estrecho (22,5-24,5º) si se compara con la de otros planetas como Marte (Laskar et al., 1993). Cuanto mayor es la oblicuidad mayor es la estacionalidad, y por lo tanto las diferencias entre la insolación recibida en verano e invierno a altas latitudes también son mayores. El efecto de la oblicuidad es mayor por lo tanto a altas latitudes. Los ciclos de oblicuidad dominantes son de ~41 kyr, aunque existe un ciclo de mayor amplitud de ~125 kyr (Shackleton et al., 1999).

## 1.3. EL PLEISTOCENO MEDIO: *MID-PLEISTOCENE TRANSITION* (MPT) Y *MID-BRUNHES EVENT* (MBE)

El inicio de las glaciaciones en el hemisferio norte tuvo lugar hace aproximadamente 2,7 Ma dentro de un contexto de progresivo enfriamiento y aumento global del volumen de hielo que comenzó hace 3,6 Ma (fig. 1.7). Este incremento gradual en el volumen de hielo se relaciona con procesos tectónicos de larga duración, como el levantamiento y erosión del Himalaya (Raymo and Ruddiman, 1992; Raymo, 1994), o el cierre del Istmo de Panamá (Keigwin, 1982; Haug and Tiedemann, 1998), pero también con procesos oceánicos como la somerización de la termoclina (Philander and Fedorov, 2003) o la estratificación en el Pacífico norte (Haug et al., 1999), y con el aumento de la amplitud de los ciclos de oblicuidad y precesión, que en última instancia modulan la insolación recibida en altas latitudes (Haug and Tiedemann, 1998; Maslin et al., 1998).

La asimetría en los ciclos climáticos aparece poco después del inicio de las glaciaciones en el hemisferio norte (Lisiecki and Raymo, 2007) y se mantiene durante todo el Pleistoceno (cuya base está en 2,58 Ma, según la última escala de tiempo geológico de la Unión Internacional de Ciencias

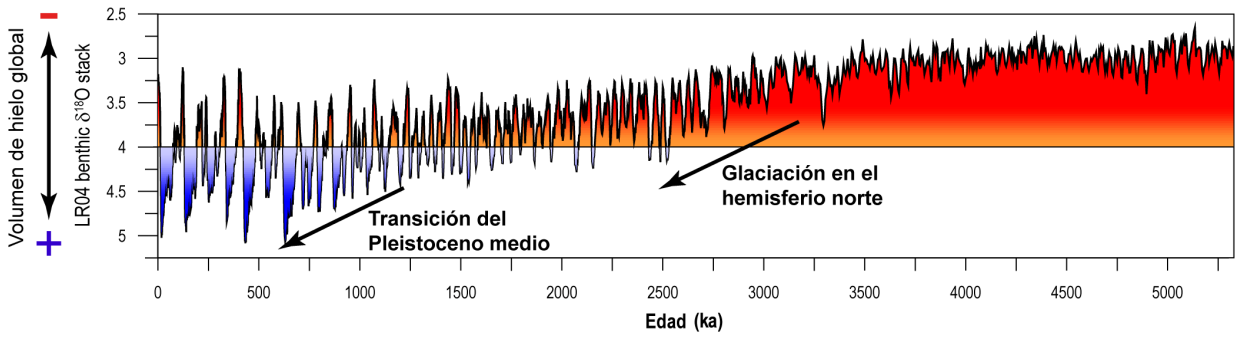


Fig. 1.7. Progresivo enfriamiento del Plio-Pleistoceno observado en la curva de isótopos de oxígeno de foraminíferos bentónicos de Lisiecki and Raymo (2005). Hemos destacado la glaciación del hemisferio norte y la transición del Pleistoceno medio están con flechas.

Geológicas, IUGS), acentuándose durante el Pleistoceno medio, cuando aumenta la duración e intensidad de los periodos glaciales (fig. 1.7). La transición del Pleistoceno medio (MPT) o revolución del Pleistoceno medio, es un periodo de reorganización climática, registrado tanto en sedimentos marinos como continentales, que tuvo lugar aproximadamente desde 1,2 Ma hasta 0,5 Ma (Head and Gibbard, 2005; Head et al., 2008). Esta reorganización afectó profundamente a la circulación tanto oceánica como atmosférica, así como a los casquetes de hielo y a la distribución y evolución de la vida en la Tierra, incluyendo a los ancestros de los seres humanos modernos. Aproximadamente hace 1,2 Ma se produjo una notable intensificación del sistema de monzones de invierno en el este de Asia (Heslop et al., 2002) y en el sur del Atlántico se intensificaron las diferencias entre la circulación de los periodos glaciales e interglaciales (Diekmann and Kuhn, 2002). Poco después, entre 1,17 y 1,11 Ma, la vegetación de Nueva Zelanda gradualmente cambió hacia flora de clima más frío (Byrami et al., 2005) y la vegetación tropical africana empezó a presentar mayores contrastes entre periodos glaciales e interglaciales en torno a 1,05 Ma (Dupont et al., 2001), con condiciones cálidas y áridas durante los interglaciales y frías y húmedas durante los glaciales entre 0,9 y 0,6 Ma. Raymo et al. (2006) sugieren que en torno a 1 Ma el progresivo enfriamiento superó un umbral que permitió que el hielo del este de la Antártida se asentara sobre la plataforma continental. En el MIS 24 (~910 ka) comienza la tendencia de incremento en el volumen de hielo global (Mudelsee and Stattegger, 1997) y además en el Atlántico norte se registra una fuerte reducción en la circulación termohalina con una clara influencia de AABW en el fondo oceánico (Ferretti et al., 2005). El MIS 22 representa el primer periodo glacial intenso del Pleistoceno durante el cual las condiciones climáticas en el norte de Eurasia fueron muy severas (Heslop et al., 2002), la reducción en la circulación termohalina también fue intensa y se produjo una caída fuerte del nivel del mar (Ferretti et al., 2005). A partir del MIS 21 un clima más frío y húmedo en Eurasia, con un paisaje más abierto favoreció la propagación de los grandes mamíferos (Palombo and Valli, 2005), incluidos los mamuts en el norte (van Kolfschoten and Markova, 2005) y los homínidos aunque no de modo definitivo (Dennell, 2003; Cuenca-Bescos et al., 2005; Petraglia, 2005). El MIS 16 es el periodo glacial en el cual los mantos de hielo del

hemisferio norte alcanzaron su máxima extensión y se produjeron las primeras grandes avenidas de icebergs del manto de Laurentia (Lisiecki and Raymo, 2005; Tzedakis et al., 2006; Hodell et al., 2008). Desde el MIS 15 al 13 se produjo una intensificación de los monzones de verano en India y Asia (Guo et al., 2000; Yin and Guo, 2008; Suganuma et al., 2009) y en el Pacífico suroeste se ha descrito que durante este intervalo hubo un aumento en el aporte de nutrientes y un periodo de baja oxigenación y ventilación en las aguas profundas del Pacífico (Hayward et al., 2005). A partir del MIS 15 los homínidos ocuparon Europa de modo continuo, aunque su máxima expansión se produjo en el MIS 11 (McNabb, 2005). Finalmente en el MIS 12 se establecen los patrones climáticos de los últimos 450 ka, con periodos glaciales e interglaciales muy extremos.

Durante el MPT los ciclos climáticos pasaron de ser predominantemente de ~41 kyr, que es la ciclicidad que se observa durante todo el Pleistoceno inferior, a ~100 kyr, que es la que se observa en los últimos 4 ciclos climáticos (Berger and Jansen, 1994). Como se muestra en la figura 1.8, análisis espectrales realizados en curvas de isótopos de oxígeno de foraminíferos bentónicos sugieren que los ciclos de ~100 kyr aumentan su importancia hace aproximadamente 650 ka, con un desfase de unos 250 ka respecto al incremento en el volumen de hielo ocurrido hace ~900 ka (Mudelsee and Schulz, 1997). La aparición de los ciclos de ~100 kyr dio lugar a ciclos climáticos aún más asimétricos y con forma aserrada, que pasaban gradualmente de un periodo interglacial a uno glacial a medida que el hielo iba acumulándose en los continentes, mientras que la deglaciación se produjo bruscamente dando paso a un periodo interglacial en pocos miles de años. Al contrario que en el inicio de las glaciaciones del hemisferio norte, durante el MPT no ocurrió ningún cambio significativo en los parámetros orbitales al cual podamos atribuir los cambios en el clima. Parece que el sistema climático terrestre pasó de ser un sistema de respuesta lineal a los parámetros orbitales a uno de respuesta fuertemente no lineal en el cual los mecanismos internos de retroalimentación pasaron a controlar los ciclos climáticos (Mudelsee and Stattegger, 1997; Maslin and Ridgwell, 2005), desarrollando largos periodos de acumulación de hielo que finalizan en un decaimiento rápido durante las terminaciones. Se han propuesto varios mecanismos internos como causas de la amplificación de los ciclos climáticos, entre ellos:

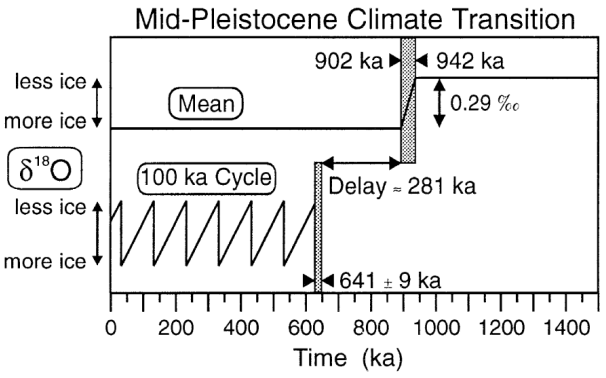


Fig. 1.8. Esquema de la transición del Pleistoceno medio, en donde se muestra el desfase entre el aumento del volumen de hielo que ocurrió hace ~900 ka y el inicio de los ciclos de ~100 kyr hace ~650 ka. Tomado de Mudelsee y Schulz (1997).

1) La tendencia de enfriamiento global a lo largo del Cenozoico pudo causar un aumento gradual en el umbral de la insolación necesaria para fundir los casquetes de hielo (Raymo, 1997; Berger et al., 1999; Huybers, 2006) lo cual les permitió perdurar entre 80 y 100 kyr. Por otro lado Tziperman y Gildor (2003)

aluden al enfriamiento asociado que se produjo en el fondo oceánico como causa del MPT a través de la formación de hielo marino y sus efectos en la temperatura atmosférica y en las tasas de acumulación y ablación de los mantos de hielo continentales.

2) El tamaño que alcanzaron los casquetes de hielo también pudo ser un factor crítico que permitió establecer una respuesta no lineal respecto a los parámetros orbitales (Imbrie et al., 1993). Este aumento de tamaño pudo estar relacionado con la erosión del regolito sobre el que se asentaron los mantos de hielo, al menos en Norte América (Clark and Pollard, 1998). Además, según Raymo et al. (2006), el asentamiento del casquete de hielo del este de la Antártida sobre la plataforma continental hace ~1 Ma pudo provocar que la ablación de verano se produjera a través de descargas de icebergs, apareciendo la señal de la precesión en el sistema climático y prolongando así los ciclos glacial-interglacial.

3) El ciclo global del carbono también pudo estar involucrado a través de la disminución en la concentración de $CO_2$ atmosférico que pudo alcanzar un umbral por debajo del cual el clima empezó a responder de forma no lineal (Mudelsee and Schulz, 1997; Mudelsee and Stattegger, 1997; Raymo et al., 1997). Ruddiman (2006) calculó que después del MPT el control climático ejercido por el $CO_2$ aumentó al 75 %, mientras que antes del MPT era de sólo un 30 %. A su vez la concentración de $CO_2$ atmosférico parece estar controlada por la dinámica oceánica del océano Antártico, por lo que en última instancia los cambios en la ventilación del océano Antártico controlarían en gran medida los cambios climáticos (Toggweiler, 1999; Sigman and Boyle, 2000; Sigman et al., 2010).

4) El levantamiento del promontorio submarino que va desde Groenlandia a Escocia hace aproximadamente 950 ka (Denton, 2000) pudo causar una migración en la zona de formación de aguas profundas del océano Ártico al NGS. Como consecuencia es posible que se produjeran cambios en la circulación oceánica, especialmente en el transporte de calor y humedad derivado de la formación de NADW (Broecker, 1991; Raymo et al., 1997) que se trasladó al NGS.

Otro evento importante registrado durante el Pleistoceno medio es el evento de mitad del cron Brunhes (*Mid-Brunhes Event*, MBE), en torno a 400-450 ka. La diferencia entre periodos glaciales e interglaciales se intensificó a partir de la Terminación V dando lugar a ciclos de 100 kyr muy marcados (Berger and Wefer, 2003; Droxler et al., 2003). Los periodos interglaciales se hicieron más intensos y la cantidad de hielo acumulado en los continentes durante los cuatro últimos periodos interglaciales (y en el presente) fue menor que en los interglaciales anteriores al MBE, como puede observarse en las curvas isotópicas de oxígeno de foraminíferos bentónicos (fig. 1.8). El $CO_2$ atmosférico también experimentó una subida respecto a los anteriores periodos interglaciales (Petit et al., 1999; Siegenthaler et al., 2005; Luthi et al., 2008). Las simulaciones del volumen de hielo en la Antártida sugieren que durante el MIS 11 hubo incluso menos hielo que actualmente (Raynaud et al., 2003). Durante el MBE se produjo una expansión en las masas de aguas cálidas del oeste del Pacífico ecuatorial que estimuló el crecimiento de arrecifes de coral

(Berger and Wefer, 2003). El MBE ha sido objeto de estudio porque a pesar de que los cambios en la insolación recibida a altas latitudes fueron relativamente pequeños durante la transición MIS 12/11, los mecanismos internos de retroalimentación produjeron una gran deglaciación que derivó en el primer interglacial extremadamente cálido. Este evento se ha asociado a modificaciones en los mecanismos de retroalimentación que regulan el clima, como la producción de NADW, el albedo, el $CO_2$ y especialmente a cambios isostáticos en las zonas donde se asientan los mantos de hielo (Berger and Wefer, 2003). Asociado al *Mid-Brunhes* se ha descrito también un intervalo en el cual se acentuó la disolución (*Mid-Brunhes dissolution interval*, MBDI) y que abarca desde ~600 a ~300 ka (Bassinot et al., 1994) y que podría estar ligado al establecimiento de los ciclos de ~100 kyr. Paradójicamente el registro de $CO_2$ de los testigos de hielo antárticos (Petit et al., 1999; Siegenthaler et al., 2005; Luthi et al., 2008) no sigue esa tendencia que muestra la disolución durante el MBDI.

A pesar de todos los esfuerzos realizados para esclarecer los motivos por los cuales se produjo este cambio en el clima terrestre, aún quedan muchas cuestiones por resolver tanto en torno al MPT como al MBE.

## 1.4. LOS FORAMINÍFEROS COMO PROXIES EN PALEOCEANOGRAFÍA Y PALEOCLIMATOLOGÍA

Los foraminíferos son microorganismos marinos unicelulares del reino Protista. Ya en el siglo XIX estos microorganismos despertaban curiosidad entre los científicos tanto por su biología y variedad en las formas de sus conchas como por su abundancia y amplia distribución en el registro geológico (Flint, 1899). Estudios a lo largo de todo el mundo demuestran que la presencia de unas especies u otras de foraminíferos está condicionada por una serie de factores ambientales como temperatura, salinidad, luminosidad, oxigenación y aportes de nutrientes. Debido al control que los factores ambientales ejercen sobre estos microorganismos, la presencia de unas u otras especies en muestras fósiles ha sido ampliamente utilizada como indicador de variaciones en las condiciones ambientales del pasado.

Además una gran parte de estos microorganismos segrega una concha carbonatada cuya composición refleja las características del agua en la que viven. La realización de análisis geoquímicos en las conchas de los foraminíferos nos permite reconstruir las propiedades fisico-quimicas del agua del océano así como de los cambios paleoclimáticos y paleoceanográficos ocurridos en el pasado. Uno de los análisis más extendidos, realizados en conchas de foraminíferos, son los análisis de isótopos estables de oxígeno y carbono. Por ejemplo, los isótopos de oxígeno realizados en foraminíferos bentónicos principalmente reflejan el volumen de hielo acumulado en los glaciares y en menor medida cambios en la temperatura y en el balance de precipitación-

evaporación (Shackleton, 1967), mientras que en los foraminíferos planctónicos la temperatura y el balance hídrico pueden llegar a tener mayor importancia que en los bentónicos. En cambio los isótopos de carbono nos ofrecen información sobre la ventilación del fondo oceánico, y en definitiva sobre la intensidad de la circulación termohalina. En esta tesis también se han realizado análisis de elementos traza en las conchas de foraminíferos planctónicos, que nos han permitido reconstruir la temperatura del agua. El estudio de los distintos elementos traza presentes en las conchas de foraminíferos está en auge, puesto que se han descubierto nuevas relaciones entre elementos traza y parámetros ambientales, como por ejemplo la relación entre el Boro y el pH del agua (Yu et al., 2007).

La escasez de foraminíferos bentónicos en el testigo estudiado ha determinado que sólo se estudiasen las asociaciones de los foraminíferos planctónicos. Los foraminíferos bentónicos se han utilizado únicamente para análisis geoquímicos. Las especies seleccionadas han sido *Cibicidoides wuellerstorfi* y *Melonis pompilioides*. *C. wuellerstofi* es una especie muy utilizada para análisis de isótopos estables porque vive sobre el fondo marino, es una especie típicamente epifaunal (Corliss, 1985), mientras que otras especies que viven de modo infaunal no registran el $\delta^{13}C$ del agua de fondo sino del agua intersticial del sedimento en el que viven (Zahn et al., 1986), por lo que no son buenos indicadores paleoceanográficos. Además, el $\delta^{13}C$ que registra *C. wuellerstofi* está en equilibrio con el del agua aunque con un desfase debido al efecto vital (McCorkle and Keigwin, 1994). En las muestras que no contenían esta especie tomamos *M. pompilioides*.

**Ecología de los foraminíferos planctónicos**

Existen dos tipos de foraminíferos planctónicos, especies espinosas y no espinosas. En la tabla 1.1 se muestra la relación de las especies que pertenecen a ambos grupos según Bé (1977). Algunas especies presentan simbiontes fotosintéticos (generalmente dinoflagelados) y otras no, y esto va a determinar en parte sus características ecológicas (Hemleben et al., 1989). La alimentación de las espinosas depende principalmente del zooplanckton (copépodos, amfípodos y tunicados), mientras que las no espinosas, a pesar de ser omnívoras, basan la mayoría de su dieta en el fitoplancton, especialmente diatomeas (Hemleben et al., 1989 y referencias citadas). Muchos de ellos siguen un ciclo de reproducción lunar o semilunar (Hemleben et al., 1989; Stangeew, 2001), siempre que las condiciones sean adecuadas para su reproducción.

En la figura 1.9 podemos ver las provincias paleobiogeográficas que se definieron en función de la distribución de las especies de foraminíferos planctónicos (Bé, 1977; Hemleben et al., 1989). Las condiciones en estas zonas no son estáticas, sino que cambian con la estación del año, y a medida que cambian las condiciones de las masas de agua las especies migran vertical y lateralmente (Tolderlund and Bé, 1971; Fraile et al., 2008). A continuación se describen las características ecológicas de las especies más abundantes en el intervalo estudiado en esta tesis doctoral. El orden de las descripciones se ha realizado en función de la provincia biogeográfica en

| Especies espinosas | Especies no espinosas |
|---|---|
| *Turborotalita quinqueloba* | *Neogloboquadrina pachyderma* sin |
| *Globigerina bulloides* | *Neogloboquadrina pachyderma* dex |
| *Globigerina rubescens* | *Neogloboquadrina dutertrei* |
| *Globigerina humilis* | *Globorotalia inflata* |
| *Globigerina falconensis* | *Pulleniatina obliquiloculata* |
| *Globigerina calida* | *Globorotalia inflata* |
| *Beella digitata* | *Globorotalia scitula* |
| *Globigerinella siphonifera* | *Globorotalia theyeri* |
| *Hastigerina digitata* | *Globorotalia crassaformis* |
| *Hastigerina pelagica* | *Globorotalia crotonensis* |
| *Globigerinoides ruber* | *Globorotalia hirsuta* |
| *Globigerinoides conglobatus* | *Globorotalia truncatulinoides* |
| *Globigerinoides sacculifer* | *Globorotalia menardi* |
| *Globigerinoides tenellus* | *Globorotalia tumida* |
| *Orbulina universa* | *Candeina nitida* |
| | *Globigerinita glutinata* |

Tabla 1.1. Especies espinosas y no espinosas según Hemleben et al. (1989).

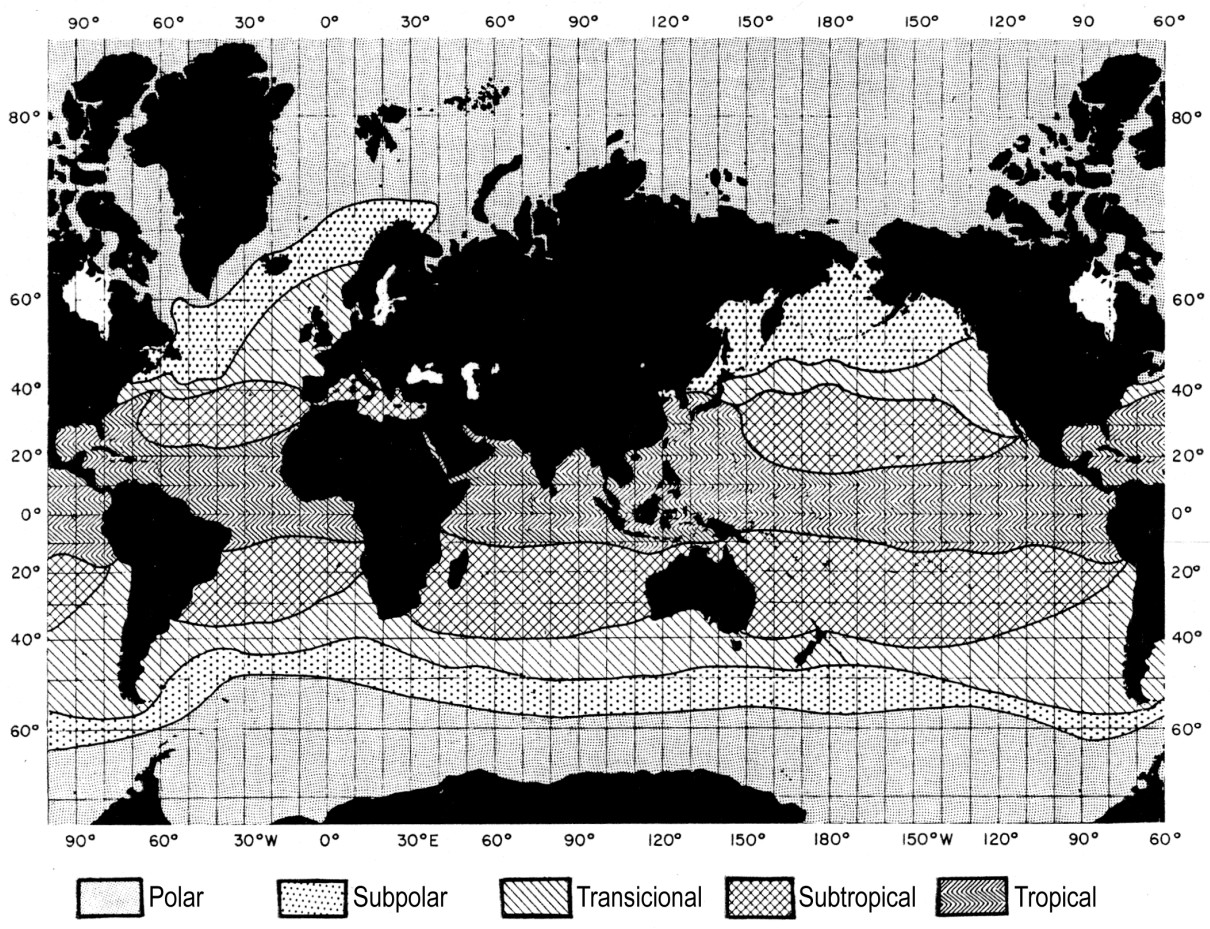


Fig. 1.9. Principales provincias paleobiogeográficas en las que se dividen las asociaciones de foraminíferos planctónicos. Tomado de Bé (1977).

la que habitan, desde la polar a la subtropical.

- *Neogloboquadrina pachyderma* sinistrorsa

Antiguamente se consideraba que la especie *N. pachyderma* (Ehrenberg) tenía dos variedades con diferente enrollamiento debido a la temperatura (Tolderlund and Bé, 1971; Bé, 1977; Hemleben et al., 1989). Estudios genéticos y morfológicos recientes han demostrado que son dos especies diferentes (Kucera and Darling, 2002; Bauch et al., 2003; Darling et al., 2004; Darling et al., 2006; Darling et al., 2007) y por eso vamos a tratarlas en apartados distintos.

*N. pachyderma* sin está considerada como la única especie plenamente adaptada al clima polar (Bé, 1977; Hemleben et al., 1989). A pesar de que admite un amplio rango de temperaturas, de -1 a 8 ºC, su máxima concentración es en torno a 2 ºC (Tolderlund and Bé, 1971). En cuanto a la salinidad, las condiciones óptimas para esta especie están en torno a 34.3 psu (Tolderlund and Bé, 1971; Spindler, 1996; Stangeew, 2001). Según Spindler (1996) los individuos de *N. pachyderma* sin son capaces de generar nuevas cámaras hasta los 50 psu, pero les cuesta mucho reproducirse y por tanto generar la calcita secundaria. También se han descrito individuos juveniles que habitan en las salmueras del hielo de la Antártida, soportando salinidades muy altas, incluso del 82 psu (Hemleben et al., 1989; Dieckmann et al., 1991; Spindler, 1996). Estos individuos son capturados en el proceso de formación de la banquisa, sobreviven gracias a la alta abundancia de diatomeas, también capturadas en el hielo, y en primavera son liberados y continúan con su ciclo vital, ya que dentro de la salmuera no pueden reproducirse. En el Ártico se cree que esto es menos frecuente debido a las diferencias en los procesos de formación del hielo (Spindler, 1990).

Respecto a la profundidad en la que vive dentro de la columna de agua, está considerada como una especie que vive en la zona fótica profunda, su máxima abundancia se encuentra por debajo del máximo profundo de clorofila, a la altura de la termoclina y picnoclina (Bé, 1977; Reynolds and Thunell, 1985; Hemleben et al., 1989; Kohfeld et al., 1996), aunque estudios más recientes con trampas de sedimento la sitúan en el propio máximo (Mortyn and Charles, 2003; King and Howard, 2005). Además se han encontrado individuos juveniles de *N. pachyderma* sin en zonas más someras de la columna de agua, pero cuando los individuos se reproducen y segregan la calcita secundaria pasan a vivir en la picnoclina (Kohfeld et al., 1996; Stangeew, 2001).

- *Turborotalita quinqueloba*

Está considerada como una especie subpolar de aguas frías, pero más cálidas que *N. pachyderma* sin, con temperaturas óptimas de entre 4.6 y 10.8 ºC y salinidades entre 34.40 y 34.95 psu (Tolderlund and Bé, 1971). Sin embargo, más recientemente, Stangeew (2001) describió que su temperatura óptima está en 12 ºC y su salinidad en 34.5 psu. Esta especie prolifera en aguas donde la capa de mezcla es profunda y por tanto hay una alta productividad fitoplanctónica (Tolderlund and Bé, 1971; Reynolds and Thunell, 1985). En el mar Nórdico, su máximo de abundancia está

ligado al gradiente térmico situado entre las aguas atlánticas y las aguas árticas (Johannessen et al., 1994).

• *Neogloboquadrina pachyderma* dextrorsa

Algunos autores, siguiendo la nomenclatura empleada por Cifelli (1973) utilizan *N. incompta* en vez de *N. pachyderma* dex, en este trabajo hemos preferido seguir la nomenclatura tradicional.

El límite de dispersión entre *N. pachyderma* dex y sin lo marca la isoterma de abril de 7.2 ºC (Ericson, 1959). Esta especie vive en aguas más cálidas y salinas que *N. pachyderma* sin, preferentemente entre 10-18 ºC y 34-35.5 psu (Tolderlund and Bé, 1971; Bé, 1977; Bé and Hutson, 1977; Hemleben et al., 1989). Habita en torno a 100 m de profundidad dentro de la columna de agua asociada a la termoclina y el máximo profundo de clorofila (Reynolds-Sautter and Thunell, 1989). Estudios recientes demuestran que en el Atlántico norte *N. pachyderma* dex presenta su máxima abundancia asociada a las aguas estratificadas y de baja productividad de verano y principios de otoño, aunque también vive en primavera en cantidades menores (Schiebel and Hemleben, 2000).

• *Globigerina bulloides*

*G. bulloides* puede vivir entre 2 y 16 ºC y entre 34.4 y 36 psu, está considerada como una especie subpolar-transicional y de zonas de upwelling (Tolderlund and Bé, 1971; Bé, 1977; Reynolds and Thunell, 1985), y aunque se le ha asociado a la zona somera-intermedia (50-100 m) de la columna de agua (Bé, 1977; Ortiz et al., 1995; Mortyn and Charles, 2003), estudios recientes demuestran que en el océano Antártico vive en aguas más superficiales (King and Howard, 2005). Esta especie está asociada a alta productividad fitoplanctónica y zonas en las que la capa de mezcla es profunda (Reynolds and Thunell, 1985; Schiebel et al., 2001), por lo tanto está considerada como una especie ligada a concentración de nutrientes más que a temperatura.

• *Globorotalia inflata*

*G. inflata* es la única especie típica de la zona de transición. Puede vivir en un amplio rango de temperaturas, aunque sus máximas abundancias se concentran entre 10.4 y 19.9 ºC, y salinidades entre 35.8 y 36.5 psu (Bé and Tolderlund, 1971). En la zona de transición esta especie presenta una distribución bimodal presentando máximas abundancias en Diciembre y Marzo, mientras que en la zona subpolar es más abundante durante el otoño (Septiembre-Noviembre). Suele habitar en profundidades por debajo del máximo profundo de clorofila (Fairbanks et al., 1980; Mortyn and Charles, 2003; King and Howard, 2005).

• Otras especies presentes generalmente en cantidades menores al 10 % son *Globigerinita glutinata,* que es una especie ubicua pero asociada a aguas ricas en nutrientes, especialmente durante la mezcla de primavera (Tolderlund and Bé, 1971; Schiebel et al., 2001) y *Globorotalia scitula* que habita en aguas profundas y frías (Bé, 1977).

• Además se han encontrado especies subtropicales en determinadas tramos, aunque en conjunto las especies subtropicales nunca superan el 5 %. Entre ellas se han encontrado *Orbulina universa*, *Globorotalia truncatulinoides*, *Globigerinoides ruber* alba, *Globigerinella siphonifera*, *Globorotalia crassaformis*, *Globorotalia hirsuta* y *Beella digitata*.

En el anexo I se pueden observar fotografías de microscopio electrónico de las especies de foraminíferos planctónicos así como de los bentónicos utilizados para los análisis isotópicos y de algunos radiolarios y ostrácodos encontrados en las muestras.

# CAPÍTULO 2.

# MATERIALES Y MÉTODOS

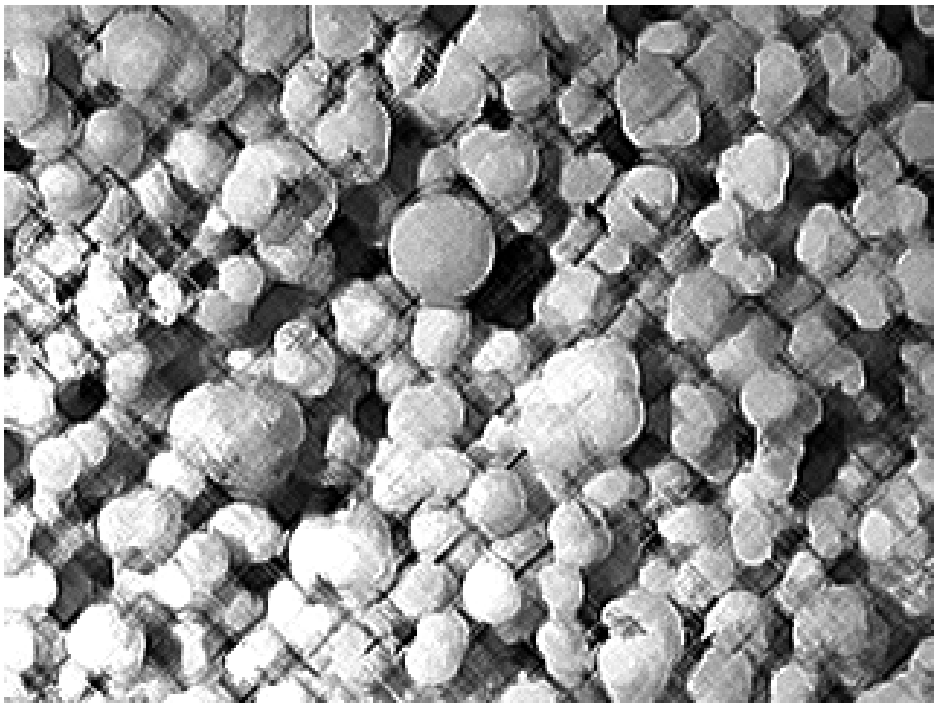

# 2. MATERIALES Y MÉTODOS

## 2.1. IODP *SITE* U1314

El sondeo estudiado en este trabajo, denominado IODP *site* 1314, fue extraído durante la expedición científica 306 del *Integrated Ocean Drilling Program* (Channell et al., 2006), realizada entre el 2 de marzo y el 25 de abril de 2005 a bordo del buque oceanográfico *JOIDES Resolution* (fig. 2.1). El *site* se encuentra situado en el Atlántico norte, al sur de Islandia, en la zona sur del Gardar Drift (fig. 2.2). Varios factores condicionaron la elección del área de perforación del sondeo. En primer lugar su situación oceanográfica, puesto que se puede monitorizar la intensidad de la corriente Noratlántica en superficie y la intensidad de la circulación termohalina en profundidad. En segundo lugar, porque debido a la alta tasa de sedimentación de la zona, es posible realizar estudios de escala milenaria. Y en tercer lugar, porque su situación geográfica permitía el registro de los eventos de avenidas de icebergs al Atlántico con la ventaja de que la tasa de sedimentación no se ve muy alterada como ocurre más al sur en el cinturón de detritos transportados por hielo o *ice-rafted debris* (*IRD belt*) donde se sedimentaron la mayoría de los fragmentos líticos que se desprendieron de los icebergs procedentes de Laurentia.

Para la extracción se utilizó un sacatestigos de pistón múltiple avanzado (*multiple advanced piston corer*, APC), con el que se perforaron 3 sondeos (A, B y C) en el mismo lugar que se solapan parcialmente en profundidad. Con el fin de obtener una secuencia sin interrupciones ni deterioros en el sedimento, los participantes de la expedición elaboraron un registro continuo compuesto, correlacionando intervalos parciales correspondientes a los tres testigos, denominado *splice*, sobre el que se ha trabajado (Channell et al., 2006).

El sedimento (fig. 2.3) básicamente está compuesto por arcillas de nanofósiles aunque también pueden encontrarse cantidades variables de diatomeas, radiolarios, foraminíferos e IRD. En la fracción arena los foraminíferos planctónicos son el componente mayoritario y generalmente

Fig. 2.1. Fotografía del buque oceanográfico *JOIDES Resolution* con el cual se realizó la campaña 306 de IODP en la que se extrajo el testigo U1314. Esta fotografía ha sido facilitada por IODP.

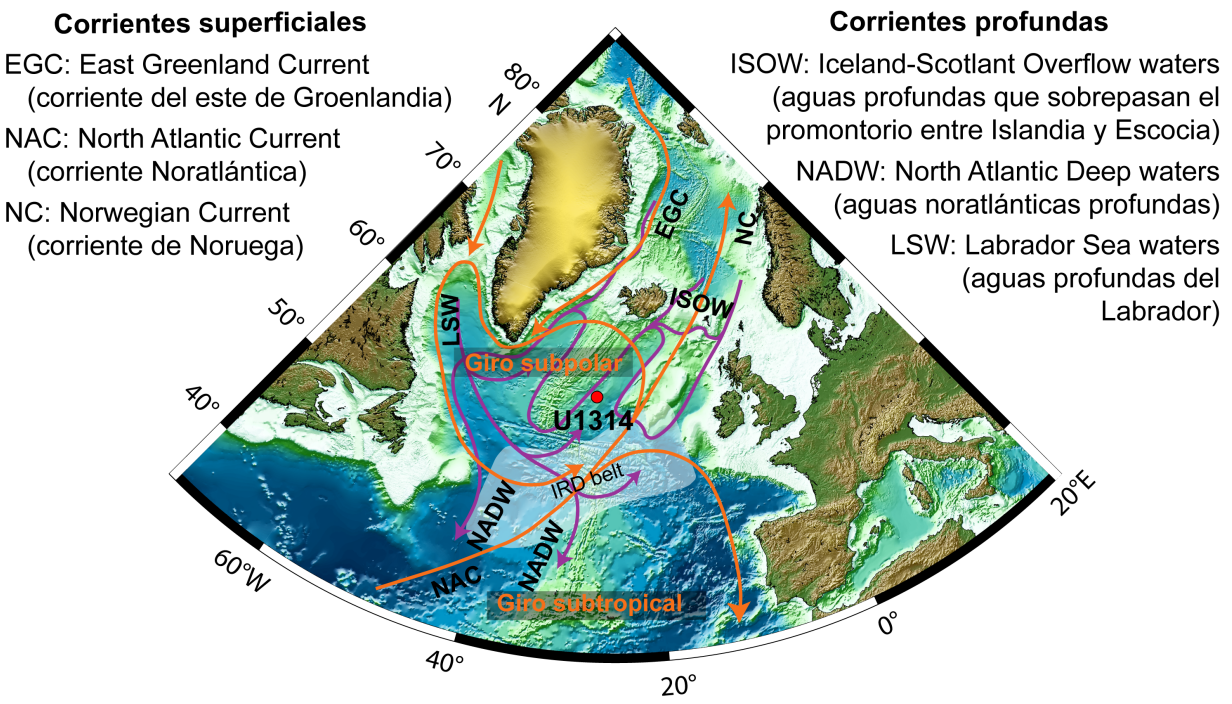


Fig. 2.2. Situación geográfica del testigo U1314 y distribución de las principales corrientes superficiales (líneas naranjas) y profundas (líneas moradas). El cinturón de mayor acumulación de IRD (*IRD belt*) está indicado con un sombreado blanco. El mapa ha sido facilitado por IODP.

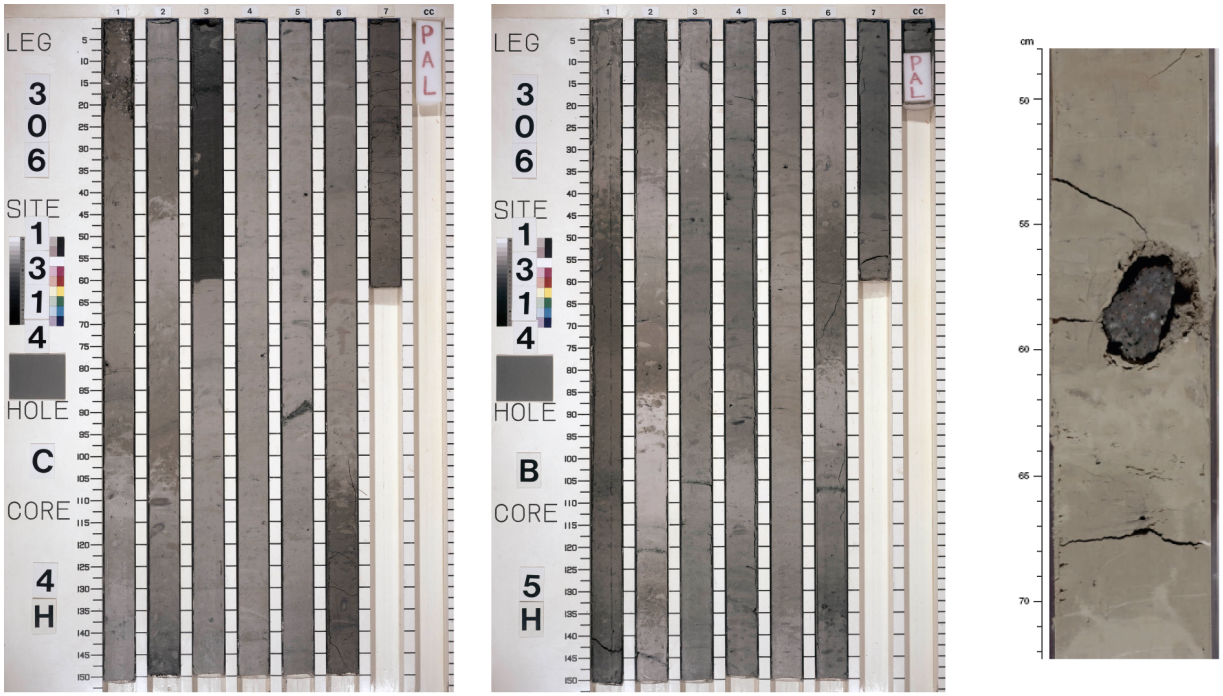


Fig. 2.3. Fotografías de los testigos después de abrirlos por la mitad. Pueden observarse cambios en el color del sedimento y en la fotografía de la derecha se muestra un IRD de gran tamaño. Estas fotografías han sido facilitadas por IODP.

están bien preservados. Además en la fracción arena podemos encontrar foraminíferos bentónicos, ostrácodos, microfósiles silíceos e IRD. El intervalo objeto de estudio comienza en el metro 32,80 del *splice* o mcd (*meters of composite depth*) y termina en el metro 59,98 mcd.

## 2.2. TOMA Y PREPARACIÓN DE MUESTRAS

La toma de muestras se realizó siguiendo el *splice*, por lo que se tomaron muestras alternando los tres testigos. Las muestras fueron tomadas cada 4 cm excepto en las profundidades donde era necesario cambiar de testigo, allí se tomaron varias muestras de los dos testigos que se superponían. Cada muestra cubre un intervalo de 2 cm en profundidad.

Para estudiar foraminíferos se toma una parte de sedimento seco y se pesa. Ese sedimento se introduce en agua para disgregarlo. Cuando las muestras se disgregan mal, como en este caso, se añade pirofosfato sódico para disgregarlas mejor. Posteriormente la muestra es tamizada bajo el grifo con un tamiz de 63 μm para eliminar las partículas finas y se deja secar. Una vez seca se vuelve a tamizar en seco, separando las fracciones de 63-150 μm y la mayor de 150 μm. El trabajo realizado en esta Tesis Doctoral se ha centrado en la fracción mayor de 150 μm.

## 2.3. RECUENTOS DE FORAMINÍFEROS PLANCTÓNICOS

Los recuentos se realizaron en muestras alternas utilizando un microscopio estereoscópico o lupa binocular (fig. 2.4). Antes de proceder con el recuento de cada muestra fue necesario realizar un cuarteo hasta obtener una alícuota que contuviera aproximadamente 400 foraminíferos planctónicos, nunca menos de 300 ya que estadísticamente la precisión del recuento disminuye y no se deben extrapolar recuentos menores de 300 individuos.

Fig. 2.4. Microscopio estereoscópico o lupa binocular con la que se realizaron los recuentos de los foraminíferos e IRD, así como el *picking* de foraminíferos.

El recuento de cada muestra incluía todas las partículas contenidas en esa alícuota, bien fueran foraminíferos planctónicos, bentónicos, ostrácodos, radiolarios, diatomeas, espículas de esponjas y de equinodermos, minerales autigénicos o fragmentos líticos. A nivel de especie sólo se han identificado los foraminíferos planctónicos y en la medida de lo posible también los bentónicos. Los ostrácodos, microfósiles silíceos y espículas sólo se han contado

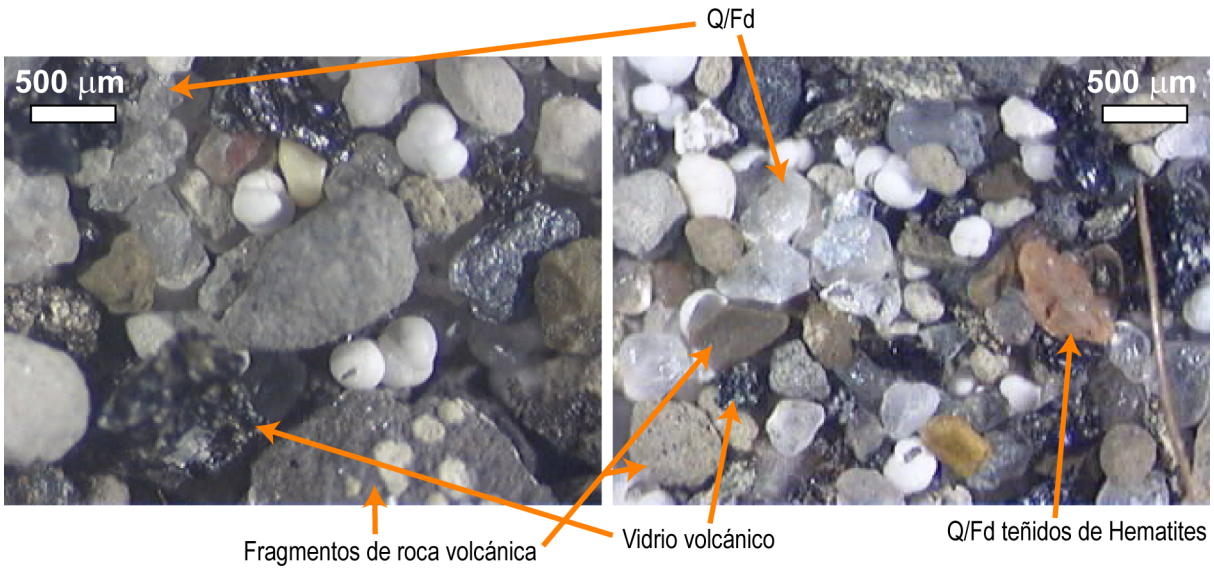


Fig. 2.5. Muestra de los principales tipos de IRD encontrados en el testigo U1314.

en su totalidad.

En cuanto a los fragmentos líticos y minerales autigénicos encontrados en las muestras, se ha diferenciado el mayor número posible de grupos separando la pirita y los sulfatos de los detritos transportados por hielo. Dentro de los IRD también se han distinguido varios grupos: cuarzo y feldespato, cuarzo y feldespato teñidos por hematites, vidrio volcánico, otros fragmentos de rocas volcánicas, micas y fragmentos de rocas plutónicas y metamórficas. Algunos de ellos se muestran en la figura 2.5.

## 2.4. ANÁLISIS FACTORIAL

En esta Tesis Doctoral se ha realizado un análisis factorial de la abundancia de las especies de foraminíferos planctónicos. El análisis factorial tiene como objetivo reducir el número de variables para hacer que la matriz de datos original sea más fácilmente interpretable. Los nuevos factores creados son una combinación de las variables originales. El análisis factorial puede orientarse tanto a la identificación de grupos de variables de comportamiento correlacionable (Modo R), como a las relaciones entre los casos (Modo Q). En este estudio se ha utilizado el Modo Q, en el cual las variables (las especies de foraminíferos) estaban en filas y los casos (las muestras) en columnas. Además también se ha seleccionado la rotación ortogonal *varimax* que rota los factores alineándolos con la dirección de máxima variabilidad, maximizando la varianza de la correlación entre las variables originales y los factores (y por tanto maximizando los *factor loadings*). La interpretación de los factores se deduce observando la relación entre los factores y las variables iniciales.

## 2.5. FUNCIONES DE TRANSFERENCIA

Las funciones de transferencia han sido ampliamente utilizadas desde los años 70 (Imbrie y Kipp, 1971) para reconstruir las condiciones del océano superficial a partir de la comparación entre muestras fósiles y muestras de una base de datos actual. Este método se ha utilizado con una gran diversidad de organismos, diatomeas, radiolarios dinoflagelados, cocolitofóridos y por supuesto con foraminíferos planctónicos. La precisión de las reconstrucciones depende en gran medida del número de muestras de la base de datos y su dispersión, de manera que cubra todos los ambientes actuales. Las bases de datos se han ido ampliando desde los años 70 (Pflaumann et al., 1996; Barrows y Juggins, 2005; Hayes et al., 2005; Kucera et al., 2005), pero aún hay zonas en las cuales tanto el número de muestras como su dispersión son bajos (Kucera et al., 2005). La eficacia de las funciones de transferencia quedó claramente demostrada con las reconstrucciones del último máximo glacial (LGM, *last glacial maximum*) realizadas por el proyecto CLIMAP (1976, 1981) y las sucesivas mejoras llevadas a cabo con los proyectos EPILOG (Mix et al., 2001), GLAMAP (Pflaumann et al., 2003; Sarnthein et al., 2003) y MARGO (Kucera et al., 2005; MARGO project members, 2009).

En esta Tesis Doctoral se han utilizado dos métodos distintos para calcular las temperaturas superficiales del océano (SST, *sea surface temperature*), el método de análogos modenos (MAT, *modern analog technique*) y redes neuronales artificiales (ANN, *artificial neural networks*). La base de datos con la que se han comparado las muestras fósiles es la base para el Atlántico norte compilada por el proyecto MARGO, que está publicada en Kucera et al. (2005) y tiene 862 muestras de sedimento superficial (fig. 2.6). En ese artículo se pusieron de manifiesto las ventajas de usar bases de datos específicas para distintas zonas, ya que las diferencias genéticas entre los foraminíferos de unas zonas y otras pueden afectar a su comportamiento ecológico. Las temperaturas asociadas a cada muestra de la base de datos representan la temperatura a 10 m de profundidad y fueron extraídas de la segunda versión del World Ocean Atlas (WOA, 1998). La base presenta temperaturas de verano (Julio-Agosto-Septiembre), invierno (Enero-Febrero-Marzo) y la media anual para cada muestra, permitiendo así hacer tres reconstrucciones, verano, invierno y media anual.

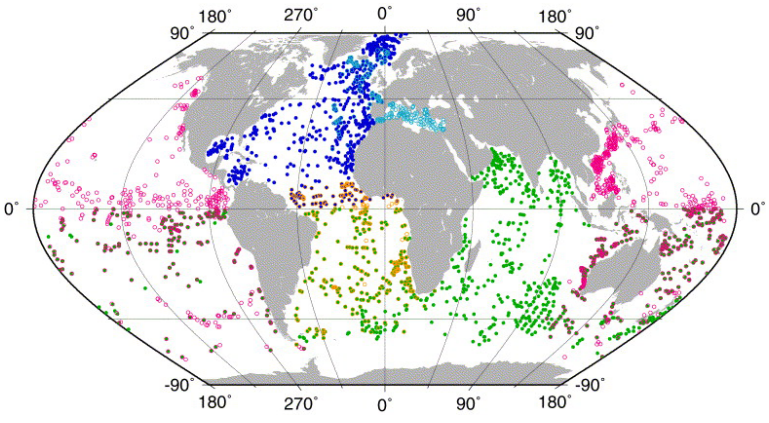


Fig. 2.6. Base de datos de foraminíferos planctónicos recopilada por el proyecto MARGO (Kucera et al., 2005). Cada punto representa el lugar donde se tomó una muestra de sedimento superficial para analizar la asociación foraminíferos planctónicos. En color azul oscuro están representadas las muestras que se utilizan en la base de datos del Atlántico Norte.

La MAT fue introducida por Hutson (1980). Este método identifica para cada muestra fósil los mejores análogos de la base de datos usando el cuadrado de la distancia (Prell, 1985). El índice de similaridad del análogo más cercano que calcula este método nos da una idea de lo parecidas que son nuestras muestras fósiles con las de la base de datos y por tanto del nivel de fiabilidad que tiene la reconstrucción. Para reconstruir las temperaturas se ha realizado una media ponderada de los 10 mejores análogos utilizando su índice de similaridad para la ponderación.

La función de transferencia basada en ANN, es una red de propagación hacia atrás (Malmgren et al., 2001) entrenada con la base de datos de MARGO para el Atlántico norte. Este método exige que las redes neuronales sean entrenadas con cada base de datos. Para el entrenamiento de una red neuronal se extrae un porcentaje de muestras y con las demás se intenta llegar al mejor cálculo de temperatura. A continuación se extrae otro porcentaje y se hace lo mismo intentando que en cada entrenamiento se mejore la precisión de los algoritmos que calculan las temperaturas. En este caso hemos usado la media de las 10 optimizaciones que se usaron en las reconstrucciones de Kucera et al. (2005). Con esas 10 optimizaciones también hemos calculado la desviación estándar, que nos indica si una muestra está bien o mal representada en la base de datos.

## 2.6. ANÁLISIS ISOTÓPICOS Y DE ELEMENTOS TRAZA

Una parte importante de esta Tesis Doctoral es el análisis de isótopos estables de oxígeno y carbono en conchas de foraminíferos planctónicos y bentónicos. En cuanto a los planctónicos se han realizado dos curvas, una a máxima resolución (tomándose individuos de todas las muestras) con la especie *Neogloboquadrina pachyderma* sinistrorsa y otra a la mitad de resolución (analizándose sólo muestras alternas) con *Neogloboquadrina pachyderma* dextrorsa. Debido a la escasez de foraminíferos bentónicos, principalmente se ha utilizado la especie *Cibicidoides wuellerstorfi*, y en su ausencia se tomaron otros *Cibicidoides* o *Melonis pompilioides*. Los *Cibicidoides* producen una señal muy similar a la de *C. wuellerstorfi*, pero los resultados de *M. pompilioides* difieren. Para poder unificar los resultados y construir una curva continua a la máxima resolución posible, en algunos tramos se realizaron análisis de las dos especies (*M. pompilioides* y *C. wuellerstorfi*). Esto nos permitió calcular la diferencia media entre los resultados de ambas especies y poder ajustar, de este modo, los valores de *M. pompilioides* a los de *C. wuellerstorfi*.

Los análisis de elementos traza nos han proporcionado datos de las relaciones Mg/Ca, Sr/Ca, Mn/Ca, Al/Ca y Cd/Ca. En cuanto a los análisis de elementos traza solamente fueron realizados en la especie *N. pachyderma* sin y en muestras alternas.

***Picking***. Para realizar estos análisis lo primero que hicimos fue seleccionar los foraminíferos cuyas conchas van a ser analizadas. Este proceso de selección se conoce como *picking*. Generalmente se elige un número concreto de foraminíferos enteros, aparentemente limpios, sin sedimento en

el interior y preferentemente de una fracción concreta. Debido a la escasez de los foraminíferos bentónicos el número de ejemplares tomados en cada muestra varía entre 1 y 8, y su tamaño generalmente entre 300 y 600 µm. Para la especie *N. pachyderma* sin se tomaron ejemplares de entre 200 y 250 µm, seleccionándose 15 para los análisis isotópicos y entre 60 y 65 para los análisis de elementos traza. Para los análisis isotópicos de la especie *N. pachyderma* dex se tomaron 12 ejemplares de entre 250 y 300 µm.

**Limpieza para análisis isotópicos**. Previamente a los análisis isotópicos es necesario eliminar impurezas que pudieran interferir en los análisis. Primero los foraminíferos se rompen suavemente entre dos portas de cristal, abriendo las cámaras y facilitando así su limpieza. Para análisis isotópicos de oxígeno y carbono sólo se ha realizado una limpieza con metanol y ultrasonidos que elimine las partículas, en su mayoría arcillosas, adheridas a las conchas.

**Limpieza para elementos traza**. Debido a la baja proporción de elementos traza en las conchas la limpieza previa a los análisis de elementos traza es mucho más compleja y debe realizarse en un laboratorio blanco para evitar contaminaciones (fig. 2.7). El protocolo de limpieza que se ha


Fig. 2.7. Fotografías del laboratorio blanco. En ellas se muestra el material utilizado durante la limpieza para los análisis de elementos traza. Arriba a la izquierda se muestra la campana de flujo laminar y la de compuestos de amoniaco

seguido en este caso es una modificación del protocolo descrito por Pena et al., (2005) que consta de 4 fases detalladamente explicadas en el anexo III. Antes de la limpieza hay que romper los foraminíferos, igual que se hace para los isótopos. La primera fase consiste en la eliminación de arcillas mediante lavados con agua ultrapura, metanol y ultrasonidos. La segunda fase es un tratamiento reductivo que en este caso se modificó a la mitad de tiempo, y que permite la eliminación de recubrimientos de óxidos de hierro y manganeso. Para este tratamiento reductivo se usa una mezcla de hidróxido de hidracina con ácido cítrico y amonio. En la tercera fase se aplica un tratamiento oxidativo con agua oxigenada e hidróxido de sodio que elimina la materia orgánica. Y finalmente se realiza una limpieza con un ácido nítrico débil para eliminar otros posibles contaminantes. Antes de ser analizadas las muestras han de disolverse en ácido nítrico ultrapuro al 1% y con rodio.

**Espectrómetros**. Los análisis isotópicos de foraminíferos planctónicos se realizaron en la Universidad de Barcelona en un espectrómetro de masas de relación isotópica Finnigan MAT 251 acoplado a un dispositivo *Carbonate Kiel* II (fig 2.8a). La calidad de los resultados se controla usando el estándar internacional NBS-19 y la precisión externa de los análisis es mejor que 0,02 ‰ para el $\delta^{13}C$ y 0,06 ‰ para el $\delta^{18}O$. Los análisis de elementos traza también se realizaron en la Universidad de Barcelona. El espectrómetro utilizado fue un espectrómetro de masas acoplado a una antorcha de plasma inducido (ICP, *induced coupled plasma*) Perkin-Elmer Elan-6000 (fig 2.8b). Los resultados obtenidos nos permiten evaluar las relaciones Mg/Ca, Sr/Ca, Mn/Ca y Al/Ca. El cadmio también se midió pero los contenidos de cadmio en las conchas eran tan bajos que prácticamente siempre estaban por debajo del límite de detección, por lo que no pueden ser utilizados. Los análisis isotópicos de foraminíferos bentónicos fueron realizados en el laboratorio de análisis de isótopos estables de la Universidad de Kiel. Se utilizó un espectrómetro

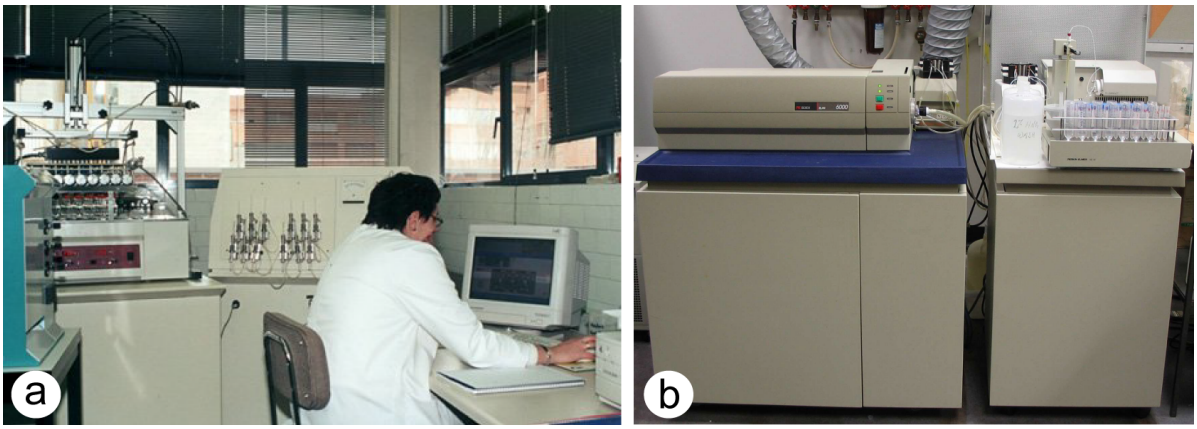


Fig. 2.8. a) Espectrómetro de masas de relación isotópica Finnigan MAT 252 de la Universidad de Barcelona utilizado para los análisis isotópicos de oxígeno y carbono en foraminíferos planctónicos. b) Espectrómetro de masas acoplado a una antorcha de plasma inducido (ICP) Perkin-Elmer Elan-6000 de la Universidad de Barcelona utilizado para los análisis de elementos traza. Ambas fotografías están tomadas de la página web de los servicios científico-técnicos de la Universidad de Barcelona (http://www.sct.ub.es/w3/wesp/hom/hom_0000.htm).

Fig. 2.9. Espectrómetro de masas Finnigan MAT 251 de la Universidad de Kiel utilizado para los análisis isotópicos de oxígeno y carbono en foraminíferos bentónicos. La fotografía se ha tomado de la página web del laboratorio Leibniz para datación radiométrica y análisis isotópicos de la Universidad de Kiel, Alemania (http://www.sct.ub.es/w3/wesp/hom/hom_0000.htm).

de masas Finnigan MAT 251 acoplado a un dispositivo *Carbonate Kiel* I (fig. 2.9) y los estándares internacionales NBS-19 y NBS-20 para controlar la calidad de los resultados. La precisión externa en este laboratorio es mejor que 0,07 ‰ para el $\delta^{18}O$ y que 0,05 ‰ para el $\delta^{13}C$. Los resultados de la precisión externa en todos los casos están referidos a la escala estándar de V-PDB (Vienna Pee Dee Belemnite) según Coplen (1996).

## 2.7. MODELO DE EDAD

El modelo de edad para el intervalo estudiado se ha elaborado comparando nuestro registro de isótopos de oxígeno realizado en foraminíferos bentónicos con la curva de temperaturas basadas en el contenido en deuterio del testigo de hielo antártico EPICA Dome C (Jouzel et al., 2007). Para realizar la correlación se ha utilizado el programa *Analyseries 2.0*. El uso de la curva de temperatura antártica como referencia para establecer el modelo de edad está basado en la hipótesis presentada por Shackleton et al. (2000), según la cual existe una alta correlación entre los registros de isótopos de oxígeno de bentónicos y la temperatura en la Antártida. Además el registro de temperatura de la Antártida presenta alta resolución lo que le convierte en una buena opción para comparar con nuestro registro que también se ha elaborado a alta resolución.

La realización y los resultados del modelo de edad se discuten más a fondo en el capítulo 3, donde también puede verse una tabla con los puntos de correlación (*tie points*) y un gráfico en el que se muestran esos puntos para cada una de las curvas.

## 2.8. TESTIGO DE HIELO ANTÁRTICO EPICA DOME CONCORDIA (EDC)

Las comparaciones con los datos del testigo de hielo antártico EDC (75º 06' S, 123º 21' E) son un punto clave en la realización de esta Tesis, no sólo por su uso en la construcción del modelo de edad. La comparación entre las temperaturas superficiales del testigo U1314 con las de EDC ha permitido una comparación interhemisférica, y las aportaciones de las comparaciones con las

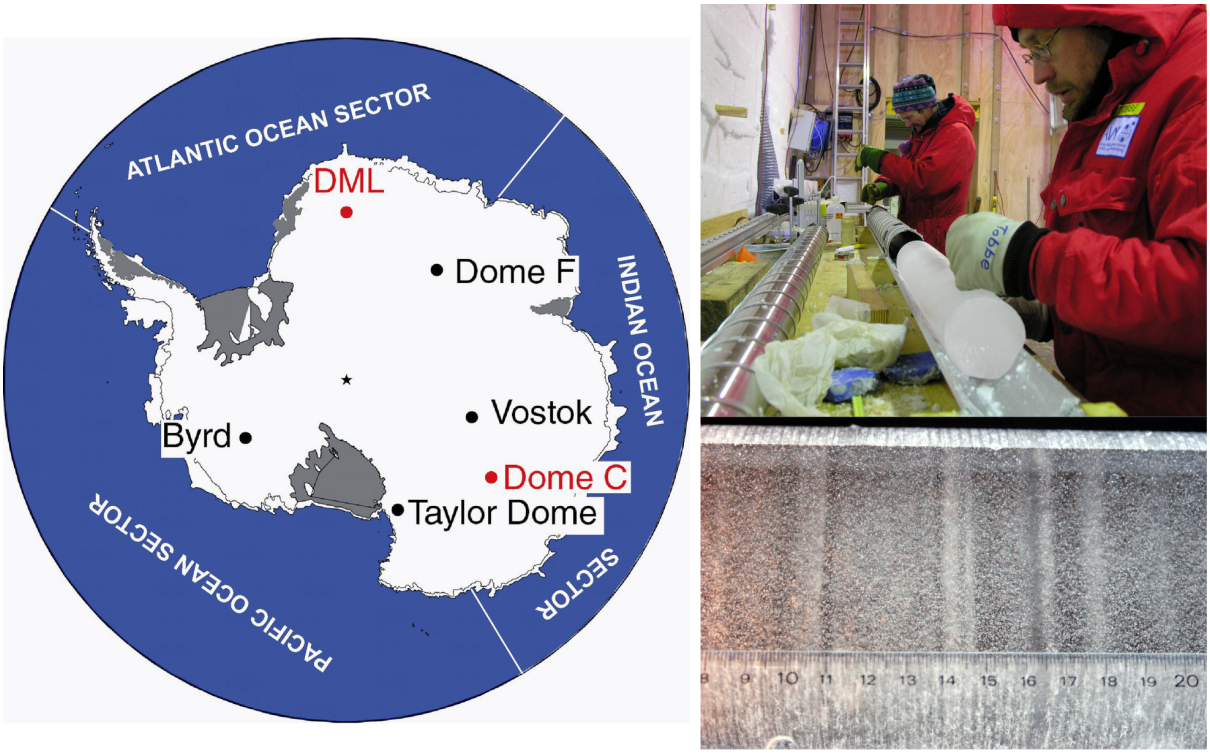


Fig. 2.10. Situación del testigo de hielo EPICA Dome C dentro del casquete antártico. A la derecha fotografías de los testigos de hielo, en la de abajo se puede apreciar un bandeado en el registro de hielo. Las imágenes se han tomado de la web del Instituto Alfred Wegener (http://www.awi.de/en/news/press_releases/detail/item/alles_im_blick/?cHash=4bef1335c7).

curvas de los gases invernadero también son de suma importancia.

Este testigo de hielo está situado en el sector índico de la Antártida (Fig. 2.10) y en la actualidad alcanza el registro de hielo más antiguo cubriendo los últimos 800 ka según el modelo de edad EDC3 de Parrenin et al. (2007). Las temperaturas antárticas fueron reconstruidas a partir de las medidas de la relación deuterio/hidrógeno en el propio hielo (Jouzel et al., 2007). Además, las vacuolas incluidas en el hielo son un archivo único que ha permitido la reconstrucción de la concentración atmosférica de gases invernadero como $CO_2$ (Siegenthaler et al., 2005; Luthi et al., 2008) y $CH_4$ (Spahni et al., 2005; Loulergue et al., 2008) a alta resolución para los últimos 800 ka.

## 2.9. ANÁLISIS DE SERIES TEMPORALES

Los análisis de series temporales son una herramienta muy importante en paleoclimatología e incluso para la predicción de fenómenos climáticos puesto que muchos de esos fenómenos se producen en ciclos de frecuencias regulares. En esta Tesis se han utilizado diversos métodos para estudiar las frecuencias dominantes y su importancia relativa.

En primer lugar se ha utilizado el método de análisis espectral Blackman-Tukey (Jenkins y Watts, 1968) que realiza una transformada de Fourier para obtener el espectro de frecuencias y con el cual se obtuvieron las frecuencias dominantes para todo el intervalo de estudio. Este análisis se ha realizado usando el programa *Analyseries 2.0* (Paillard et al., 1996).

En segundo lugar, se ha realizado un análisis espectral denominado *continuous wavelet analysis* (Daubechies, 1992), el cual nos permite evaluar cuáles eran las frecuencias dominantes en cada momento del intervalo de estudio. La ventaja de este método frente al análisis de Fourier es que la resolución temporal de la ventana de estudio es flexible y se ajusta a la escala de cada frecuencia investigada. Este tipo de análisis nos permite ver cómo las frecuencias dominantes van variando a lo largo del tiempo. Observar si existen cambios significativos en las frecuencias dominantes es importante puesto que el intervalo de estudio está dentro de la transición del Pleistoceno medio (MPT, ver capítulo 1.3). En este caso se ha llevado a cabo un análisis espectral de tipo Morlet *wavelet* utilizando una serie de scripts de *Matlab* llamados SOWAS (Maraun y Kurths, 2004). Además de realizar los análisis espectrales, el paquete de software SOWAS nos ha permitido comparar registros dos a dos realizando un espectro cruzado (*cross wavelet spectrum*). El estudio de la correlación que existe entre los análisis espectrales de ambos registros (coherencia) y el retraso o desfase entre ambos (fase) a diferentes frecuencias nos indica cuando hubo cambios en la respuesta de las frecuencias dominantes. En este tipo de análisis (tanto para el espectro normal como para el cruzado) se trabaja con series finitas y esto hace que los mayores errores de cálculo se producen al principio y al final de la serie que es donde no hay muestras para llenar toda la ventana de estudio. Para advertir del error que pudiera producirse en los extremos de la serie estudiada se usa el cono de influencia (*cone of influence*), que es la región del espectro en la cual los efectos de la ausencia de muestras en un extremo de la ventana son significativos. Cuanto menor es la frecuencia investigada mayor será la zona por debajo del cono, puesto que la ventana necesaria es mayor.

En tercer lugar, se han realizado filtros Gaussianos que destacan la importancia que presenta una frecuencia concreta en un parámetro a lo largo del intervalo temporal estudiado. Para hacer los filtros Gaussianos también se ha utilizado el programa *Analyseries 2.0* (Paillard et al., 1996). Los valores de frecuencia y ancho de banda utilizados para realizar los filtros se muestran en la tabla 2.1. La combinación de los filtros Gaussianos y la coherencia y fase del espectro cruzado de varios registros han sido muy útiles en este trabajo para evaluar cambios en las repuestas climáticas.

# CAPÍTULO 3.

## OCEAN CIRCULATION, ICE SHEET GROWTH AND INTERHEMISPHERIC COUPLING OF MILLENNIAL CLIMATE VARIABILITY DURING THE MID-PLEISTOCENE (ca. 800-400 ka)

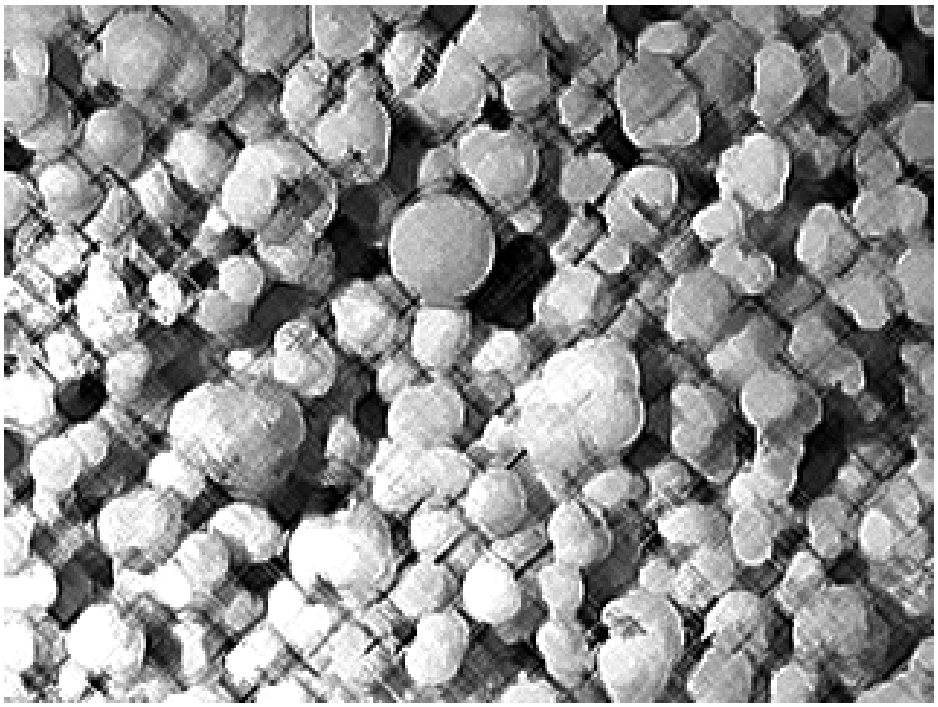

# 3. OCEAN CIRCULATION, ICE SHEET GROWTH AND INTERHEMISPHERIC COUPLING OF MILLENNIAL CLIMATE VARIABILITY DURING THE MID-PLEISTOCENE (ca. 800-400 ka)

M. Alonso-Garcia[1]*, F. J. Sierro[1], M. Kucera[2], J. A. Flores[1], I. Cacho[3] and N. Andersen[4]

1 Department of Geology (Paleontology), Faculty of Science, University of Salamanca, Pza. de la Merced s/n, 37188 Salamanca, Spain
2 Institute of Geosciences (Micropaleontology), University of Tübingen, Sigwartstrasse 10, DE-72076 Tübingen, Germany
3 Department of Stratigraphy, Paleontology and Marine Geosciences, Faculty of Geology, University of Barcelona, Martí i Franquès s/n, 08028 Barcelona, Spain
4 Leibniz Laboratory for Radiometric Dating and Stable Isotope Research, University of Kiel, Max-Eyth-Str. 11, 24118 Kiel, Germany

*Corresponding author. Department of Geology (Paleontology), Faculty of Science, University of Salamanca, Pza. de la Merced s/n, 37188 Salamanca, Spain. Tel. +34 923 294497; Fax +34 923 294514. E-mail address: montseag@usal.es (M. Alonso-Garcia).

**Abstract**

Stable carbon and oxygen isotopes from benthic and planktic foraminifers, planktic foraminifer assemblages and ice rafted debris from the intermediate-deep North Atlantic Site U1314 (Integrated Ocean Drilling Program Expedition 306) were studied, over the time interval from ca. 800 to 400 ka. This article attempts to shed light on orbital and millennial-scale climate variability in the North Atlantic and its impact on global circulation focusing on the development of glacial periods during Mid-Pleistocene.

Glacial inceptions were characterized by a sharp cooling in the North Atlantic that was transferred to the Southern Ocean through the AMOC. Two stages were recognized in the major glaciations recorded in our study. During the first stage of the glaciations ice sheets growth was continuous due to a transfer of freshwater to the continents, and the AMOC was not disturbed. Whereas during the second stage ice sheet growth was punctuated by millennial-scale ice sheet collapse events (ISCE) which returned to the ocean part of the freshwater accumulated in the continents. The structure of these ISCE is defined by an ice-rafting event followed by an abrupt warming event, which is similar to the sequence of a Heinrich event and the subsequent interstadial event described for the last glacial period. Terminations were interpreted as large ISCE that were amplified by stronger feedbacks probably related with major reorganizations of deep ocean circulation.

During the studied interval the Atlantic Meridional overturning circulation (AMOC) over glacial-interglacial cycles showed a similar behaviour to that recorded in the last 400 ka. This study highlights that ice sheet growth and Terminations present similar patterns to the last glacial-interglacial period, even though Mid-Pleistocene climate conditions were slightly different.

**Keywords**: North Atlantic, Mid-Pleistocene, stable isotopes, foraminifera, IODP Site U1314, IRD

## 1. Introduction

During the last glacial period ice sheet growth was interrupted by several ice-rafting events, known as Heinrich events (HE), which were associated to major reductions in the Atlantic Meridional overturning circulation (AMOC) and followed by prominent warming events, known as interstadial events (Chapman and Shackleton, 1999; Shackleton et al., 2000; Arz et al., 2007). Besides, it has been reported that rapid global sea level rises occurred as a result of the ice sheet collapse during the HE and/or to the meltwater generated during the interstadial event (Chapman and Shackleton, 1999; Siddall et al., 2003; Arz et al., 2007; Sierro et al., 2009). The progressive growth of the ice sheets during the last glacial period was therefore punctuated by episodes of ice sheet collapse that gave rise to temporal sea level rises.

Similar ice-rafting events associated to reductions in the AMOC have been reported in the North Atlantic during mid-late Pleistocene glacial periods (Oppo et al., 1995; Raymo et al., 1997; Venz et al., 1999; Flower et al., 2000; Hodell et al., 2003; Raymo et al., 2004). These ice-rafting events prove that ice sheet growth was not a continuous process during past glacial cycles but it was punctuated by several waning episodes. In this work we analyzed benthic and planktic stable oxygen and carbon isotopes, planktic foraminifer assemblages and ice rafted debris (IRD) fluxes over the time interval from 800 to 400 ka in order to reconstruct ice sheet growth and the impact of the major episodes of iceberg discharges in surface and deep ocean circulation.

The location of Site U1314 (Southern Gardar drift, 56º 21.8’ N, 27º 53.3’ W, 2820 m water depth, see fig. 3.1), in the subpolar gyre but in the main course of the North Atlantic current (NAC), provides an extraordinary opportunity to explore past changes in surface subpolar gyre circulation and migrations of the Arctic front. Since Site U1314 was drilled deeper than other nearby subpolar North Atlantic sites (ODP 980, 982, 983 or 984) studying benthic foraminifer stable isotopes at this site provides a unique record that allows new insight into the Mid-Pleistocene deep ocean circulation changes in the high latitude North Atlantic. The elevated sedimentation rates typical of the Gardar Drift (Channell et al., 2006) allowed us to analyse millennial-scale events from ca. 800 to 400 ka and compare them with the better-known millennial events of the late Pleistocene glacial cycles (Bond et al., 1993; McManus et al., 1994; Chapman and Shackleton, 1999; Shackleton et al., 2000; Rasmussen and Thomsen, 2004). Furthermore, the high resolution that was possible to achieve in Site U1314 allowed a comparison with EPICA Dome C (EDC) ice core records (EPICA Community Members, 2004), in order to investigate climatic coupling between both Hemispheres during this time period.

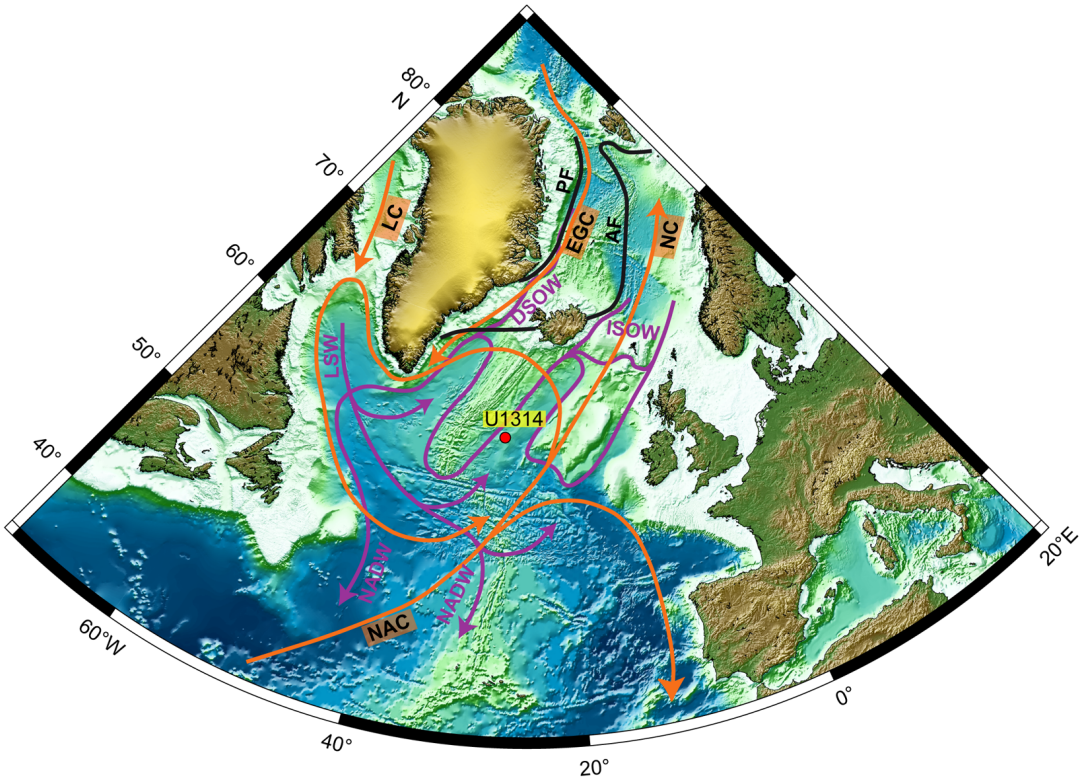


Fig. 3.1. Location of IODP Site U1314 (red dot). Orange arrows represent North Atlantic surface circulation after Schmitz and McCartney (1993). Purple arrows represent deep ocean circulation after Dickson et al. (1990). The map was provided by IODP. East Greenland Current (EGC), Norwegian Current (NC), Labrador Current (LC), North Atlantic Current (NAC), Denmark Strait Overflow water (DSOW), Iceland Scotland Overflow water (ISOW), Labrador Sea water (LSW) and North Atlantic Deep water (NADW).

## 2. Materials and methods

In order to obtain a high resolution record samples were taken every 4 cm from the composite section made from the 3 holes of Site U1314 (Channell et al., 2006). Each sample was washed under distilled water through a 63 μm mesh to eliminate clay and other fine-grained particles. Then samples were dry-sieved through a 150 μm mesh and separated into two fractions, 63-150 μm and over 150 μm. Census counts and stable oxygen and carbon isotope analyses of foraminifera were based on specimens from the coarse fraction.

Benthic stable isotope analyses were carried out at the Leibniz laboratory for radiometric dating and Isotope research, in the University of Kiel. Analyses were performed on an automated carbonate preparation Kiel device I (prototype) coupled to a Finnigan MAT 251 mass spectrometer. International standards NBS-19 and NBS-20 were used with an external precision better than 0.07 ‰ for $\delta^{18}O$ and better than 0.05 ‰ for $\delta^{13}C$. Results are reported with respect to the Vienna Pee Dee Belemnite (VPDB) standard scale (Coplen, 1996). Due to the scarcity of benthic foraminifers a composite of two genera, *Melonis* and *Cibicidoides*, was required to achieve a continuous high

resolution record of benthic stable oxygen and carbon isotopes. Where available, 1 to 8 specimens of *Cibicidoides* (mainly *C. wuellerstorfi*, but sometimes *C. pachyderma* or *Cibicidoides* spp) bigger than 300 μm (most were between 300 and 600 μm) were analysed. Where *Cibicidoides* was absent about 6 specimens of *M. pompilioides* were analysed from the same size fraction as *Cibicidoides*.

Planktic stable isotope analyses were carried out using a Finnigan MAT 252 mass spectrometer at the University of Barcelona. International standard NBS-19 was used with an external precision better than 0.06 ‰ for $\delta^{18}O$. Results are reported with respect to the VPDB standard scale as well. The continuous planktic isotopic record was based on the subpolar foraminifer *Neogloboquadrina pachyderma* dextral (dex). On average 12 specimens of *N. pachyderma* dex from the 250-300 μm fraction were picked for isotopic analyses from every other sample. The resolution of planktic isotope analyses is lower than in benthic because we chose the same resolution as for census counts, and we considered this resolution was enough for comparing with EDC records.

Prior to isotopic analyses, the picked benthic and planktic specimens of each sample were gently crushed between two glass slides under the stereomicroscope to open chambers and facilitate cleaning of adhering sediment. The crushed shell fragments were ultrasonicated for 20 seconds in methanol, which was then removed to eliminate clays and other contaminating particles. Finally the samples were air-dried overnight into the gas hood to avoid contamination.

Census counts of planktic foraminifer assemblages were done at every other sample like planktic isotopes. Each sample was split using a microsplitter as many times as necessary until the remaining aliquot contained roughly 400 planktic foraminifer specimens (300 at minimum). Reconstructions of mean annual sea surface temperature (SST) at 10 m depth were calculated from planktic foraminifer assemblages using a transfer function technique based on a back propagating artificial neural network (ANN) (Malmgren et al., 2001) trained on the North Atlantic MARGO dataset (Kucera et al., 2005). The same set of ten neural networks as in Kucera et al., (2005) was used in this study, providing 10 different mean annual temperature reconstructions. The average values of these 10 temperatures were used for the final reconstruction and the standard deviation (StDev) of the ten networks was used to determine how well a fossil sample is represented in the calibration data set (Kucera et al., 2005). Additionally, in order to calculate a similarity index and corroborate the ANN results, we applied a Modern Analog Technique (MAT, Prell, 1985) on the fossil data using the same MARGO modern dataset as was used for the training of the ANNs (Kucera et al., 2005).

## 3. Results

### 3.1. Stable isotopes from planktic and benthic foraminifers

In order to adjust *M. pompilioides* isotope data to those of *C. wuellerstofi* we calculated the difference between both species in 74 samples where both species were analysed. The mean difference is the factor we used to adjust both records, -0.11 ‰ for the oxygen and +0.59 ‰ for the carbon isotopes. Benthic $\delta^{18}O$ record (fig. 3.2 and 3.3) varies between 2.8 and 5 ‰ and show 4 major glacial cycles in the studied interval. The intervals interpreted as Terminations (fig. 3.3) exhibit sharp shifts with amplitudes from 0.7 to 1.8 ‰.

Benthic $\delta^{13}C$ record (fig. 3.3) ranges from -0.35 ‰ to 1.5 ‰. The sharpest changes in benthic $\delta^{13}C$, with amplitudes around 1 ‰, were recorded at Terminations as well, and within Marine Isotope Stage (MIS) 15 (fig. 3.3).

*N. pachyderma* dex oxygen isotopes range between 1 and 4.7 ‰. Main trends are similar to benthic $\delta^{18}O$ with Terminations presenting the largest gradients, up to 3.1 ‰, but being more abrupt than in the benthic record.

### 3.2. Chronological framework

Following Shackleton et al. (2000) we constructed an age model (fig. 3.2) for the studied section based on the assumption that changes in the benthic foraminifer oxygen isotopes were synchronous with shifts in the Antarctic EDC deuterium temperature record (Jouzel et al., 2007). It is noteworthy that our benthic $\delta^{18}O$ record and EDC deuterium temperature record are very similar even without performing the age scaling in our record (fig. 3.2). *Analyseries 2.0* software (Paillard et al., 1996) was used to identify the 37 tie points used for the correlation (see fig. 3.2 and table 3.1) and to perform the interpolation between both records.

Constraining the age of the youngest and oldest sample of our record was difficult but we found some control points. We took into account that our first sample still records full interglacial conditions, in terms of benthic $\delta^{18}O$ values and SST, within the MIS 11 (fig. 3.3 and 3.4), and thus the age of this sample must be at least prior to the beginning of the climate deterioration dated at 398-396 ka (de Abreu et al., 2005; Stein et al., 2009). Besides, our record presents a cold event in early MIS 11 (represented by a subtle increase in *N. pachyderma* sin and a decrease in SST at 33.72 cm mcd, see fig. 3.3 and 3.4) that correlates well with the cold event recorded in the high resolution record of IODP Site U1313 (Stein et al., 2009) around 412 ka. For the oldest samples the Brunhes-Matuyama paleomagnetic transition at 59.1 mcd (Channell et al., 2006) dated at ~772.5 ka (Channell and Kleiven, 2000) was helpful at establishing a tie point.

Before tuning the age model to Antarctic temperature, we constructed alternative age models

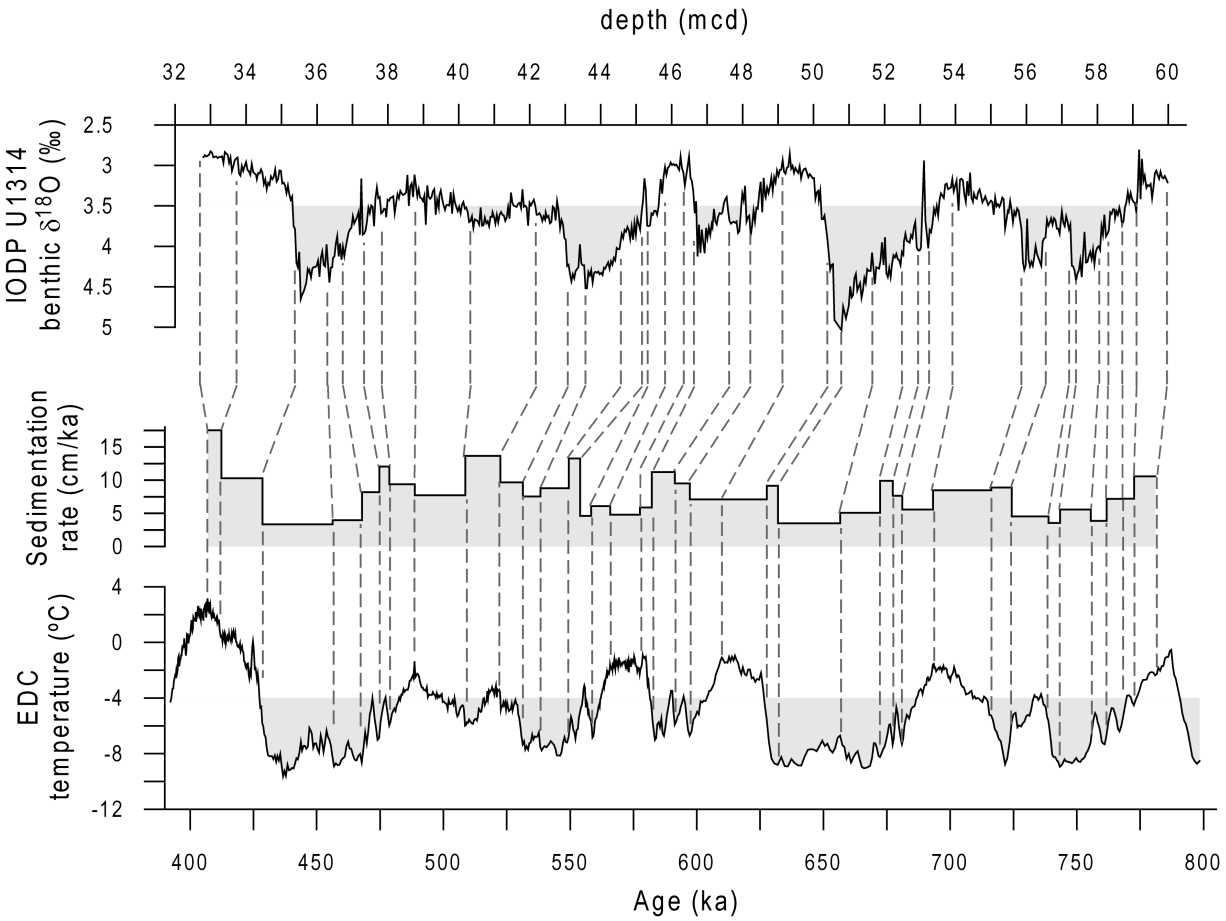


Fig. 3.2. The construction of the age model was performed correlating Antarctic temperature and Site U1314 benthic $\delta^{18}O$. Tie points of both records are joined with grey dashed lines. From top to bottom: U1314 benthic $\delta^{18}O$ in meters of composite depth (mcd); Sedimentation rate of Site U1314 after tuning; and Antarctic temperature record from EPICA Dome C (EDC) (Jouzel et al., 2007).

using the orbitally tuned global benthic oxygen isotope stack from Lisiecki and Raymo (2005, hereafter LR04) and the depth-derived age model generated by Huybers (2007) as tuning targets. We chose EDC deuterium temperature ages (Parrenin et al., 2007) as the tuning target because of its higher resolution and higher amplitude of events. This correlation allowed us to match millennial-scale events and, therefore, to achieve a correlation with higher resolution than glacial-interglacial cycles. Small discrepancies can be observed between LR04 and EDC deuterium temperature ages, especially at some Terminations (Jouzel et al., 2007), as a result of the different methods used in their respective age models (Lisiecki and Raymo, 2005; Parrenin et al., 2007). The same age discrepancies can also be observed comparing LR04 record and our benthic $\delta^{18}O$ record tuned with EDC deuterium temperature (fig. 3.3).

Sedimentation rates calculated on the basis of the preferred age model show relatively muted changes (fig. 3.2), although it is worth mentioning that during glacial periods the rates were lower than during interglacials, and within the interglacial periods the sedimentation rates were generally higher at the beginning. The mean sedimentation rate was 7.27 cm/ka, in agreement with the rate

| Site 1314 depth (m) | EDC time (ka) |
|---|---|
| 32.8 | 407.031 |
| 33.72 | 412.277 |
| 35.38 | 428.444 |
| 36.31 | 456.156 |
| 36.77 | 467.74 |
| 37.33 | 474.576 |
| 37.81 | 478.562 |
| 38.75 | 488.555 |
| 40.29 | 508.493 |
| 42.19 | 522.403 |
| 43.05 | 531.284 |
| 43.57 | 538.194 |
| 44.55 | 549.348 |
| 45.15 | 553.874 |
| 45.35 | 558.214 |
| 45.81 | 565.745 |
| 46.37 | 577.447 |
| 46.65 | 582.213 |
| 47.67 | 591.301 |
| 48.23 | 597.19 |
| 49.13 | 609.854 |
| 50.39 | 627.597 |
| 50.79 | 631.964 |
| 51.65 | 656.55 |
| 52.45 | 672.29 |
| 52.95 | 677.33 |
| 53.23 | 680.987 |
| 53.91 | 693.188 |
| 55.86 | 716.162 |
| 56.58 | 724.233 |
| 57.24 | 738.799 |
| 57.4 | 743.325 |
| 58.08 | 755.475 |
| 58.32 | 761.692 |
| 58.74 | 767.558 |
| 59.1 | 772.553 |
| 59.98 | 780.863 |

Table 3.1. Tie points used in the correlation between U1314 benthic $\delta^{18}O$ and EDC Antarctic temperature. Between tie points ages were calculated by linear interpolation.

determined during Expedition 306 for the first 115 mcd (Channell et al., 2006). According to the preferred age model, the resolution between samples is on average 550 years for the full resolution records and 1100 years for the every other sample records.

### 3.3. *N. pachyderma* sin record and SST reconstruction

At present *N. pachyderma* sin inhabits Polar and Arctic waters with optimum temperature around 2 ºC (Tolderlund and Bé, 1971; Bé, 1977; Johannessen et al., 1994). In the studied section this species shows sharp changes in relative abundance between glacial and interglacial periods which correlate with sharp changes of the reconstructed mean annual SST (fig. 3.4, 3.5, 3.6 and 3.7). During glacial intervals the abundance of *N. pachyderma* sin ranged between 65 and ≥ 90 %, and SST ranged between 5 ºC and ≤ 1 ºC, whereas during interglacial periods the abundance of this species was generally below 20 %, even reaching values as low as 1 %, and the reconstructed temperatures varied from 10 to 15 ºC. We observed that the abundance of this species controlled the reconstructed SST for most of the record. Only during intervals where its abundance was low (less than 15 %) were SST reconstructions controlled by the abundances of other species (e.g., *Globorotalia inflata* and *Globigerina bulloides*).

StDev of the calculated SST was low throughout the record (generally below 0.5°C) and is poorly correlated with temperature ($R^2$ = 0.1325, see fig. 3.8). This suggests that the assemblages of planktic foraminifera in the analysed fossil samples are well represented in the modern dataset and that the SST reconstructions are not affected by no-analog artefacts (Kucera et al., 2005). This conclusion is supported by high values of the similarity index of MAT, above 0.9 for most of the samples (fig. 3.8).

### 3.4. IRD record

Despite its location outside the main IRD belt (Bond and Lotti, 1995), IRD fluxes in the studied section reached values up to 24000 grains/cm$^2$ka and the average size of IRD was up to 0.5 cm. Ice-rafting events in the studied record (fig. 3.3) were more frequent during glacial stages and the higher fluxes were usually associated with Terminations. The most abundant

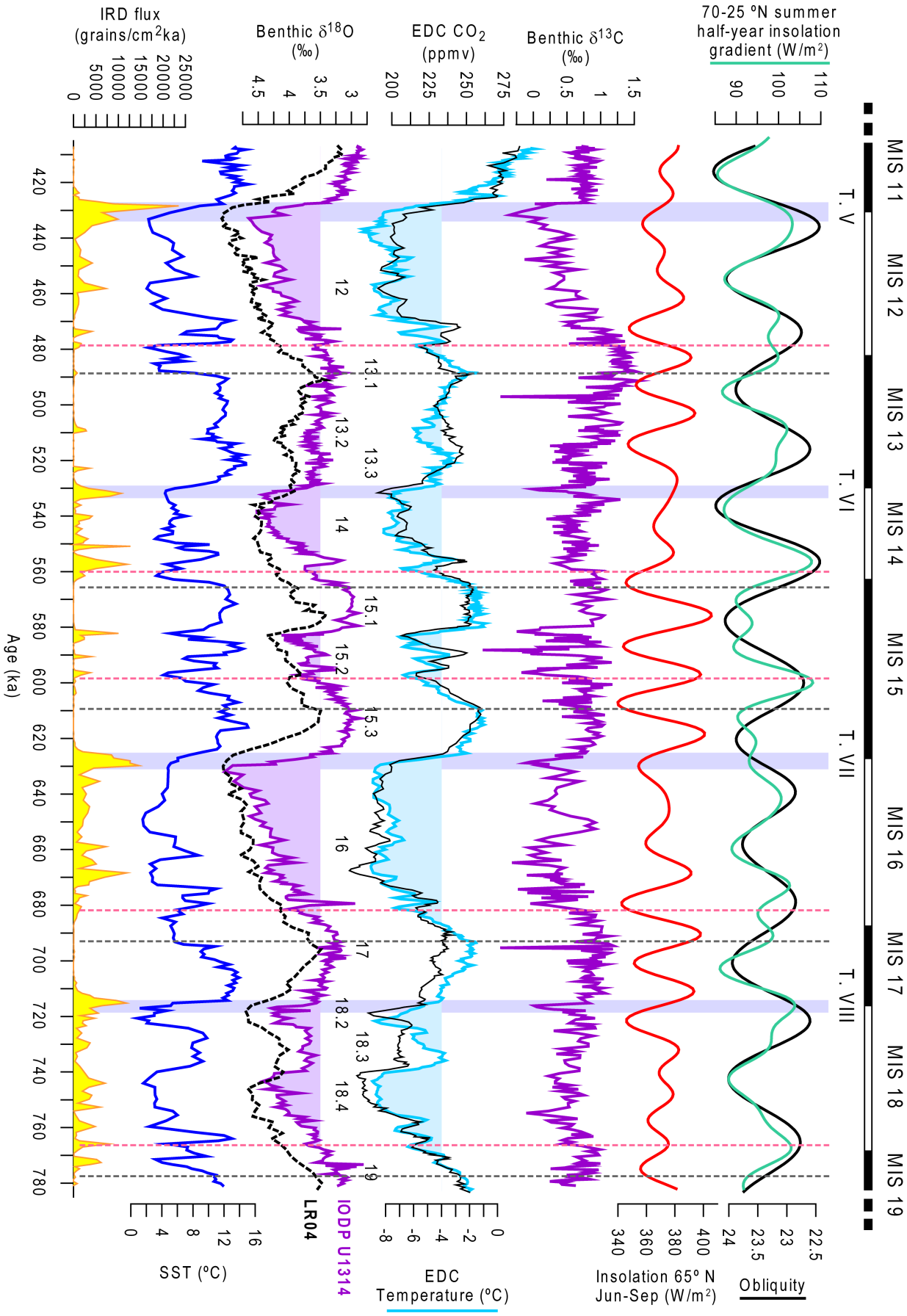
IRD flux
(grains/cm2ka)
Benthic δ18O
(‰)
EDC CO2
(ppmv)
Benthic δ13C
(‰)
70-25 ºN summer
half-year insolation
gradient (W/m2)
MIS 11
MIS 12
MIS 13
MIS 14
MIS 15
MIS 16
MIS 17
MIS 18
MIS 19
T. V
T. VI
T. VII
T. VIII
12
13.1
13.2
13.3
14
15.1
15.2
15.3
16
17
18.2
18.3
18.4
19
Age (ka)
SST (ºC)
LR04
IODP U1314
EDC
Temperature (ºC)
Insolation 65º N
Jun-Sep (W/m2)
Obliquity

Fig. 3.3. IODP U1314 records from ca. 800 to 400 ka compared with EPICA Dome C (EDC) and insolation records (Laskar et al., 2004). From top to bottom: insolation gradient of summer half-year (March-September) between 25º N and 70º N (green line) and obliquity; mean summer (June-September) insolation at 65º N (red line)(Laskar et al., 2004); Site U1314 benthic $\delta^{13}C$; EDC temperature (blue line) and $CO_2$ (black line) records, DT is filled up to -4ºC, the glacial threshold; Site U1314 benthic $\delta^{18}O$ (purple line) and benthic $\delta^{18}O$ LR04 stack (black dashed line) (Lisiecki and Raymo, 2005), U1314 record is filled up to 3.5 ‰, the glacial threshold; sea surface temperature (SST) based on planktic foraminifer assemblages from Site U1314; IRD fluxes from Site U1314. Marine Isotope Stages (MIS) are shown at the top (glacials in white and interglacials in black) and substages are indicated with numbers above benthic $\delta^{18}O$. Terminations are depicted with violet vertical bars and roman numbers from V to VIII. Vertical grey dashed lines depict glacial inceptions (benthic $\delta^{18}O$ inflections) and vertical red dashed lines depict when the thermohaline circulation become disturbed.

lithic fragments were quartz and feldspar (including hematite stained grains) and volcanic rock fragments (including volcanic glass).

## 4. Discussion

### 4.1. Glacial-interglacial climate changes

Four climate cycles, with an average duration of ~100 kyr, were recognised in the studied section, including MIS 13-12 (fig. 3.4), MIS 15-14 (fig. 3.5), MIS 17-16 (fig. 3.6) and MIS 19-18 (fig. 3.7). The benthic $\delta^{18}O$ record indicates that between 800 and 400 ka the largest northern Hemisphere ice sheets were developed during MIS 12 and 16, which were the coldest and longest glacial periods lasting ~51 and ~57 kyr, respectively, whereas MIS 14 and 18 were milder. This pattern is also shown in EDC ice core records (Siegenthaler et al., 2005; Jouzel et al., 2007; Loulergue et al., 2008; Luthi et al., 2008) and the global isotope stack LR04 (Lisiecki and Raymo, 2005). On the other hand, the most prominent interglacial periods were recorded during MIS 15.1 and MIS 15.3 but the benthic $\delta^{18}O$ values of these interglacial periods were still lower than the values of interglacial periods after MIS 12.

The flux of IRD to the Gardar drift was almost absent during most interglacial periods, but it rapidly increased during the glacial intervals when northern Hemisphere ice sheets reached certain size. Consistent with data from ODP Site 980 (McManus et al., 1999), major IRD events at Site U1314 in the studied interval occurred always when a 3.5 ‰ threshold in the benthic $\delta^{18}O$ was surpassed. This indicates that large instabilities of the ice sheets took place only when their volume was large enough. The lack of dolomite and limestone, which is very abundant in the main IRD belt (Heinrich, 1988; Bond et al., 1992), suggest that North America was not the main source of icebergs for the studied Site. By contrast, the abundance of quartz, feldspar and volcanic glass in the IRD and the regional Atlantic surface circulation strongly argue in favour of Greenland and

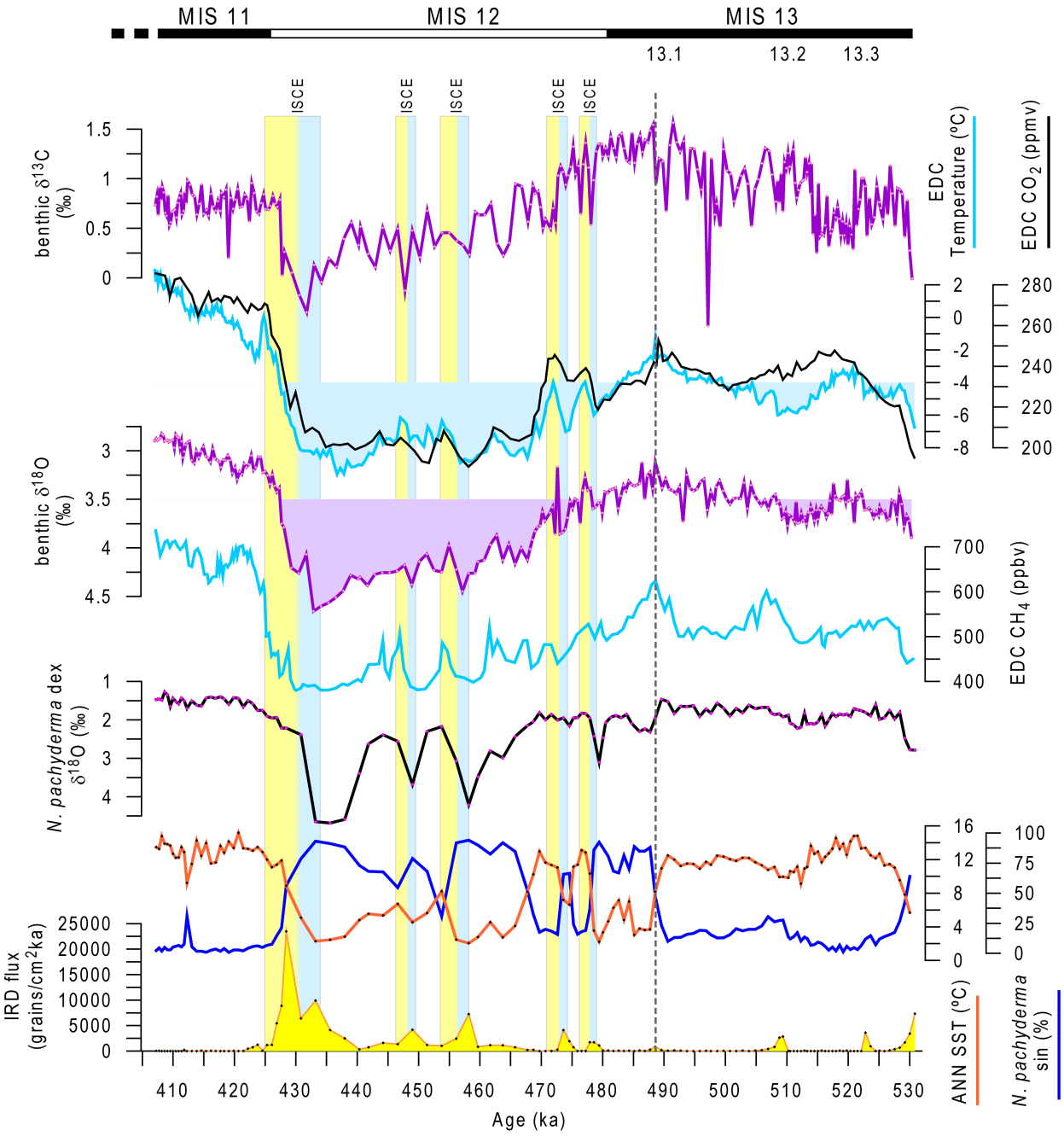


Fig. 3.4, 3.5, 3.6 and 3.7. Detailed records of each glacial cycle MIS 11-13 (fig. 3.4), MIS 14-15 (fig. 3.5), MIS 16-17 (fig. 3.6), MIS 18-19 (fig. 3.7). From top to bottom: Site U1314 benthic $\delta^{13}C$ record; EDC $CO_2$ record (black) and EDC temperature record (blue); Site U1314 benthic $\delta^{18}O$ record; EDC $CH_4$ record; *N. pachyderma* dex $\delta^{18}O$ record of Site U1314; sea surface temperature (SST) based on planktic foraminifer assemblages obtained with ANN (orange) and *N. pachyderma* sin abundance (dark blue) of Site U1314; IRD fluxes from Site U1314. Marine Isotope Stages (MIS) and substages are shown for reference. Vertical bars indicate ice sheet collapse events (ISCE), including the ones linked to deglaciations. The cooling phase of the ISCE in the Northern Hemisphere is in blue and the warming phase in yellow. Vertical grey dashed lines indicate glacial inceptions.

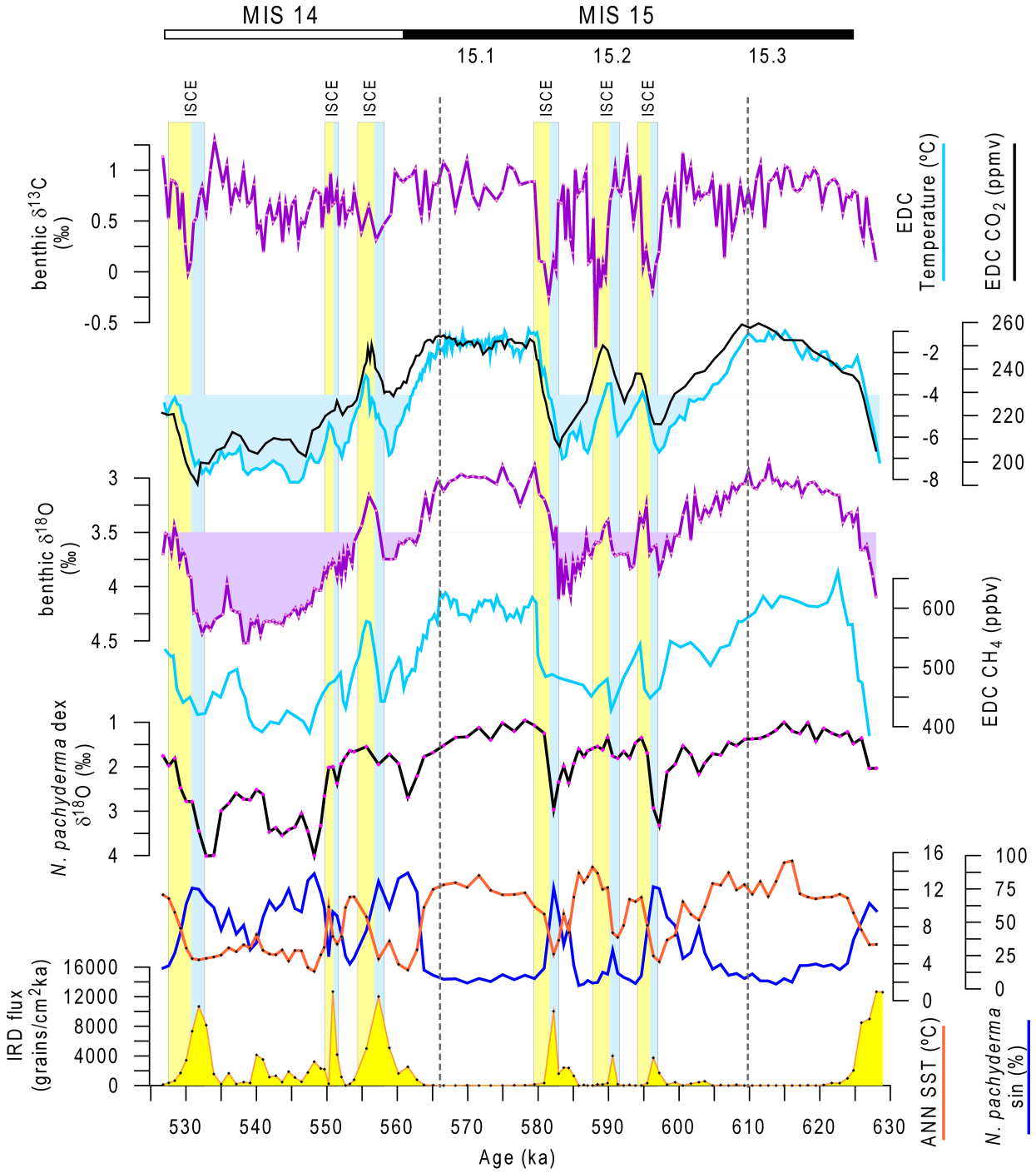


Fig. 3.5.

Iceland as the main source of the icebergs that reached Site U1314, although we cannot totally discard a Scandinavian or Svalbard origin (Moros et al., 2004).

Mean annual SST during interglacial periods at Site U1314 was relatively stable, around 12 ºC. This temperature was slightly warmer than today's SST at the studied site, about 10 ºC according to the World Ocean Atlas data (Locarnini et al., 2006). During glacial periods temperatures were on average much lower, between 5 and 1 ºC, but short abrupt temperature changes occurred.

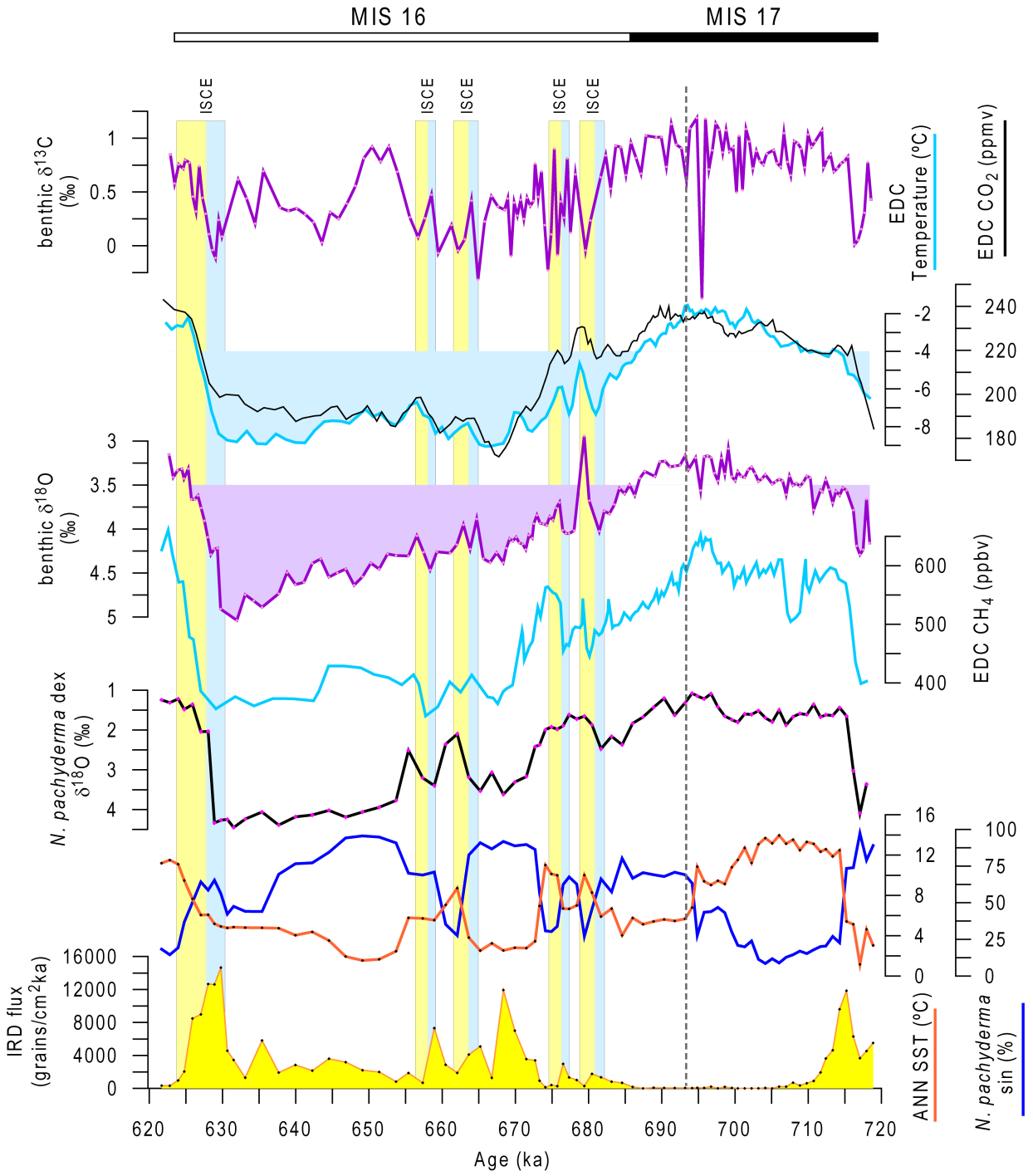


Fig. 3.6.

These abrupt changes were particularly important at the early glacial times when the ice sheets were still relatively small, with temperature changes of about 6 to 10 ºC occurring in less than 9 kyr. Linked to the abrupt temperature changes we found rapid migrations of the Arctic front, revealed by the sharp changes in the abundance of the polar species *N. pachyderma* sin. In the Norwegian Greenland Seas (NGS), this species has been related to the cold and low salinity waters of the Polar and Arctic waters (Johannessen et al., 1994; Simstich et al., 2003) and, hence, to perennial and seasonal sea ice during glacial periods (Fronval et al., 1998; Wright and Flower,

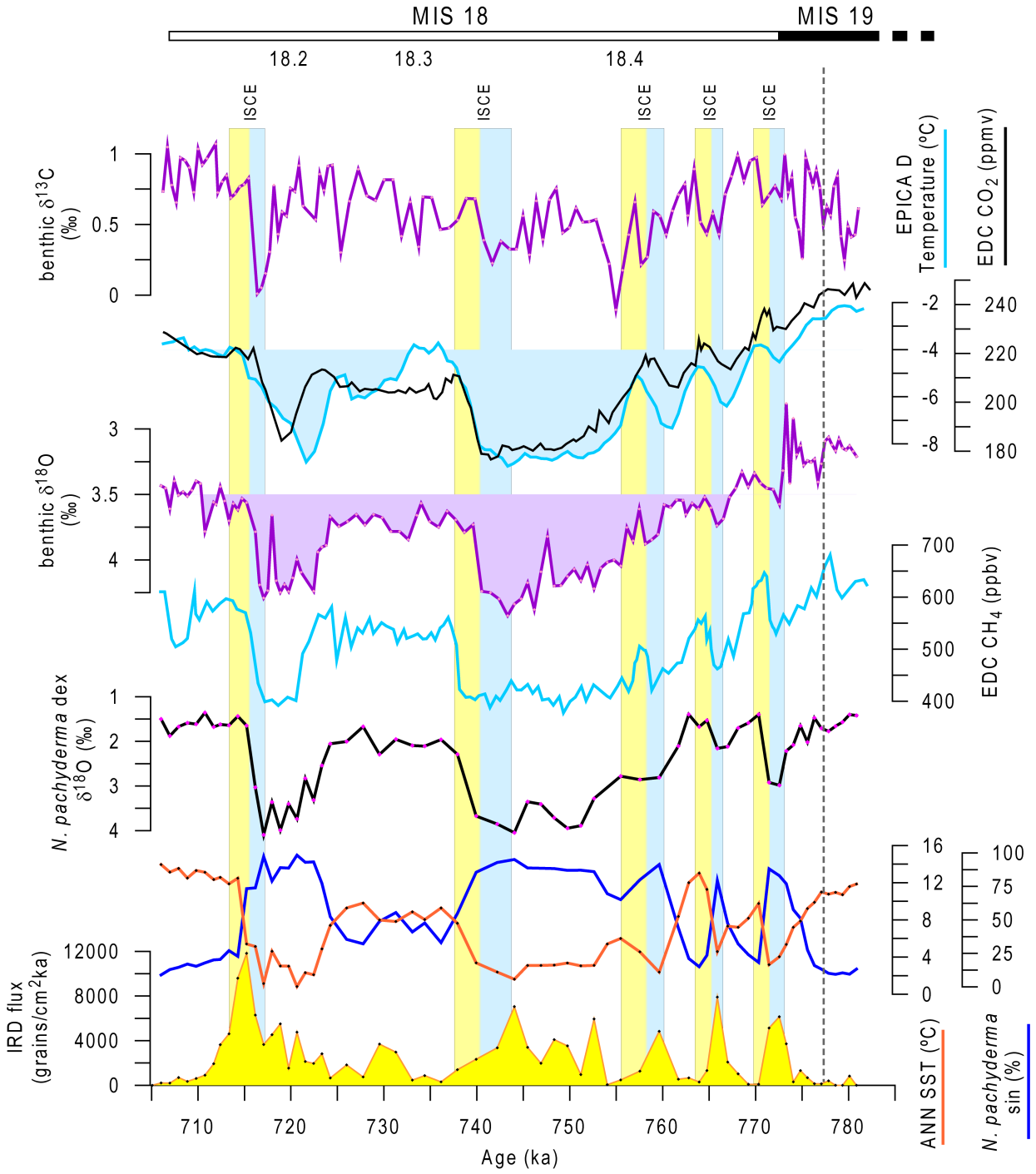


Fig. 3.7.

2002). The periods of minimum SST in Site U1314 and maximum abundance of *N. pachyderma* sin (above 70-80 %) indicate sea ice formation (Johannessen et al., 1994) in the North Atlantic at Site U1314 latitude and northwards. However, the high fluxes of planktic foraminifers during *N. pachyderma* sin maximum abundances suggest the sea-ice cover was only seasonal at the latitude of the studied site (Alonso-Garcia et al., submitted, see chapter 4).

Heavy benthic carbon isotopes at Site U1314 during interglacial periods (fig. 3.3) were

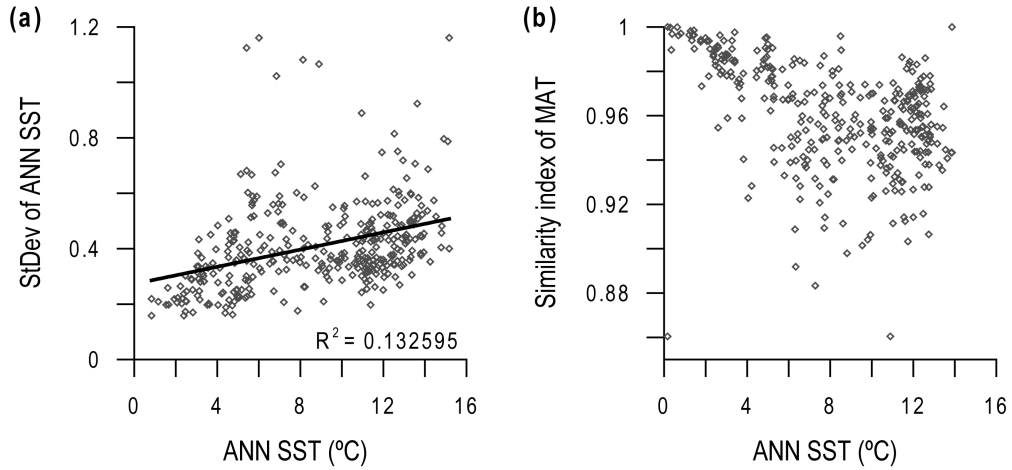


Fig. 3.8. Cross-correlation between the artificial neural networks (ANN) sea surface temperature (SST) and their Standard Deviation (a) and between the ANN SST and the similarity index of modern analog technique (MAT) (b). The low correlation coefficient ($R^2$) and the high similarity index indicate that the studied samples are well represented in the modern dataset and the temperatures calculated are not biased by no-analog situations.

interpreted as advection of nutrient-poor North Atlantic Deep water (NADW) generated by intense open sea convection in the NGS and the Labrador Sea (Broecker, 1991; Schmitz, 1995). This is consistent with the high SST and ice free conditions described above for the latitude of Site U1314 and other northernmost sites (646, 919, 980, 983 and 984) during MIS 11, 13, 15, 17 and 19 (Koç and Flower, 1998; Koç et al., 1999; Wright and Flower, 2002; St. John et al., 2004; de Vernal and Hillaire-Marcel, 2008). However, the low benthic $\delta^{13}C$ values recorded during glacial periods of the studied interval, especially in MIS 12 and MIS 16, indicated that the glacial AMOC was disturbed. A clear relationship was observed between the intervals with high flux of IRD and lower benthic $\delta^{13}C$, suggesting that ice sheet instabilities and the subsequent freshwater delivery to the North Atlantic severely affected deep water formation in the North Atlantic. During late Pleistocene glacial periods a sharp chemocline was developed in the Atlantic Ocean at ~2500 m (Ninnemann and Charles, 2002; Marchitto and Broecker, 2006) that separated the well ventilated and nutrient depleted waters (high $\delta^{13}C$) of Glacial North Atlantic intermediate water (GNAIW) from the poorly ventilated nutrient enriched waters (low $\delta^{13}C$) of AABW or brine rejection NGS deep water overflow at the Northern North Atlantic (Raymo et al., 2004; Yu et al., 2008). The low benthic $\delta^{13}C$ values recorded during the glacial periods of the studied section reflect that during the glacial periods from 800 to 400 ka Site U1314 was below this chemocline and benthic foraminifers inhabited either in AABW waters or brine rejection NGS overflow waters.

### 4.2. Coupling between North Atlantic and Antarctic temperatures

The SST record calculated at Site U1314 follows the glacial interglacial cycles recorded by the benthic $\delta^{18}O$ record and the Antarctic temperature but during the early glacial periods displayed changes of much higher amplitude (fig. 3.3). *N. pachyderma* dex $\delta^{18}O$ record mirrors

the SST changes, suggesting that a large fraction of the $\delta^{18}O$ change in surface waters is driven by temperature. Since modern *N. pachyderma* dex lives preferably during summer-fall when the waters are more stratified in the North Atlantic (Schiebel and Hemleben, 2000; Chapman, 2010) and within the first 100 m, associated with the thermocline and deep chlorophyll maximum (Fairbanks et al., 1982; Reynolds-Sautter and Thunell, 1989), their isotopic results may not reflect what happened near surface but at ~100 m. The influence of freshwater delivery to the ocean at times of ice sheet collapse could affect oxygen isotopes of surface dwellers (Flower et al., 2004) but if the waters were stratified *N. pachyderma* dex oxygen isotopes might not be affected. Conversely if the waters are well mixed the meltwater effect might result in short-term discrepancies with the SST record, for instance at ~474, ~591 or ~677 ka (fig. 3.4, 3.5 and 3.6).

The comparison of U1314 SST record in the North Atlantic with Antarctic temperature shows that most of the changes in SST in the North Atlantic have their counterpart events in the Southern Hemisphere. This similar temperature behaviour strongly argues in favour of a narrow coupling

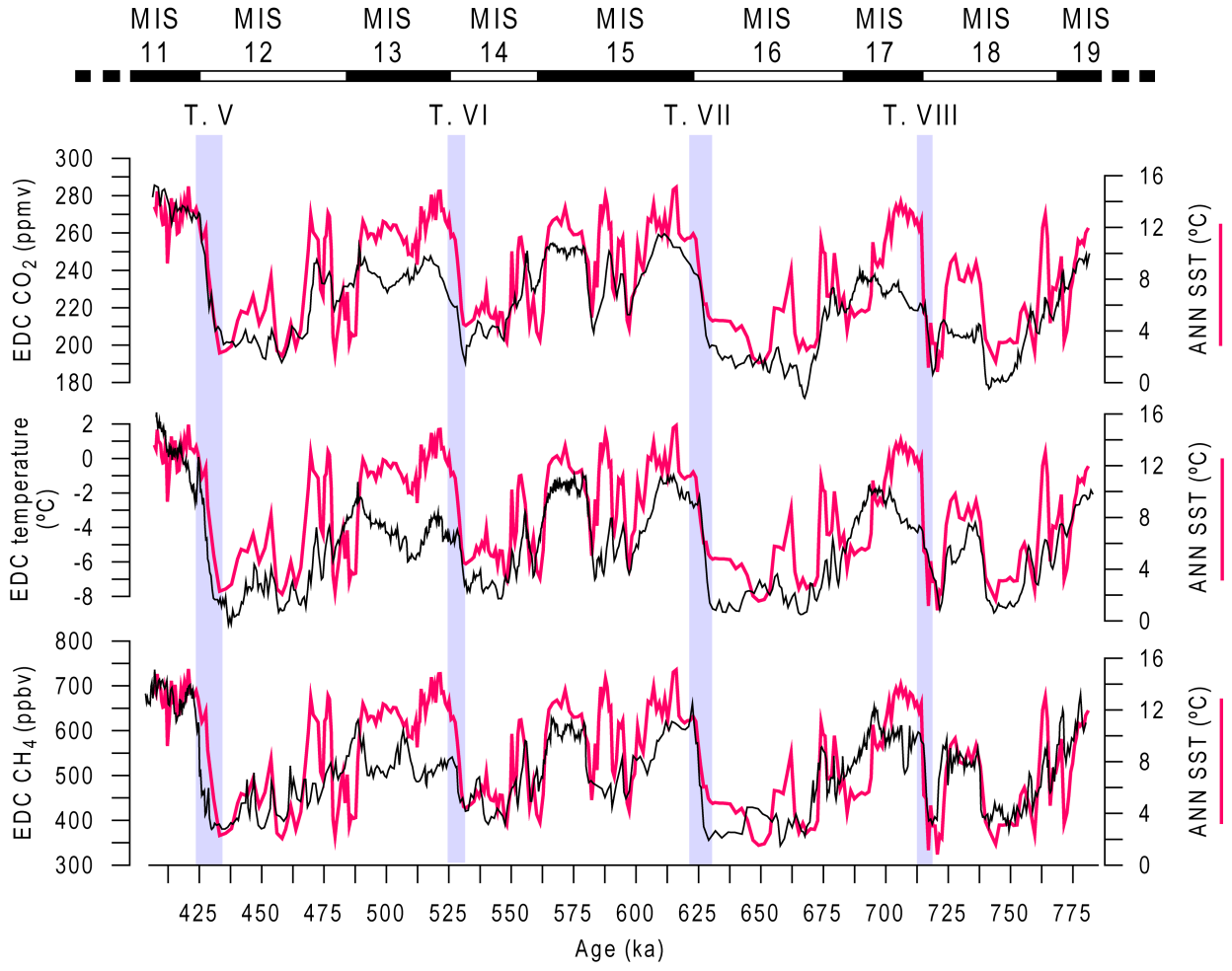


Fig. 3.9. Sea surface temperature (SST) based on planktic foraminifer assemblages and calculated with artificial neural networks (ANN) compared with EDC $CO_2$ record, EDC temperature, and EDC $CH_4$. Marine Isotope Stages (MIS) and Terminations (violet bars) are shown for reference.

between both hemispheres during the studied interval. The tuning methods used to synchronize with EDC temperature record do not allow us to accurately constrain the timing of climate events in the North Atlantic and, consequently, the phase relationship with their counterparts in the Southern Hemisphere. However, a "seesaw effect" between both Hemispheres similar to that mentioned during MIS 3 (Blunier et al., 1998) may have happened at millennial events although this is not easy to demonstrate in most of the cases due to age model uncertainties.

In order to test the accuracy of our age model, we compared the U1314 SST with the Antarctic $CH_4$ record (fig. 3.9), commonly used as a Northern Hemisphere proxy of warm climate and wetland expansion during the last glacial-interglacial cycle (Chappellaz et al., 1993; Blunier and Brook, 2001; Landais et al., 2006). Abrupt warming events in the Northern Hemisphere are correlated with $CH_4$ rises owing to a rapid northward shift of the Intertropical Convergence Zone (ITCZ) and the subsequent increase in precipitations over Asia and Africa. Based on this assumption $CH_4$ has been widely used to synchronize ice core records of both Hemispheres at MIS 3 (Blunier et al., 1998; Blunier and Brook, 2001). The coupling between Site U1314 SST and EDC $CH_4$ record, especially at millennial-scale events supports the high correlation between Site U1314 and EDC records and validates the age model construction.

### 4.3. Glacial inceptions between 400-800 ka

After Terminations the benthic $\delta^{18}O$ values in the studied section remained low during the interglacial periods, reflecting relatively stable warm climate. An inflection in the benthic $\delta^{18}O$ record towards heavier values marks the onset of a new glacial period or glacial inception (vertical grey dashed lines in fig. 3.3, 3.4, 3.5, 3.6 and 3.7). We observed that each glacial inception in the studied interval was associated with a pronounced cooling (observed in ANN SST) and a southward expansion of winter sea ice (inferred from *N. pachyderma* sin abundance) in the North Atlantic, synchronous with a Southern Hemisphere cooling (observed in the EDC deuterium temperatures). In MIS 17 the northern cooling was gradual, and even appears to have preceded the global glaciation by a few kyr, whereas in MIS 15.3 the cooling took place a few kyr after the inflection in the benthic $\delta^{18}O$ record. All glacial-inception North Atlantic temperature drops occurred after subtle IRD events dated at 488, 562, 605, 699 and 778 ka (fig. 3.4, 3.5, 3.6 and 3.7). The magnitude of the temperature change was 7 to 9 ºC in a period of less than 9 kyr (the sharpest events in 3-4 kyr). During these rapid climate deteriorations in the North Atlantic *N. pachyderma* sin abundances shifted from less than 10 % to more than 70 %, reflecting the rapid southward migration of the Arctic Front and the expansion of seasonal sea ice across the high latitudes of the North Atlantic. However, benthic $\delta^{13}C$ record remained almost unaffected for several kyr, suggesting that no major changes in deep water circulation occurred at glacial inceptions. Only during the subtle IRD events it is common to find a brief negative excursion in the benthic $\delta^{13}C$ record.

The increasing trend in the benthic $\delta^{18}O$ suggests that the ice sheets started to grow and/or deep water cooled at the glacial inceptions. We propose that the cooling of the Northern North Atlantic surface waters caused cooling in the NADW and, hence, benthic $\delta^{18}O$ values decreased. This is in agreement with the sea level and deep temperature models of Bintanja et al. (2005), in which they depicted that at glacial inceptions deep sea temperatures decreased rapidly and subsequently sea level began to drop. The timing of the onset of cooling in the Northern and Southern Hemisphere seems to be similar, within age model uncertainties, suggesting a strong coupling between both hemispheres at glacial inceptions. This coupling may be explained by the heat exchange between both Hemispheres through the AMOC, as predicted with Earth System models (Ganopolski and Roche, 2009). In other words, a North Atlantic cooling can be transferred to the Southern Ocean via colder NADW and, hence, the thermal vertical gradient between the colder NADW and the warmer surface currents that transported heat from the Southern to the Northern Hemisphere increased. This gradient may enhance Southern Ocean cooling through the arrival of colder NADW and heat loss through the surface currents. This coupling process, as remarked in Ganopolski and Roche (2009), is completely different to the "seesaw effect".

The fact that the glacial inception was linked to an abrupt cooling event points to a rapid expansion of sea ice in the high latitudes of the North Atlantic and a rapid expansion of the continental surface perennially covered by snow, even though the thickness of the ice sheets was still very reduced. Low summer insolation in the high latitudes of the Northern Hemisphere may gradually increase the snow-covered surface in North America and NW Europe triggering ice sheets growth. The albedo produced by the expansion of ice and sea ice would have strongly amplified the gradual effect of insolation when certain threshold was reached (Crucifix and Loutre, 2002), promoting the rapid expansion of sea ice that took place in glacial inceptions. A similar scenario of a glacial inception seems to occur during the last glacial cycle, at MIS 5e, when the Northern North Atlantic cooled in response to a decrease in June insolation at 65 ºN, while the mid latitudes were still relatively warm (Cortijo et al., 1994; Fronval and Jansen, 1997; Tzedakis, 2005).

The relatively high benthic $\delta^{13}C$ values observed during several kyr after glacial inceptions indicate that the AMOC was still active even though the NADW was colder. This "lagging NADW production" was observed as well at Site 980 from 1000 to 500 ka (Wright and Flower, 2002) and at MIS 5e/5d transition (McManus et al., 2002). The persistence of an active AMOC during the first stage of the glacial periods studied was likely caused by a density intensification of the NAC through North Atlantic cooling and through the extraction of freshwater at mid latitudes and its subsequent transfer and accumulation in the continents (Duplessy and Shackleton, 1985). The warm temperatures recorded at Site 980 at late MIS 19, 17 and 15 (Wright and Flower, 2002) suggest that the flow of Atlantic waters to the NGS was still active although the Arctic Front had moved southward. It is likely that the Arctic Front was somewhere between Site U1314 and Site

980 and the NAC flowed as a narrow current over the Rockall Plateau and or the Rockall channel but not westwards. Consequently, the subpolar gyre was colder than the East North Atlantic and SST at Site U1314 was colder too.

### 4.4. Ice sheet growth during glacial periods punctuated by millennial-scale ice sheet collapse events.

The ice sheet growth, which started at glacial inceptions, was not interrupted by iceberg discharges until the ice sheets exceeded certain size (the 3.5 ‰ threshold in benthic $\delta^{18}O$). For instance, the cooling event that marks the onset the glaciation at MIS 13/12 is dated at 488 ka whereas the first ice-rafting event was recorded at 480 kyr ago (fig. 3.4). A similar lag is observed in MIS 17/MIS 16 transition (fig. 3.6). The rapid increase in benthic $\delta^{18}O$ at glacial inceptions show that the early stage of the glaciations was characterized by a dominant transfer of freshwater from the ocean to the continents that led to a rapid growth of the ice sheets in the Northern Hemisphere. Low summer insolation at high latitudes can promote the accumulation of snow in the continents, but low insolation is not enough to produce large ice sheet growth, and other feedbacks like albedo, atmospheric $CO_2$ drops and ocean circulation patterns must have been involved (Crucifix and Loutre, 2002; Wang and Mysak, 2002; Landais et al., 2006; Bonelli et al., 2009). Additionally, the summer half-year (March 21-September 21) insolation gradient between 25 and 70º N was high at all glacial inceptions over the studied interval (fig. 3.3), and at least ~10 kyr afterwards. This gradient was suggested to regulate the poleward transport of moisture and heat (Raymo and Nisancioglu, 2003). Therefore, insolation gradients could also favoured snow precipitation and accumulation during the first stage of the glacial periods.

The second stage of the glaciations started with the first significant pulse of iceberg delivery to the North Atlantic (e.g. at 480 ka in MIS 12, fig. 3.4). The major IRD flux peaks were recorded in response to large instabilities in the northern Hemisphere ice-sheets. The freshwater delivery to the North Atlantic as a consequence of ice sheets instabilities is correlated with low benthic $\delta^{13}C$ values, suggesting that during this second stage of the glaciation the Atlantic thermohaline circulation was largely affected. Over the studied interval, the longest periods of disturbed AMOC (low benthic $\delta^{13}C$) were the longest glacial periods MIS 12 and 16 when the Northern Hemisphere ice-sheets reached the maximum volume too. However the strongest shut downs of the AMOC occurred at Terminations and during MIS 15.2, probably associated to large inputs of freshwater to sensitive North Atlantic areas (the deep water formation areas).

During this second stage of the glaciation, the northern hemisphere long-term gradual ice sheets growth towards the glacial maximum was punctuated by millennial-scale events of ice sheet instability. Hereafter we will refer to these millennial-scale interruptions of the ice sheet growth as ice sheet collapse events (ISCE), which are associated with small negative excursions in the benthic $\delta^{18}O$ and $\delta^{13}C$. In the ocean surface, the ISCE are initiated with a significant peak

of IRD flux and cool SST, immediately followed by a rapid decline of the IRD flux and an abrupt warming. These ISCE are similar to the succession of a HE followed by a prominent interstadial at the base of the Bond cycles in MIS 3 (Bond et al., 1993) and similar events were also identified at Site 980 from MIS 13 to 10 (Oppo et al., 1998).

The early stage of the glaciations was dominated by freshwater transfer towards the continents, whereas during the second stage of the glaciations, periods of ice sheet growth alternated with ISCE, which return large amounts of freshwater to the ocean, either within the first phase of the ISCE associated to the iceberg calving or due to the ice melting during the warming phase of the ISCE. Whatever the mechanism that triggered these ISCE they all caused a major slow down of the thermohaline circulation (reflected by a drop in the benthic $\delta^{13}C$) and a strong decrease in SST due to lower rates of oceanic heat transport at surface, which is followed by resumption of the AMOC and abrupt warming. The negative benthic $\delta^{18}O$ excursions during these ISCE, with an average amplitude of 0.5 ‰, are probably too high to be only associated to ice volume, since this would represent a sea level rise of around 50 m. Part of the benthic $\delta^{18}O$ decrease may be related to deep sea hydrographic changes due to the dampening of the AMOC (replacement of high $\delta^{18}O$ NADW by low $\delta^{18}O$ AABW and/or deep water generated by brine rejection in the NGS) similarly to what has been reported for the last glacial period (Skinner et al., 2003; Skinner and Elderfield, 2007; Yu et al., 2008), and the other part could be associated to millennial-scale waning of global ice volume, similarly to the millennial sea level rises associated to the HE or the most prominent interstadials during the Bond cycles in MIS 3 (Siddall et al., 2003; Arz et al., 2007; Sierro et al., 2009).

We consider it is worth paying special attention to the ISCE observed in MIS 15.2 (fig. 3.5). The glacial inception of late MIS 15.3 took place several kyr before the first surface cooling, at ~604 ka. Additionally, the first significant iceberg discharge and benthic $\delta^{13}C$ drop was recorded even later, at ~598 ka. From the inception to ~598 ka, the increase in benthic $\delta^{18}O$ reflects the stage of ice sheet growth and decreasing deep water temperature. Three major ISCE were recorded in MIS 15.2. The massive iceberg discharge of the third ISCE gave rise to the deglaciation of MIS 15.2 at ~582 ka. The average recurrence of ISCE events in MIS 15.2 is between 6 to 7 kyr, which is very similar to that of HEs in MIS 3 (Bond et al., 1993). The three episodes of ice sheet collapse in the Northern Hemisphere, including the one that ended with the glacial period, caused a prominent reduction in the AMOC as evidenced by three high amplitude drops in the benthic $\delta^{13}C$ of almost 1 ‰. Similar benthic $\delta^{13}C$ and SST drops were observed during the last glacial period linked to HEs (Chapman and Shackleton, 1998). Consequently, heat transport towards the North Atlantic was severely restricted, causing significant warming in the Southern Hemisphere. The "seesaw effect" during the ISCE is very apparent, especially in the third one (deglaciation) when there is a lag of 2-3 kyr between the gradual temperature increase in Antarctica and the abrupt rise in $CH_4$ (interpreted as Northern Hemisphere warming indicator). Similar ISCE can be

observed in MIS 12, MIS 14, MIS 16 and MIS 18 (fig. 3.4, 3.5, 3.6 and 3.7) but with lower benthic $\delta^{13}C$ oscillations. Commonly, ISCE of larger amplitude were recorded when the ice sheets were relatively small. When the ice sheets reached certain size (≥ 4 ‰ in our benthic $\delta^{18}O$ data), glacial conditions became more stable and the following ISCE presented smaller amplitude changes until the Termination, except in MIS 15.2 where the ice sheet stopped growing and the third ISCE caused a deglaciation.

In the EDC records the ISCE were typically linked to periods of rising temperatures and $CO_2$ (fig. 3.4, 3.5, 3.6 and 3.7) that ended at the beginning of the Northern Hemisphere warming phase and the inflection towards heavier benthic $\delta^{18}O$ values that may represent the renewal of ice sheet growth and the resumption of the AMOC. It is likely that $CO_2$ helped to warm the Northern Hemisphere through increasing the greenhouse effect. The resumption of the AMOC after the IRD and meltwater discharges may have restarted the transfer of heat to the Northern Hemisphere bringing the Antarctic temperatures and $CO_2$ down and, in turn, diminishing the greenhouse effect which helped to cool Northern Hemisphere again.

At the end of glacial periods benthic $\delta^{18}O$ values were high (fig. 3.3), North Atlantic and Antarctic temperatures were low (fig. 3.9) and greenhouse gasses were low as well (fig. 3.9). All Terminations recorded in the investigated section were associated with large-scale ISCEs, as can be observed by the larger flux of IRD (fig. 3.3, 3.4, 3.5, 3.6 and 3.7) at these times and the high-amplitude anomalies in the benthic $\delta^{13}C$. It seems that massive iceberg discharges produced a prominent shutdown of the thermohaline circulation. As a result, a major reorganization of the global ocean and atmosphere circulation may have increased Southern Ocean ventilation releasing huge amounts of $CO_2$ to the atmosphere (Dickson et al., 2008; Schmittner and Galbraith, 2008; Anderson et al., 2009; Toggweiler, 2009; Anderson and Carr, 2010; Sigman et al., 2010; Skinner et al., 2010). As can be seen from figures 3.3 and 3.9, the large-scale ISCEs recorded at Terminations are always related to high amplitude sharp increases in atmospheric $CO_2$ in the Antarctic ice record. $CO_2$ has been frequently suggested to boost ice melting during Terminations and to drive the 100 kyr cycles (Raymo, 1997; Ruddiman, 2006b; Ruddiman, 2006a; Toggweiler, 2008). We believe that the huge $CO_2$ leakage during the ISCE at Terminations may have played a major role, amplifying the warming of the Northern Hemisphere and, hence, the ice sheet melting that led to the end of the glacial periods studied.

## 6. Conclusions

The study of benthic and planktic stable isotopes from Site U1314 in the North Atlantic, as well as planktic foraminifer assemblages and IRD content, allowed us to reconstruct climate variability, changes in sea-ice extent and ice sheet growth at millennial and orbital timescales

between 800 and 400 ka. Four climatic cycles with an average duration of 100 kyr were recorded during this period. The comparison of SST in the North Atlantic with the EDC Antarctic temperature (Jouzel et al., 2007) revealed that both hemispheres were closely coupled at millennial timescales over the four glacial-interglacial cycles studied (fig. 3.9).

Glacial inceptions started with a sharp cooling at the latitude of Site U1314 linked to a rapid southward expansion of Arctic waters. The prevalence of an active AMOC during this initial stage of the glaciation, as indicated by the high benthic $\delta^{13}C$ values, could have played a significant role in transferring this cooling to the Southern Hemisphere via NADW. During the first stage of the glaciation the increase in the benthic $\delta^{18}O$ suggests rapid ice sheet growth, though part of this isotopic change may be due to the advection of colder deep waters to the studied site. Therefore, during this first stage freshwater was preferentially transferred from the oceans to the continents and accumulated in the ice sheets. That turned North Atlantic waters saltier and denser making them more conductive to maintain the thermohaline circulation.

The second stage of glaciations was characterized by long term ice sheet growth punctuated by millennial-scale events of ice sheet waning or ISCE, in other words, periods of freshwater transfer to the continents alternated with short episodes of freshwater return to the ocean. The ISCE were initiated by iceberg calving in the continental margins which freshened the North Atlantic preventing NADW/GNAIW formation. After the IRD discharge, SST increased and planktic $\delta^{18}O$ decreased, indicating much warmer conditions that caused partial melting of the ice sheets. In consequence, these ISCE were associated to short-term negative anomalies in the benthic $\delta^{18}O$ which were related to short interruptions in the progressive ice sheet growth during the glacial periods. This succession is similar to the one described for the HE and the subsequent major interstadials during the last glacial period (Bond et al., 1993; Chapman and Shackleton, 1998). In the Antarctic records the ISCE were linked to periods of rising temperatures and $CO_2$ that ended with resumption of the AMOC and rapid warming of the Northern Hemisphere. Terminations, as recorded in the studied section, were associated to large-scale ISCE that caused a prominent shutdown of the AMOC. This shut down could induce a major reorganization of ocean and atmosphere (e. g. Schmittner and Galbraith, 2008; Anderson et al., 2009; Toggweiler, 2009) that increased Southern Ocean ventilation and released huge amounts of $CO_2$ to the atmosphere, which may have played a major role in amplifying the ice sheet melting.

# CAPÍTULO 4.

## MID-PLEISTOCENE SHIFTS OF THE ARCTIC FRONT IN THE SUBPOLAR NORTH ATLANTIC FROM 800 TO 400 ka

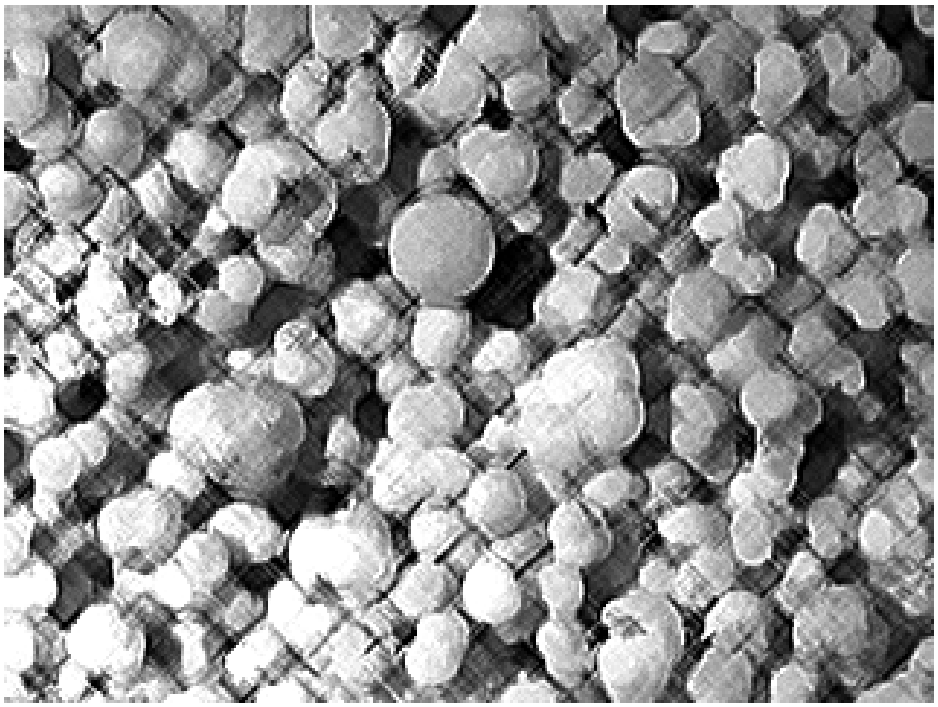

# 4. MID-PLEISTOCENE SHIFTS OF THE ARCTIC FRONT IN THE SUBPOLAR NORTH ATLANTIC FROM 800 TO 400 ka

Montserrat Alonso-Garcia[1], Francisco J. Sierro[1] and José A. Flores[1]

1 Department of Geology (Paleontology), University of Salamanca, Pza. de la Merced s/n, 37188, Salamanca, SPAIN

*Corresponding author. Department of Geology (Paleontology), Faculty of Science, University of Salamanca, Pza. de la Merced s/n, 37188 Salamanca, Spain. Tel. +34 923 294497; Fax +34 923 294514. E-mail address: montseag@usal.es (M. Alonso-Garcia).

## Abstract

Surface water conditions were inferred from planktonic foraminifer assemblages from the end of Marine Isotope Stage (MIS) 19 to the beginning of MIS 11 (ca. 800-400 ka) at IODP Site U1314 (Southern Gardar Drift, 56º 21.8' N, 27º 53.3' W, 2820 m depth). Factor analysis of planktonic foraminifer assemblages suggests that the assemblage was controlled by three factors. The first factor has been associated with the presence of cold and low saline surface waters (the Arctic waters). The second factor points to warm and salty surface waters (the Atlantic waters). And the third factor, linked to a significant presence of T. quinqueloba, reflects the closeness of the Arctic front (which separates Atlantic from Arctic waters).

Planktonic foraminifer abundances from Site U1314 and their factor analysis, combined with planktonic foraminifer and diatom abundances data from other already published North Atlantic sites, allowed us to estimate the position of the Arctic front across glacial-interglacial cycles. We associated Arctic front migrations with changes in the subpolar North Atlantic water masses and therefore with the North Atlantic Current strength and the thermohaline circulation. According to these interpretations and to previous ice sheet growth reconstructions we have divided each climatic cycle in five stages, early interglacial stages, late interglacial stages, first stage of glacial periods, second stage of glacial periods and late glacial periods-Termination. These stages may be applied to the last four climatic cycles as well

**Keywords**: planktonic foraminifers, subpolar North Atlantic, Arctic front, factor analysis, Mid-Pleistocene.

## 1. Introduction

In the modern ocean and during interglacial periods, production of North Atlantic deep waters (NADW) mainly takes place in the Norwegian Greenland Seas (NGS) where winter convection promotes the sinking of cold dense waters (Swift, 1986). It is widely known that during glacial stages the warm and salty waters of the North Atlantic current (NAC) became colder and fresher and, in turn, less heat was supplied to high latitudes allowing sea ice to cover most of the NGS. Thus NADW production was reduced, shifting to Glacial North Atlantic intermediate water (GNAIW) production in the northern North Atlantic (Boyle and Keigwin, 1987; Venz et al., 1999). In this regard surface water characteristics of the subpolar North Atlantic are particularly important because changes in deep water ventilation and in the strength of the thermohaline circulation are driven by temperature and salinity shifts of the subpolar North Atlantic surface waters (Broecker and Denton, 1989).

Planktonic foraminifers are a very valuable proxy to study surface water masses since they provide valuable information of sea surface temperature and salinity (Kucera et al., 2005; Pflaumann et al., 2003). Ruddiman and Glover (1975) were pioneers describing subpolar North Atlantic circulation changes and the position of the Polar front and the Subarctic Convergence (equivalent to the Arctic front) for the last 18,000 years using planktic foraminifer abundances. In the NGS planktonic foraminifer assemblages characterize the different surface water masses and they are considered as a proxy for surface water temperature, salinity and sea ice coverage (Johannessen et al., 1994). Several authors used the relationship between several planktic foraminifer species abundances as a proxy to infer the Polar and Arctic front (PF and AF) positions for different Pleistocene intervals (Fronval et al., 1998; St. John et al., 2004; Wright and Flower, 2002). Moreover, other planktic organisms have been used to infer front positions such as diatom assemblages (Koç and Flower, 1998).

Here, we analysed a high resolution record of planktic foraminifer assemblages from a subpolar North Atlantic site (Site U1314) in order to infer changes in surface water characteristics over glacial-interglacial cycles of the Mid-Pleistocene (ca. 800-400 ka). We took advantage of the location of Site U1314, in the subpolar gyre, and compared our data with published data from other North Atlantic sites to reconstruct the approximate extent of winter sea ice coverage and the AF migrations over climatic cycles. We suggest the study of subpolar surface waters can be very helpful to interpret some changes in the Atlantic Meridional Overturning Circulation (AMOC). The knowledge of surface water masses distribution in the Northern North Atlantic is essential for a better understanding of climate changes in the North Atlantic and the whole Earth.

## 2. Regional setting

IODP Site U1314 was drilled in southern Gardar drift, south of Iceland (56º 21.8' N, 27º 53.3' W) at 2820 m water depth (fig. 4.1). Site U1314 is located inside the subpolar gyre (fig. 4.1), nowadays influenced by the NAC which flows northeastwards across the North Atlantic into the Nordic Seas. NAC passes between subtropical and subpolar gyres drawing water from them (Hansen and Østerhus, 2000). Near Iceland, the Irminger Current (IC) splits from the NAC and flows towards the Greenland coasts mixing with the cold East Greenland Current (EGC). The EGC flows to the Labrador Sea and mixes with the Labrador Current whose waters flow towards the NAC and begin the gyre again (Hansen and Østerhus, 2000; Tomczak and Godfrey, 1994). At present, according to Swift (1986), in the NGS three surface water masses can be distinguished, Polar, Arctic and Atlantic waters. The cold and low salinity Polar waters (which correspond to the EGC) are separated by the PF from the cold but saltier Arctic waters (fig. 4.1). The PF is close to the summer sea ice edge, thus Polar waters are perennially under the sea ice. The AF is the boundary between the Arctic waters and the warm and high salinity Atlantic waters of the Norwegian Current (NC). Since the maximum sea ice edge is slightly west of the AF, Arctic waters are seasonally covered by ice and suffer winter convection due to the ice formation, which in turn lead to NGS deep water formation (Swift, 1986; Tomczak and Godfrey, 1994). Water masses characteristics of the NGS are very important since during glacial periods these water masses spread southwards along with sea ice expansion.

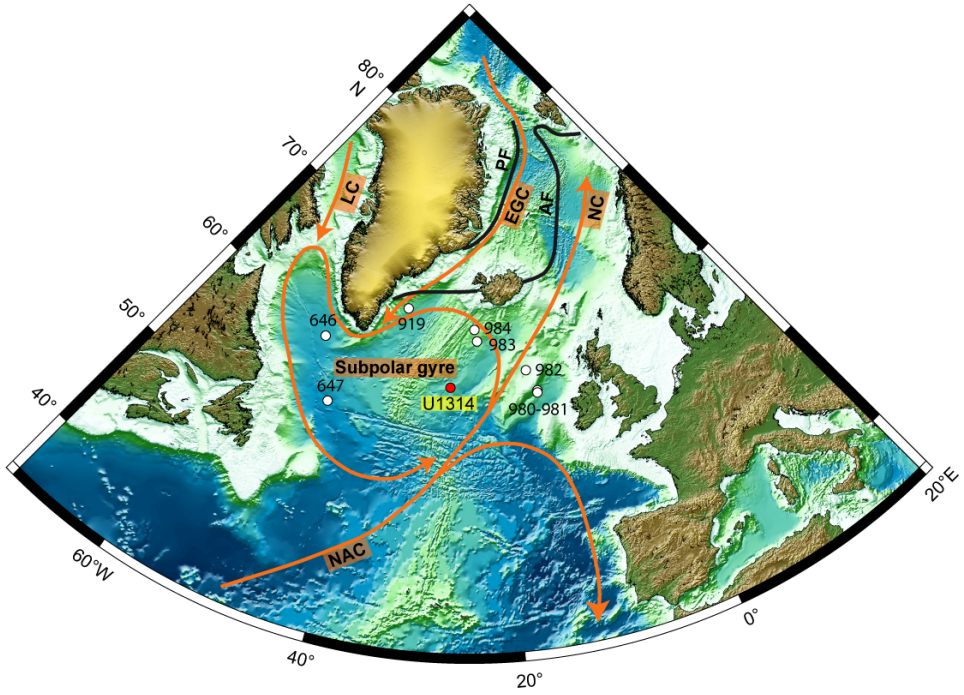


Fig. 4.1. Location of the IODP site U1314 and other north Atlantic sites which were useful to reconstruct the Arctic Front position. Orange arrows represent main surface currents according to Schmitz and McCartney (1993). Present location of the Arctic and Polar fronts (AF and PF) is depicted according to Swift (1986). The map was provided by Integrated Ocean Drilling Program (IODP).

## 3. Materials and methods

Sediments at Site U1314 mainly consist of calcareous nannofossils and clay with minor and varying proportions of diatoms, radiolarians, foraminifers and IRD. Generally well preserved planktic foraminifers are the dominant component in the sand fraction, with lower proportions of benthic foraminifers, ostracodes, siliceous microfossils and IRD (Channell et al., 2006). The high sedimentation rate of the Gardar drift makes this site suitable for a high resolution study of glacial-interglacial climate shifts.

The interval presented in this study encompasses from 32.80 to 59.98 mcd (meters of composite depth). Planktic foraminifer assemblages were studied every 8 cm. Each sample was sieved under water with a 63 μm mesh to eliminate fine-grained particles. Then, samples were divided into two fractions, 63-150 μm and above 150 μm. Counts were performed on the coarse fraction. Each sample was split as many times as necessary until there were roughly 400 planktic foraminifers (300 minimum) in order to calculate relative abundances, specimens per gram and fluxes.

## 4. Results

### 4.1. Age model framework

The age model for the studied interval was published in Alonso-Garcia et al. (submitted) and was performed correlating the Antarctic deuterium temperature ages from EPICA Dome C (EDC) ice core record (Jouzel et al., 2007; Parrenin et al., 2007) with the benthic $\delta^{18}O$ record of Site U1314. The interval encompasses from ca. 800 to 400 ka, within the so-called mid-Pleistocene transition. Mean sedimentation rate of the interval was 7.27 cm/ka, similar to the rate described on board (Channell et al., 2006). Resolution between samples for the foraminifer census counts is on average 1100 years.

### 4.2. Planktic foraminifer assemblages

Despite the fact that 16 planktic foraminifer species were identified, only five of them present abundances high enough to be considered. Those species are *N. pachyderma* sin, *N. pachyderma* dex, *Globorotalia inflata*, *Globigerina bulloides* and *Turborotalita quinqueloba* (fig. 4.2).

Census counts reveal two clear groups of fauna. During glacial stages diversity was very low and the assemblage was almost monospecific, dominated by the species *N. pachyderma* sin,

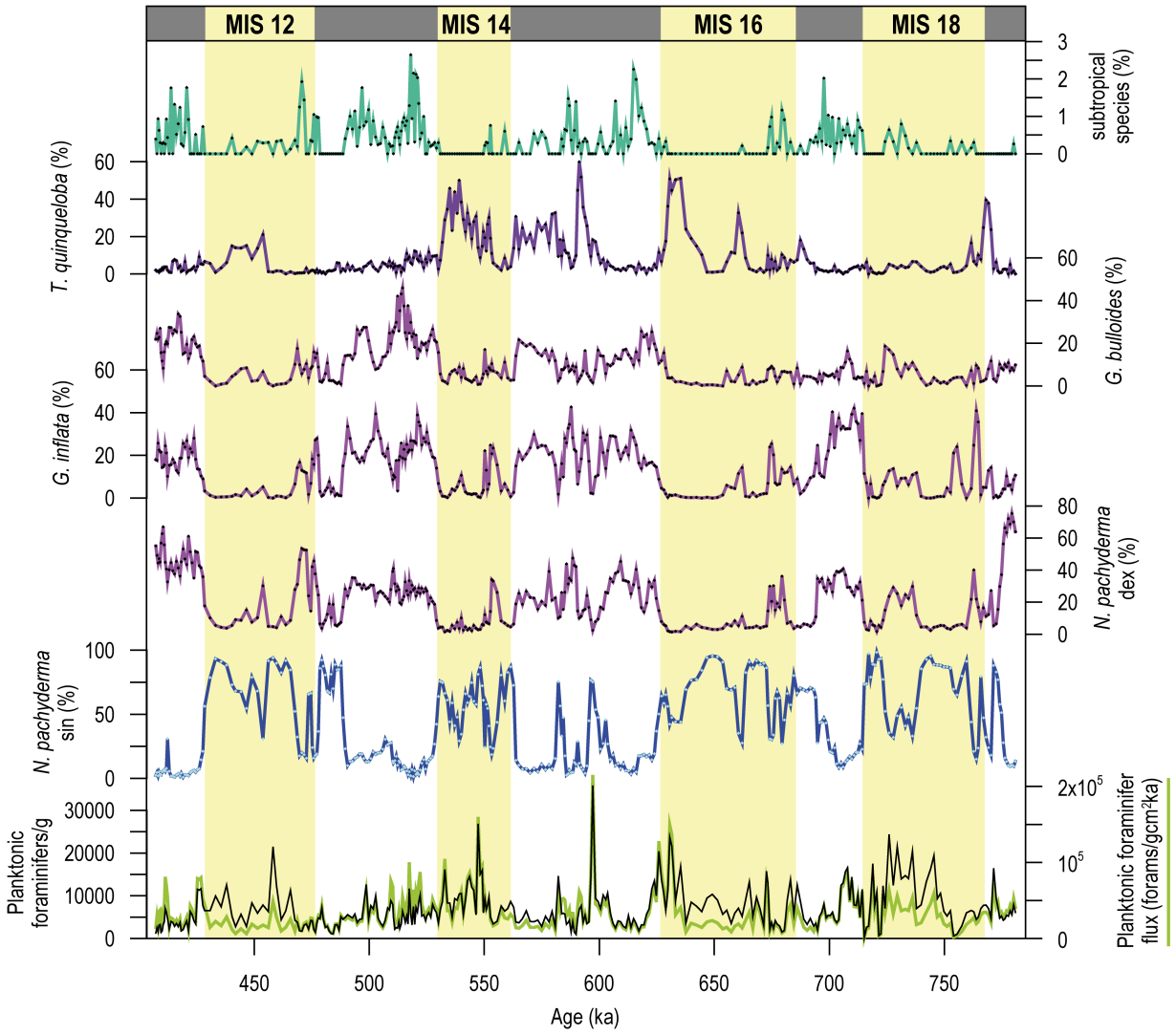


Fig. 4.2. Planktonic foraminifer assemblage of site U1314. Relative abundance of the different species, from top to bottom: subtropical species, *T. quinqueloba*, *G. Bulloides G. inflata*, *N. pachyderma* dex and *N. pachyderma* sin. At the bottom of the graph planktonic foraminifers per gram of dry sediment (black line) and planktonic foraminifer flux (green line) are depicted. Glacial Marine Isotope Stages (MIS) are shown with vertical yellow bars.

accompanied by variable amounts of *T. quinqueloba* and low percentages of *N. pachyderma* dex, *G. inflata* and *G. bulloides* (fig. 4.2). *N. pachyderma* sin shows sharp changes in relative abundance between glacial and interglacial periods, ranging between 65 and 98 % during glacial periods whereas during interglacial periods this species was generally below 15 %, even reaching values of about 1 %. This species lives in polar environments between -1 and 8 ºC (Bauch et al., 1997; Bé, 1977; Pflaumann et al., 2003; Tolderlund and Bé, 1971).

On the other hand, during interglacial periods a more diversified microfauna was found (fig. 4.2). Three species are the main components of the assemblage, *N. pachyderma* dex, *G. inflata* and *G. bulloides*, accompanied by variable amounts of *T. quinqueloba,* and little amounts

of subtropical and ubiquitous species. *N. pachyderma* dex, *G. inflata* and *G. bulloides* reached relative abundances of 60-70 %, 30-40 % and 20-40 % respectively during the interglacial periods whereas during glacial times *N. pachyderma* dex abundance was about 5 %, *G. bulloides* below 5 % and *G. inflata* near zero. *N. pachyderma* dex and *G. bulloides* live in subpolar environments preferably between 10 and 18 ºC (Bé, 1977; Hemleben et al., 1989; Reynolds and Thunell, 1985; Tolderlund and Bé, 1971) whereas *G. inflata* is a transitional species that lives in a wide temperature range, but preferably between 10 and 20 ºC (Bé and Tolderlund, 1971). These three species accounted for the major part of the transitional-subpolar assemblage.

*T. quinqueloba* presented higher abundances at certain intervals either during glacial or interglacial periods, ranging between approximately 0 and 50 % (fig. 4.2). This species thrives nowadays in periods of high phytoplankton productivity when the mixed layer is deep (Simstich et al., 2003; Stangeew, 2001). Johannessen et al. (1994) reported the maximum abundance of *T. quinqueloba* in the Nordic Seas just east of the Arctic front covering the thermal gradient between the Arctic waters and the Atlantic waters.

Among the less abundant species *Globigerinita glutinata* and *Globorotalia scitula* were recorded in percentages below 20 and 10 % respectively. Besides, many subtropical species like *Globorotalia truncatulinoides*, *Neogloboquadrina dutertrei*, *Orbulina universa*, *Globigerinoides ruber* white, *Globorotalia crassaformis*, *Globorotalia hirsuta* and *Beella digitata* were found below 2 % altogether (fig. 4.2).

Preservation in the studied interval was analysed regarding at the planktic foraminifer fragment index, which represents in percentage the amount of fragments respect to the total amount of foraminifers plus fragments (Thunell, 1976). The index is generally lower than 20 %, indicating very good preservation in the samples, except for some short intervals where dissolution increased but hardly reaches 40 %. Miao et al. (1994) described in samples from the China Sea that the assemblages began to suffer modifications due to dissolution when the 40 % of fragments was exceeded. Therefore, we can assume that the assemblages presented here are not modified by dissolution and they are a suitable proxy for inferring water masses characteristics.

## 5. Discussion

### 5.1. Factor analysis of planktic foraminifer assemblages

Although two groups of microfauna can be easily distinguished, planktic foraminifer relative abundance data was reduced using factor analysis. We performed a Q-mode factor analysis of the

downcore assemblages with varimax rotation. 96 % of the variance was explained taking three factors (see Appendix IV). We rejected the fourth factor and followings because the variance explained by them was lower than 5 %. Species scores for the three factors are listed in table 4.1 and factor loadings are depicted in figure 4.3 and the values are available in supplementary data (Appendix IV). Factor 1 explained 49.07 % of the variance. The highest factor scores of this factor were found in transitional-subpolar water species (*N. pachyderma* dex, *G. inflata* and *G. bulloides*, see table 4.1). Factor 2 explained 37.34 % of the variance and was only related to the polar species *N. pachyderma* sin. In the third factor, which explained 9.64 % of the variance, only *T. quinqueloba* presented high factor scores. Factor loadings of factor 1 and 2 are generally opposite, however high factor loadings of factor 3 co-occurred with medium-high values of factor 1 or 2 indistinctly (see Appendix IV).

Factor 1 is related to the transitional-subpolar water species indicating the influence of the temperate waters of the subpolar NAC where these species thrive at present (Bé, 1977; Bé and Tolderlund, 1971; Hemleben et al., 1989; Reynolds and Thunell, 1985; Tolderlund and Bé, 1971). A similar conclusion was obtained for factor 2, it is linked to the cold and low salinity waters in which *N. pachyderma* sin thrives nowadays (Bé, 1977; Hemleben et al., 1989; Reynolds and

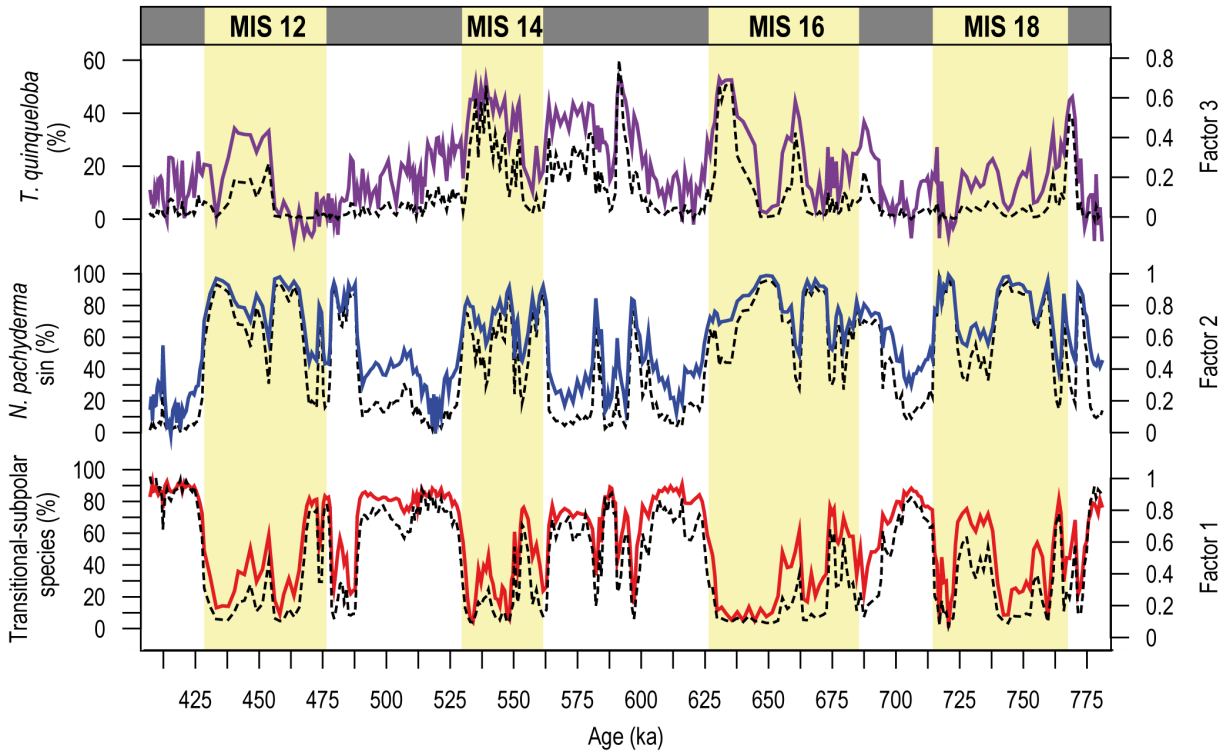


Fig. 4.3. Comparison between factor loadings and the abundance of the more important species of each factor. a) Factor 1 (blue line) and the subpolar species (*N. pachyderma* dex + *G. inflata* + *G. bulloides*) relative abundance (black dashed line); b) Factor 2 (red line) and the polar species *N. pachyderma* sin relative abundance (black dashed line); and c) Factor 3 (purple line) and *T. quinqueloba* relative abundance (black dashed line). Glacial MIS are shown with vertical yellow bars.

| Species | Factor scores | | |
|---|---|---|---|
| | Factor 1 | Factor 2 | Factor 3 |
| *O. universa* | -0.626939 | -0.339986 | -0.371842 |
| *G. ruber* (w) | -0.702879 | -0.312522 | -0.409562 |
| *G. siphonifera* | -0.688493 | -0.313648 | -0.402060 |
| *G. bulloides* | 1.366.476 | -0.321384 | 0.311304 |
| *B. digitata* | -0.758138 | -0.300600 | -0.397085 |
| *T. quinqueloba* | -0.435578 | 0.049417 | 3.342.697 |
| *N. pachyderma* (s) | -0.202129 | 3.386.966 | -0.194820 |
| *N. dutertrei* | -0.736524 | -0.290743 | -0.430577 |
| *N. pachyderma* (d) | 1.934.903 | 0.382150 | -0.651943 |
| *G. inflata* | 1.774.594 | -0.560992 | 0.244901 |
| *G. truncatulinoides* | -0.686507 | -0.330202 | -0.420716 |
| *G. crassaformis* | -0.626366 | -0.350627 | -0.421583 |
| *G. scitula* | -0.350287 | -0.348483 | 0.003828 |
| *G. glutinata* | 0.737868 | -0.349345 | -0.202541 |

Table 4.1. Factor scores obtained from the planktic foraminifer factor analysis. The highest factor scores are highlighted in grey indicating which species are important in each factor.

Thunell, 1985; Simstich et al., 2003; Stangeew, 2001; Tolderlund and Bé, 1971). The high factor scores of *T. quinqueloba* in factor 3 suggest that this factor is indicating the presence of the AF near the site (Johannessen et al., 1994). The fact that high factor loadings of factor 3 are coeval with high factor loadings of factors 1 (or 2) reflects that the site was near the AF but mainly influenced by the NAC (or by the Arctic waters).

Glacial and interglacial faunas are clearly defined by factors 2 and 1 respectively (fig. 4.3), and changes from low to high values were often sharp, within about 3300 years or even less, indicating that migrations of the AF were rather fast. There is a strong parallelism between the abundance of subpolar-transitional species and Factor 1, and between the abundance of *N. pachyderma* sin and Factor 2. However, factor 3 shows changes that are not so obvious in the *T. quinqueloba* abundance (fig. 4.3). Thus, we reckon that Factor 3 is more helpful to analyse AF migrations than the mere abundance of *T. quinqueloba*. Shifts in factor loadings of Factor 3 suggest that the AF was not in the same location during all glacial (or interglacial) periods but its location was highly variable. Our factor analysis combined with planktic foraminifer abundances allowed us to reconstruct surface water masses affinity to NAC, AF and Arctic waters over glacial-interglacial periods and, hence, to reconstruct AF fluctuations near to Site U1314.

### 5. 2. Arctic front migrations over ca. 800-400 ka

In this section we inferred AF migrations in the North Atlantic combining our planktic foraminifer assemblages and their factor analysis with planktic foraminifer and diatom records from other subpolar North Atlantic sites. Since all glacial-interglacial cycles show a common pattern, we divided each cycle in 5 stages of development, even though each climatic cycle presents several inherent features (fig. 4.4). Benthic oxygen isotopes and sea surface temperatures (SST) from Site U1314 (Alonso-Garcia et al., submitted to QSR) are shown in figure 4.4 to track ice volume growth and temperature shifts and relate them with the AF fluctuations.

**Early interglacial stage**. After Terminations planktic foraminifer assemblages indicate that the AF was further north and NAC waters influenced Site U1314. The gradual decrease in *N. pachyderma* sin and *T. quinqueloba* percentages (as well as in Factor 3) indicates that the AF was retreating during the early stage of interglacial periods. This retreat is linked to a slightly increase in mean annual SST. Low but significant abundances of *N. pachyderma* sin and *T. quinqueloba* suggest that winters were relatively cold after the Terminations and progressively became milder as *N. pachyderma* sin and *T. quinqueloba* decreased. Hence, mean annual temperatures increased because winters got milder (fig. 4.4). At ODP Sites 980, 984 and 647 *N. pachyderma* sin percentages decreased as well in the early interglacial stages (Aksu et al., 1989; Wright and Flower, 2002) although at Site 646 only MIS 11, 13 and 17 presented significant transitional-subpolar species abundances indicating that MIS 15 and 19 were slightly colder in the Labrador Sea. It is likely that deep water formation in the Labrador Sea was enhanced and the Irminger current contributed to warm the Labrador Sea waters, especially during MIS 11, 13 and 17. Additionally the high diatom production at ODP Sites 983 and 919 (Koç and Flower, 1998; Koç et al., 1999) suggest that the PF was further north of both sites. Based on these data, we consider that after the Terminations the AF gradually migrated northwestwards until it reached the present position or perhaps even more northwesterly (fig. 4.5a), keeping Arctic waters northwards in both the NGS and the Labrador Sea.

**Late interglacial stage**. The first slight increases of *N. pachyderma* sin and *T. quinqueloba* abundances (Factor 3, in figure 4.4, shows more clearly this increases in the importance of *T. quinqueloba* in the assemblage) suggest that interglacial conditions over the studied interval began to deteriorate. This deterioration initiated a period in which annual SST at Site U1314 started to decrease and the AF progressively migrated southwards towards the position of Site U1314, as indicated by the increasing values of Factor 3 loadings and *T. quinqueloba*, which suggest more severe winter cooling. In Sites 984, 647 and 646 *N. pachyderma* sin and *T. quinqueloba* rose to high values indicating that Arctic waters prevailed at these areas and even southeastwards (Aksu et al., 1989; Wright and Flower, 2002). Whereas in Site 980 *N. pachyderma* sin and *T. quinqueloba* percentages were relatively low and high SST prevailed even after the glacial inceptions (Wright and Flower, 2002), indicating that the NAC still flowed over Site 980. During the late stage of the interglacial periods studied benthic $\delta^{18}O$ shows that ice sheets were not growing, in fact the $\delta^{18}O$ was slightly decreasing, which suggests that they were still waning. Although the ice sheets were not growing, records from all the sites mentioned suggest the AF progressively moved southeastwards and the NAC migrated to the east (fig. 4.5b). This migration might have been triggered by a decrease in deep water formation at the Labrador Sea, which weakened the Irminger current. Consequently the EGC was the main source of surface waters and the subpolar gyre cooled. Despite the lack of planktic foraminifer records from the NGS we assume that the AF might have moved similarly to what was reported for late Eemian (Fronval et al., 1998).

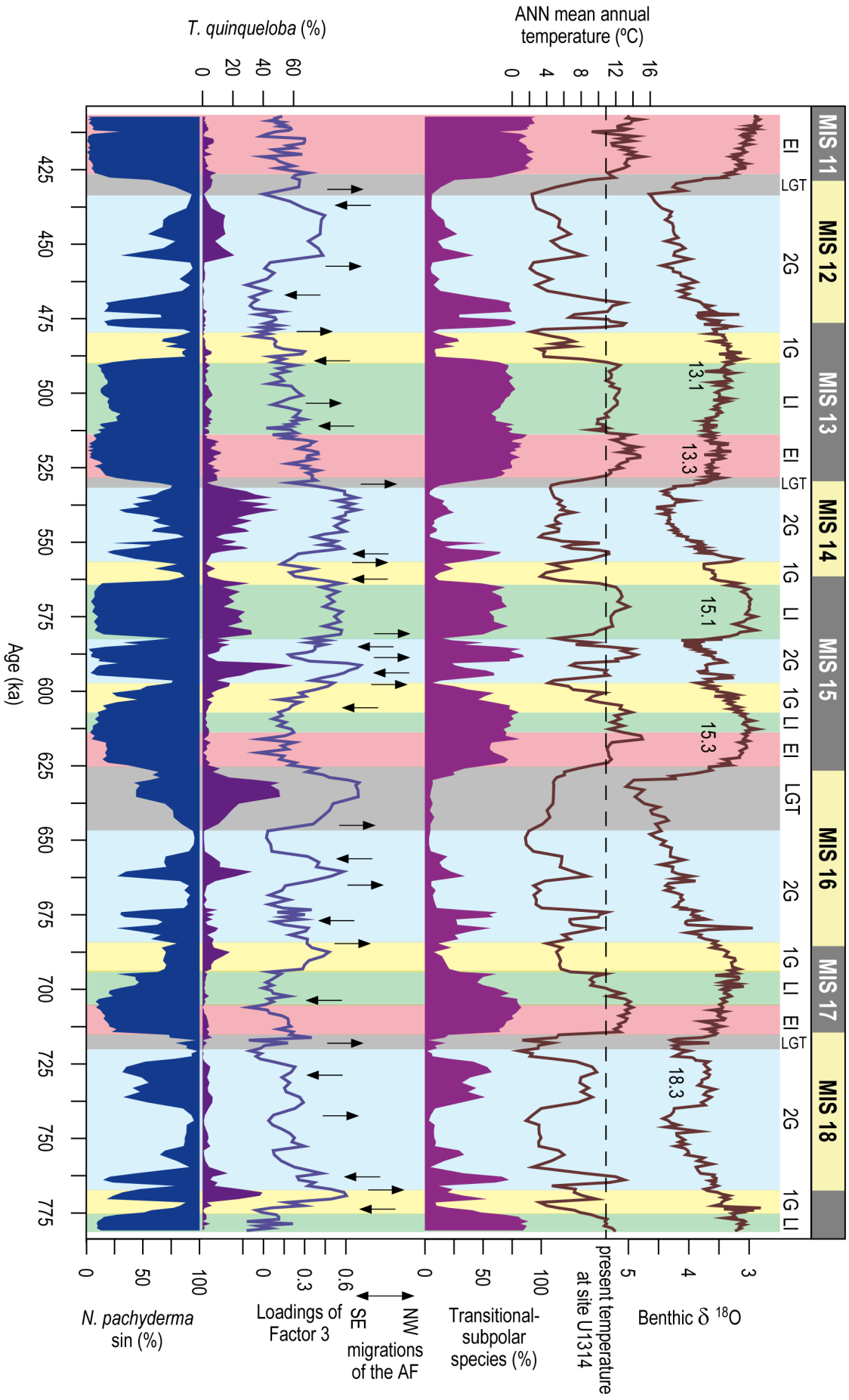
T. quinqueloba (%)
ANN mean annual temperature (ºC)
MIS 11
MIS 12
MIS 13
MIS 14
MIS 15
MIS 16
MIS 17
MIS 18
EI
LGT
2G
1G
LI
13.1
13.3
15.1
15.3
18.3
Age (ka)
N. pachyderma sin (%)
Loadings of Factor 3
SE
NW
migrations of the AF
Transitional-subpolar species (%)
present temperature at site U1314
Benthic δ 18O

Fig. 4.4. Different stages of development of climatic cycles based on AF migrations and ice sheet size: early interglacial stages (EI), late interglacial stages (LI), first stage of glacial periods (1G), second stage of glacial periods (2G) and late glacial periods-Termination (LGT). *N. pachyderma* sin, *T. quinqueloba* and the subpolar species (*N. pachyderma* dex + *G. inflata* + *G. bulloides*) relative abundances and Factor 3 were used to infer surface water masses characteristics and AF shifts. Fill colour of *N. pachyderma* sin is inverted in order to better appreciate the coupling with *T. quinqueloba* when the Arctic front is near site U1314. Mean annual temperature from ANN and benthic $\delta^{18}O$ are from Alonso-Garcia et al. (submitted, see chapter 3). Ice sheet growth and decay through climatic cycles was reflected in benthic $\delta^{18}O$.

**First stage of glacial periods.** Glacial inceptions were defined at Site U1314 by an inflection towards high benthic $\delta^{18}O$ values (Alonso-Garcia et al., submitted) which indicates that ice sheets started to grow. Around glacial inceptions SST at Site U1314 decreased rapidly while *N. pachyderma* sin percentages increased to glacial values. In Sites 983, 984, 919, 646 and 647 these conditions were similar or even harsher, the northernmost sites were rapidly covered by perennial sea ice (Aksu et al., 1989; Koç and Flower, 1998; Koç et al., 1999; Wright and Flower, 2002). However, the high SST at Site 980 suggests an active flow of NAC over this site (Wright and Flower, 2002). Benthic stable carbon isotopes from this site and from Site U1314 (Alonso-Garcia et al., submitted) also support that the AMOC was active during the early stage of glaciations. We advocate that the NAC flowed east of Site U1314, probably as a narrow stream, over the Rockall Plateau and Trough, and reached the NGS where it sank to generate the NADW which maintained the AMOC active (fig. 4.5c). It is likely that during this stage NADW was mainly generated in the NGS because almost all the Labrador Sea was perennially sea ice covered. However, we can not discard that intermediate or deep waters were generated at the western North Atlantic in areas with annually sea ice cover. If NADW was only generated in the NGS it is likely that the volume of deep water production was significantly reduced weakening the AMOC to some extent.

**Second stage of glacial periods.** When the second stage of glacial periods started the polar assemblage was already dominant in Sites U1314, 984, 646 and 647 but not in Site 980 (Aksu et al., 1989; Wright and Flower, 2002). At Site 980 this stage is characterised by a decrease in SST and a significant increase in *N. pachyderma* sin which mostly co-occur with *T. quinqueloba* (Wright and Flower, 2002). This suggests that the AF was south of all the sites mentioned but 980, which was mostly near the AF. Several ice sheet collapse events (ISCE) interrupted ice sheet growth during the second stage of glacial periods as reported in Alonso-Garcia et al. (submitted). During the warm phase of these ISCE SST raised considerably (even surpassing present temperatures) and the transitional-subpolar assemblage throve for a few thousand years at Site U1314, indicating that the AF shifted northwards of this site for short intervals (fig. 4.4 and 4.5e). Therefore, during the second stage of glacial periods the AF was not steady in a southern position but experienced several fluctuations. Moreover, the second stage of glacial periods is the most diverse. Diatom data from Sites 919 and 983 indicate that these areas were perennially ice-covered only during MIS

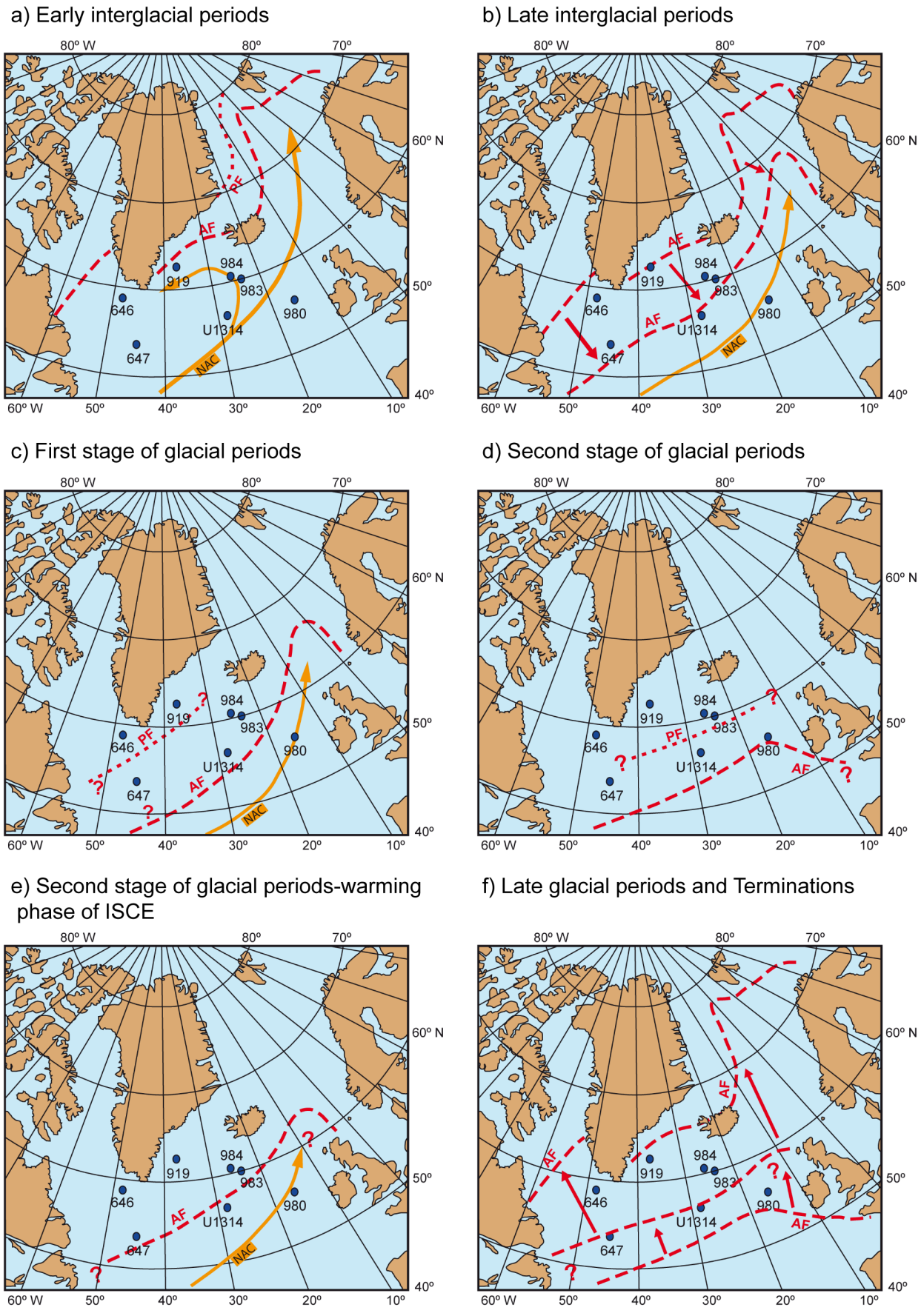


Fig. 4.5. Inferred position of the AF and PF in the North Atlantic for each stage of climatic cycles.

16 and 12 (Koç and Flower, 1998; Koç et al., 1999). In Site U1314 planktic foraminifer fluxes (fig. 4.2) were high during all glacial periods indicating that sea ice cover was only seasonal. We suggest that during the periods with the maximum ice sheet extent of the studied interval (MIS 12 and 16) the PF was south of Iceland but north of Site U1314 whereas during MIS 14 and 18 the PF was north of Sites 919 and 983. During MIS 18 *N. pachyderma* sin decreased near to interglacial values for a prolonged period of time between ~738 and 725 ka in Sites U1314, 647 and 980 (Aksu et al., 1989; Wright and Flower, 2002). This suggests that the AF shifted northwards longer than the few thousand years of the warm phase of the ISCEs. Hence, during cold period of MIS 18 the AF was located in a similar position to that recorded for MIS 16 and 12, but during the warm period 18.3 the AF was further north. Finally, during MIS 14, which was a shorter glacial period and with smaller ice sheets, slightly lower percentages of *N. pachyderma* sin and higher values of *T. quinqueloba* than in MIS 16 and 12 were recorded at Site U1314. A similar record reported at Sites 647 and 980 (Aksu et al., 1989; Wright and Flower, 2002) supports that MIS 14 was slightly warmer in the North Atlantic and the AF was rather near Sites 647, U1314 and 980.

**Late glacial periods-Termination.** A few thousand years before the Termination *N. pachyderma* sin gradually began to decrease at Site U1314, and the subpolar species (*N. pachyderma* dex, *G. inflata* and *G. bulloides*), *T. quinqueloba* and Factor 3 increased indicating that the AF moved somewhat northwards while benthic $\delta^{18}O$ still continued increasing. In South Labrador Sea, Site 647 indicates that polar waters were gradually replaced by subpolar waters (Aksu et al., 1989). At Site 980 the subpolar species and *T. quinqueloba* also increased before the Termination but not in Site 984 (Wright and Flower, 2002). As shown in figure 4.5f the AF slightly retreated northwestwards and the NAC probably penetrated north of Site 980 bringing warmth and moisture to European mid-latitudes, which probably enhanced winter snow accumulation. During Terminations the AF moved northwestwards rather fast and subpolar-transitional assemblages settled in the North Atlantic. MIS 16 is the longest glacial period of the studied interval. In fact, the late glacial-Termination stage identified in Site U1314 for MIS 16 was the longest of the glacial periods studied (fig. 4.4). At the end of MIS 16 there was a long period in which the AF slightly retreated but conditions were still cold for transitional-subpolar fauna and only *T. quinqueloba* and *N. pachyderma* sin throve. Additionally during the Termination there was a small reversal in *N. pachyderma* sin abundance that was identified as well in Site 980 as a Younger Dryas-like period (Wright and Flower, 2002).

It is worth mentioning the case of MIS 15 (fig. 4.4). Based on the LR04 stack (Lisiecki and Raymo, 2005) this interglacial period was divided into two interglacial substages (MIS 15.3 and 15.1) separated by a glacial substage (MIS 15.2). During the second stage of glaciation at MIS 15.2 ice sheets melted rapidly and a small deglaciation took place. Subsequently, during MIS 15.1 mean annual temperatures were slightly colder than during the early interglacial periods and *T. quinqueloba* percentages were high suggesting colder winters and, hence, a southern position of

the AF like in the late stage of interglacial periods. Data from Sites 984, 980, 646 and 647 support this position of the AF. In conclusion, MIS 15.1 does not present the early stage of interglacial periods and directly began with the second stage.

## 6. Summary and conclusions

The high resolution of the planktic foraminifer assemblages of Site U1314, their factor analysis, and additional planktic foraminifer and diatom data from other subpolar North Atlantic sites allowed us to track the migrations of the AF over the studied interval (ca. 800-400 ka) and, in turn, record the paleoceanographic changes of North Atlantic surface water. Each climatic cycle has been divided in five stages attending to ice volume, AF position and the distribution of surface water masses.

During the early interglacial stages Site U1314 was mainly influenced by the NAC (fig. 4.5a). The data from the North Atlantic sites analysed suggests that the AF position was similar to present day and, hence, we assume that the PF was in a similar position as well. The NAC flowed across the subpolar North Atlantic as a broad current displacing the subpolar gyre westwards. The NAC waters, warm and with high salinity, reached the Labrador Sea, via the Irminger current, and the NGS where they cooled and sank to generate NADW. This situation allowed a great transport of heat and moisture to high latitudes maintaining the AF further north in the NGS and in the Labrador Sea.

During the late interglacial stages SST and *N. pachyderma* sin and *T. quinqueloba* abundances indicate that the AF gradually moved southeastwards and winters cooled whereas benthic $\delta^{18}O$ records suggest the ice sheets were not growing. The Arctic waters expanded, particularly in the Labrador Sea where it is likely that a decrease in deep water formation weakened the Irminger current (fig. 4.5b). As a consequence the subpolar gyre waters turned cool and fresh mainly influenced by the EGC. The NGS waters cooled due to severe winters but they got dense enough to sink and maintain the AMOC active or even stronger (Alonso-Garcia et al., submitted; Wright and Flower, 2002) due to the colder temperature of the water. NADW produced during these periods got gradually colder, particularly at the end of the interglacial periods, and contributed to deep ocean cooling (Alonso-Garcia et al., submitted).

During the first stage of glacial periods the AF was southwards of all sites but 980, which was near the AF but in the Atlantic waters (fig. 4.5c). The NAC flowed as a narrow current over the eastern North Atlantic but still reached the NGS generating NADW. Almost all the Labrador Sea was perennially sea ice covered which prevented NADW formation at this area. Since NADW

was only generated in the NGS, the decrease in deep water volume production might gradually weakened the AMOC to some extent.

The second stage of the glacial periods began with the first ISCE (Alonso-Garcia et al., submitted). As a result of the iceberg and melt water discharges the AMOC was disturbed and deep water convection at the NGS slowed down. The reduction in the deep water formation led to a decrease in the NAC flow and, in turn, enhanced the NGS cooling, triggering perennial sea ice coverage. During the coldest periods seasonal sea ice was widespread through the subpolar North Atlantic and the AF was south of all the sites mentioned but 980, which was mostly near the AF, and the PF was south of Iceland but north of Site U1314 (fig. 4.5d). Convection may have occurred between the Polar and Arctic fronts, like nowadays in the NGS, but the water was not dense enough to sink deeply and GNAIW was generated. However, during this stage the AF fluctuated at each ISCE. During the warm phase of the ISCE, the NAC was reinforced and for a few thousand years Atlantic waters prevailed at Site U1314 and 980, indicating that the AF shifted northwards of these sites for short intervals (fig. 4.5e).

At the late glacial periods the AF started to move northwards (fig. 4.5f) and Arctic waters were gradually replaced by Arctic front waters at the southernmost Sites (U1314, 980 and 647). During Terminations the AF moved northwestwards and rapidly reached a position similar to present. The NAC flowed again across the North Atlantic to highest latitudes bringing warm a high salinity water to the NGS and the Labrador Sea. Deep water convection was resumed and, hence, the AMOC was activated.

# CAPÍTULO 5.

## MID-PLEISTOCENE SEA SURFACE TEMPERATURES, SEASONALITY AND SEAWATER $\delta^{18}O$ CHANGES IN THE NORTHERN NORTH ATLANTIC SITE U1314

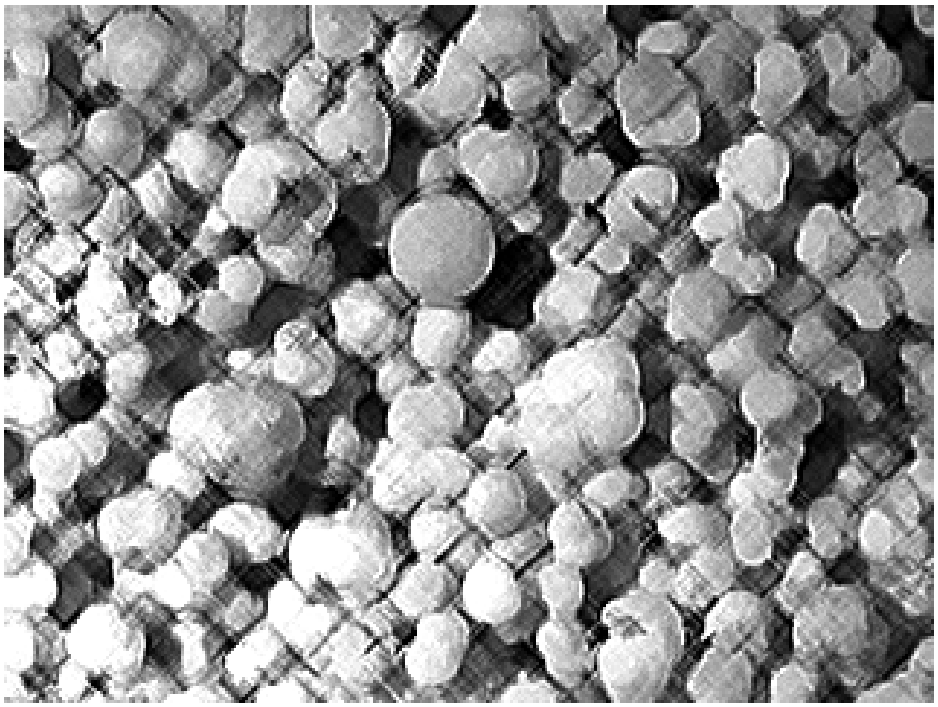

# 5. MID-PLEISTOCENE SEA SURFACE TEMPERATURES, SEASONALITY AND SEAWATER $\delta^{18}O$ CHANGES IN THE NORTHERN NORTH ATLANTIC SITE U1314

Montserrat Alonso-Garcia[1]*, Francisco J. Sierro[1], Isabel Cacho[2], Michal Kucera[3] and José A. Flores[1]

1 Department of Geology (Paleontology), Faculty of Science, University of Salamanca, Pza. de la Merced s/n, 37188 Salamanca, Spain
2 Department of Stratigraphy, Paleontology and Marine Geosciences, Faculty of Geology, University of Barcelona, Martí i Franquès s/n, 08028 Barcelona, Spain
3 Institute of Geosciences (Micropaleontology), University of Tübingen, Sigwartstrasse 10, DE-72076 Tübingen, Germany

*Corresponding author. Department of Geology (Paleontology), Faculty of Science, University of Salamanca, Pza. de la Merced s/n, 37188 Salamanca, Spain. Tel. +34 923 294497; Fax +34 923 294514. E-mail address: montseag@usal.es (M. Alonso-Garcia).

**Abstract**

Paleotemperatures of the subpolar North Atlantic Site U1314 (56º 21.8' N, 27º 53.3' W) from ~800 to 400 ka were calculated using Mg/Ca paleothermometry in *N. pachyderma* sin and transfer functions for planktic foraminifer assemblages. We suggest that Mg/Ca paleotemperatures during interglacials reflect winter temperatures because *N. pachyderma* sin lives either during the winter or in the deep waters with remnant winter temperatures. However, after glacial inceptions the Arctic waters influenced Site U1314 and Mg/Ca paleotemperatures reliability decreased. The ~3 ºC difference between winter ANN and Mg/Ca paleotemperatures during interglacial periods can be a consequence of problems with the reconstruction methods because neither of them produced temperatures similar to the present temperatures at Site U1314.

The $\delta^{18}O$ records of *N. pachyderma* sin and dex allowed us to infer surface water conditions and seasonality, particularly during interglacial periods when *N. pachyderma* sin reflects winter conditions and *N. pachyderma* dex summer conditions. The difference between *N. pachyderma* sin and dex $\delta^{18}O$ records during MIS 15, 11 and during the interstadials indicates that winter and summer conditions were very different and strong thermal stratification was developed during the summer. Conversely, during MIS 17 and 13 more similar $\delta^{18}O$ values were recorded. We suggest that enhanced summer-fall winds partially prevented summer stratification during these periods lowering the seasonal differences in surface water temperatures.

Seawater $\delta^{18}O$ was reconstructed using *N. pachyderma* sin and dex $\delta^{18}O$ records and the paleotemperature reconstructions. Major changes in $\delta^{18}O_w$ were recorded at Terminations, glacial inceptions and abrupt Arctic front shifts. During Terminations the fresh water input owing to iceberg discharges and ice sheets melting produced short and abrupt falls of $\delta^{18}O_w$. At glacial inceptions the influence of Arctic waters at Site U1314 lowered $\delta^{18}O_w$. Similar changes took place associated with the first ice sheet collapse events of glacial periods. Many of the ice-rafting events were not associated with strong depletions in $\delta^{18}O_w$ at Site U1314.

**Keywords**: Subpolar North Atlantic, planktic foraminifers, Mg/Ca, transfer functions, $\delta^{18}O$.

## 1. Introduction

Transfer functions have been used to calculate SST since the 1970s and are based on the assumption that planktic foraminifer assemblages reflect SST and their ecology remained steady through time, at least for recent times (Hutson, 1980; Imbrie and Kipp, 1971; Prell, 1985). The accuracy of these calculations depends on the coverage of modern samples dataset and on the equations utilized. Modern datasets improved the coverage of the oceans, which led to better understanding of modern assemblages (Barrows and Juggins, 2005; Hayes et al., 2005; Kucera et al., 2005; Pflaumann et al., 1996). The profitability of transfer functions was widely demonstrated with the Last Glacial Maximum (LGM) reconstruction of the CLIMAP Project (1976, 1981) and the subsequent upgrades with the EPILOG (Mix et al., 2001), GLAMAP (Pflaumann et al., 2003; Sarnthein et al., 2003) and MARGO (Kucera et al., 2005; Members, 2009) reconstructions.

The relationship between the magnesium content of biogenic carbonates and temperature was discovered in the early 20$^{th}$ century (Clarke and Wheeler, 1922). However, it was not until late 1990s when magnesium relationship was profitably used in paleoclimatology. Calibrations have been improved using culturing experiments (Lea et al., 1999; Mashiotta et al., 1999; Nürnberg et al., 1996; von Langen et al., 2005), sediment trap samples (Anand et al., 2003) and core top samples (Dekens et al., 2002; Elderfield and Ganssen, 2000; Lea et al., 2000; Rosenthal et al., 1997). In addition cleaning techniques have been reassessed (Barker et al., 2003; Martin and Lea, 2002; Pena et al., 2005; Rosenthal et al., 2004). Despite all the progress, paleotemperature calibrations using *N. pachyderma* sin in the northern North Atlantic still remain uncertain owing to the steep temperature and salinity gradients in between Polar, Arctic and Atlantic surface water masses (Bauch et al., 2003; Kozdon et al., 2009; Simstich et al., 2003).

Oxygen isotopes were used as well to reconstruct paleotemperatures, first with molluscs (Epstein et al., 1953) and later with planktic foraminifers (Emiliani, 1955). Shackleton (1967) pointed out that $\delta^{18}O$ in calcite primarily reflected the $\delta^{18}O$ of seawater (as a result of changes in ice volume and to a lesser extent of the evaporation-precipitation balance) and thus paleotemperature reconstructions done before must have been reevaluated. Recently Mg/Ca analyses in combination with oxygen isotopes were used to reconstruct SST and seawater $\delta^{18}O$ (Flower et al., 2004; Lea et al., 2000; Mashiotta et al., 1999; Meland et al., 2006; Pena et al., 2008).

In this paper we used the North Atlantic IODP Site U1314 sediments to compare the results of paleotemperature reconstructions based on two methods, Mg/Ca ratios and planktic foraminifer census counts, through several glacial-interglacial cycles of the Mid-Pleistocene (ca. 800-400 ka). Temperature calculations were significantly different in some intervals. We used stable oxygen isotopes of *N. pachyderma* sin and *N. pachyderma* dex and the Arctic front shifts reconstruction (Alonso-Garcia et al., submitted, see chapter 4) to asses the reliability of the different methods and

to investigate the possible environmental causes for different temperature results. Furthermore, once the paleotemperature proxies were assessed we reconstructed seawater $\delta^{18}O$ from MIS 19 to 11.

## 2. Material and methods

IODP Site U1314 is located in southern Gardar drift (56º 21.8' N, 27º 53.3' W), at 2820 m water depth (fig. 5.1). Nowadays this site is placed in the warmer side of the subpolar gyre, where the North Atlantic Current (NAC) supplies warm and saline waters (Hansen and Østerhus, 2000; Simstich et al., 2003; Tomczak and Godfrey, 1994). However, the oceanographic conditions of the North Atlantic considerably changed through glacial-interglacial cycles. As a result during colder intervals the Arctic Front moved southwards and the northern North Atlantic was under the influence of the cold and lower salinity Arctic waters (Wright and Flower, 2002); Alonso-García et al., submitted b, see chapter 4).

Sediment at this site is mostly composed of calcareous nannofossils and clay. However, in

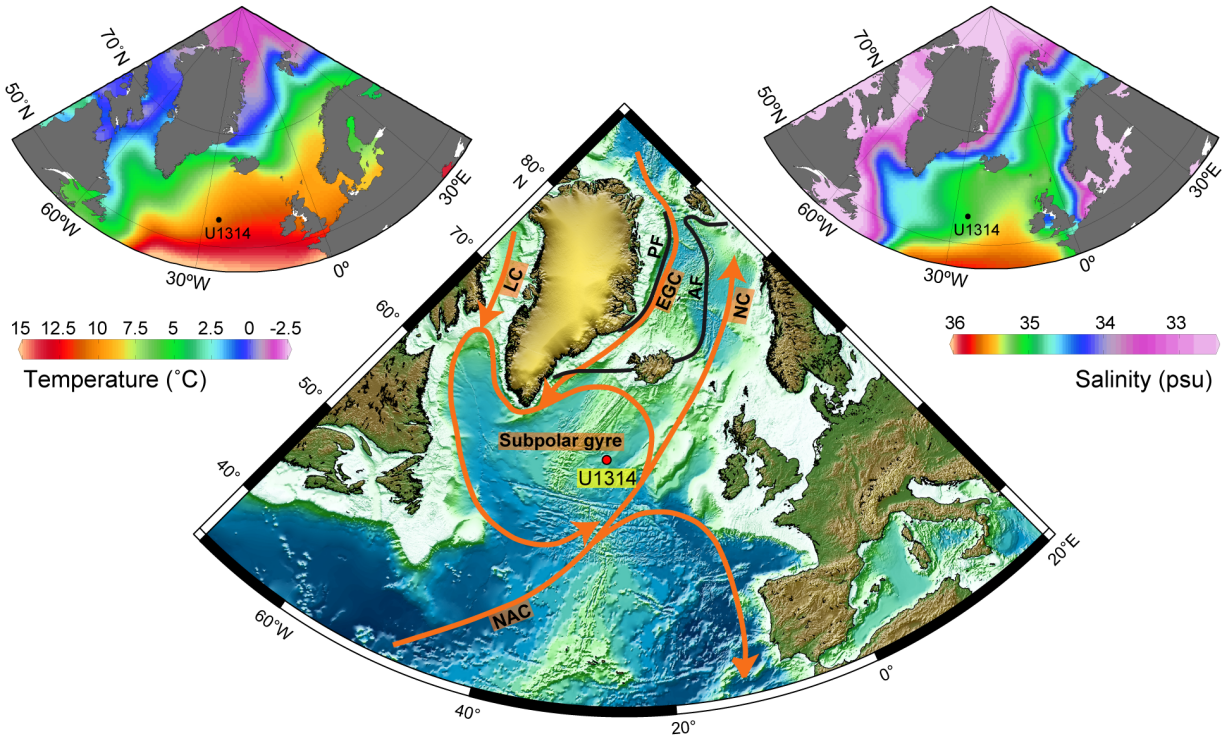


Fig. 5.1. Location of the IODP site U1314. Orange arrows in the middle map represent main surface currents according to Schmitz and McCartney (1993). Present location of the Arctic and Polar fronts (AF and PF) was sketched according to Swift (1986). Left and right maps depict subpolar North Atlantic temperature and salinity at present. The map in the middle was provided by Integrated Ocean Drilling Program (IODP), temperature and salinity maps were performed with ODV (Schlitzer, 2009) using the World Ocean Atlas 2005 (Locarnini et al., 2006).

the sand fraction, well preserved planktic foraminifers are the dominant component, with lower proportions of benthic foraminifers, ostracodes, siliceous microfossils and IRD (Channell et al., 2006). Each sample was sieved under water with a 63 μm mesh to eliminate clay and fossil ooze. Then the sample was dry-sieved to separate two fractions, 63-150 μm and over 150 μm. Planktic foraminifer census counts and picking for the trace elements and oxygen isotopes analyses were focused on the coarser fraction. Samples were taken every 8 cm except for the *N. pachyderma* sin oxygen isotope record which was sampled every 4 cm. Following the age model proposed in Alonso-Garcia et al. (submitted a, see chapter 3) the sampling interval represents an average resolution of 1100 years for trace elements analysis, census counts and *N. pachyderma* dex oxygen isotopes and 550 years for *N. pachyderma* sin oxygen isotopes.

### 2.1. Planktic foraminifer stable oxygen isotopes

Here we present the analyses of two planktic species *N. pachyderma* sin and *N. pachyderma* dex. On average 15 specimens of *N. pachyderma* sin were picked from the fraction between 200-250 μm and 12 specimens of *N. pachyderma* dex from the 250-300 μm fraction were needed. Prior to isotopic analyses, the picked specimens of each sample were gently crushed between two glass slides under the stereomicroscope to open chambers and facilitate cleaning of adhering sediment. The crushed shell fragments were ultrasonicated for 20 seconds in methanol, which was then removed to eliminate clays and other contaminating particles. Finally, the samples were air-dried overnight into the gas hood to avoid contamination. Planktic stable isotope analyses were carried out using a Finnigan MAT 252 mass spectrometer linked to a CarboKiel-II carbonate preparation device at the University of Barcelona. International standard NBS-19 was used with an external reproducibility better than 0.06 ‰ for $\delta^{18}O$. Results are reported with respect to the Vienna Pee Dee Belemnite (VPDB) standard scale (Coplen, 1996).

### 2.2. Mg/Ca paleothermometry

For trace elements analyses 65 specimens of *N. pachyderma* sinistral between 200 μm and 250 μm were taken from each sample. Specimens were gently crushed between two glasses to open chambers and facilitate cleaning. They were cleaned following the trace elements procedure of Pena et al., (2005) but with a reduction of half time in the reductive step. This modification was introduced in the procedure because foraminifers were very susceptible to dissolution during this step owing to their small size and half time of the reductive cleaning was enough to remove the Mn-Fe-oxide coatings.

The first step of the cleaning procedure was the clay removal. It entails washing and softly sonicating the samples with ultrapure water and methanol. Special attention was paid during this step because the site is in the subpolar North Atlantic and the low Mg/Ca ratios of foraminifers from cold water areas are more prone to significant contamination by clay and IRD (Barker et

al., 2003). After this, a reductive treatment was applied to eliminate Mn-Fe-oxide coatings using a reagent composed of hydrous hydrazine in a citric acid-ammonia buffer. Mg content in this oxide coatings is generally low (Barker et al., 2003), but we decided to use the reductive step because in samples from cold areas Mg contamination by coatings might strongly disturb Mg/Ca ratios. In order to remove organic matter, an oxidative step was done with an alkali-buffered solution of $H_2O_2$. Finally, a weak acid leaching was applied. Before doing the trace elements analyses, samples were dissolved adding 400 µl of ultra-pure 1 % $HNO_3$ + Rh. The analyses were performed on a Perkin-Elmer Elan-6000 Inductively Coupled Plasma Mass Spectrometer (ICP-MS). Calcium concentrations typically were in the ranges of 10–50 ppm which did not make a calcium matrix correction necessary. Standard solution prepared from high purity standards was routinely analyzed every four samples and produced a mean accuracy of 0.04 % and a precision of 2.60 %. Systematically, Mn/Ca and Al/Ca ratios were monitored in order to identify any potential contamination problems in samples. Additionally, to ensure clean conditions during the sample preparation, procedure blanks were measured for each sample batch. Blanks yielded in all cases values at the detection limit. Both cleaning and analytical measurements were performed in the University of Barcelona (Spain).

### 2.3. Transfer Functions

Sea surface temperatures (SST) were as well calculated using transfer functions for planktic foraminifer assemblages. Before counting, each sample was split, using a microsplitter, as many times as necessary until the remaining aliquot contained roughly 400 planktic foraminifer specimens (300 at minimum).

The calibration data set used for the transfer functions is the North Atlantic planktic foraminifer database, compiled by the MARGO project (Kucera et al., 2005), which includes 862 coretop samples. Following Kucera et al. (2005) recommendations we used this specific data set in order to minimise the "noise" in the paleotemperature reconstruction triggered by the regional distribution of different planktic foraminifer genetic types (cryptic species). Modern temperatures from the calibration data set were extracted from the World Ocean Atlas version 2 (WOA, 1998) at 10 m water depth. SST can be calculated for summer (July-August-September), winter (January-February-March) and even the annual mean.

#### 2.3.a. Modern Analog Technique (MAT)

MAT, introduced by Hutson (1980), allows us to reconstruct environmental variables comparing a fossil faunal assemblage with a calibration data set. MAT identifies for a sample given the best analogs in the calibration dataset using the squared chord distance (Prell, 1985). This technique calculates a similarity index that shows the similarity coefficient of the best analog used and it is used to determine if the temperature calculated for the fossil sample can be trusted

(samples below 0.8 are less reliable). Since the database is large and the samples are widely distributed, we used the 10 best analogs for the paleotemperature estimation. Paleotemperatures were calculated as an average of the temperatures associated with those 10 best analogs weighed by the similarity coefficient.

### 2.3.b. Artificial Neural Networks (ANN)

This transfer function technique is based on a back propagating artificial neural network (ANN) (Malmgren et al., 2001) trained on the North Atlantic MARGO dataset (Kucera et al., 2005). The same set of ten neural networks as in Kucera et al. (2005) was used in this study, providing 10 different temperature reconstructions for summer, winter and mean annual. The average values of these 10 temperatures were used for the final reconstruction and the standard deviation (StDev) of the ten networks was used to determine how well a fossil sample is represented in the calibration data set.

## 3. Results

### 3.1. Planktic foraminifer stable oxygen isotopes

Oxygen isotopes of *N. pachyderma* sin and dex show similar trends across glacial-interglacial cycles (fig. 5.2). However their values show a strong offset during interglacial periods, particularly during MIS 11 and 15 when the values of both species show a difference of even 1 ‰. *N. pachyderma* sin $\delta^{18}O$ values range between 1.3-4.7 ‰ while *N. pachyderma* dex between 1 and 4.7 ‰; and consequently isotopic depletions at Terminations are larger in the *N. pachyderma* dex record (up to 3.1 ‰).

In order to obtain the variations in the $\delta^{18}O$ of the sea water ($\delta^{18}O_w$) we applied the equation of Shackleton (1974) using both Mg/Ca and ANN temperatures, to remove the temperature effect. The ice volume sign was subtracted using the ice sheet contribution to the marine isotope signal curve, relative to present, from Bintanja and van de Wal (2008). Salinity was calculated with the GEOSECS (1987) equation from $\delta^{18}O_w$ curves.

### 3.2. Mg/Ca paleothermometry

Mn/Ca and Al/Ca ratios were measured to monitor contamination from diagenetic and detrital sources. Correlation coefficient between Mg/Ca and Al/Ca (fig. 5.3a) is very low ($R^2$=0.016), indicating that clay contamination can be rejected. Correlation coefficient of Mg/Ca and Mn/Ca (fig. 5.3b) is higher but still not significant ($R^2$=0.417). Mn/Ca values are below 0.5 mmol/mol and, thus, they are relatively low compared with samples proved to be contaminated by Mn oxides and Mn-rich carbonates (> 1 mmol/mol). Considering these results we suggest that Mg contamination associated to Mn coatings does not interfere with our results.

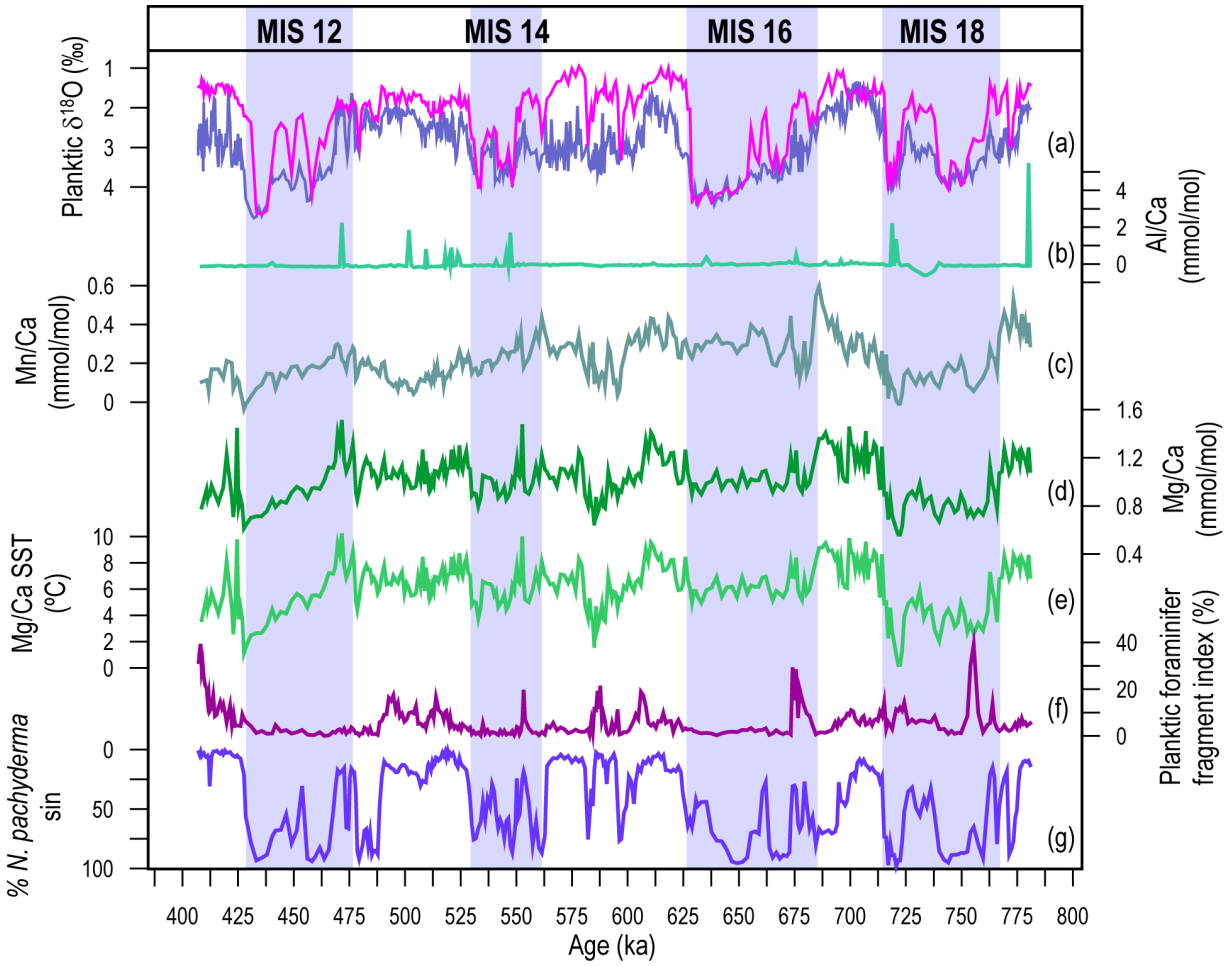


Fig. 5.2. Trace elements and stable oxygen isotopes. (a) Stable oxygen isotopes performed on *N. pachyderma* sin (blue line) and *N. pachyderma* dex (pink line). Trace elements ratios: (b) Al/Ca; (c) Mn/Ca; (d) Mg/Ca. (e) Sea surface temperature reconstruction based on Mg/Ca ratios. (f) Planktic foraminifer fragmentation index shows that dissolution was not significant to modify Mg/Ca ratios. (f) *N. pachyderma* sin abundance. Marine isotope stages (MIS) are indicated on the top, and vertical bars show the duration of glacial periods.

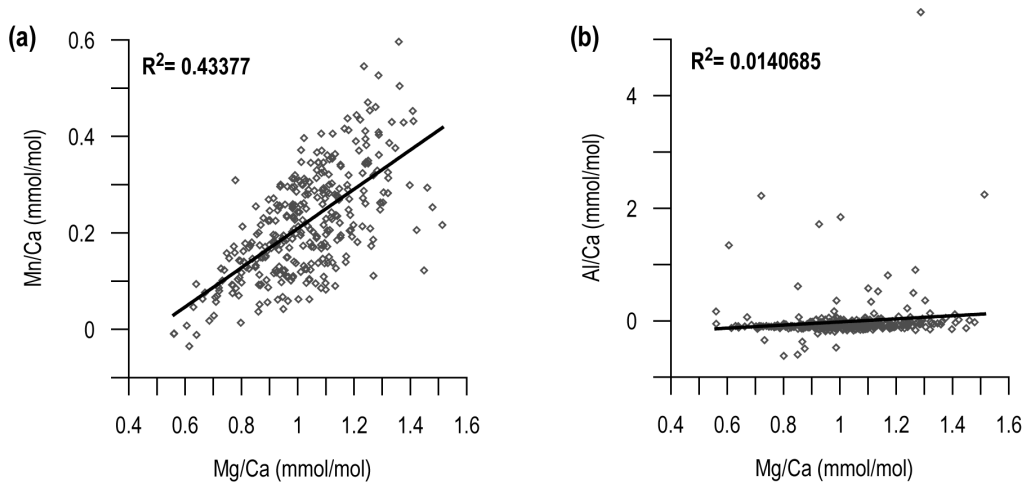


Fig. 5.3. Low correlation between Mg/Ca results and Mn/Ca (a) and between (b) Mg/Ca and Al/Ca indicates no clay and oxide coatings contamination was present in the foraminifer tests.

Mg/Ca ratios range from 0.56 and 1.51 mmol/mol, with minimum values during glacial periods. Paleotemperatures were reconstructed with the equation put forward in Mashiotta et al. (1999) based on *N. pachyderma* sin from North Atlantic core tops (Nürnberg, 1995). Temperatures based on Mg/Ca ratios range from 0.2 and 10.24 ºC. It is remarkable that during the glacial period MIS 16 Mg/Ca ratios and their associated temperatures were anomalously high for a major glacial period.

### 3.3. Transfer functions

Summer, winter and mean annual SST calculated with ANN and MAT are rather similar (fig. 5.4) and there is a strong linear relationship ($R^2$=0.963) between both SST records (fig. 5.5a). However, ANN produced slightly warmer temperatures, particularly for summer and during the warmer intervals. Summer ANN results range between 18.36 and 3.06 ºC whereas summer MAT results range between 17.23 and 1.90 ºC. For winter ANN SST fluctuate between 13.18 and -0.23 ºC and MAT SST between 11.42 and -0.79 ºC. And the annual mean SST reconstruction range between 15.17 and 0.83 ºC with ANN and between 13.86 and 0.17 ºC with MAT. The Root Mean Square Error of Prediction (RMSEP) for the MAT and ANN was calculated in Kucera et al. (2005) and the values for winter summer and annual estimations are shown in table 5.1. Maximum differences between both methods are around 3 ºC, however the mean difference is less than 1ºC for all the temperatures calculated (summer, winter and annual, see table 5.1).

Present mean annual SST at 10 m depth at Site U1314 is around 10.5 ºC (fig. 5.4), which is slightly lower than the mean annual SST calculated with ANN for the interglacial periods (fig. 5.4). Present winter temperature at 10 m depth at Site U1314, around 8 ºC (Locarnini et al., 2006), is also slightly lower than ANN and MAT paleotemperatures (fig. 5.4). However, present summer temperature at 10 m depth is 12 ºC (Locarnini et al., 2006), which is significantly lower than ANN paleotemperatures, often more than 4 degrees lower.

The low correlation between ANN SST and their standard deviation (Stdev) and between MAT SST and their Stdev (fig. 5.5) indicates that the accuracy of the prediction is not depending on the temperature and therefore cold and warm temperatures present high and low standard deviations. The correlation between similarity index and MAT SST is low as well, but it shows that better analogs were found for low temperature reconstructions, though analogs are rather good for all the samples. It is not clear how far back in time can we use the transfer functions since we don't know for how long the species ecology has persisted. Nevertheless, we argue that the use of transfer functions for the studied interval is reliable because the assemblages of Site U1314 samples and the North Atlantic dataset are very similar (similarity index above 0.9 for most of the samples, see fig. 5.4 and 5.5).

Since ANN and MAT paleotemperatures are rather close, hereafter we only use the ANN temperatures to simplify the comparison with Mg/Ca paleothermometry.

## 4. Discussion

### 4.1. Preservation

Preservation in the studied interval was analysed using the planktic foraminifer fragment index (fig. 5.4), which represents in percentage the amount of fragments respect to the total amount of foraminifers plus fragments (Thunell, 1976). Assemblages began to suffer modifications due to dissolution over a planktic foraminifer fragment index of 40 % (Miao et al., 1994). Here, the planktic foraminifer fragment index is generally lower than 20 %, indicating very good preservation in the samples, except some little intervals where dissolution increased but hardly reaches 40 %. Therefore, we can assume that the assemblages studied were not modified by dissolution and they are a suitable proxy for transfer functions.

Since Mg-calcite presents preferential dissolution respect to normal calcite (Brown and Elderfield, 1996), Mg/Ca paleothermometry may be affected by dissolution as well. Our Mg/

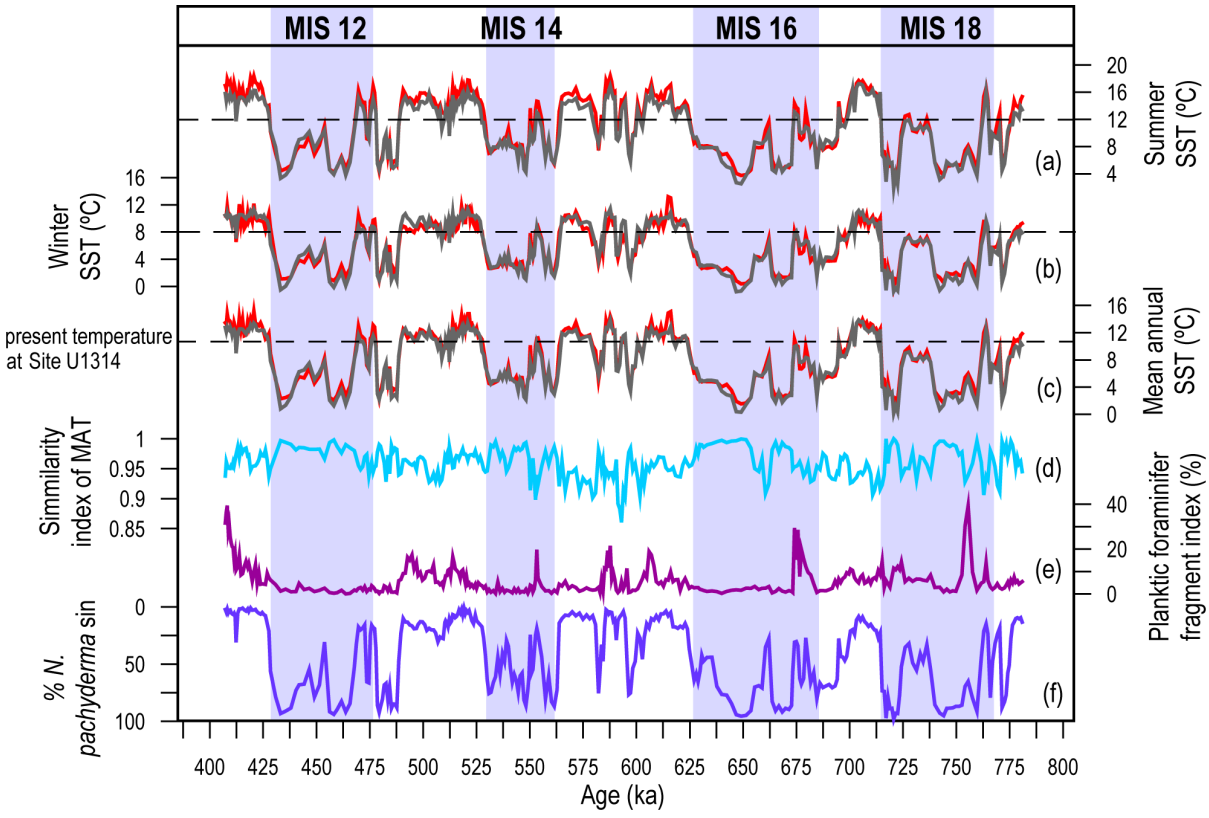


Fig. 5.4. Transfer functions paleotemperatures for summer (a), winter (b) and the mean annual (c), calculated with ANN (red line) and MAT (grey line). (d) Simmilarity index of MAT, values above 0.8 indicate high similarity between the samples studied and the dataset. (e) Planktic foraminifer fragmentation index indicates that dissolution is negligible. (f) *N. pachyderma* sin abundance shows that temperatures are controlled to a large extent by the presence of this polar species. Marine isotope stages (MIS) are indicated on the top, and vertical bars show the duration of glacial periods.

| | Summer | Winter | Annual |
|---|---|---|---|
| MAT RMSE (ºC) | 1.42 | 1.32 | 1.26 |
| ANN RMSE (ºC) | 1.14 | 0.96 | 0.96 |
| Max ANN SST (ºC) | 18.36 | 13.18 | 15.17 |
| Max MAT SST (ºC) | 17.23 | 11.42 | 13.86 |
| Min ANN SST (ºC) | 3.06 | -0.23 | 0.83 |
| Min MAT SST (ºC) | 1.9 | -0.79 | 0.17 |
| Max difference (ºC) | 3.48 | 3.13 | 2.99 |
| Mean difference (ºC) | 0.94 | 0.73 | 0.68 |

Table 5.1. Sea surface temperatures prediction errors in ºC for both of the transfer functions methods, Modern Analog Technique (MAT) and Artificial Neural Networks (ANN) after Kucera et al. (2005), maximum and minimum temperatures calculated with both methods and the maximum and mean difference between both methods.

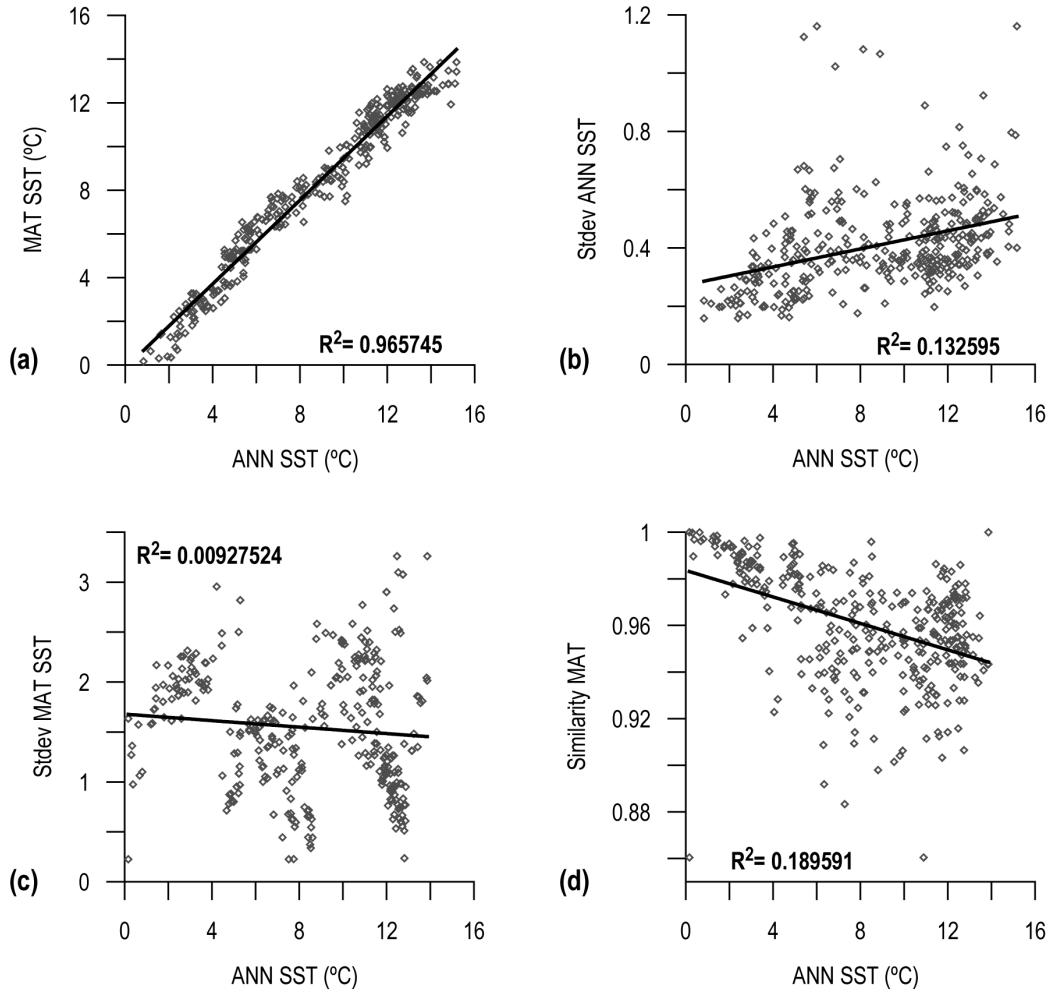


Fig. 5.5. (a) SST generated by ANN and MAT present strong linear relationship ($R^2$=0.963) because their results are rather similar. (b) The low correlation between ANN SST and their standard deviation and between (c) MAT SST and their standard deviation indicates that the accuracy of the prediction is not depending on the temperature. (d) Correlation between similarity index and MAT SST is low but better analogs are found for lower temperature samples.

Ca record and the planktic foraminifer fragment index do not show covariance (fig. 5.2) and present very low correlation (fig. 5.6). Therefore, we argue that the effect of dissolution in planktic foraminifer Mg/Ca ratios was negligible and, in turn the results of Mg/Ca paleothermometry were not modified by preservation.

### 4.2. Differences between paleotemperature proxies

The optimum habitat of *N. pachyderma* sin is in high latitude environments between -1 and 8 ºC (Bauch et al., 1997; Bé, 1977; Pflaumann et al., 2003; Tolderlund and Bé, 1971) and near the pycnocline within a wide depth range, from surface waters to 100-200 m (Carstens and Wefer, 1992; Nyland et al., 2006; Simstich et al., 2003; Stangeew, 2001). At present *N. pachyderma* sin thrives in different seasons at different areas (Fraile et al., 2009a). At the latitude of Site U1314 area *N. pachyderma* sin thrives during winter-spring (Fraile et al., 2009a; Fraile et al., 2009b; Reynolds and Thunell, 1985) when there is no thermal gradient in the water column. In the NGS *N. pachyderma* sin calcifies during the summer but it has been related to the cold stratified waters below the thermocline and, therefore this species records winter conditions (Nyland et al., 2006). In summary, although *N. pachyderma* sin peaks at different seasons depending on the latitude, this species always records winter temperatures.

Since Mg/Ca paleotemperatures were reconstructed with *N. pachyderma* sin, they reflect winter conditions at probably 100-200 m depth. Nevertheless, Mg/Ca paleotemperatures during interglacial periods are slightly colder than present winter temperatures at Site U1314 (fig. 5.7), about 8 ºC (Locarnini et al., 2006). This difference cannot be accounted by the water depth in which *N. pachyderma* sin lives because the temperature for the first 200 m depth is the same during the winter (Locarnini et al., 2006). The Mid-Pleistocene Mg/Ca temperatures can be slightly colder than during recent temperatures due to inaccuracies of the equation used to calculate paleotemperatures or just because during the studied interval winter temperatures were colder at least during interglacial periods.

SST estimates based on planktic foraminifer transfer functions have revealed lower reliability when summer temperatures are below 4-5 ºC (Pflaumann et al., 1996; Pflaumann et al., 2003) owing to the low planktic diversity at the "cold end" (Arctic and Polar waters). This effect must be accounted during the glacial periods when the Arctic waters expanded across the subpolar North Atlantic (Alonso-Garcia et al, submitted b, see chapter 4) but not during interglacial periods. ANN and Mg/Ca temperatures during interglacial periods (fig. 5.7) present similar trends but an average offset of 3 ºC was recognized. Winter temperatures of interglacial periods appear more constant in the Mg/Ca record (fig. 5.7), perhaps because ANN winter temperatures are biased by the spring, summer and fall components of the assemblage or because *N. pachyderma* sin prefers gradually deeper habitats with increasing SST, thus counterbalancing absolute temperature variations (Kozdon et al., 2009).

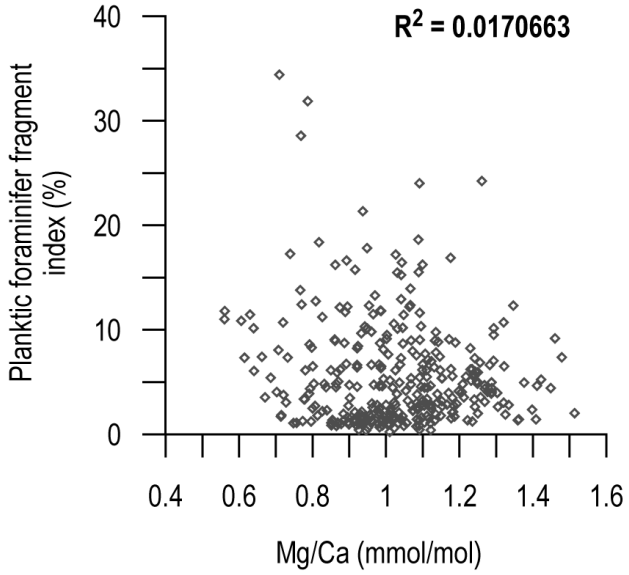


Fig. 5.6. Relationship between Mg/Ca ratios and planktic foraminifer fragmentation index shows lower correlation, indicating that dissolution was not controlling Mg content in the tests.

On the other hand during glacial periods Mg/Ca and ANN winter temperatures are mostly different in both trends and values. Similar values are only found during the warm phase of the first ice sheet collapse events of each glacial period (ISCE, Alonso-Garcia et al., submitted a, see chapter 3), in which near to interglacial temperatures were reached. Glacial ANN paleotemperatures calculated at Site U1314 might be slightly overestimated due to the "cold end" effect, as it was reported by Kucera et al. (2005) for the LGM reconstruction. Present Mg/Ca ratios from sites that are annually covered by sea ice are generally too high (Meland et al., 2006; Nürnberg, 1995) and the relationship between Mg/Ca ratio and temperature is poorly correlated or even inversed when summer temperatures are below 3 ºC, i.e. in Arctic and Polar waters (Kozdon et al., 2009). Additionally it has been suggested that Mg/Ca ratios increase with lower pH (Lea et al., 1999; Russell et al., 2004) and it has been proposed that the anomalously high Mg/Ca ratios in Arctic and Polar waters could be due to the low values of $[CO_3^{2-}]$ (Meland et al., 2006).

In summary, we suggest that during interglacial conditions, from the Termination to the expansion of Arctic waters nearby Site U1314 at glacial inceptions (Alonso-Garcia et al., submitted a and b, chapters 3 and 4), Mg/Ca winter temperatures are reliable though perhaps slightly colder respect to present temperatures. These periods are remarked with orange rectangles in figure 5.7. However, ANN paleotemperatures are warmer than present SST and it is difficult to know which paleotemperatures are more accurate. On the other hand from the glacial inceptions to Terminations Mg/Ca temperature reliability decreases because the influence of the Arctic waters at Site U1314 modified the Mg/Ca-temperature relationship generating inconsistencies between both paleotemperature reconstructions. During glacial periods we believe that transfer functions paleotemperatures are more accurate although perhaps warmer like it happened during interglacial periods.

### 4.3. Oxygen isotope differences between *N. pachyderma* dex and sin

Planktic oxygen isotopes follow the long-term trends of the benthic $\delta^{18}O$ record of Site U1314 (Alonso-Garcia et al., submitted a, see chapter 3). Oxygen isotope values were low during interglacial periods and progressively increased towards glacial periods, as ice volume increased, indicating that ice volume controlled the long-term changes in $\delta^{18}O$ values of the planktic foraminifers (fig. 5.8). The *N. pachyderma* sin and the benthic oxygen isotope records show lower amplitude changes in the abrupt millennial-scale climate events than the $\delta^{18}O$ record of *N. pachyderma* dex. Significant differences are observed not only between benthic and planktic records, but also between both planktic $\delta^{18}O$ records. The difference between the $\delta^{18}O$ values of both planktic species might be interpreted as a consequence of different interspecific vital effects (Bauch et al., 2003) but the fact that the difference between both species is not constant through time suggests that physico-chemical properties of seawater may have been involved in the variability of $\delta^{18}O$ values. The variable difference between the $\delta^{18}O$ records of *N. pachyderma* sin and *G. bulloides* in the Northeast Atlantic was attributed to changes in the seasons in which these species lived (according to this authors at present *N. pachyderma* sin calcifies in winter and *G. bulloides* in spring in the Northeast Atlantic) and/or to variations in the stratification of the water column (Dickson et al., 2008).

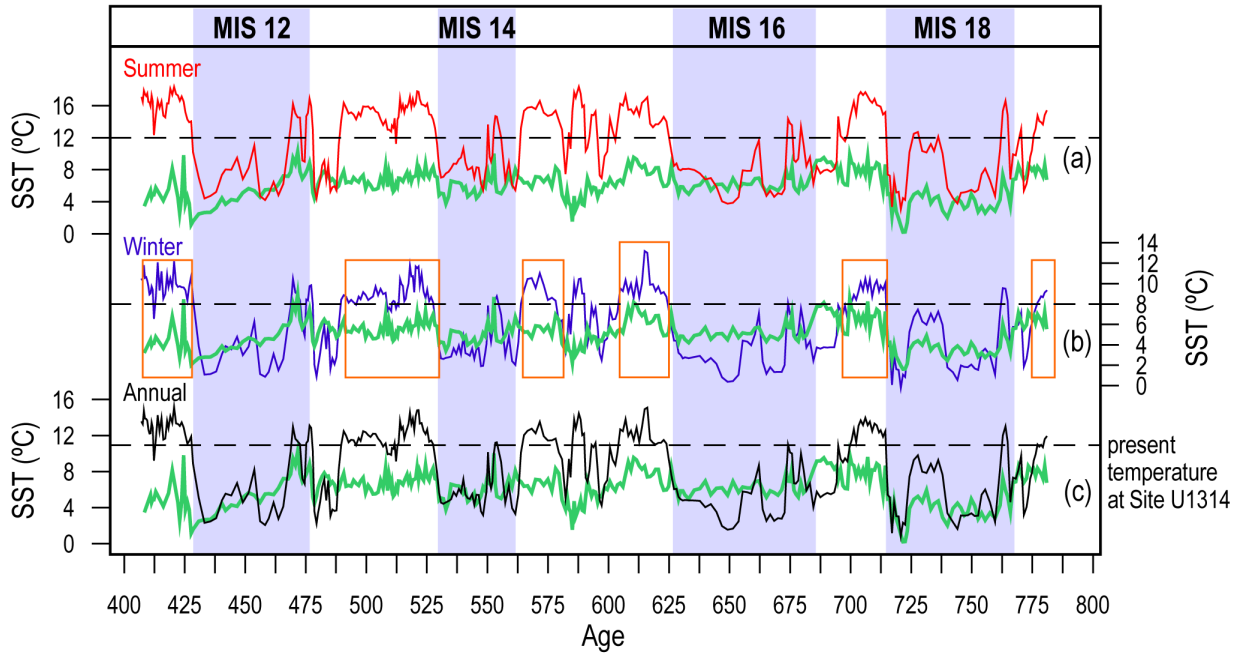


Fig. 5.7. Comparison between Mg/Ca temperatures (green line), calculated using Mashiotta et al. (1999) equation, and ANN summer (a), winter (b) and annual mean (c) temperatures. During interglacial periods Mg/Ca temperatures are similar to ANN winter temperatures although slightly colder (orange rectangles). Whereas during glacial periods Mg/Ca temperatures are similar to ANN annual temperatures but with several intervals of inconsistency either by colder or warmer Mg/Ca temperatures respect to ANN annual mean. Marine isotope stages (MIS) are indicated on the top, and vertical bars show the duration of glacial periods.

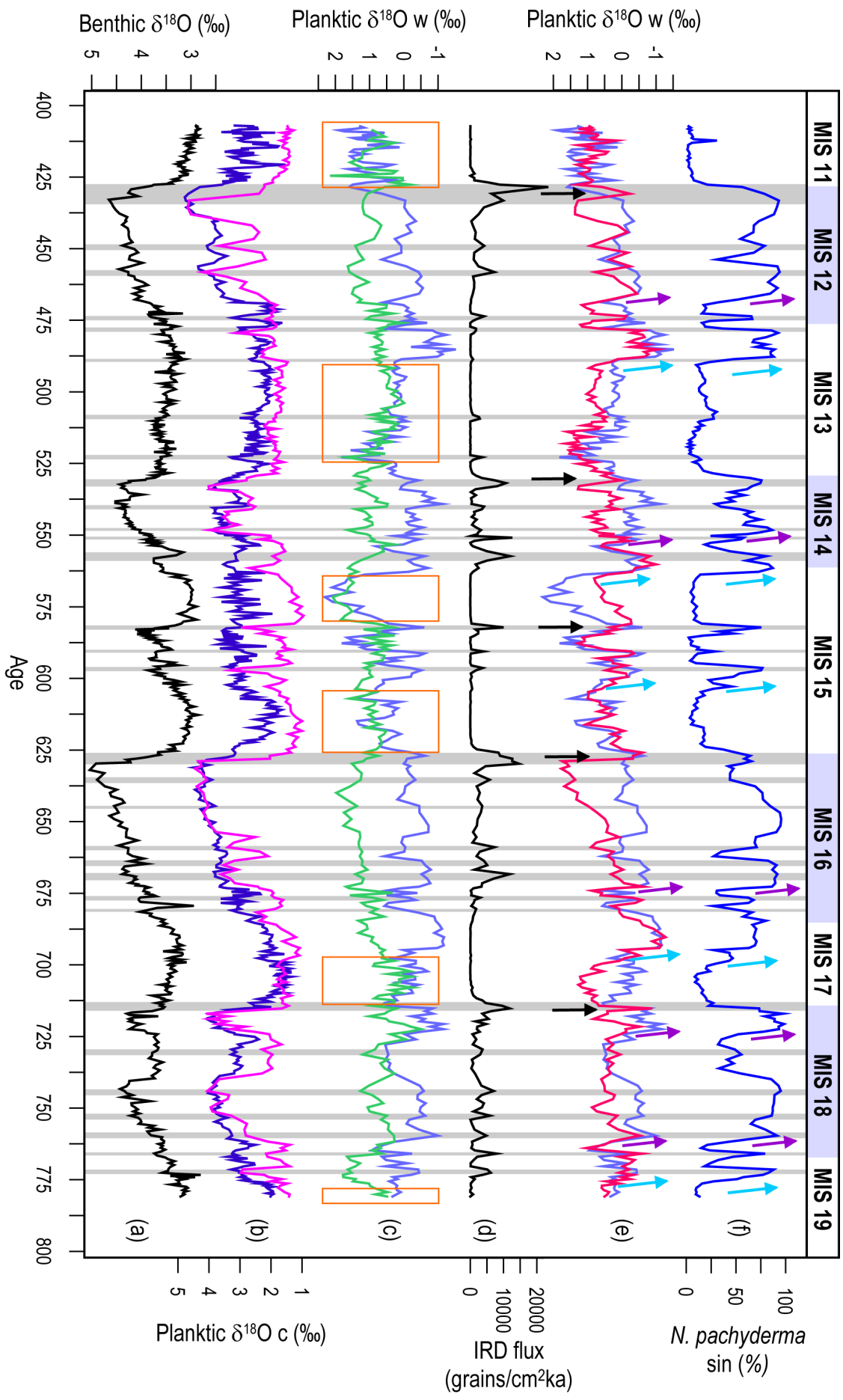
Benthic δ18O (‰)
Planktic δ18O w (‰)
Planktic δ18O w (‰)
Age
MIS 11
MIS 12
MIS 13
MIS 14
MIS 15
MIS 16
MIS 17
MIS 18
MIS 19
(a)
(b)
(c)
(d)
(e)
(f)
Planktic δ18O c (‰)
IRD flux
(grains/cm2ka)
N. pachyderma
sin (%)

Fig. 5.8. Reconstructions of $\delta^{18}O_w$, calculated using Shackleton (1974) equation. (a) Benthic $\delta^{18}O$ from site U1314 (Alonso-Garcia et al., submitted a, see chapter 3) as a reference for ice volume. (b) Original $\delta^{18}O_c$ of *N. pachyderma* sin (blue line) and *N. pachyderma* dex (pink line). (c) $\delta^{18}O_w$ calculated using *N. pachyderma* sin $\delta^{18}O_c$ and Mg/Ca temperatures plus 3 ºC (green line) and ANN winter temperatures (blue line). Orange rectangles show the interglacial intervals in which both $\delta^{18}O_w$ calculations are consistent. (d) IRD fluxes show the major intervals of ice-rafting, and possibly of fresh water input, which are also depicted as vertical grey bars. (e) $\delta^{18}O_w$ calculated using *N. pachyderma* sin $\delta^{18}O_c$ and ANN winter temperatures (blue line) and using *N. pachyderma* dex $\delta^{18}O_c$ and ANN annual mean temperatures (dark pink line). (f) *N. pachyderma* sin abundances show when the Arctic front migrated southwards (light blue and purple arrows) and as a consequence $\delta^{18}O_w$ decreased dramatically due to the influence of Arctic waters in the calcification of both species. Black arrows indicate the strong depletions in $\delta^{18}O_w$ during Terminations. Light blue arrows indicate depletions in $\delta^{18}O_w$ during glacial inceptions due to the expansion of Arctic waters, and purple arrows indicate subsequent Arctic front migrations that took place after interstadial events. Marine isotope stages (MIS) are indicated on the top.

In the area Site U1314 winter and spring temperature is nearly constant in the upper 200 m of the water column. Conversely, during summer, warming of surface waters results in strong stratification of the water column producing a vertical thermal gradient between the surface waters and the water immediately below the thermocline, which maintains the winter temperature. *N. pachyderma* sin lives near the pycnocline (Carstens and Wefer, 1992; Nyland et al., 2006; Simstich et al., 2003; Stangeew, 2001) reflecting the conditions of the winter (Nyland et al., 2006) whereas *N. pachyderma* dex lives preferably between 10-18 ºC, within the first 50-100 m, associated with the thermocline and deep chlorophyll maximum (Fairbanks et al., 1982; Reynolds-Sautter and Thunell, 1989, 1991), and it has been related to the warm and stratified surface waters of the summer-autumn in the Northeast Atlantic and the NGS (Chapman, 2010; Nyland et al., 2006; Schiebel and Hemleben, 2000; Schiebel et al., 2001). During the interglacial periodsof the studied interval *N. pachyderma* dex $\delta^{18}O$ values are generally lower than *N. pachyderma* sin $\delta^{18}O$ values. The differences between $\delta^{18}O$ values of both species are larger during the interglacial periods MIS 15, 11 and during the warm intervals of the glacial periods (interstadials). Since *N. pachyderma* sin reflects winter conditions and *N. pachyderma* dex summer conditions, seasonality appears to be the main factor controlling the differences between $\delta^{18}O$ values of both species during interglacial periods and during the interstadials.

The large difference between $\delta^{18}O$ values of *N. pachyderma* dex and sin during MIS 15, 11 and the interstadials (fig. 5.8) indicates strong temperature differences between winter and summer, and hence strong summer stratification. We suggest that strong seasonal changes may have occurred during MIS 15 and 11, particularly during MIS 15.1. Low winter temperatures were observed as well in the Mg/Ca paleotemperature record of MIS 15.1 and MIS 11 (fig. 5.7), and the high *T. quinqueloba* percentages of MIS 15.1 (Alonso-Garcia et al., submitted b, see chapter 4) suggest that winter and spring temperatures were low but the Arctic waters were still northwards of Site U1314. It is likely that winter temperatures were remarkably lower, especially during MIS

15.1, whereas summer and fall were particularly warm and the water column was strongly stratified. However, at MIS 17 $\delta^{18}O$ values of *N. pachyderma* dex were slightly higher than in MIS 15 or 11 (fig. 5.8) and very similar to *N. pachyderma* sin values, suggesting reduced summer temperatures during this period. Similar conditions were observed at MIS 13 with a small offset between *N. pachyderma* sin and dex $\delta^{18}O$ values. The low $\delta^{18}O$ values of *N. pachyderma* sin during MIS 17, MIS 15.1 and 13 suggest that winter temperatures were less cold. The higher winter temperatures of these periods are also supported by Mg/Ca paleothermometry (fig. 5.7). Hence, it appears that during MIS 17 and 13 seasonality was lower with less cold winters and less warm summers respect to MIS 15 and 11. The occurrence of mixing during the summer or a weaker stratification of the water column during MIS 17 and 13 might explain the low summer temperatures recorded by $\delta^{18}O$. A weaker stratification might be generated by anomalously stronger winds in the North Atlantic, particularly during the summer-fall, which avoided thermal stratification. Strong East Asian summer monsoon activity has also been reported at MIS 13 (Guo et al., 2009; Yin and Guo, 2008).

At glacial inceptions *N. pachyderma* sin $\delta^{18}O$ tend to higher values because of the Arctic waters influence, at least during the winter season. Winter and summer temperature differences increased at interstadials due to the increasing seasonality, except between 480-470 ka when winters appeared anomalously warmer and similar to summer conditions. During glacial periods, the $\delta^{18}O$ values of *N. pachyderma* sin and dex were very close. We cannot be sure if we analysed the real *N. pachyderma* dex or aberrant right-coiling *N. pachyderma* sin specimens because there were very few *N. pachyderma* dex and hence this similar $\delta^{18}O$ values of *N. pachyderma* sin and *N. pachyderma* dex might be attributed to the fact that all of them correspond to *N. pachyderma* sin. However, it is also possible that both species recorded similar $\delta^{18}O$ values because both species calcified in the same water masses contrary to present. During winter, sea ice covered the area of Site U1314 and foraminifers could not calcify under these conditions. When sea ice melted, during summer, it is likely that a lid of low saline waters might have prevented water mixing. We suggest that as a result of this strong stratification both species lived and calcified during summer and at similar water depths, in other words in the same water mass below the low saline water lid.

### 4.4. Seawater $\delta^{18}O$ ($\delta^{18}O_w$) variations

We calculated $\delta^{18}O_w$ variations using *N. pachyderma* sin and dex oxygen isotopes and our temperature reconstructions. *N. pachyderma* sin $\delta^{18}O$ record allowed us to reconstruct two different curves of $\delta^{18}O_w$, one with Mg/Ca paleotemperature and the other with the ANN reconstruction. As *N. pachyderma* sin reflects winter conditions we used the winter ANN paleotemperatures to make the $\delta^{18}O_w$ reconstruction shown in fig. 5.8c. The actual value of $\delta^{18}O_w$ is difficult to evaluate because of the 3 ºC difference between both paleotemperature proxies. In order to obtain more similar results between both reconstructions we added 3 ºC to Mg/Ca temperatures to approach them to ANN temperatures. During the periods in which we considered Mg/Ca as a reliable winter

paleotemperature proxy (orange rectangles in fig. 5.7 and 5.8), the $\delta^{18}O_w$ records obtained with both temperatures were similar in trends and also in values due to the artefact of adding 3ºC. The fact that both $\delta^{18}O_w$ records present similar trends supports the interpretations of the $\delta^{18}O_w$ record.

A third reconstruction of $\delta^{18}O_w$ was performed using *N. pachyderma* dex oxygen isotopes and the mean annual ANN temperatures (fig. 5.8e). Summer ANN temperatures were calculated for 10 m depth but *N. pachyderma* dex calcified at ~50-100 m depth where temperatures are about 1-2 ºC lower at present (Locarnini et al., 2006). Consequently, we used the annual temperature in order to reduce the overestimation of the $\delta^{18}O_w$ calculated with *N. pachyderma* dex. During the periods in which stratification was weaker *N. pachyderma* sin and dex $\delta^{18}O$ values were closer and ANN annual temperatures should be lower because summers were milder and, hence, $\delta^{18}O_w$ must be overestimated. During the glacial periods both species calcified in the same water mass and hence $\delta^{18}O_w$ calculated using *N. pachyderma* dex could be overestimated too. On average we suggest that $\delta^{18}O_w$ reconstructed with *N. pachyderma* sin and winter ANN temperatures is more reliable than *N. pachyderma* dex reconstruction.

Major changes in $\delta^{18}O_w$ were recorded at Terminations, glacial inceptions and abrupt Arctic front shifts. During Terminations short and abrupt falls of $\delta^{18}O_w$ were recorded (highlighted with black arrows in fig. 5.8), especially in the *N. pachyderma* dex $\delta^{18}O_w$ record, that indicate periods of considerable fresh water input owing to iceberg discharges and ice sheets melting. *N. pachyderma* dex recorded these events more clearly because it lives during the summer when most of the ice was melted. After Terminations the $\delta^{18}O_w$ progressively increased, showing the increasing influence of the more saline waters of the NAC with heavier $\delta^{18}O$ values in response to the intensification of the AMOC.

A remarkable drop of $\delta^{18}O_w$ has been recognized in both species during glacial inceptions (light blue arrows of fig. 5.8) due to the expansion of the Arctic waters with typically lower salinities and $\delta^{18}O$ values. During glacial inceptions the abrupt increases in *N. pachyderma* sin support that the Arctic front shifted south of Site U1314. During the first ice sheet collapse events the Arctic front retreated northwards of Site U1314 and $\delta^{18}O_w$ increased owing to the intensification of the northward flow of the NAC towards the northern North Atlantic (Alonso-Garcia et al., submitted b, see chapter 3). After that an abrupt $\delta^{18}O_w$ drop accompanied by an increase of *N. pachyderma* sin (indicated by purple arrows in fig. 5.8) suggests that the Arctic front moved southwards and Arctic waters influenced the area of Site U1314 again.

Strikingly many of the ice-rafting events were not associated with strong depletions in $\delta^{18}O_w$ but with slight increases. It is likely that during these events the cooling produced by iceberg discharges counterbalanced the salinity decrease and hence $\delta^{18}O_w$ values were higher. Other possibility is that icebergs produced a strong cooling in the area but they hardly melted at

this latitude and therefore salinity was hardly affected. Salinities calculated for these events are strongly overestimated.

## 5. Conclusions

The reconstruction of marine paleotemperatures at high latitudes appears to be rather complex and it needs from a careful interpretation of the proxies. The combination of different proxies allowed us to analyse more in detail the actual meaning of the reconstructions providing higher confidence in the interpretations. We found that Mg/Ca is an excellent proxy of winter paleotemperatures during interglacial periods but during glacial periods the presence of Arctic waters interfered in the Mg/Ca-temperature relationship and the values are less reliable, confirming previous results from the NGS (Kozdon et al., 2009; Nyland et al., 2006). The ~3 ºC difference between winter ANN and Mg/Ca temperatures is probably due to problems with the reconstruction methods because neither of the methods produced temperatures similar to the present winter temperatures. It would be useful to reassess both Mg/Ca and transfer functions equations to achieve more similar results.

Seasonality and surface water conditions were analysed using *N. pachyderma* sin and dex $\delta^{18}O$ records. Since at present *N. pachyderma* sin calcifies under winter conditions and *N. pachyderma* dex during the summer, the differences between $\delta^{18}O$ values of both species during interglacial periods and interstadials reflect the differences between winter and summer temperatures. Seasonality was higher during MIS 15, 11 and during the interstadials, when strong summer thermal stratification developed. Seasonality was particularly strong during MIS 15.1 and 11 when winter conditions were extremely cold. Conversely *N. pachyderma* sin and dex $\delta^{18}O$ values during MIS 17 and 13 were closer indicating lower seasonality. Mg/Ca temperatures suggest that winters during MIS 17 and 13 were less cold than in MIS 15 and 11, and the low $\delta^{18}O$ *N. pachyderma* dex values indicate that summers were less warm. It is likely that summer winds were stronger during MIS 17 and 13 in the North Atlantic and summer-fall stratification was weaker. Hence, during MIS 17 and 13 winter and summer surface water conditions were more similar.

During glacial periods similar $\delta^{18}O$ values between both species might have been a result of the fact that both species calcified in the same water mass. We suggest that both species calcified during the summer in a strongly stratified water mass under the low saline lid produced by sea ice melting. Nevertheless, we cannot completely rule out that we the specimens analysed were actually aberrant right coiling *N. pachyderma* sin specimens instead of *N. pachyderma* dex.

Three different $\delta^{18}O_w$ records were elaborated, two with *N. pachyderma* sin and one with *N. pachyderma* dex. The reconstructions with *N. pachyderma* sin $\delta^{18}O$ reflect similar trends during

interglacial periods. Major changes in $\delta^{18}O_w$ were recorded at Terminations, glacial inceptions and abrupt Arctic front shifts. During Terminations short and abrupt falls of $\delta^{18}O_w$ were recorded as a consequence of considerable fresh water input owing to iceberg discharges and ice sheets melting. *N. pachyderma* dex recorded these events more clearly because it lives during the summer when most of the ice was melted.

At glacial inceptions $\delta^{18}O_w$ drop as a result of the influence of the low salinity and $\delta^{18}O$ values of the Arctic waters. The abrupt changes in $\delta^{18}O_w$ record support the strong surface water conditions that took place associated with the Arctic front shifts at glacial inceptions and during the first ice sheet collapse events of glacial periods.

Many of the ice-rafting events were not associated with strong depletions in $\delta^{18}O_w$ probably because the cooling produced by iceberg discharges counterbalanced the salinity decrease and/or because icebergs produced a strong cooling in the area but they hardly melted at this latitude.

# CAPÍTULO 6.

# MID-PLEISTOCENE CHANGES IN CYCLICITY

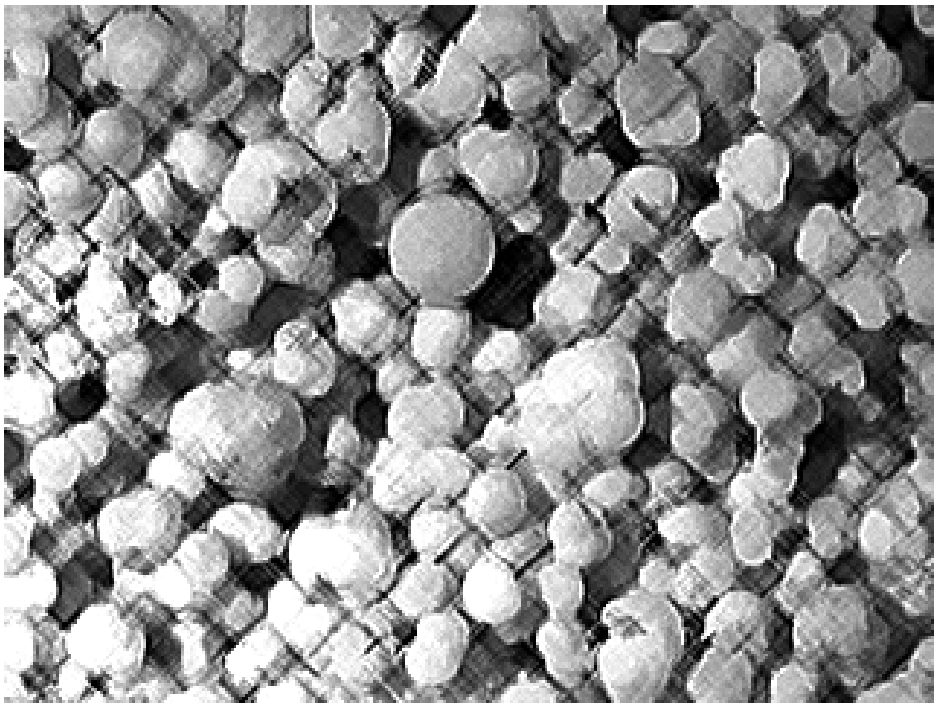

# 6. MID-PLEISTOCENE CHANGES IN CYCLICITY

The Mid-Pleistocene transition (MPT) is defined as the period in which the climatic cyclicity dominance shifted from the ~41 ka cycles, related to obliquity, to the ~100 ka cycles, related to eccentricity (Berger and Jansen, 1994). At ~900 ka the glacial ice sheets size increased and also the severity of the glacial cycles. Orbital forcing did not underwent any change during this interval (as it did at the onset of Northern Hemisphere glaciations), therefore the changes towards the long-term ~100 kyr glacial-interglacial variability have been attributed to changes in the internal feedbacks of the dynamics of the climate system (Maslin and Ridgwell, 2005; Mudelsee and Stattegger, 1997).

In order to evaluate when different Milankovitch frequencies occurred as a function of geological time, over the time interval between 800 and 400 ka, we performed time series analysis on IODP Site U1314 records. The results from U1314 time series analyses were compared with the same kind of analysis performed on EPICA Dome C (EDC) ice core records (Jouzel et al., 2007; Loulergue et al., 2008; Luthi et al., 2008; Siegenthaler et al., 2005; Spahni et al., 2005) to find a global interpretation. Since eccentricity cycles evolved at ~900 ka (Mudelsee and Schulz, 1997), the time period studied in this work corresponds to the first 100 kyr cycles, which present slightly different climatic features compared with the last four glacial-interglacial cycles. We were interested on the changes in cyclicity over the studied interval and when they took place, therefore, after applying the Blackman-Tukey method we decided to perform other types of time series analyses that allow us to evaluate these changes in cyclicity at the different astronomical periodicities over the time. The techniques selected were wavelet spectral analysis, wavelet cross spectral analysis and Gaussian filters. All the techniques used here were thoroughly described in chapter 2.

## 6.1. SPECTRAL ANALYSIS RESULTS

### 6.1.1. Blackman-Tukey

Spectral analysis was initially performed using the Blackman-Tukey method (Jenkins and Watts, 1968). This method revealed the dominant frequencies of the whole interval studied. Eccentricity, obliquity and precession frequencies are well represented in the studied section (fig. 6.1). Eccentricity cycles show the strongest power in all the parameters analysed not only in Site U1314 records but also in EDC records. Obliquity cycles shows lower spectral power and the obliquity peaks are often rather subtle. At the precession band lower spectral power is also observed but the peaks show higher amplitude, particularly in Site U1314 SST (fig. 6.1).

### 6.1.2. Wavelet spectral analyses

Morlet wavelet spectral analysis was performed using SOWAS software (Maraun and Kurths, 2004). This software allows us to perform a continuous wavelet spectral analysis and afterwards to evaluate the coherency and phase of the wavelet cross spectrum between different parameters.

Continuous wavelet spectral analysis of Site U1314 records (fig. 6.2) shows strong power of the eccentricity cycles (~100 kyr period) in all the records and over the entire interval analysed. This periodicity is mostly under the cone of influence and these results are less reliable due to the edge effect. However, in the global spectrum, eccentricity cycles are over the 90 % of confidence and in the Blackman-Tukey method eccentricity cycles present the highest power. Thus we consider that eccentricity power results in the wavelet spectral analysis may be reliable.

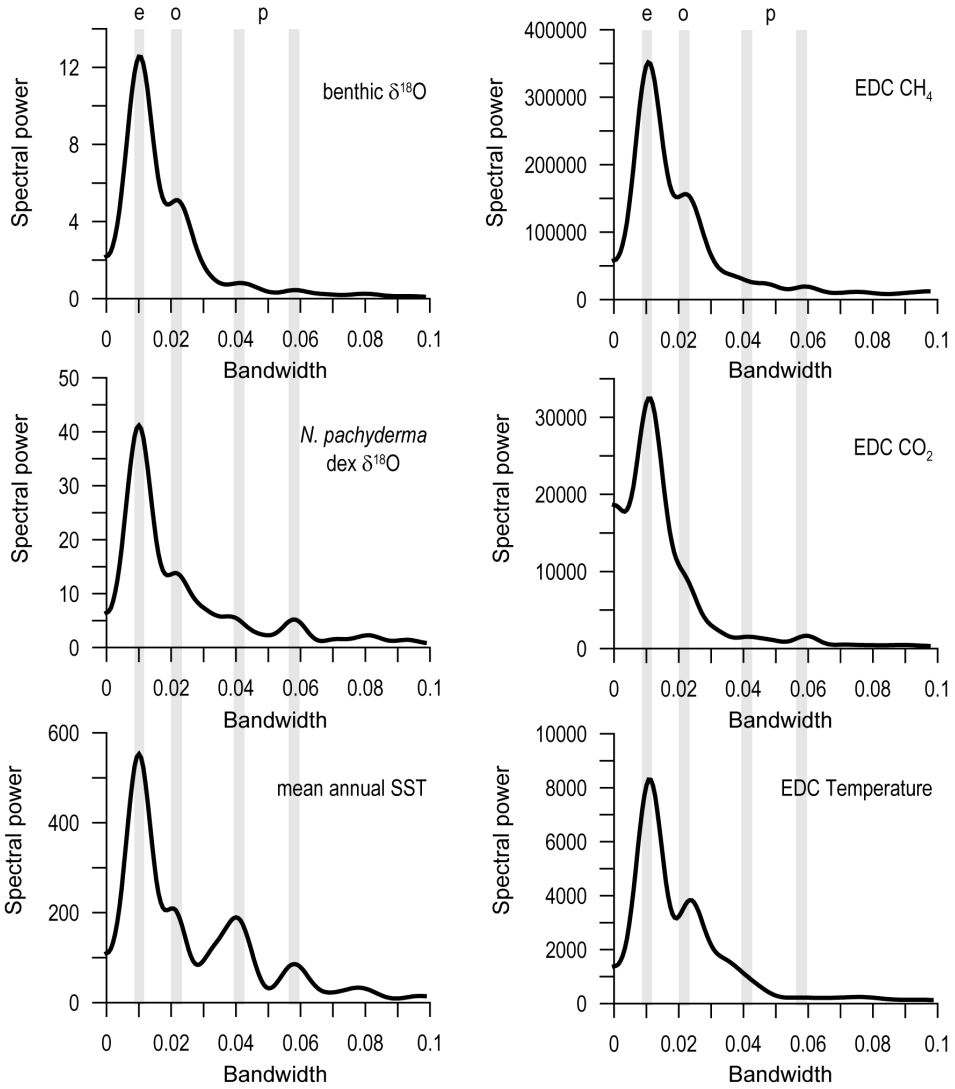


Fig. 6.1. Spectral analysis of the studied interval using the Blackman-Tuckey method. The more powerful frequencies are highlighted with grey vertical bars: eccentricity (e), obliquity (o) and precession (p) at ~19 and ~23 kyr.

At the obliquity period (~41 kyr) the power in the wavelet spectra is strong as well, but the power decreased at most parameters studied between 550 and 450 ka. Precession cycle power (~19-23 kyr) is somewhat weaker than obliquity and eccentricity but still significant. The power strength is not continuous and we recognise two weak intervals in most of the parameters measured, from 710 to 650 ka and from 550 to 450 ka.

Similar results can be observed in the wavelet analysis of EDC records (fig. 6.3). Eccentricity cycles present the strongest and more constant power but mostly below the cone of influence. Obliquity power reveals strong power but with two weaker intervals from 725 to 650 ka and from 550 to 450 ka. The first weaker interval is not present in U1314 spectra but in the benthic $\delta^{18}O$ spectrum. At the precession periodicity, the power is weaker like in Site U1314 spectra but significant. The lowest values occurred during the intervals from 710 to 650 and from 550 to 450 ka as well. The spectrum of the sum of normalized eccentricity, tilt, and precession (ETP) (Imbrie et al., 1984) is also depicted in order to show that the weaker spectral power intervals observed in the spectral analyses of both U1314 and EDC records are not related with changes in the orbital parameters.

### 6.1.3. Gaussian filtering and wavelet cross spectral analyses

Gaussian filtering at ~100 kyr period (fig. 6.4, bottom panel) shows high and steady amplitude in all the records filtered. There are no significant changes in amplitude or phase between the filtered records shown in fig. 6.4. A subtle change can be observed comparing the filtered records of *N. pachyderma* sin abundance and EDC temperature and $CO_2$, *N. pachyderma* sin led before ~500 ka and afterwards *N. pachyderma* sin lagged. In the coherency of the cross spectra (fig. 6.5 and 6.6) we saw no significant changes at the eccentricity period. Coherency values are above 0.8 in most of the cross spectra and only slight changes in phase are observed at the eccentricity period in some of the cross spectra beginning at 725 and at 550 ka.

At the obliquity band Gaussian filters clearly show amplitude flattening between ca. 550 and 450 ka and phase changes (fig. 6.4, middle panel). Coherency of the cross spectra at the obliquity band is not as constant as in the eccentricity periods (fig. 6.5 and 6.6), although there are intervals with rather high values (over 0.8). The intervals in which low coherency is observed at the obliquity band mainly occurred between ~725 and 650 ka and between ~525 and 450 ka and show strong to moderate changes in phase.

Gaussian filters at the precession band (fig. 6.4, top panel) show large differences with respect to the precession parameter (Laskar et al., 2004) and important changes in phase, particularly when the precession parameter amplitude is low. Amplitude flattening in the filtered curves and the most important changes in phase between the parameters filtered occurred at the 725-650 and 550-450 ka intervals. Coherency of the cross spectra at the precession period is lower than in eccentricity

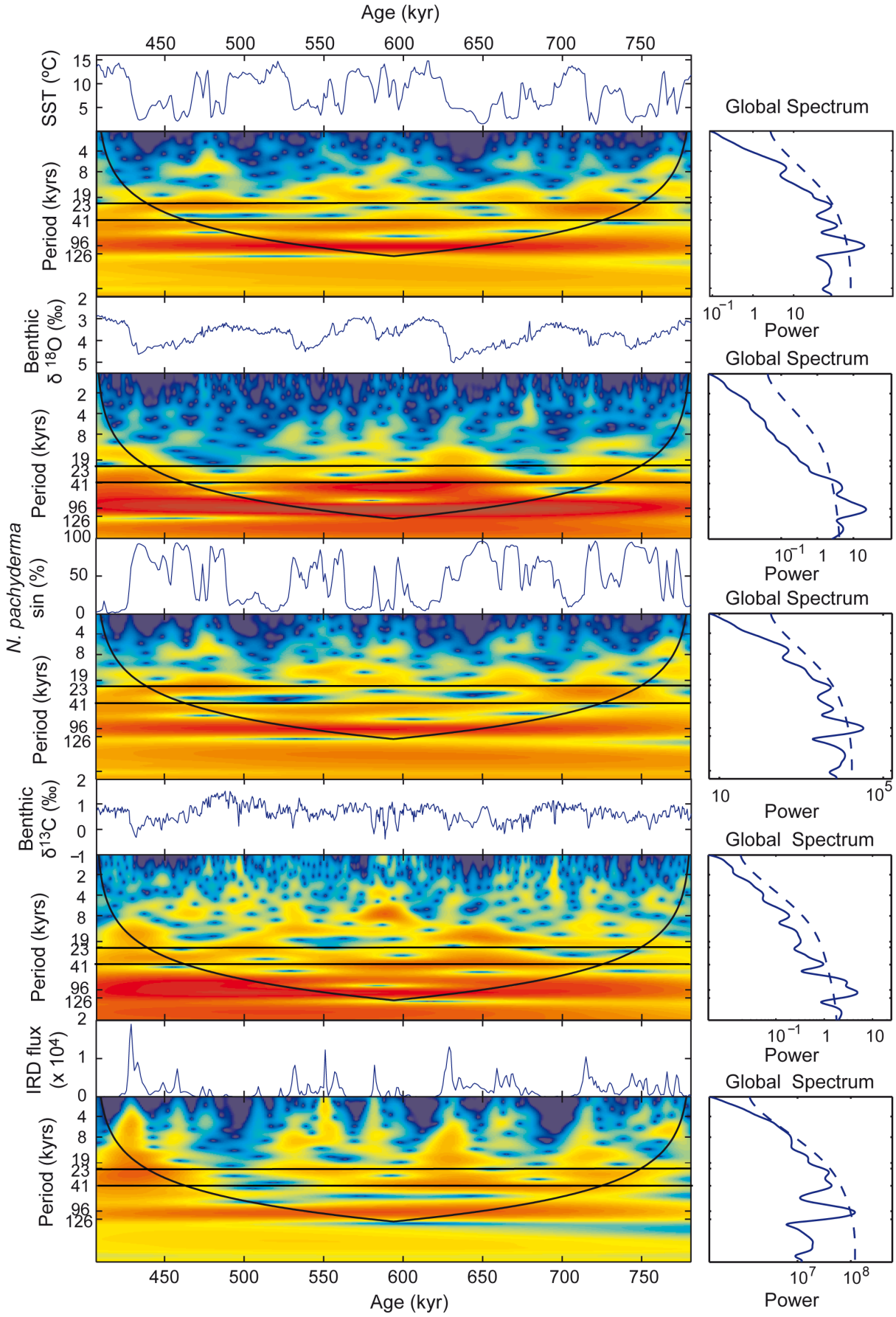
Age (kyr)
450
500
550
600
650
700
750
SST (ºC)
15
10
5
Period (kyrs)
4
8
19
23
41
96
126
2
Benthic δ 18O (‰)
3
4
5
2
4
8
19
23
41
96
126
100
N. pachyderma sin (%)
50
0
4
8
19
23
41
96
126
Benthic δ13C (‰)
2
1
0
−1
2
4
8
19
23
41
96
126
IRD flux (x 10⁴)
2
1
0
4
8
19
23
41
96
126
Global Spectrum
10−1
1
10
Power
Global Spectrum
10−1
1
10
Power
Global Spectrum
10
10⁵
Power
Global Spectrum
10−1
1
10
Power
Global Spectrum
10⁷
10⁸
Power
Age (kyr)
450
500
550
600
650
700
750

Fig. 6.2. Continuous wavelet spectral analyses of Site U1314 records from ca. 800 to 400 ka. From top to bottom spectra of mean annual SST (performed with the Artificial Neural Networks of Kucera et al. (2005) and the North Atlantic dataset), oxygen isotopes from benthic foraminifers, *N. pachyderma* sin abundances, carbon isotopes from benthic foraminifers and IRD fluxes. The results below the cone of influence are dubious. The dashed line in the global spectrum depicts the 90 % of confidence level.

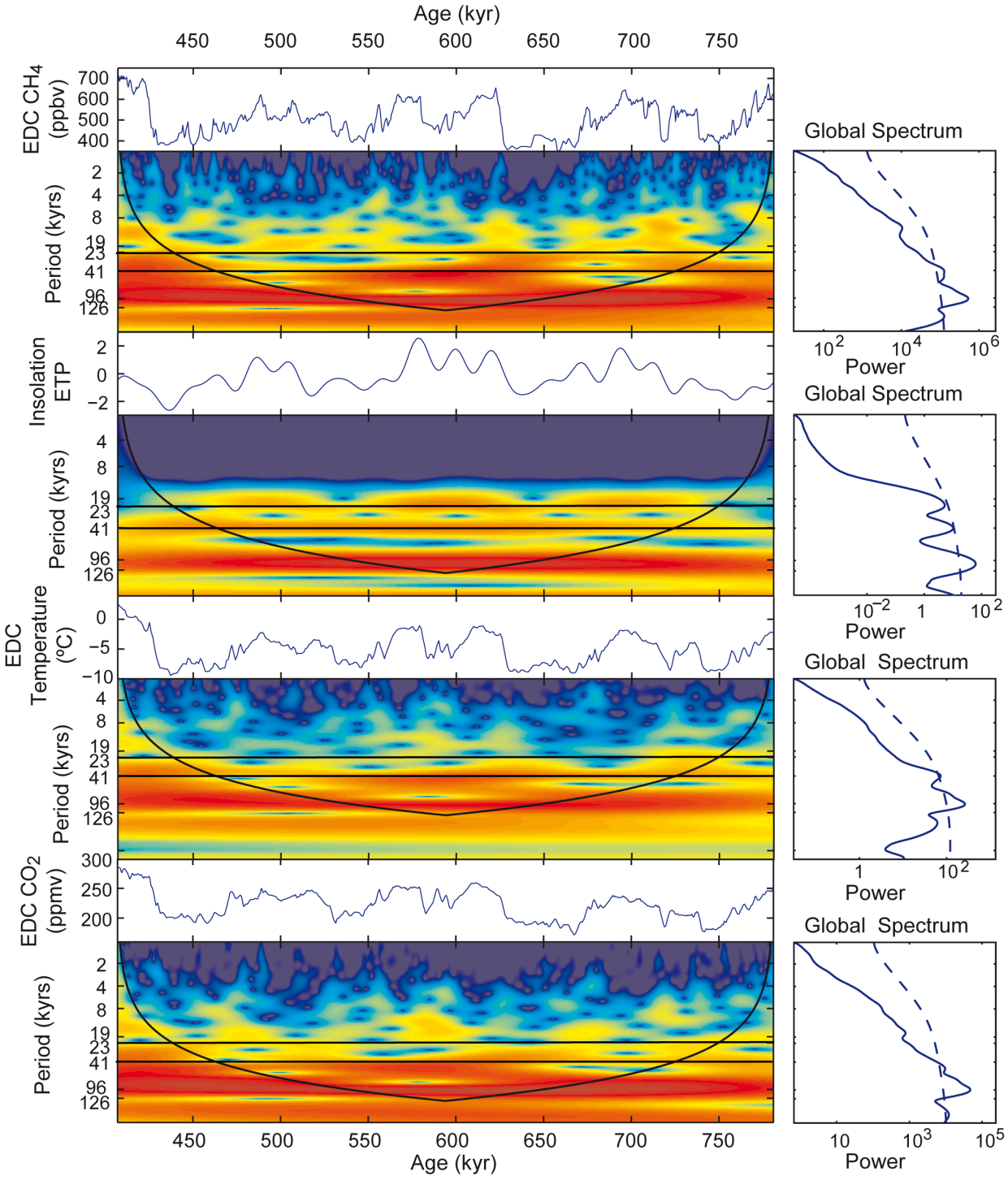


Fig. 6.3. Continuous wavelet spectral analyses of EDC records and ETP insolation from ca. 800 to 400 ka. From top to bottom spectra of $CH_4$ (Spahni et al., 2005; Loulergue et al., 2008), ETP insolation (Berger and Loutre, 1991), Deuterium temperature (Jouzel et al., 2007) and $CO_2$ (Siegenthaler et al., 2005; Luthi et al., 2008). The results below the cone of influence are dubious. The dashed line in the global spectrum depicts the 95 % of confidence level.

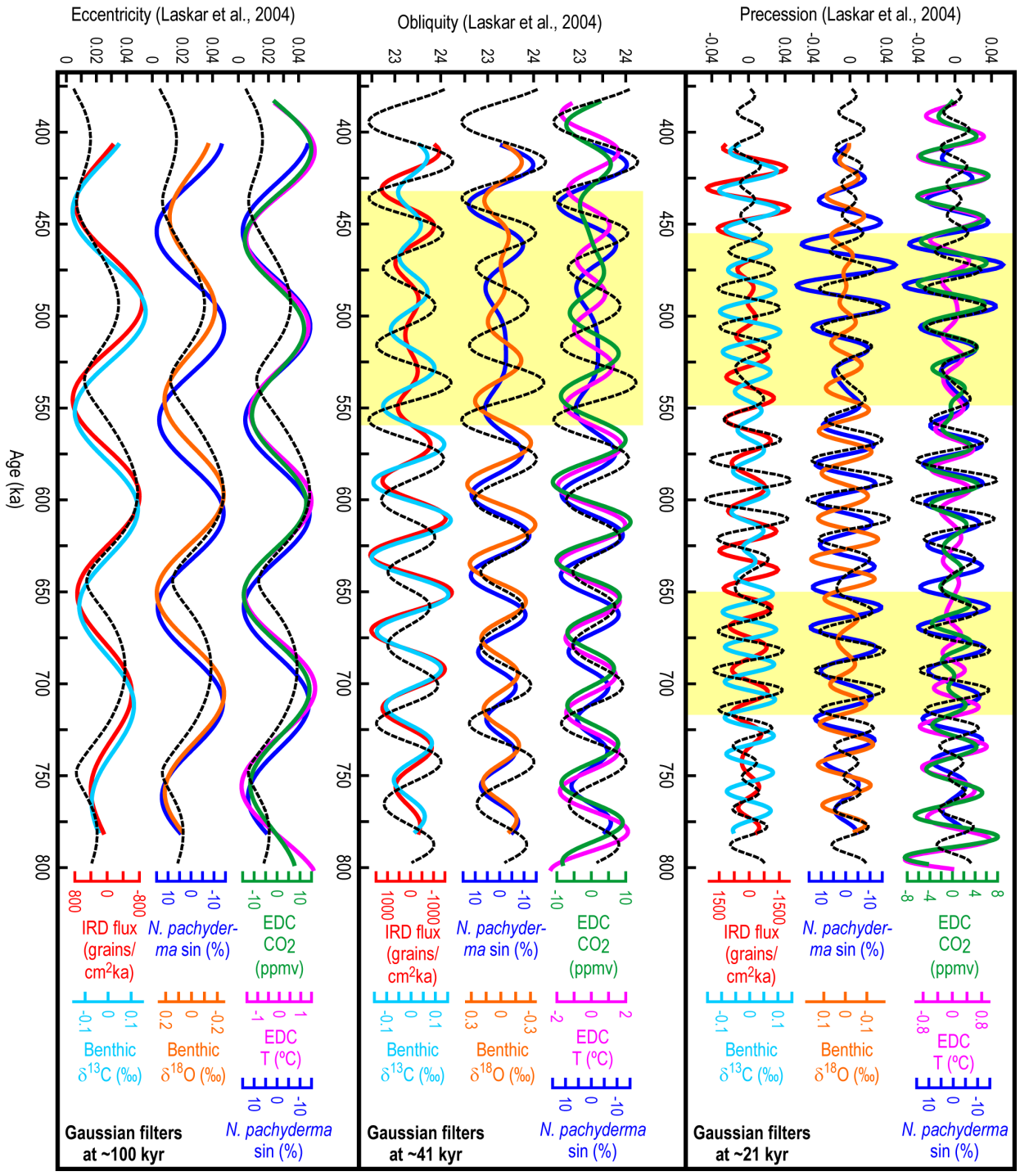


Fig. 6.4. Gaussian filters at precession (~21 kyr top panel), obliquity (~41 kyr, middle panel) and eccentricity (~100 kyr, bottom panel) of both U1314 and EDC records from ca. 800 to 400 ka. Yellow squares show the intervals with decoupling between the different filtered records and/or lower amplitude of the filtered records.

and obliquity periods (fig. 6.5 and 6.6) but in agreement with the results of the obliquity, low coherency intervals and changes in phase occurred at ~525-450 and ~725-650 ka.

At the obliquity band Gaussian filters show in phase or nearly in phase relationships between the parameters filtered and the obliquity parameter (fig. 6.4). The in phase relationship between IRD fluxes in the North Atlantic and benthic $\delta^{13}C$ indicate that at the obliquity band iceberg discharges and the disturbance of the thermohaline circulation occurred in phase. However at the precession band these parameters were in opposite phase from ~780 to 620 ka and from ~575 to 475 ka, suggesting some decouplings between thermohaline circulation and iceberg discharges.

The filtered records of *N. pachyderma* sin abundance and benthic $\delta^{18}O$ were nearly in phase at the obliquity band, except for the period between ~550-450 ka, suggesting that ice volume and North Atlantic sea surface conditions were in phase at this band. Nonetheless at the precession band ice volume and North Atlantic sea surface conditions (*N. pachyderma* sin abundance and benthic $\delta^{18}O$) were coupled from ~750-700 ka and after ~450 ka.

Atmospheric $CO_2$ and Antarctic temperatures were in phase at the obliquity band except for the period between 550 and 450 ka and temperatures lead. The out of phase relationship at the obliquity band from ~725 ka between *N. pachyderma* sin abundance and EDC records show that Northern and Southern Hemisphere climatic responses started to be out of phase at ~720 ka. At the precession band EDC temperature and $CO_2$ were not in phase from ~700 to 600 ka and from ~550 to 500 ka suggesting a decoupling between atmospheric $CO_2$ and Antarctic temperatures. Nonetheless $CO_2$ and *N. pachyderma* sin abundance were mostly in phase. Northern and Southern Hemisphere temperatures were not in phase at the precession band until 475 ka but atmospheric $CO_2$ and *N. pachyderma* sin abundance were slightly out of phase during short periods, from ~725 to 675 ka and from ~575 to 525 ka, suggesting that Northern hemisphere temperatures imprinted some control on atmospheric $CO_2$ concentrations.

## 6. 2. CHANGES IN THE DYNAMICS OF THE CLIMATE SYSTEM DURING THE MID-PLEISTOCENE TRANSITION

The changes in the dynamics of the climate system during the long-term cooling trend of the Plio-Pleistocene are still poorly understood. Prior to ~1 Ma ice volume changes occurred controlled by the local summer insolation of each hemisphere (Raymo et al., 2006). Since Earth's orbital precession is out of phase between hemispheres, precession changes in ice volume in each hemisphere cancel out in globally integrated proxies such as benthic $\delta^{18}O$, leaving the in phase obliquity component of insolation to dominate those records. Only a modest mass change in Antarctica is required to effectively cancel out a much larger northern ice volume signal according to Raymo et al. (2006). Moreover, Raymo et al. (2006) suggested that at ~1 Ma high latitude

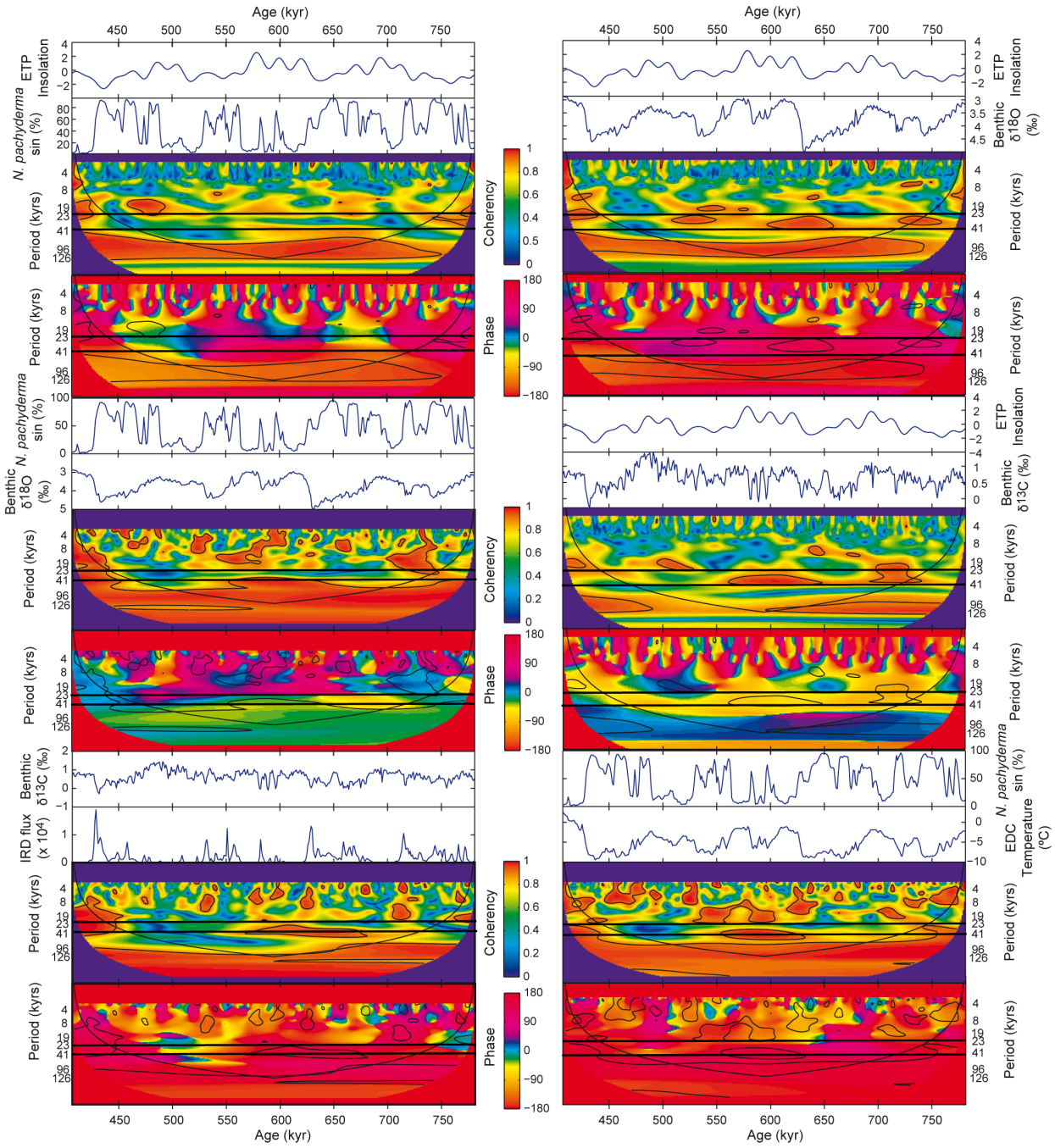


Fig. 6.5 and 6.6. Cross spectral analysis. Here we show a selection of the most representative coherency and phase spectra. The records crossed are depicted at the top of every panel. The black contours indicate the 95 % of confidence in coherency.

climate had cooled to the extent that it was no longer warm enough for an extensive terrestrial melting margin to exist on East Antarctica and marine-based margins replaced the terrestrial ice margins of the East Antarctic Ice Sheet (EAIS). As a consequence ablation occurred primarily by calving and a progressive thickening of the East Antarctic Ice Sheet (EAIS) started (Raymo et al., 2006). Since calving was driven by the sea level changes caused by the Northern Hemisphere ice sheet fluctuations, the behaviour of Northern and Southern Hemispheres could have shifted

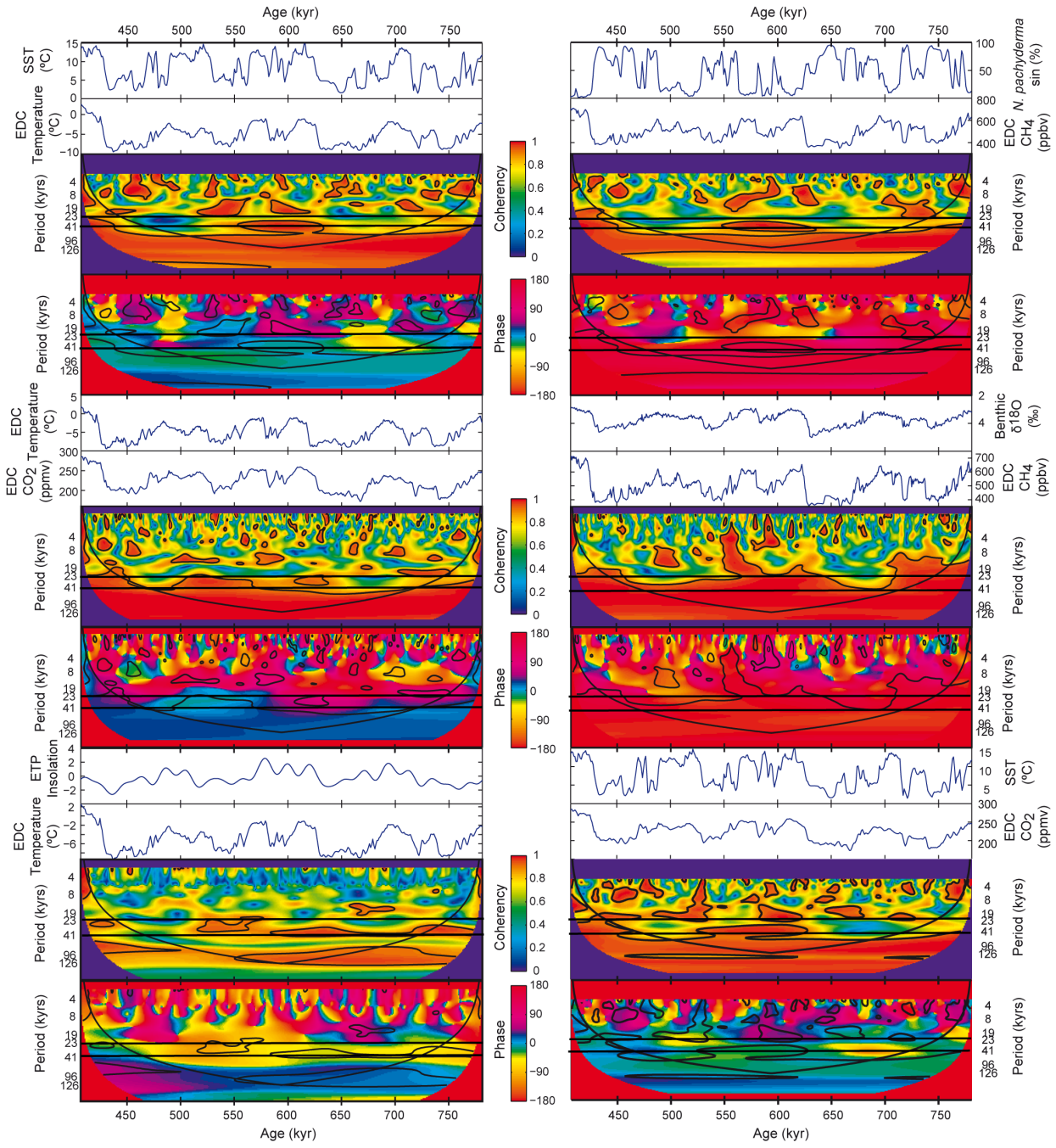


Fig. 6.6. Cross spectral analysis.

to in-phase ice volume changes and ice volume started to vary in phase at both obliquity and precession frequencies. Therefore, at ~1 Ma a strengthening of precession signal in ice volume records was initiated and possibly positive globally synchronous feedbacks (such as albedo and $CO_2$ levels) at the precession frequency were established (Raymo et al., 2006). This change to in-phase conditions was not necessarily an abrupt transition (Raymo et al., 2006), and here we propose that the Southern Hemisphere response fluctuated between in and out of phase from ~1 Ma to MIS 12, when both hemispheres started to respond in phase.

After ~1 Ma EAIS progressively began to grow and thicken in phase with Northern Hemisphere driven sea level changes, but it is likely that Northern Hemisphere ice sheet growth was still mainly controlled by obliquity because at latitudes above 50º N obliquity rhythm dominates (Ruddiman and McIntyre, 1984). At ~725 ka Site U1314 filtered record of *N. pachyderma* sin abundance and EDC records started to be out of phase at the obliquity band, indicating that obliquity was not the only control of climate and sea level changes In the precession band EDC temperature and $CO_2$ Gaussian filters present an out of phase interval between ~700 and 600 whereas *N. pachyderma* sin abundance and EDC $CO_2$ were mostly on phase. That suggests a decoupling between Antarctic temperature and $CO_2$ built up and a coupling with Northern Hemisphere temperatures. Similar conclusions can be obtained from the analysis of the wavelet cross spectra (fig. 6.4 and 6.6)

According to Ruddiman (2006), before the MPT the $CO_2$ feedback only accounted for 30 % of the ice volume response, whereas after the MPT the $CO_2$ feedback accounted for 75 %. The establishment of marine-based ice sheets in East Antarctica may have promoted a northward migration of the Subantarctic front, which may have cooled the Southern Ocean and decreased ventilation through the reduction of the Southern Ocean Meridional Overturning Circulation (Fischer et al., 2010). The alkenone SST record of ODP Site 1090 supports the cooling of the Southern Ocean from the beginning of the MPT to Termination V (Martínez-Garcia et al., 2009). It is likely that at the early MPT changes in the subantarctic sea ice extent started to control atmospheric $CO_2$ concentrations in phase with ice volume changes. Ice accumulation in the Northern Hemisphere decreased sea level and promoted a progressive ice sheets expansion in the Antarctic shelves which probably increased sea ice extent. Additionally the Northern Hemisphere cooling/warming was transferred to the Southern Hemisphere through the AMOC and it started to control the expansion/reduction of sea ice. Atmospheric $CO_2$ was built up due to sea ice expansion and reduced ventilation in the Southern Ocean at the beginning of glacial periods. Northern and Southern hemispheres mainly respond to obliquity before ~725 ka because Northern Hemisphere ice sheet growth was mainly controlled by obliquity.

At ~725 ka some feedbacks like the albedo or the $CO_2$ (largely controlled by changes in the AMOC) might have strengthened and ice accumulation in the Northern Hemisphere became out of phase with Southern Hemisphere, because in the Northern Hemisphere precession and obliquity controlled climate changes whereas in the Southern Hemisphere obliquity was the main control. A clear example of this decoupling is the glacial period MIS 18.2 when $CO_2$ and North Atlantic temperatures became decoupled with Antarctic temperature (fig. 6.7). It is likely that the Southern Hemisphere forcing was opposite to the Northern Hemisphere forcing at precession but the Northern Hemisphere forcing was stronger and that produced a period in which the precession response was superimposed to the obliquity.

The appearance of the precessional signal at the early MPT introduced an important change in the internal dynamics of the climate system, initiating the dominance of longer climatic cycles.

The development of the first large ice sheet in the Northern Hemisphere (with similar ice volume as in the last four glacial periods) took place in MIS 16, when the benthic $\delta^{18}O$ reached maximum values (over 4.25 ‰ at Site U1314) and the largest ice sheets were developed in Europe (Ehlers and Gibbard, 2007; Toucanne et al., 2009). Our spectral analyses show changes between ~725-650 ka at the obliquity and precession bands. This interval preceded the development of the large ice sheet that took place at MIS 16. We suggest that at MIS 16 a threshold that allowed larger ice volume accumulation had been surpassed for the first time (probably during the interval ~725-650 ka). There were several conditions that allowed the climate system to overcome this threshold: the erosion of the regolith (Clark and Pollard, 1998) that allowed higher ice sheet growth; the enlargement of climatic cycles through the introduction of the precession in the internal dynamics of the climate system; the low atmospheric $CO_2$ levels (fig. 6.7) driven by the larger extension of the Subantarctic sea ice and the transfer of the Northern Hemisphere cooling to the Southern Ocean; and the increasing albedo in the Northern Hemisphere.

The interval between ~900 ka and ~400 ka is well known as the interval of the lukewarm interglacial periods (e.g. Tzedakis et al., 2009) due to the high benthic $\delta^{18}O$ and low Antarctic deuterium temperatures. In contrast, North Atlantic surface temperatures were high during these interglacial periods. We cannot attribute the high North Atlantic temperatures to atmospheric $CO_2$

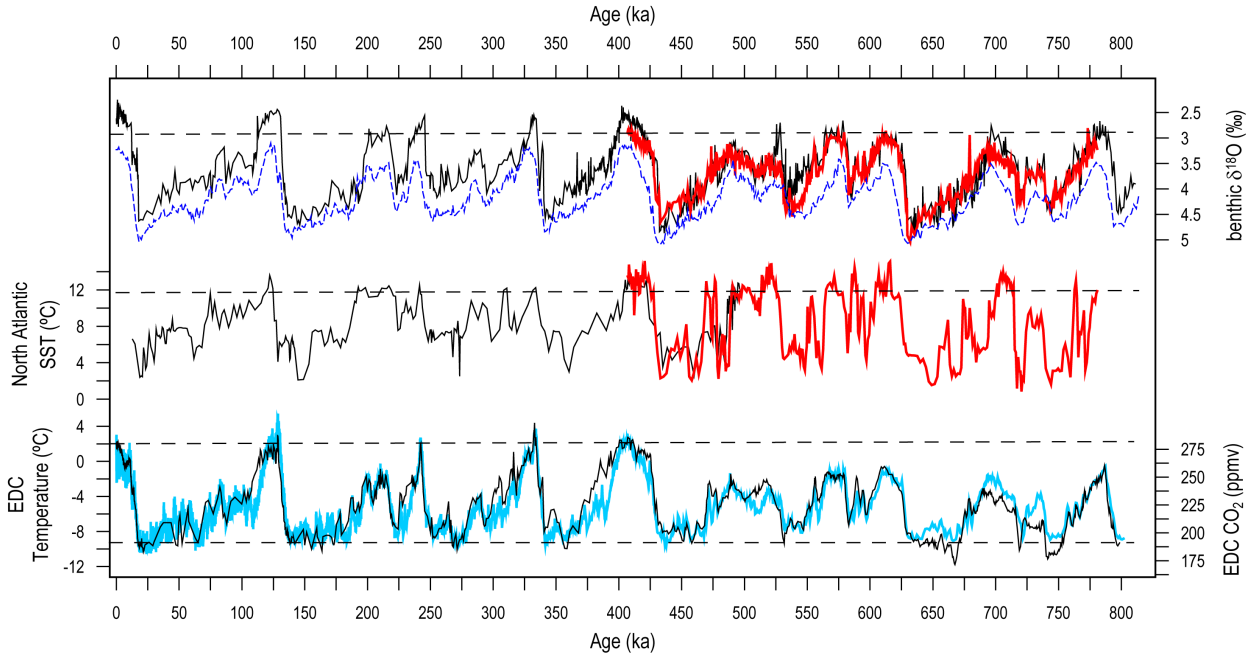


Fig. 6.7. Differences between ice volume and temperature records of the Mid-Pleistocene. Benthic oxygen isotopes from LR04 (Lisiecki and Raymo, 2005, blue dashed line), Site ODP 980 (Flower et al., 2000, black line) and Site U1314 (red line) show lower ice volume during interglacial periods after MIS 12. Sea surface temperatures from Site U1314 (red line) and the near Site GIK23414 (Kandiano and Bauch, 2003, black line) show that North Atlantic temperatures were similar during interglacial periods before and after MIS 12. Antarctic temperatures (Jouzel et al., 2007, black line) and atmospheric $CO_2$ (Luthi et al., 2008; Petit et al., 1999; Siegenthaler et al., 2005, red line) were lower during interglacial periods before MIS 12.

levels because they were moderate. However, a northernmost position of the ITCZ could have played a major role warming Northern Hemisphere because of the low-to-high latitude insolation gradient, which is almost dominated by obliquity, controls the poleward heat and moisture fluxes in the atmosphere (Raymo and Nisancioglu, 2003). We suggest that warm and humid conditions in Europe and Asia may have been associated to enhanced fluxes of heat and moisture to the Northern Hemisphere high latitudes boosted by the northernmost position of the ITCZ. The wider extent of the subantarctic sea ice could have shifted all the wind belts northwards shifting the Intertropical Convergence zone (ITCZ) further north in the Northern Hemisphere. This shift in the ITCZ produced a strong asymmetry between Southern and Northern Hemisphere, as suggested for MIS 13 (Guo et al., 2009). Several records support that the ITCZ might have been located northwards during the interglacial periods before the Mid-Brunhes Event, strengthening Indian and Asian monsoons (Bassinot et al., 1994; Guo et al., 2000; Suganuma et al., 2009; Sun et al., 2006). In fact interglacial temperatures at Site U1314 from ~800 to 400 ka were similar or even warmer than present temperatures. Warm temperatures were also inferred at the Baikal region (Prokopenko et al., 2002), the Tibetan Plateau (Chen et al., 1999), south of Greenland (de Vernal and Hillaire-Marcel, 2008; Liu and Herbert, 2004) and in Europe (Markovic et al., 2009; Tzedakis et al., 2006; Vandenberghe, 2000). Additionally, the increase in the meridional SST gradient reduced air temperature and increased snowfall over the Northern latitudes, particularly in North America (Brierley and Fedorov, 2010), which probably contributed to build a larger ice sheet at MIS 16.

The wavelet spectra of most of the parameters analysed suggest a strong obliquity control for the climatic cycles between MIS 16 and 13 (fig. 6.2 and 6.3) because the large ice sheets in Antarctica cancel out the influence of precession on the global sea level response. Coherency is also high and the Gaussian filters at the precession band show out of phase records except for the interval between 600 and 550 ka, when insolation changes in the Northern Hemisphere present rather high amplitudes due to high precession amplitude. We associate this precessional response to the coupling between $CO_2$ and the Northern Hemisphere climate via the AMOC. When the $CO_2$ concentration was high, the Northern Hemisphere insolation drove the climate through the $CO_2$ feedback, whereas when $CO_2$ concentration decreased at MIS 14 obliquity controlled climate changes. At Termination VI (MIS 14/13), and probably at MIS 15.2/15.1 transition, the meridional low-to-high Northern latitude insolation gradient was low and it likely starved snow accumulation leading to a premature ice sheet decay (fig. 3.3).

MIS 13 was the last interglacial period with moderate ice volume and interhemispheric asymmetry. At ~500-450 ka more Gaussian filters at the precession band became on phase and ice volume mainly responded to Northern Hemisphere precession changes since then. It is likely that during MIS 12 the internal dynamics of the climate system achieved more stable conditions with a nearly in phase response of both hemispheres in ~100 kyr cycles and a long glacial period

developed. After MIS 12 the Subantarctic front retreated reaching a position similar to present, as recorded in the diatom records of Site 1090 (Cortese and Gersonde, 2008). Hence the ITCZ was nearer to the Equator, the interhemispheric asymmetry gave rise to a more symmetric state and more arid conditions were established in the Northern Hemisphere (Markovic et al., 2009; Tzedakis et al., 2006). Late Pleistocene climate dynamics was established at MIS 12. In MIS 11 and the subsequent interglacial periods, we believe that less ice volume was stored in Antarctica that produced the difference between the lukewarm interglacials and interglacials after MBE because a smaller mass change in Antarctica is required to achieve the same ice volume effect in the benthic $\delta^{18}O$ (Raymo et al., 2006).

## 6. 4. SUMMARY AND CONCLUSIONS

The significant strengthening of the 100 kyr eccentricity power in the past 800 ka is one of the intriguing questions of climate history. Here we analysed North Atlantic and Antarctic records in order to identify the changes that the internal dynamics of the climate system underwent to evolve to the long-term cyclicity of the Late Pleistocene.

The establishment of the marine based EAIS at the MPT gave rise to a progressive appearance of the precession signal which produced an in phase climate response of both hemispheres and, in turn, enlarged climate cycles. During this progressive appearance of longer climate cycles Southern Hemisphere response fluctuated in and out of phase until the MBE, and since then both Hemispheres responded in phase.

The marine based ice sheet probably promoted the expansion of sea ice in the Southern Ocean that disturbed ventilation and promoted a $CO_2$ built up. Changes in the North Atlantic circulation also contributed to store or outgass $CO_2$ in the Southern Ocean. The expansion of the Southern Ocean sea ice also shifted the ITCZ northwards generating an interhemispheric asymmetry in the distribution of the wind belts. The changes in atmospheric $CO_2$ turned into a strong feedback for climate changes driving the ~100 kyr cycles. The shift in the ITCZ produced an increase in temperature and precipitation in the Northern Hemisphere strengthening summer monsoons. The low $CO_2$ levels in phase with Northern Hemisphere climate changes, the higher transfer of water vapour, the exposure of the bedrock in Laurentia and the enlargement of climatic cycles promoted a vast ice accumulation in Northern Hemisphere generating the first large ice sheet of the Mid-Late Pleistocene (MIS 16 ice sheet).

After MIS 16 climatic cycles were mostly obliquity forced because the large ice sheets in Antarctica cancel out the precession influence on global sea level change. The response of $CO_2$ in phase with the Northern Hemisphere climate change acted as a feedback, enhancing warming with high $CO_2$ concentrations and cooling with low concentrations. When glacial conditions began,

obliquity controlled climate changes because the feedbacks that enhanced northern hemisphere climate were low and because the low-to-high latitude gradient favoured obliquity forcing. At ~500-450 ka the Southern Hemisphere became in phase with the Northern, the ITCZ migrated near the Equator and Northern-Southern Hemisphere asymmetry was flattened, more arid conditions were initiated in the Northern Hemisphere and warmer interglacials occurred in the Southern Hemisphere. At the MBE the internal dynamics of the climate system that prevailed during the Late Pleistocene climate cycles (the last 400 ka) was established.

# CAPÍTULO 7.

# CONCLUSIONES/ CONCLUSIONS

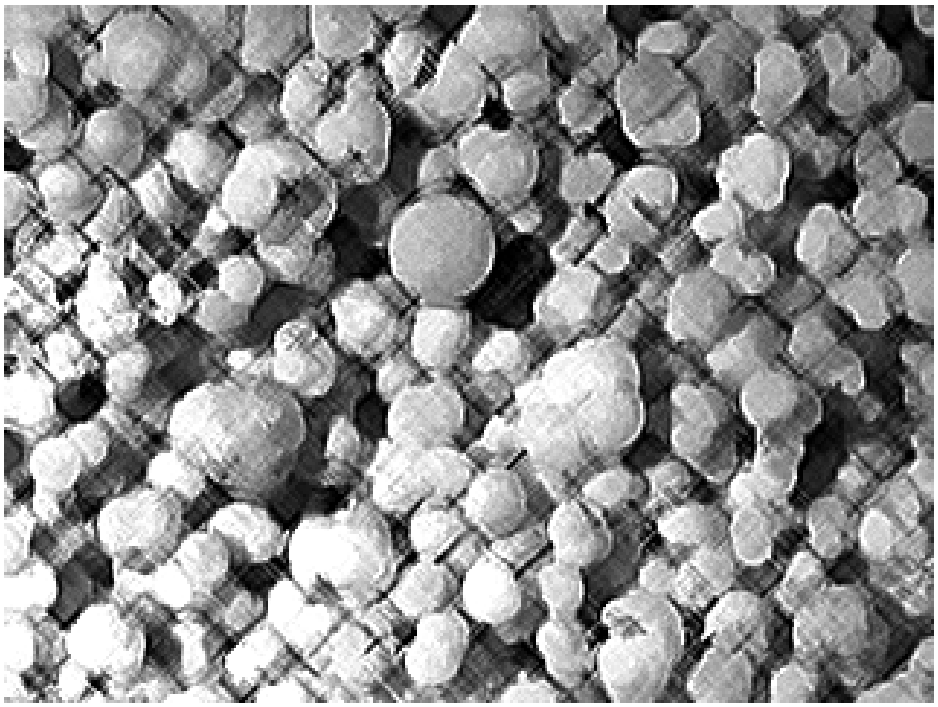

# 7. CONCLUSIONES

En primer lugar se ha establecido un **modelo de edad** para el intervalo estudiado sincronizando los isótopos de oxígeno de foraminíferos bentónicos del testigo U1314 con el registro de temperatura antártica del testigo de hielo EDC. El registro estudiado comprende aproximadamente desde 779 a 407 ka, incluyendo desde el estadio isotópico marino 19 al 11.

El estudio combinado de los registros de isótopos estables de oxígeno y carbono en foraminíferos bentónicos y planctónicos así como de las asociaciones de foraminíferos planctónicos, las abundancias de IRD y los cálculos de paleotemperaturas a partir de Mg/Ca y de funciones de transferencia para foraminíferos planctónicos, nos ha permitido reconocer una serie de **patrones en las variaciones climáticas, oceanográficas y en el crecimiento de los mantos de hielo**. De acuerdo con estos patrones hemos establecido una división del ciclo glacial-interglacial en **cinco fases**.

1) **Fase inicial de los periodos interglaciales**. Durante esta fase la circulación termohalina era muy activa y los frentes Ártico y Polar estaban situados aproximadamente en el mismo lugar que ocupan en el presente, o posiblemente algo más al noroeste. La NAC cruzaba el Atlántico llegando hasta el NGS y el Mar del Labrador donde se enfriaba y se hundía dando lugar a la NADW como ocurre hoy en día.
2) **Fase tardía de los periodos interglaciales**. Esta fase se caracteriza por la migración del frente Ártico hacia el sureste debido probablemente a un recrudecimiento de los inviernos aunque aún no se ha empezado a acumular hielo en los continentes. La corriente termohalina continúa activa, pero es posible que la formación de aguas profundas en el Mar del Labrador disminuyese, quedando el NGS como zona principal de formación de la NADW.
3) **Primera fase de los periodos glaciales**. Esta fase se caracteriza por el comienzo de la acumulación de hielo en los continentes con una circulación termohalina aún activa. Sin embargo, sólo se generaban aguas profundas en el NGS porque los frentes Ártico y Polar estaban muy al sureste y casi toda la zona del Mar del Labrador estaba cubierta por una banquisa de hielo perenne. El avance de las aguas Árticas en el Atlántico subpolar se hace patente también en la disminución brusca en el delta del agua y la salinidad. La NAC fluía solamente sobre la meseta submarina de Rockall-Hatton y el canal de Rockall pero aún llegaba al NGS. Durante esta fase el crecimiento de los mantos de hielo del hemisferio Norte fue rápido gracias al funcionamiento activo de la circulación termohalina que permitía el transporte de vapor de agua desde el océano al continente. Esto también favoreció la continuidad de la circulación termohalina ya que las aguas de la NAC aumentaban su salinidad con la extracción de vapor de agua. La NADW probablemente fue enfriándose paulatinamente, incluso desde la fase anterior, y este enfriamiento se transmitió al hemisferio Sur a través de la circulación termohalina.

4) **Segunda fase de los periodos glaciales**. Esta fase comienza con la primera descarga de icebergs que interrumpe el crecimiento de los mantos de hielo y ralentiza la circulación termohalina, que pasa a estar alimentada por la formación de aguas intermedias, la GNAIW. Esta fase se caracteriza por el progresivo crecimiento de los casquetes de hielo que se vio interrumpido por varios eventos bruscos de escala milenaria en los cuales los mantos de hielo retrocedieron. Hemos denominado a estos eventos como ISCE (*ice sheet collapse events*). Estos eventos comienzan con una descarga de IRD hacia el Atlántico norte que ralentiza la formación de GNAIW y produce un calentamiento en el hemisferio sur por el efecto *see-saw* que a su vez da lugar a la liberación de $CO_2$ del océano a la atmósfera. A esta primera etapa de enfriamiento extremo en el hemisferio norte le sucede un calentamiento brusco del agua superficial que incrementa la ablación de las grandes masas del hielo en el hemisferio norte. Este calentamiento brusco es probablemente inducido por el aumento de $CO_2$ atmosférico y por una reactivación de la circulación termohalina. Durante las etapas frías de crecimiento de los casquetes polares el Atlántico subpolar estaba cubierto de hielo estacional al menos hasta los 55º N. Los frentes Ártico y Polar estaban situados muy al sur, con una dirección casi este-oeste y la NAC apenas llegaba al Site 980. La GNAIW probablemente se generaba al sur de los 60º N. Sin embargo, durante los periodos cálidos de los ISCE el frente Ártico migró rápidamente hacia el norte (al menos en el Atlántico este) y la NAC posiblemente llegaba a la latitud de Escocia, formando GNAIW más al norte.
5) **Fase final de los periodos glaciales y terminación**. Al final de los periodos glaciales el frente Ártico comienza a retroceder lentamente hasta que se produce una migración brusca al noroeste cuando empieza la terminación. La NAC va penetrando hacia el norte y reactiva la circulación termohalina formando NADW tanto en el NGS como en el Mar del Labrador. Durante las terminaciones grandes cantidades de agua dulce se vierten al Atlántico norte disminuyendo la salinidad del agua superficial por un corto espacio de tiempo.

Las **asociaciones de foraminíferos planctónicos** nos muestran cambios muy bruscos entre la asociación predominante en los **periodos cálidos**, donde dominan las especies transicionales-subpolares *N. pachyderma* dex, *G. inflata* y *G. bulloides*, y la asociación prácticamente monoespecífica de *N. pachyderma* sin que predomina durante los **periodos fríos**. Estos cambios bruscos se deben a la **posición del frente Ártico**, que determina la presencia de aguas de la corriente noratlántica o aguas Árticas en la zona del testigo. Además podemos determinar cuando el frente Ártico estaba cerca del área de estudio por los altos porcentajes de *T. quinqueloba*.

Los **cálculos de paleotemperaturas** a partir de la relación Mg/Ca y de las asociaciones de foraminíferos planctónicos nos muestran que las temperaturas de Mg/Ca en latitudes altas son fiables durante los periodos interglaciales, cuando el frente Ártico estaba al norte del Site U1314, mientras que la presencia de las aguas árticas interfiere en la relación del Mg/Ca con la temperatura, corroborando estudios previos. El análisis de las temperaturas junto a los **análisis del $\delta^{18}O$ en las**

conchas de los foraminíferos planctónicos **N. pachyderma sin y dex** nos muestra que durante los periodos interglaciales la diferencia entre ambas especies indica **estacionalidad y mezcla en la columna de agua**. Los MIS 15 y 11 presentaron una mayor estacionalidad con veranos más cálidos e inviernos más fríos que los MIS 17 y 13, en parte como consecuencia de una mayor estratificación de la columna de agua durante el verano. Estas diferencias en la estratificación pudieron estar relacionadas con un aumento en la fuerza de los vientos durante los veranos de los MIS 17 y 13. Durante los periodos glaciales la presencia de banquisa de hielo durante la mayor parte del año favoreció que ambas especies vivieran en la misma estación y en la misma masa de agua dentro de la columna dado que es posible que el deshielo de la banquisa produjera una gran estratificación. Las descargas de icebergs no produjeron cambios significativos en el $\delta^{18}O$ del agua excepto en las Terminaciones.

El **análisis de la ciclicidad** de los diferentes registros elaborados en esta Tesis y su comparación con los registros de EDC, nos ha permitido observar un **progresivo aumento en la importancia de la precesión en los ciclos climáticos**. Desde el establecimiento casquete de hielo del este de la Antártida sobre la plataforma marina el hemisferio Sur ha alternado entre estar en fase o desfasado respecto al hemisferio norte hasta que en el MIS 12 se establece en fase. Este periodo de adaptación provocó un desplazamiento en la ITCZ hacia el norte que aumentó el transporte de vapor de agua al hemisferio norte contribuyendo a la formación de grandes masas de hielo que alcanzaron su máximo desarrollo en el MIS 16. Desde el MIS 16 al 12 la insolación sobre altas latitudes del hemisferio norte controlaba los cambios climáticos globales y la concentración de $CO_2$, pero el clima estaba aún estaba influido por la oblicuidad. A partir del MIS 12 la ITCZ se situó más cerca del ecuador, las temperaturas durante los interglaciales aumentaron en el hemisferio sur y los cambios de volumen de hielo se produjeron en fase en ambos hemisferios.

# 7. CONCLUSIONS

First of all, a **chronological framework** for the studied interval was established synchronising the benthic oxygen isotope record of Site U1314 with the Antarctic temperature record from EDC ice core. The studied interval encompasses from 779 to 407 ka, which includes from MIS 19 to MIS 11.

The study of stable oxygen and carbon isotopes from benthic and planktic foraminifers, planktic foraminifer assemblages, IRD abundances, paleotemperature reconstructions made with Mg/Ca paleothermometry and transfer functions allowed us to identify a set of **patterns in oceanic and climatic variability as well as in ice sheet growth**. According to these patterns we divided the glacial-interglacial cycles in **five stages**.

1) **Early interglacial stage**. During this stage the thermohaline circulation was strong and the Arctic and Polar fronts were located in a similar position to present or perhaps even northwards. The NAC flowed though the Atlantic and reached the NGS and the Labrador Sea where it sank generating NADW as it happens at present.
2) **Late interglacial stage**. During this stage the Arctic front migrated southeastwards owing to a cooling of winters although no ice was accumulating in the continents. The thermohaline circulation was active, but it is likely that deep water formation in the Labrador Sea was reduced and the NGS was the main deep water source of NADW.
3) **First stage of glacial periods**. During this stage ice started to accumulate in the continents but the thermohaline circulation remained active. However, deep water convection only occurred in the NGS because the Arctic and Polar fronts were further south and the Labrador Sea was almost perennially sea ice covered. The presence of Arctic waters in the subpolar Atlantic also indicates by the decrease in salinity and seawater $\delta^{18}O$. The NAC flowed only over the Rockall-Hatton and the Rockall channel, but still reached the NGS. The Northern Hemisphere ice sheet growth was fast owing to the active thermohaline circulation that allowed the transport of water vapour from the oceans to the continents. The extraction of freshwater also helped to maintain the thermohaline circulation active increasing seawater salinity. It is likely that the NADW was progressively getting cooler and this cooling was transmitted to the Southern Hemisphere via the thermohaline circulation.
4) **Second stage of glacial periods**. This stage began with the first ice-rafting event which interrupted the ice sheet growth and disturbed the thermohaline circulation. The generation of NADW was replaced by GNAIW. During this stage the long-term ice sheet growth was punctuated by sharp millennial-scale events in which the ice sheets waned. We denominated these events as ice sheet collapse events (ISCE). The ISCE began with iceberg discharges to the North Atlantic that dampened the formation of GNAIW and produced a warming event in the Southern Hemisphere due to the see-saw effect. During this warming $CO_2$ was outgassed

from the ocean to the atmosphere. After the iceberg discharges, an abrupt warming took place in the Northern Hemisphere as a result of the increase in atmospheric $CO_2$ and the resume of the thermohaline circulation. During the cool phases in which ice sheets were growing, the subpolar North Atlantic was seasonally covered by sea ice at least until 55ºN. The Arctic and Polar fronts were located further south, approximately with an East-West direction and the NAC hardly reached Site 980.The GNAIW was probably generated south of 60ºN. Conversely, during the warm periods of the ISCE, the Arctic front migrated northwards rapidly (at least in the East Atlantic) and it is likely that the NAC reached latitudes near Scotland and GNAIW was generated northernmost.

5) **Late glacial periods-termination**. At the end of glacial periods the Arctic front slowly began to retreat. However during the termination the Arctic front migrated abruptly northwestwards and the NAC was progressively entering towards the NGS and the Labrador Sea, resuming NADW formation. During terminations, there was a vast input of freshwater to the North Atlantic which decreased surface salinity during short periods.

**Planktic foraminifer assemblages** show sharp changes between warm and cold periods. During **warm periods** the transitional-subpolar species *N. pachyderma* dex, *G. inflata* y *G. bulloides* dominate the assemblage, whereas an almost monospecific *N. pachyderma* sin assemblage throve during **cold periods**. These abrupt shifts are controlled by the **position of the Arctic front**, which determines the presence of NAC waters or Arctic waters in the studied area. Additionally the high percentages of *T. quinqueloba* allowed us to track when the Arctic front was near Site U1314.

Paleotemperature reconstructions performed with transfer functions for planktic foraminifers and Mg/Ca paleothermometry showed that Mg/Ca paleothermometry is reliable when the Arctic front was north of Site U1314 whereas the presence of the Arctic waters interfered in the Mg/Ca-temperature relationship, supporting previous works. Additionally the analysis of temperatures and $\delta^{18}O$ records on planktic foraminifer tests of *N. pachyderma* sin and dex suggests that during interglacial periods the difference between both species is related to seasonality and stratification of the water column. During MIS 15 and 11 seasonality was higher, with cooler winters and warmer summers than during MIS 17 and 13 summer stratification of the water column was higher than during MIS 17 and 13. The differences in seasonality might be related with the strength of summer winds. During interglacial periods the presence of sea ice during most of the year favoured that both species lived during the same season and in the same water mass because the sea ice melting might have produced a low salinity lid that prevented water mixing. The iceberg discharges did not produce significant changes in the seawater $\delta^{18}O$ except at the Terminations.

Time series analyses performed on the different records of the Thesis and their comparison with the spectral analyses of EDC records, showed a progressive importance of the precession band in the climatic cycles. From the marine-establishment of the East Antarctic Ice Sheet the Southern Hemisphere fluctuated between in and out phase responses respect to the Northern hemisphere

until MIS 12. This change produced a northward shift in the ITCZ increasing moisture transport to higher latitudes and contributing to the snow accumulation and the large ice sheet growth of MIS 16. From MIS 16 to 12 high latitude northern hemisphere insolation controlled global climate changes and the $CO_2$ concentration, but the climate was still highly influenced by obliquity. After MIS 12 the ITCZ migrated near the equator, sea surface temperatures in the Southern Hemisphere increased and ice volume changes occurred in phase.

# BIBLIOGRAFÍA

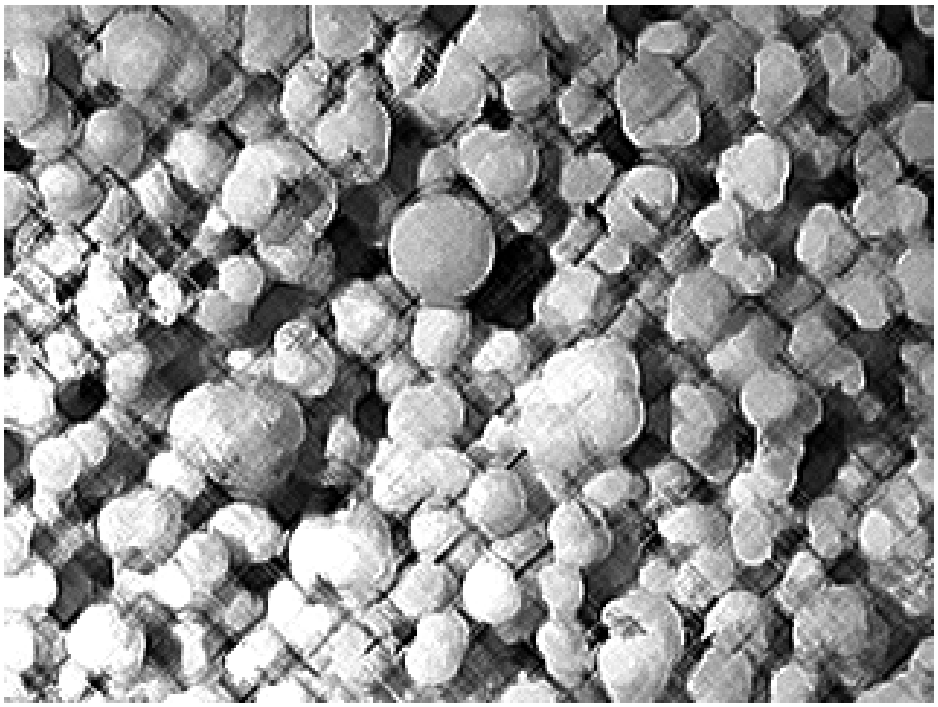

# BIBLIOGRAFÍA

Aksu, A.E., de Vernal, A., Mudie, P.J., 1989. High-resolution foraminifer, palynologic, and stable isotopic records of upper Pleistocene sediments from the Labrador Sea: paleoclimatic and paleoceanographic trends, In: Srivastava, S.P., Arthur, M., Clement, B. (Eds.), Proceedings of the Ocean Drilling Program, Scientific results, pp. 617-652.

Anand, P., Elderfield, H., Conte, M.H., 2003. Calibration of Mg/Ca thermometry in planktonic foraminifera from a sediment trap time series. Paleoceanography 18.

Anderson, R.F., Ali, S., Bradtmiller, L.I., Nielsen, S.H.H., Fleisher, M.Q., Anderson, B.E., Burckle, L.H., 2009. Wind-Driven Upwelling in the Southern Ocean and the Deglacial Rise in Atmospheric CO2. Science 323, 1443-1448.

Anderson, R.F., Carr, M.-E., 2010. Uncorking the Southern Ocean's Vintage CO2. Science 328, 1117-1118.

Arz, H.W., Lamy, F., Ganopolski, A., Nowaczyk, N., Pätzold, J., 2007. Dominant Northern Hemisphere climate control over millennial-scale glacial sea-level variability. Quaternary Science Reviews 26, 312-321.

Barker, S., Greaves, M., Elderfield, H., 2003. A study of cleaning procedures used for foraminiferal Mg/Ca paleothermometry. Geochem. Geophys. Geosyst. 4, doi: 10.1029/2003GC000559.

Barrows, T.T., Juggins, S., 2005. Sea-surface temperatures around the Australian margin and Indian Ocean during the Last Glacial Maximum. Quaternary Science Reviews 24, 1017-1047.

Bassinot, F.C., Beaufort, L., Vincent, E., Labeyrie, L.D., Rostek, F., Müller, P.J., Quidelleur, X., Lancelot, Y., 1994. Coarse Fraction Fluctuations in Pelagic Carbonate Sediments from the Tropical Indian Ocean: A 1500-Kyr Record of Carbonate Dissolution. Paleoceanography 9, 579-600.

Bauch, D., Carstens, J., Wefer, G., 1997. Oxygen isotope composition of living Neogloboquadrina pachyderma (sin.) in the Arctic Ocean. Earth and Planetary Science Letters 146, 47-58.

Bauch, D., Darling, K., Simstich, J., Bauch, H.A., Erlenkeuser, H., Kroon, D., 2003. Palaeoceanographic implications of genetic variation in living North Atlantic Neogloboquadrina pachyderma. Nature 424, 299-302.

Bé, A.W.H., 1977. An ecological, zoogeographic and taxonomic review of recent planktonic foraminifera, In: Ramsay, A.T.S. (Ed.), Oceanic Micropalaeontology. Academic Press, London, pp. 1-100.

Bé, A.W.H., Hutson, W.H., 1977. Ecology of planktonic foraminifera and biogeographic patterns of life and fossil assemblages in the Indian Ocean. Micropaleontology 23, 369-414.

Bé, A.W.H., Tolderlund, D.S., 1971. Distribution and ecology of living planktonic foraminifera in surface waters of the Atlantic and Indian Oceans, In: Funnell, B., Riedel, W.R. (Eds.), The Micropaleontology of the Oceans. Cambridge University Press, London, pp. 105-149.

Becquey, S., Gersonde, R., 2002. Past hydrographic and climatic changes in the Subantarctic Zone of the South Atlantic - The Pleistocene record from ODP Site 1090. Palaeogeography, Palaeoclimatology, Palaeoecology 182, 221-239.

Berger, A., 1988. Milankovitch Theory and Climate. Rev. Geophys. 26, 624–657.

Berger, A., Li, X.S., Loutre, M.F., 1999. Modelling northern hemisphere ice volume over the last 3 Ma. Quaternary Science Reviews 18, 1-11.

Berger, A., Loutre, M.F., 1991. Insolation values for the climate of the last 10 million years. Quaternary Science Reviews 10, 297-317.

Berger, W.H., Jansen, E., 1994. Mid-Pleistocene climate shift-The Nansen connection, In: Johannessen, O.M., Muench, R.D., Overland, J.E. (Eds.), The Polar Oceans and their Role in Shaping the Global Environment. AGU, Washington D.C., pp. 295-311.

Berger, W.H., Wefer, G., 2003. On the Dynamics of the Ice Ages: Stage-11 Paradox, Mid-Brunhes Climate Shift, and 100-ky Cycle, In: Droxler, A.W., Poore, R.Z., Burkle, L.H. (Eds.), Earth's Climate and Orbital Eccentricity. The Marine Isotope Stage 11 Question. Geophysical Monograph, 137. Americal Geophysical Union, Washington D.C., pp. 41-59.

Bintanja, R., van de Wal, R.S.W., 2008. North American ice-sheet dynamics and the onset of 100,000-year glacial cycles. Nature 454, 869-872.

Bintanja, R., van de Wal, R.S.W., Oerlemans, J., 2005. Modelled atmospheric temperatures and global sea levels over the past million years. Nature 437, 125-128.

Blunier, T., Brook, E.J., 2001. Timing of Millennial-Scale Climate Change in Antarctica and Greenland During the Last Glacial Period. Science 291, 109-112.

Blunier, T., Chappellaz, J., Schwander, J., Dallenbach, A., Stauffer, B., Stocker, T.F., Raynaud, D., Jouzel, J., Clausen, H.B., Hammer, C.U., Johnsen, S.J., 1998. Asynchrony of Antarctic and

Greenland climate change during the last glacial period. Nature 394, 739-743.

Bond, G., Broecker, W., Johnsen, S., McManus, J., Labeyrie, L., Jouzel, J., Bonani, G., 1993. Correlations between climate records from North Atlantic sediments and Greenland ice. Nature 365, 143-147.

Bond, G., Heinrich, H., Broecker, W., Labeyrie, L., McManus, J., Andrews, J., Huon, S., Jantschik, R., Clasen, S., Simet, C., Tedesco, K., Klas, M., Bonani, G., Ivy, S., 1992. Evidence for massive discharges of icebergs into the North Atlantic ocean during the last glacial period. Nature 360, 245-249.

Bond, G.C., Lotti, R., 1995. Iceberg Discharges into the North Atlantic on Millennial Time Scales During the Last Glaciation. Science 267, 1005-1010.

Bonelli, S., Charbit, S., Kageyama, M., Woillez, M.N., Ramstein, G., Dumas, C., Quiquet, A., 2009. Investigating the evolution of major Northern Hemisphere ice sheets during the last glacial-interglacial cycle. Clim. Past 5, 329-345.

Boyle, E.A., Keigwin, L., 1987. North Atlantic thermohaline circulation during the past 20,000 years linked to high-latitude surface temperature. Nature 330, 35-40.

Brierley, C.M., Fedorov, A.V., 2010. Relative importance of meridional and zonal sea surface temperature gradients for the onset of the ice ages and Pliocene-Pleistocene climate evolution. Paleoceanography 25, PA2214, doi:2210.1029/2009PA001809.

Broecker, W.S., 1991. The Great Ocean Conveyor. Oceanography 4, 79-89.

Broecker, W.S., Denton, G.H., 1989. The role of ocean-atmosphere reorganizations in glacial cycles. Geochimica et Cosmochimica Acta 53, 2465-2501.

Brown, S.J., Elderfield, H., 1996. Variations in Mg/Ca and Sr/Ca Ratios of Planktonic Foraminifera Caused by Postdepositional Dissolution: Evidence of Shallow Mg-Dependent Dissolution. Paleoceanography 11, 543-551.

Byrami, M.L., Newnham, R.M., Alloway, B.V., Pillans, B., Ogden, J., Westgate, J., Mildenhall, D.C., 2005. A late Early Pleistocene tephrochronological and pollen record from Auckland, New Zealand. Geological Society, London, Special Publications 247, 183-208.

Carstens, J., Wefer, G., 1992. Recent distribution of planktonic foraminifera in the Nansen Basin, Arctic Ocean. Deep Sea Research Part A. Oceanographic Research Papers 39, S507-S524.

Cifelli, R., 1973. Observations on Globigerina pachyderma (Ehrenberg) and Globigerina incompta Cifelli from the North Atlantic. Journal of Foraminiferal Research 3, 157-166.

Clark, P.U., Pollard, D., 1998. Origin of the Middle Pleistocene Transition by Ice Sheet Erosion of Regolith. Paleoceanography 13, 1-9.

Clarke, F.W., Wheeler, W.C., 1922. The inorganic constituents of marine invertebrates. USGS Professional Paper 124, 55.

CLIMAP project members, 1976. The Surface of the Ice-Age Earth. Science 191, 1131-1137.

CLIMAP project members, 1981. Seasonal reconstruction of the Earth's Surface at the Last Glacial Maximum. MC-36 1-18. Map and chart series, Geol. Soc. Am.

Coplen, T.B., 1996. More Uncertainty than Necessary. Paleoceanography 11, 369-370, DOI: 310.1029/1096PA01420.

Corliss, B.H., 1985. Microhabitats of benthic foraminifera within deep-sea sediments. Nature 314, 435-438.

Cortese, G., Gersonde, R., 2008. Plio/Pleistocene changes in the main biogenic silica carrier in the Southern Ocean, Atlantic Sector. Marine Geology 252, 100-110.

Cortijo, E., Duplessy, J.C., Labeyrie, L., Leclaire, H., Duprat, J., van Wearing, T.C.E., 1994. Eemian cooling in the Norwegian Sea and North Atlantic ocean preceding continental ice-sheet growth. Nature 372, 446-449.

Crucifix, M., Loutre, F., 2002. Transient simulations over the last interglacial period (126-115 kyr BP): feedback and forcing analysis. Climate Dynamics 19, 417-433.

Cuenca-Bescos, G., Rofes, J., Garcia-Pimienta, J., 2005. Environmental change across the Early-Middle Pleistocene transition: small mammalian evidence from the Trinchera Dolina cave, Atapuerca, Spain. Geological Society, London, Special Publications 247, 277-286.

Curry, W.B., Oppo, D.W., 2005. Glacial water mass geometry and the distribution of δ 13 C of Sigma CO 2 in the western Atlantic Ocean. Paleoceanography 20, 1-12.

Channell, J.E.T., Kanamatsu, T., Sato, T., Stein, R., Alvarez Zarikian, C.A., Malone, M.J., and the Expedition Scientists, 2006. 303/306 Expedition reports, North Atlantic Climate, Proceedings of the Integrated Ocean Drilling Program, College Station TX (Integrated Ocean Drilling Program Management International, Inc.).

Channell, J.E.T., Kleiven, H.F., 2000. Geomagnetic palaeointensities and astrochronological ages for the Matuyama-Brunhes boundary and the boundaries of the Jaramillo Subchron: palaeomagnetic and oxygen isotope records from ODP Site 983. Philosophical Transactions of the Royal Society of London. Series A: Mathematical, Physical and Engineering Sciences 358, 1027-1047.

Chapman, M.R., 2010. Seasonal production patterns of planktonic foraminifera in the NE Atlantic Ocean: Implications for paleotemperature and hydrographic reconstructions. Paleoceanography 25, PA1101, doi:1110.1029/2008PA001708.

Chapman, M.R., Shackleton, N.J., 1998. Millennial-scale fluctuations in North Atlantic heat flux during the last 150,000 years. Earth and Planetary Science Letters 159, 57-70.

Chapman, M.R., Shackleton, N.J., 1999. Global ice-volume fluctuations, North Atlantic ice-rafting events, and deep-ocean circulation changes between 130 and 70 ka. Geology 27, 795-798.

Chappellaz, J., Bluniert, T., Raynaud, D., Barnola, J.M., Schwander, J., Stauffert, B., 1993. Synchronous changes in atmospheric CH4 and Greenland climate between 40 and 8 kyr BP. Nature 366, 443-445.

Chen, F.H., Bloemendal, J., Zhang, P.Z., Liu, G.X., 1999. An 800 ky proxy record of climate from lake sediments of the Zoige Basin, eastern Tibetan Plateau. Palaeogeography, Palaeoclimatology, Palaeoecology 151, 307-320.

Darling, K.F., Kucera, M., Kroon, D., Wade, C.M., 2006. A resolution for the coiling direction paradox in Neogloboquadrina pachyderma. Paleoceanography 21, doi: 10.1029/2005PA001189.

Darling, K.F., Kucera, M., Pudsey, C.J., Wade, C.M., 2004. Molecular evidence links cryptic diversification in polar planktonic protists to Quaternary climate dynamics. Proceedings of the National Academy of Sciences 101, 7657-7662.

Darling, K.F., Kucera, M., Wade, C.M., 2007. Global molecular phylogeography reveals persistent Arctic circumpolar isolation in a marine planktonic protist. Proceedings of the National Academy of Sciences 104, 5002-5007.

Daubechies, I., 1992. Ten Lectures on Wavelets. Society for Industrial and Applied Mathematics.

de Abreu, L.c., Abrantes, F.t.F., Shackleton, N.J., Tzedakis, P.C., McManus, J.F., Oppo, D.W., Hall, M.A., 2005. Ocean climate variability in the eastern North Atlantic during interglacial marine isotope stage 11: A partial analogue to the Holocene? Paleoceanography 20, doi: 10.1029/2004PA001091.

de Vernal, A., Hillaire-Marcel, C., 2008. Natural Variability of Greenland Climate, Vegetation, and Ice Volume During the Past Million Years. Science 320, 1622-1625.

Dekens, P.S., Lea, D.W., Pak, D.K., Spero, H.J., 2002. Core top calibration of Mg/Ca in tropical foraminifera: Refining paleotemperature estimation. Geochem. Geophys. Geosyst. 3, doi: 10.1029/2001GC000200.

Dennell, R., 2003. Dispersal and colonisation, long and short chronologies: how continuous is the Early Pleistocene record for hominids outside East Africa? Journal of Human Evolution 45, 421-440.

Denton, G.H., 2000. Does an asymmetric thermohaline-ice-sheet oscillator drive 100 000-yr glacial cycles? Journal of Quaternary Science 15, 301-318.

Dickson, A.J., Austin, W.E.N., Hall, I.R., Maslin, M.A., Kucera, M., 2008a. Centennial-scale evolution of Dansgaard-Oeschger events in the northeast Atlantic Ocean between 39.5 and 56.5 ka B.P. Paleoceanography 23, 1-13.

Dickson, A.J., Leng, M.J., Maslin, M.A., 2008b. Mid-depth South Atlantic Ocean circulation and chemical stratification during MIS-10 to 12: implications for atmospheric CO2. Clim. Past 4, 333-344.

Dickson, R.R., Gmitrowicz, E.M., Watson, A.J., 1990. Deep-water renewal in the northern North Atlantic. Nature 344, 848-850.

Dieckmann, G.S., Spindler, M., Lange, M.A., Ackley, S.F., Eicken, H., 1991. Antarctic sea ice; a habitat for the foraminifer Neogloboquadrina pachyderma. Journal of Foraminiferal Research 21, 182-189.

Diekmann, B., Kuhn, G., 2002. Sedimentary record of the mid-Pleistocene climate transition in the southeastern South Atlantic (ODP Site 1090). Palaeogeography, Palaeoclimatology, Palaeoecology 182, 241-258.

Droxler, A.W., Poore, R.Z., Burkle, L.H., 2003. Earth's Climate and Orbital Eccentricity. The Marine Isotope Stage 11 Question. Americal Geophysical Union, Washington D.C.

Duplessy, J.-C., Shackleton, N.J., 1985. Response of global deep-water circulation to Earth's climatic change 135,000-107,000 years ago. Nature 316, 500-507.

Dupont, L.M., Donner, B., Schneider, R., Wefer, G., 2001. Mid-Pleistocene environmental change in tropical Africa began as early as 1.05 Ma. Geology 29, 195-198.

Ehlers, J., Gibbard, P.L., 2007. The extent and chronology of Cenozoic Global Glaciation. Quaternary International 164-165, 6-20.

Elderfield, H., Ganssen, G., 2000. Past temperature and [delta]18O of surface ocean waters inferred from foraminiferal Mg/Ca ratios. Nature 405, 442-445.

Emiliani, C., 1955. Pleistocene Temperatures. The Journal of Geology 63, 538-578.

EPICA Community members, 2004. Eight glacial cycles from an Antarctic ice core. Nature 429, 623-628.

Epstein, S., Buchsbaum, R., Lowenstam, H.A., Urey, H.C., 1953. Revised carbonate-water isotopic temperature scale. Geological Society of America Bulletin 64, 1315–1326.

Ericson, D.B., 1959. Coiling Direction of Globigerina pachyderma as a Climatic Index. Science 130, 219-220.

Fairbanks, R.G., Sverdlove, M., Free, R., Wiebe, P.H., Be, A.W.H., 1982. Vertical distribution and isotopic fractionation of living planktonic foraminifera from the Panama Basin. Nature 298, 841-844.

Fairbanks, R.G., Wiebe, P.H., Be, A.W.H., 1980. Vertical Distribution and Isotopic Composition of Living Planktonic Foraminifera in the Western North Atlantic. Science 207, 61-63.

Ferretti, P., Shackleton, N.J., Rio, D., Hall, M.A., 2005. Early-Middle Pleistocene deep circulation in the western subtropical Atlantic: southern hemisphere modulation of the North Atlantic Ocean. Geological Society, London, Special Publications 247, 131-145.

Fischer, H., Schmitt, J., Lüthi, D., Stocker, T.F., Tschumi, T., Parekh, P., Joos, F., Köhler, P., Völker, C., Gersonde, R., Barbante, C., Le Floch, M., Raynaud, D., Wolff, E., 2010. The role of Southern Ocean processes in orbital and millennial CO2 variations - A synthesis. Quaternary Science Reviews 29, 193-205.

Flint, J.M., 1899. Recent Foraminifera: A descriptive catalogue of specimens dreged by the U.S. Fish Commission Steamer Albatross.

Flower, B.P., Hastings, D.W., Hill, H.W., Quinn, T.M., 2004. Phasing of deglacial warming and Laurentide Ice Sheet meltwater in the Gulf of Mexico. Geology 32, 597-600.

Flower, B.P., Oppo, D.W., McManus, J.F., Venz, K.A., Hodell, D.A., Cullen, J.L., 2000. North Atlantic intermediate to deep water circulation and chemical stratification during the past 1 Myr. Paleoceanography 15, 388-403.

Fraile, I., Schulz, M., Mulitza, S., Kucera, M., 2008. Predicting the global distribution of planktonic foraminifera using a dynamic ecosystem model. Biogeosciences 5, 891-911.

Fraile, I., Schulz, M., Mulitza, S., Merkel, U., Prange, M., Paul, A., 2009. Modeling the seasonal distribution of planktonic foraminifera during the Last Glacial Maximum. Paleoceanography 24, PA2216, doi : 2210.1029/2008PA001686.

Fronval, T., Jansen, E., 1997. Eemian and Early Weichselian (140-60 ka) Paleoceanography and

Paleoclimate in the Nordic Seas With Comparisons to Holocene Conditions. Paleoceanography 12, 443-462.

Fronval, T., Jansen, E., Haflidason, H., Sejrup, J.P., 1998. Variability in surface and deep water conditions in the Nordic seas during the last interglacial period. Quaternary Science Reviews 17, 963-985.

Ganopolski, A., Roche, D.M., 2009. On the nature of lead-lag relationships during glacial-interglacial climate transitions. Quaternary Science Reviews 28, 3361-3378.

GEOSECS, 1987. Atlantic, Pacific and Indian Ocean Expeditions Shorebased data and graphics., In: Ostlund, H.G., Craig, H., Broecker, S.W.S., Spencer, D. (Eds.), GEOSECS Executive Committee. National Science Foundation 7.

Guo, Z., Biscaye, P., Wei, L., Chen, X., Peng, S., Liu, T., 2000. Summer monsoon variations over the last 1.2 Ma from the weathering of loess‐soil sequences in China. Geophys. Res. Lett. 27, 1751-1754.

Guo, Z.T., Berger, A., Yin, Q.Z., Qin, L., 2009. Strong asymmetry of hemispheric climates during MIS-13 inferred from correlating China loess and Antarctica ice records. Climate of the Past 5, 21-31.

Hansen, B., Østerhus, S., 2000. North Atlantic-Nordic Seas exchanges. Progress In Oceanography 45, 109-208.

Haug, G.H., Sigman, D.M., Tiedemann, R., Pedersen, T.F., Sarnthein, M., 1999. Onset of permanent stratification in the subarctic Pacific Ocean. Nature 401, 779-782.

Haug, G.H., Tiedemann, R., 1998. Effect of the formation of the Isthmus of Panama on Atlantic Ocean thermohaline circulation. Nature 393, 673-676.

Hayes, A., Kucera, M., Kallel, N., Sbaffi, L., Rohling, E.J., 2005. Glacial Mediterranean sea surface temperatures based on planktonic foraminiferal assemblages. Quaternary Science Reviews 24, 999-1016.

Hayward, B.W., Grenfell, H.R., Sabaa, A.T., Sikes, E., 2005. Deep-sea benthic foraminiferal record of the mid-Pleistocene transition in the SW Pacific. Geological Society, London, Special Publications 247, 85-115.

Head, M.J., Gibbard, P.L., 2005. Early-Middle Pleistocene transitions: an overview and recommendation for the defining boundary. Geological Society, London, Special Publications 247, 1-18.

Head, M.J., Pillans, B., Farquhar, S.A., 2008. The Early-Middle Pleistocene Transition: characterization and proposed guide for the defining boundary. Episodes 31, 255-259.

Heinrich, H., 1988. Origin and consequences of cyclic ice rafting in the Northeast Atlantic Ocean during the past 130,000 years. Quaternary Research 29, 142-152.

Hemleben, C., Spindler, M., Anderson, O.R., 1989. Modern Planktonic Foraminifera. Springer-Verlag, New York.

Heslop, D., Dekkers, M.J., Langereis, C.G., 2002. Timing and structure of the mid-Pleistocene transition: records from the loess deposits of northern China. Palaeogeography, Palaeoclimatology, Palaeoecology 185, 133-143.

Hodell, D.A., Channell, J.E.T., Curtis, J.H., Romero, O.E., Röhl, U., 2008. Onset of "Hudson Strait" Heinrich events in the eastern North Atlantic at the end of the middle Pleistocene transition (~640 ka)? Paleoceanography 23.

Hodell, D.A., Venz-Curtis, K.A., 2006. Late Neogene history of deepwater ventilation in the Southern Ocean. Geochem. Geophys. Geosyst. 7, Q09001, doi:09010.01029/02005GC001211.

Hodell, D.A., Venz, K.A., Charles, C.D., Ninnemann, U.S., 2003. Pleistocene vertical carbon isotope and carbonate gradients in the South Atlantic sector of the Southern Ocean. Geochem. Geophys. Geosyst. 4, 1004, doi:1010.1029/2002GC000367.

Huber, R., Meggers, H., Baumann, K.-H., Raymo, M.E., Henrich, R., 2000. Shell size variation of the planktonic foraminifer Neogloboquadrina pachyderma sin. in the Norwegian-Greenland Sea during the last 1.3 Myrs: implications for paleoceanographic reconstructions. Palaeogeography, Palaeoclimatology, Palaeoecology 160, 193-212.

Hurdle, B.G., 1986. The Nordic Seas. Springer Verlag, New York.

Hutson, W.H., 1980. The Agulhas Current During the Late Pleistocene: Analysis of Modern Faunal Analogs. Science 207, 64-66.

Huybers, P., 2006. Early Pleistocene Glacial Cycles and the Integrated Summer Insolation Forcing. Science 313, 508-511.

Huybers, P., 2007. Glacial variability over the last two million years: an extended depth-derived agemodel, continuous obliquity pacing, and the Pleistocene progression. Quaternary Science Reviews 26, 37-55.

Imbrie, J., Berger, A., Boyle, E.A., Clemens, S.C., Duffy, A., Howard, W.R., Kukla, G., Kutzbach, J., Martinson, D.G., McIntyre, A., Mix, A.C., Molfino, B., Morley, J.J., Peterson, L.C., Pisias,

N.G., Prell, W.L., Raymo, M.E., Shackleton, N.J., Toggweiler, J.R., 1993. On the Structure and Origin of Major Glaciation Cycles 2. The 100,000-Year Cycle. Paleoceanography 8, 699–735.

Imbrie, J., Boyle, E.A., Clemens, S.C., Kutzbach, J., Martinson, D.G., McIntyre, A., Mix, A.C., Molfino, B., Morley, J.J., Peterson, L.C., Pisias, N.G., Prell, W.L., Raymo, M.E., Shackleton, N.J., Toggweiler, J.R., 1992. On the Structure and Origin of Major Glaciation Cycles 1. Linear responses to Milankovitch forcing. Paleoceanography 7, 701-738.

Imbrie, J., Kipp, N.G., 1971. A new micropaleontological method for quantitative paleoclimatology. Application to a late Pleistocene Caribbean core, In: Turekian, K.K. (Ed.), The Late Cenozoic glacial ages. Yale University Press, New Haven, pp. 71–131.

Jenkins, G.M., Watts, D.G., 1968. Spectral Analysis and its Applications. Holden-Day, San Francisco.

Johannessen, T., Jansen, E., Flatoy, A., Ravelo, A.C., 1994. The relationship between surface water masses, oceanographic fronts and paleoclimatic proxies in surface sediments of the Greenland, Iceland, Norwegian seas, In: Zahn, R., Pederesen, T. F., Kaminski, M. A., Labeyrie, L (Ed.), Carbon Cycling in the Glacial Ocean, *NATO ASI Series I*. Springer-Verlag, Berlin Heidelberg, p. 580.

Jouzel, J., Masson-Delmotte, V., Cattani, O., Dreyfus, G., Falourd, S., Hoffmann, G., Minster, B., Nouet, J., Barnola, J.M., Chappellaz, J., Fischer, H., Gallet, J.C., Johnsen, S., Leuenberger, M., Loulergue, L., Luethi, D., Oerter, H., Parrenin, F., Raisbeck, G., Raynaud, D., Schilt, A., Schwander, J., Selmo, E., Souchez, R., Spahni, R., Stauffer, B., Steffensen, J.P., Stenni, B., Stocker, T.F., Tison, J.L., Werner, M., Wolff, E.W., 2007. Orbital and Millennial Antarctic Climate Variability over the Past 800,000 Years. Science 317, 793-796.

Keigwin, L., 1982. Isotopic Paleoceanography of the Caribbean and East Pacific: Role of Panama Uplift in Late Neogene Time. Science 217, 350-353.

King, A.L., Howard, W.R., 2005. d18O seasonality of planktonic foraminifera from Southern Ocean sediment traps: Latitudinal gradients and implications for paleoclimate reconstructions. Marine Micropaleontology 56, 1-24.

Kleiven, H.F., Jansen, E., Curry, W.B., Hodell, D.A., Venz, K.A., 2003. Atlantic Ocean thermohaline circulation changes on orbital to suborbital timescales during the mid-Pleistocene. Paleoceanography 18, 1008.

Koç, N., Flower, B.P., 1998. High-resolution Pleistocene diatom biostratigraphy and paleoceanography of Site 919 from the Irminger Basin, In: Saunders, A.D., Larsen, H.C., Wise, S.W., Jr. (Eds.), Proceedings of the Ocean Drilling Program, Scientific Results, 152, College

Station, TX (Ocean Drilling Program), pp. 209–219.

Koç, N., Hodell, D.A., Kleiven, H.F., Labeyrie, L., 1999. High-resolution Pleistocene diatom biostratigraphy of Site 983 and correlations with isotope stratigraphy, In: Raymo, M.E., Jansen, E., Blum, P., Herbert, T. (Eds.), Proceedings of the Ocean Drilling Program, Scientific Results, 162, College Station, TX (Ocean Drilling Program), pp. 51-62.

Kohfeld, K.E., Fairbanks, R.G., Smith, S.L., Walsh, I.D., 1996. Neogloboquadrina Pachyderma (sinistral coiling) as Paleoceanographic Tracers in Polar Oceans: Evidence from Northeast Water Polynya Plankton Tows, Sediment Traps, and Surface Sediments. Paleoceanography 11, 679-699.

Kozdon, R., Eisenhauer, A., Weinelt, M., Meland, M.Y., Nürnberg, D., 2009. Reassessing Mg/Ca temperature calibrations of Neogloboquadrina pachyderma (sinistral) using paired d44/40Ca and Mg/Ca measurements. Geochem. Geophys. Geosyst. 10, Q03005, doi:03010.01029/02008GC002169.

Kucera, M., Darling, K.F., 2002. Cryptic species of planktonic foraminifera: their effect on paleoceanographic reconstructions. Phil. Trans. R. Soc. Lond. A 360, 695-718.

Kucera, M., Weinelt, M., Kiefer, T., Pflaumann, U., Hayes, A., Weinelt, M., Chen, M.-T., Mix, A.C., Barrows, T.T., Cortijo, E., Duprat, J., Juggins, S., Waelbroeck, C., 2005. Reconstruction of sea-surface temperatures from assemblages of planktonic foraminifera: multi-technique approach based on geographically constrained calibration data sets and its application to glacial Atlantic and Pacific Oceans. Quaternary Science Reviews 24, 951-998.

Landais, A., Masson-Delmotte, V., Jouzel, J., Raynaud, D., Johnsen, S., Huber, C., Leuenberger, M., Schwander, J., Minster, B., 2006. The glacial inception as recorded in the NorthGRIP Greenland ice core: timing, structure and associated abrupt temperature changes. Climate Dynamics 26, 273-284.

Laskar, J., Joutel, F., Robutel, P., 1993. Stabilization of the Earth's obliquity by the Moon. Nature 361, 615-617.

Laskar, J., Robutel, P., Joutel, F., Gastineau, M., Correia, A.C.M., Levrard, B., 2004. A long-term numerical solution for the insolation quantities of the Earth. Astron.Astrophys. 428, 261-285.

Lea, D.W., Mashiotta, T.A., Spero, H.J., 1999. Controls on magnesium and strontium uptake in planktonic foraminifera determined by live culturing. Geochimica et Cosmochimica Acta 63, 2369-2379.

Lea, D.W., Pak, D.K., Spero, H.J., 2000. Climate Impact of Late Quaternary Equatorial Pacific

Sea Surface Temperature Variations. Science 289, 1719-1724.

Lisiecki, L.E., Raymo, M.E., 2005. A Pliocene-Pleistocene stack of globally distributed benthic δ18O records. Paleoceanography 20, DOI: 10.1029/2004PA001071.

Lisiecki, L.E., Raymo, M.E., 2007. Plio-Pleistocene climate evolution: trends and transitions in glacial cycle dynamics. Quaternary Science Reviews 26, 56-69.

Liu, Z., Herbert, T.D., 2004. High-latitude influence on the eastern equatorial Pacific climate in the early Pleistocene epoch. Nature 427, 720-723.

Locarnini, R.A., Mishonov, A.V., Antonov, J.I., Boyer, T.P., Garcia, H.E., 2006. World Ocean Atlas 2005, Volume 1: Temperature. S. Levitus Ed. U.S. Government Printing Office, Washington, D.C.

Loulergue, L., Schilt, A., Spahni, R., Masson-Delmotte, V., Blunier, T., Lemieux, B., Barnola, J.-M., Raynaud, D., Stocker, T.F., Chappellaz, J., 2008. Orbital and millennial-scale features of atmospheric CH4 over the past 800,000 years. Nature 453, 383-386.

Luthi, D., Le Floch, M., Bereiter, B., Blunier, T., Barnola, J.-M., Siegenthaler, U., Raynaud, D., Jouzel, J., Fischer, H., Kawamura, K., Stocker, T.F., 2008. High-resolution carbon dioxide concentration record 650,000-800,000 years before present. Nature 453, 379-382.

Malmgren, B.r.A., Kucera, M., Nyberg, J., Waelbroeck, C., 2001. Comparison of Statistical and Artificial Neural Network Techniques for Estimating Past Sea Surface Temperatures from Planktonic Foraminifer Census Data. Paleoceanography 16, 520-530.

Maraun, D., Kurths, J., 2004. Cross wavelet analysis: significance testing and pitfalls. Nonlinear Processes in Geophysics 11, 505-514.

Marchitto, T.M., Broecker, W.S., 2006. Deep water mass geometry in the glacial Atlantic Ocean: A review of constraints from the paleonutrient proxy Cd/Ca. Geochem. Geophys. Geosyst. 7, Q12003.

MARGO project members, 2009. Constraints on the magnitude and patterns of ocean cooling at the Last Glacial Maximum. Nature Geoscience 2, 127-132.

Markovic, S.B., Hambach, U., Catto, N., Jovanovic, M., Buggle, B., Machalett, B., Zöller, L., Glaser, B., Frechen, M., 2009. Middle and Late Pleistocene loess sequences at Batajnica, Vojvodina, Serbia. Quaternary International 198, 255-266.

Martin, P.A., Lea, D.W., 2002. A simple evaluation of cleaning procedures on fossil benthic foraminiferal Mg/Ca. Geochem. Geophys. Geosyst. 3, 8401, doi:8410.1029/2001GC000280.

Martínez-Garcia, A., Rosell-Melé, A., Geibert, W., Gersonde, R., Masqué, P., Gaspari, V., Barbante, C., 2009. Links between iron supply, marine productivity, sea surface temperature, and CO2 over the last 1.1 Ma. Paleoceanography 24.

Mashiotta, T.A., Lea, D.W., Spero, H.J., 1999. Glacial-interglacial changes in Subantarctic sea surface temperature and d18O-water using foraminiferal Mg. Earth and Planetary Science Letters 170, 417-432.

Maslin, M.A., Li, X.S., Loutre, M.F., Berger, A., 1998. The contribution of orbital forcing to the progressive intensification of Northern Hemisphere glaciation. Quaternary Science Reviews 17, 411-426.

Maslin, M.A., Ridgwell, A.J., 2005. Mid-Pleistocene revolution and the 'eccentricity myth'. Geological Society, London, Special Publications 247, 19-34.

McCorkle, D.C., Keigwin, L.D., 1994. Depth Profiles of d13C in Bottom Water and Core Top C. wuellerstorfi on the Ontong Java Plateau and Emperor Seamounts. Paleoceanography 9, 197-208.

McManus, J.F., Bond, G.C., Broecker, W.S., Johnsen, S., Labeyrie, L., Higgins, S., 1994. High-resolution climate records from the North Atlantic during the last interglacial. Nature 371, 326-329.

McManus, J.F., Oppo, D.W., Cullen, J.L., 1999. A 0.5-Million-Year Record of Millennial-Scale Climate Variability in the North Atlantic. Science 283, 971-975.

McManus, J.F., Oppo, D.W., Keigwin, L.D., Cullen, J.L., Bond, G.C., 2002. Thermohaline Circulation and Prolonged Interglacial Warmth in the North Atlantic. Quaternary Research 58, 17-21.

McNabb, J., 2005. Hominins and the Early-Middle Pleistocene transition: evolution, culture and climate in Africa and Europe. Geological Society, London, Special Publications 247, 287-304.

Meland, M.Y., Jansen, E., Elderfield, H., Dokken, T.M., Olsen, A., Bellerby, R.G.J., 2006. Mg/Ca ratios in the planktonic foraminifer Neogloboquadrina pachyderma (sinistral) in the northern North Atlantic/Nordic Seas. Geochem. Geophys. Geosyst. 7, Q06P14, doi:10.1029/2005GC001078.

Miao, Q., Thunell, R.C., Anderson, D.M., 1994. Glacial-Holocene Carbonate Dissolution and Sea Surface Temperatures in the South China and Sulu Seas. Paleoceanography 9, 269-290.

Milankovitch, M., 1941. Canon of insolation in the Ice-Age problem. (English translation by the Israel Program for scientific translation, Jerusalem, 1969). R. Serbian Acad. Spec. Publ. 132.

Mix, A.C., Bard, E., Schneider, R., 2001. Environmental processes of the ice age: land, oceans, glaciers (EPILOG). Quaternary Science Reviews 20, 627-657.

Moros, M., Emeis, K., Risebrobakken, B., Snowball, I., Kuijpers, A., McManus, J., Jansen, E., 2004. Sea surface temperatures and ice rafting in the Holocene North Atlantic: climate influences on northern Europe and Greenland. Quaternary Science Reviews 23, 2113-2126.

Mortyn, P.G., Charles, C.D., 2003. Planktonic foraminiferal depth habitat and d18O calibrations: Plankton tow results from the Atlantic sector of the Southern Ocean. Paleoceanography 18, 1037, doi:10.1029/2001PA000637.

Mudelsee, M., Schulz, M., 1997. The Mid-Pleistocene climate transition: onset of 100 ka cycle lags ice volume build-up by 280 ka. Earth and Planetary Science Letters 151, 117-123.

Mudelsee, M., Stattegger, K., 1997. Exploring the structure of the mid-Pleistocene revolution with advanced methods of time-series analysis. Geologische Rundschau 86, 499-511.

Ninnemann, U.S., Charles, C.D., 2002. Changes in the mode of Southern Ocean circulation over the last glacial cycle revealed by foraminiferal stable isotopic variability. Earth and Planetary Science Letters 201, 383-396.

Nürnberg, D., 1995. Magnesium in tests of Neogloboquadrina pachyderma sinistral from high northern and southern latitudes. Journal of Foraminiferal Research 25, 350-368.

Nürnberg, D., Bijma, J., Hemleben, C., 1996. Assessing the reliability of magnesium in foraminiferal calcite as a proxy for water mass temperatures. Geochimica et Cosmochimica Acta 60, 803-814.

Nyland, B.F., Jansen, E., Elderfield, H., Andersson, C., 2006. Neogloboquadrina pachyderma (dex. and sin.) Mg/Ca and d18O records from the Norwegian Sea. Geochem. Geophys. Geosyst. 7, Q10P17, doi:10.1029/2005GC001055.

Oppo, D.W., McManus, J.F., Cullen, J.L., 1998. Abrupt Climate Events 500,000 to 340,000 Years Ago: Evidence from Subpolar North Atlantic Sediments. Science 279, 1335-1338.

Oppo, D.W., Raymo, M.E., Lohmann, G.P., Mix, A.C., Wright, J.D., Prell, W.L., 1995. A d13C Record of Upper North Atlantic Deep Water During the Past 2.6 Million Years. Paleoceanography 10, 373–394.

Ortiz, J.D., Mix, A.C., Collier, R.W., 1995. Environmental Control of Living Symbiotic and Asymbiotic Foraminifera of the California Current. Paleoceanography 10.

Paillard, D., Labeyrie, L., Yiou, P., 1996. Macintosh program performs time-series analysis. Eos 77, 379.

Palombo, M.R., Valli, A.M.F., 2005. Highlighting the Early-Middle Pleistocene transition in Italian and French large-mammal faunas: similarities and faunal renewals. Geological Society, London, Special Publications 247, 263-276.

Parrenin, F., Barnola, J.M., Beer, J., Blunier, T., Castellano, E., Chappellaz, J., Dreyfus, G., Fischer, H., Fujita, S., Jouzel, J., Kawamura, K., Lemieux-Dudon, B., Loulergue, L., Masson-Delmotte, V., Narcisi, B., Petit, J.R., Raisbeck, G., Raynaud, D., Ruth, U., Schwander, J., Severi, M., Spahni, R., Steffensen, J.P., Svensson, A., Udisti, R., Waelbroeck, C., Wolff, E., 2007. The EDC3 chronology for the EPICA Dome C ice core. Clim. Past 3, 485-497.

Pena, L.D., Cacho, I., Ferretti, P., Hall, M.A., 2008. El Niño-Southern Oscillation-like variability during glacial terminations and interlatitudinal teleconnections. Paleoceanography 23.

Pena, L.D., Calvo, E., Cacho, I., Eggins, S., Pelejero, C., 2005. Identification and removal of Mn-Mg-rich contaminant phases on foraminiferal tests: Implications for Mg/Ca past temperature reconstructions. Geochem. Geophys. Geosyst. 6, Q09P02.

Petit, J.R., Jouzel, J., Raynaud, D., Barkov, N.I., Barnola, J.M., Basile, I., Bender, M., Chappellaz, J., Davis, M., Delaygue, G., Delmotte, M., Kotlyakov, V.M., Legrand, M., Lipenkov, V.Y., Lorius, C., Pepin, L., Ritz, C., Saltzman, E., Stievenard, M., 1999. Climate and atmospheric history of the past 420,000 years from the Vostok ice core, Antarctica. Nature 399, 429-436.

Petraglia, M.D., 2005. Hominin responses to Pleistocene environmental change in Arabia and South Asia. Geological Society, London, Special Publications 247, 305-319.

Pflaumann, U., Duprat, J., Pujol, C., Labeyrie, L.D., 1996. SIMMAX: A Modern Analog Technique to Deduce Atlantic Sea Surface Temperatures from Planktonic Foraminifera in Deep-Sea Sediments. Paleoceanography 11, 15-35.

Pflaumann, U., Sarnthein, M., Chapman, M., d'Abreu, L., Funnell, B., Huels, M., Kiefer, T., Maslin, M., Schulz, H., Swallow, J., van Kreveld, S., Vautravers, M., Vogelsang, E., Weinelt, M., 2003. Glacial North Atlantic: Sea-surface conditions reconstructed by GLAMAP 2000. Paleoceanography 18, 1065, doi: 10.1029/2002PA000774.

Philander, S.G., Fedorov, A.V., 2003. Role of tropics in changing the response to Milankovich forcing some three million years ago. Paleoceanography 18, 1045, doi:1010.1029/2002PA000837.

Prell, W.L., 1985. The stability of low-latitude sea-surface temperatures: An evaluation of the CLIMAP reconstruction with emphasis on the positive SST anomalies, Washington, D. C.

Prokopenko, A.A., Williams, D.F., Kuzmin, M.I., Karabanov, E.B., Khursevich, G.K., Peck, J.A., 2002. Muted climate variations in continental Siberia during the mid-Pleistocene epoch. Nature

418, 65-68.

Rasmussen, T.L., Thomsen, E., 2004. The role of the North Atlantic Drift in the millennial timescale glacial climate fluctuations. Palaeogeography, Palaeoclimatology, Palaeoecology 210, 101-116.

Raymo, M.E., 1994. The Initiation of Northern Hemisphere Glaciation. Annual Review of Earth and Planetary Sciences 22, 353.

Raymo, M.E., 1997. The Timing of Major Climate Terminations. Paleoceanography 12, 577-585.

Raymo, M.E., Lisiecki, L.E., Nisancioglu, K.H., 2006. Plio-Pleistocene Ice Volume, Antarctic Climate, and the Global d18O Record. Science 313, 492-495.

Raymo, M.E., Nisancioglu, k., 2003. The 41 kyr world: Milankovitch's other unsolved mystery. Paleoceanography 18, doi: 10.1029/2002PA000791.

Raymo, M.E., Oppo, D.W., Curry, W.B., 1997. The mid-Pleistocene climate transition: A deep sea carbon isotopic perspective. Paleoceanography 12, 546-559.

Raymo, M.E., Oppo, D.W., Flower, B.P., Hodell, D.A., McManus, J.F., Venz, K.A., Kleiven, H.F., McIntyre, K., 2004. Stability of North Atlantic water masses in face of pronounced climate variability during the Pleistocene. Paleoceanography 19, 10.1029/2003PA000921.

Raymo, M.E., Ruddiman, W.F., 1992. Tectonic forcing of late Cenozoic climate. Nature 359, 117-122.

Raynaud, D., Loutre, M.F., Ritz, C., Chappellaz, J., Barnola, J.M., Jouzel, J., Lipenkov, V.Y., Petit, J.R., Vimeux, F., 2003. Marine Isotope Stage (MIS) 11 in the Vostok ice core: CO2 forcing and stability of East Antarctica, In: Droxler, A.W., Poore, R.Z., Burkle, L.H. (Eds.), Earth's Climate and Orbital Eccentricity. The Marine Isotope Stage 11 Question. Geophysical Monograph, 137. Americal Geophysical Union, Washington D.C., pp. 27-40.

Reynolds-Sautter, L., Thunell, R.C., 1989. Seasonal succession of planktonic foraminifera; results from a four-year time-series sediment trap experiment in the Northeast Pacific. Journal of Foraminiferal Research 19, 253-267.

Reynolds-Sautter, L., Thunell, R.C., 1991. Seasonal Variability in the d18O andd13C of Planktonic Foraminifera from an Upwelling Environment: Sediment Trap Results from the San Pedro Basin, Southern California Bight. Paleoceanography 6, 307-334.

Reynolds, L., Thunell, R.C., 1985. Seasonal succession of planktonic foraminifera in the subpolar North Pacific. Journal of Foraminiferal Research 15, 282-301.

Rosenthal, Y., Boyle, E.A., Slowey, N., 1997. Temperature control on the incorporation of magnesium, strontium, fluorine, and cadmium into benthic foraminiferal shells from Little Bahama Bank: Prospects for thermocline paleoceanography. Geochimica et Cosmochimica Acta 61, 3633-3643.

Rosenthal, Y., Perron-Cashman, S., Lear, C.H., Bard, E., Barker, S., Billups, K., Bryan, M., Delaney, M.L., deMenocal, P.B., Dwyer, G.S., Elderfield, H., German, C.R., Greaves, M., Lea, D.W., Marchitto, T.M., Jr., Pak, D.K., Paradis, G.L., Russell, A.D., Schneider, R.R., Scheiderich, K., Stott, L., Tachikawa, K., Tappa, E., Thunell, R., Wara, M., Weldeab, S., Wilson, P.A., 2004. Interlaboratory comparison study of Mg/Ca and Sr/Ca measurements in planktonic foraminifera for paleoceanographic research. Geochem. Geophys. Geosyst. 5, doi: 10.1029/2003GC000650.

Ruddiman, W.F., 2006a. Ice-driven CO2 feedback on ice volume. Clim. Past 2, 43-55.

Ruddiman, W.F., 2006b. Orbital changes and climate. Quaternary Science Reviews 25, 3092-3112.

Ruddiman, W.F., Glover, L.K., 1975. Subpolar North Atlantic circulation at 9300 yr BP: Faunal evidence. Quaternary Research 5, 361-389.

Russell, A.D., Hönisch, B., Spero, H.J., Lea, D.W., 2004. Effects of seawater carbonate ion concentration and temperature on shell U, Mg, and Sr in cultured planktonic foraminifera. Geochimica et Cosmochimica Acta 68, 4347-4361.

Sarnthein, M., Pflaumann, U., Weinelt, M., 2003. Past extent of sea ice in the northern North Atlantic inferred from foraminiferal paleotemperature estimates. Paleoceanography 18, 1047.

Schiebel, R., Hemleben, C., 2000. Interannual variability of planktic foraminiferal populations and test flux in the eastern North Atlantic Ocean (JGOFS). Deep Sea Research Part II: Topical Studies in Oceanography 47, 1809-1852.

Schiebel, R., Waniek, J., Bork, M., Hemleben, C., 2001. Planktic foraminiferal production stimulated by chlorophyll redistribution and entrainment of nutrients. Deep Sea Research Part I: Oceanographic Research Papers 48, 721-740.

Schlitzer, R., 2009. Ocean Data View, http://odv.awi.de.

Schmittner, A., Galbraith, E.D., 2008. Glacial greenhouse-gas fluctuations controlled by ocean circulation changes. Nature 456, 373-376.

Schmitz, W.J., 1995. On the Interbasin-Scale Thermohaline Circulation. Rev. Geophys. 33, 151-173.

Schmitz, W.J., McCartney, M., 1993. On the North Atlantic Circulation. Rev. Geophys. 31, 29-49.

Shackleton, N., 1967. Oxygen Isotope Analyses and Pleistocene Temperatures Re-assessed. Nature 215, 15-17.

Shackleton, N.J., 1974. Attainment of isotopic equilibrium between ocean water and the benthonic foraminifera genus uvigerina: Isotopic changes in the ocean during the last glacial. Colloq. Int. CNRS 219, 203–209.

Shackleton, N.J., Crowhurst, S.J., Weedon, G.P., Laskar, J., 1999. Astronomical calibration of Oligocene--Miocene time. Philosophical Transactions of the Royal Society of London. Series A: Mathematical, Physical and Engineering Sciences 357, 1907-1929.

Shackleton, N.J., Hall, M.A., Vincent, E., 2000. Phase Relationships Between Millennial-Scale Events 64,000-24,000 Years Ago. Paleoceanography 15, 565-569.

Siddall, M., Rohling, E.J., Almogi-Labin, A., Hemleben, C., Meischner, D., Schmelzer, I., Smeed, D.A., 2003. Sea-level fluctuations during the last glacial cycle. Nature 423, 853-858.

Siegenthaler, U., Stocker, T.F., Monnin, E., Luthi, D., Schwander, J., Stauffer, B., Raynaud, D., Barnola, J.-M., Fischer, H., Masson-Delmotte, V., Jouzel, J., 2005. Stable Carbon Cycle-Climate Relationship During the Late Pleistocene. Science 310, 1313-1317.

Sierro, F.J., Andersen, N., Bassetti, M.A., Berné, S., Canals, M., Curtis, J.H., Dennielou, B., Flores, J.A., Frigola, J., Gonzalez-Mora, B., Grimalt, J.O., Hodell, D.A., Jouet, G., Pérez-Folgado, M., Schneider, R., 2009. Phase relationship between sea level and abrupt climate change. Quaternary Science Reviews 28, 2867-2881.

Sigman, D.M., Boyle, E.A., 2000. Glacial/interglacial variations in atmospheric carbon dioxide. Nature 407, 859-869.

Sigman, D.M., Hain, M.P., Haug, G.H., 2010. The polar ocean and glacial cycles in atmospheric CO2 concentration. Nature 466, 47-55.

Simstich, J., Sarnthein, M., Erlenkeuser, H., 2003. Paired [delta]18O signals of Neogloboquadrina pachyderma (s) and Turborotalita quinqueloba show thermal stratification structure in Nordic Seas. Marine Micropaleontology 48, 107-125.

Skinner, L.C., Elderfield, H., 2007. Rapid fluctuations in the deep North Atlantic heat budget during the last glacial period. Paleoceanography 22, PA1205, doi:1210.1029/2006PA001338.

Skinner, L.C., Fallon, S., Waelbroeck, C., Michel, E., Barker, S., 2010. Ventilation of the Deep

Southern Ocean and Deglacial CO2 Rise. Science 328, 1147-1151.

Skinner, L.C., Shackleton, N.J., Elderfield, H., 2003. Millennial-scale variability of deep-water temperature and d18Odw indicating deep-water source variations in the Northeast Atlantic, 0-34 cal. ka BP. Geochem. Geophys. Geosyst. 4, 1098, doi:1010.1029/2003GC000585.

Spahni, R., Chappellaz, J., Stocker, T.F., Loulergue, L., Hausammann, G., Kawamura, K., Fluckiger, J., Schwander, J., Raynaud, D., Masson-Delmotte, V., Jouzel, J., 2005. Atmospheric Methane and Nitrous Oxide of the Late Pleistocene from Antarctic Ice Cores. Science 310, 1317-1321.

Spindler, M., 1990. A comparison of Arctic and Antarctic sea ice and effects of different properties on sea ice biota, In: Bleil, U., Thiede, J. (Eds.), Geological History of the Polar Oceans: Arctic versus Antarctic. Kluwer Academic Publishers, London, p.H3-186.

Spindler, M., 1996. On the salinity tolerance of the planktonic foraminifer *Neogloboquadrina pachyderma* from antarctic sea ice. Proc. NIPR Symp. Polar Biol. 9, 85-91.

St. John, K., Flower, B.P., Krissek, L., 2004. Evolution of iceberg melting, biological productivity, and the record of Icelandic volcanism in the Irminger basin since 630 ka. Marine Geology 212, 133-152.

Stangeew, E., 2001. Distribution and Isotopic Composition of Living Planktonic Foraminifera *N. pachyderma* (sinistral) and *T. quinqueloba* in the High Latitude North Atlantic, Ph.D. dissertation, Mathematisch-Naturwissenschaftlichen Fakultät. Christian-Albrechts-Universität, Kiel, Germany, p. 98.

Stein, R., Hefter, J., Grützner, J., Voelker, A., Naafs, B.D.A., 2009. Variability of surface water characteristics and Heinrich-like events in the Pleistocene midlatitude North Atlantic Ocean: Biomarker and XRD records from IODP Site U1313 (MIS 16-9). Paleoceanography 24.

Suganuma, Y., Yamazaki, T., Kanamatsu, T., 2009. South Asian monsoon variability during the past 800 kyr revealed by rock magnetic proxies. Quaternary Science Reviews 28, 926-938.

Sun, Y., Clemens, S.C., An, Z., Yu, Z., 2006. Astronomical timescale and palaeoclimatic implication of stacked 3.6-Myr monsoon records from the Chinese Loess Plateau. Quaternary Science Reviews 25, 33-48.

Swift, J., 1986. The Arctic Waters, In: Hurdle, B.G. (Ed.), The Nordic Seas. Springer, New York, pp. 129-151.

Thunell, R.C., 1976. Optimum indices of calcium carbonate dissolution, in deep-sea sediments.

Geology 4, 525-528.

Toggweiler, J., 1999. Variation of Atmospheric CO 2 by Ventilation of the Ocean's Deepest Water. Paleoceanography 14, 571-588.

Toggweiler, J.R., 2008. Origin of the 100,000-year timescale in Antarctic temperatures and atmospheric CO2. Paleoceanography 23.

Toggweiler, J.R., 2009. CLIMATE CHANGE: Shifting Westerlies. Science 323, 1434-1435.

Tolderlund, D.S., Bé, A.W.H., 1971. Seasonal distribution of planktonic foraminifera in the western North Atlantic. Micropaleontology 17, 297-329.

Tomczak, M., Godfrey, J.S., 1994. Regional Oceanography: an introduction. Pergamon, London.

Toucanne, S., Zaragosi, S., Bourillet, J.F., Gibbard, P.L., Eynaud, F., Giraudeau, J., Turon, J.L., Cremer, M., Cortijo, E., Martinez, P., Rossignol, L., 2009. A 1.2 Ma record of glaciation and fluvial discharge from the West European Atlantic margin. Quaternary Science Reviews 28, 2974-2981.

Tzedakis, P.C., 2005. Towards an understanding of the response of southern European vegetation to orbital and suborbital climate variability. Quaternary Science Reviews 24, 1585-1599.

Tzedakis, P.C., Hooghiemstra, H., Pälike, H., 2006. The last 1.35 million years at Tenaghi Philippon: revised chronostratigraphy and long-term vegetation trends. Quaternary Science Reviews 25, 3416-3430.

Tzedakis, P.C., Raynaud, D., McManus, J.F., Berger, A., Brovkin, V., Kiefer, T., 2009. Interglacial diversity. Nature Geosci 2, 751-755.

Tziperman, E., Gildor, H., 2003. On the mid-Pleistocene transition to 100-kyr glacial cycles and the asymmetry between glaciation and deglaciation times. Paleoceanography 18, 1001, doi:1010.1029/2001pa000627.

van Kolfschoten, T., Markova, A.K., 2005. Response of the European mammalian fauna to the mid-Pleistocene transition. Geological Society, London, Special Publications 247, 221-229.

Vandenberghe, J., 2000. A global perspective of the European chronostratigraphy for the past 650 ka. Quaternary Science Reviews 19, 1701-1707.

Venz, K.A., Hodell, D.A., 2002. New evidence for changes in Plio-Pleistocene deep water circulation from Southern Ocean ODP Leg 177 Site 1090. Palaeogeography, Palaeoclimatology, Palaeoecology 182, 197-220.

Venz, K.A., Hodell, D.A., Stanton, C., Warnke, D.A., 1999. A 1.0 Myr record of Glacial North Atlantic Intermediate Water variability from ODP site 982 in the northeast Atlantic. Paleoceanography 14, 42-52.

von Langen, P.J., Pak, D.K., Spero, H.J., Lea, D.W., 2005. Effects of temperature on Mg/Ca in neogloboquadrinid shells determined by live culturing. Geochem. Geophys. Geosyst. 6.

Wang, Z., Mysak, L.A., 2002. Simulation of the last glacial inception and rapid ice sheet growth in the McGill Paleoclimate Model. Geophys. Res. Lett. 29, 2102.

Wanner, H., Brönnimann, S., Casty, C., Gyalistras, D., Luterbacher, J., Schmutz, C., Stephenson, D.B., Xoplaki, E., 2001. North Atlantic oscillation-concepts and studies. Surveys in Geophysics 22, 321-382.

Weedon, G., 2003. Time-series Analysis and Cyclostratigraphy. Cambridge University Press, p. 259.

WOA, 1998. World Ocean Atlas 1998, Version 2, http://www.nodc.-noaa.gov/oc5/woa98.html. Tch.rep., National Oceanographic Data Center, Silver Spring, Maryland.

Wright, A.K., Flower, B.P., 2002. Surface and deep ocean circulation in the subpolar North Atlantic during the mid-Pleistocene revolution. Paleoceanography 17, 1068.

Yin, Q.Z., Guo, Z.T., 2008. Strong summer monsoon during the cool MIS-13. Climate of the Past 4, 29-34.

Yu, J., Elderfield, H., Hönisch, B., 2007. B/Ca in planktonic foraminifera as a proxy for surface seawater pH. Paleoceanography 22, PA2202, doi: 10.1029/2006PA001347.

Yu, J., Elderfield, H., Piotrowski, A.M., 2008. Seawater carbonate ion-[delta]13C systematics and application to glacial-interglacial North Atlantic ocean circulation. Earth and Planetary Science Letters 271, 209-220.

Zahn, R., Winn, K., Sarnthein, M., 1986. Benthic foraminiferal δ13C and accumulation rates of organic carbon: Uvigerina peregrina group and Cibicidoides wuellerstorfi. Paleoceanography 1, 27-42.

# ANEXOS

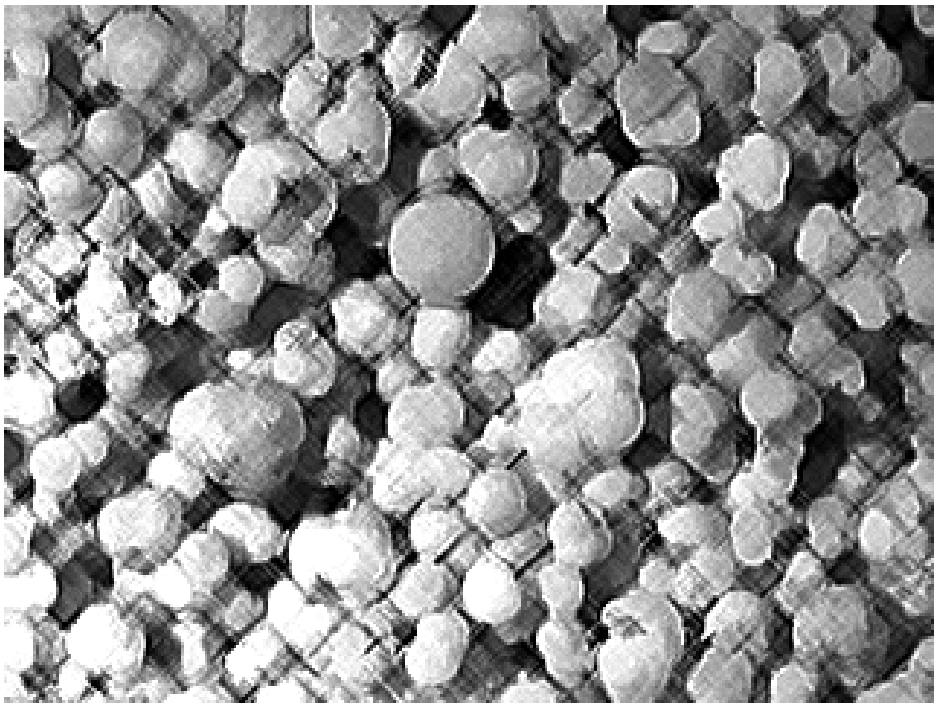

# A. I. ACRÓNIMOS Y ABREVIATURAS

A continuación se ha realizado una recopilación de los acrónimos y abreviaturas más utilizados en esta Tesis Doctoral, con el fin de facilitar su lectura. La mayoría son acrónimos que proceden del inglés, y por ello además de su significado en inglés se ha intentado buscar una traducción adecuada aunque no siempre ha sido posible.

| | |
|---|---|
| **AF** | Arctic front/ Frente Ártico |
| **AMOC** | Atlantic Meridional Overturning Circulation/ |
| **ANN** | Artificial neural networks/ Redes neuronales artificiales |
| **CLIMAP** | Climate: Long range Investigation, Mapping, and Prediction/ Proyecto de investigación climática para realizar mapas del pasado y predicciones |
| **e.g.** | exempli gratia/ por ejemplo |
| **EAIS** | East Antarctic ice sheet/ Casquete de hielo al este de la Antártida |
| **EDC** | EPICA Dome C (nombre de uno de los testigos de hielo de la Antártida) |
| **EGC** | East Greenland current/ Corriente del este de Groenlandia |
| **EPICA** | European project for ice coring in Antarctica/ Proyecto europeo para obtener testigos de hielo en la Antártida |
| **EPILOG** | Environmental Processes of the Ice Age: Land, Oceans, Glaciers/ Proyecto de investigación sobre los procesos ambientales durante las glaciaciones en los continentes, océnos y glaciares |
| **et al.** | et alii/ y colaboradores |
| **ETP** | Eccentricity, tilt and precession/ Excentricidad, obliquidad y precesión |
| **GNAIW** | Glacial North Atlantic intermediate water/ Aguas Noratlánticas intermedias glaciales |
| **i.e.** | id est/ en otras palabras |
| **IODP** | Integrated Ocean Drilling program/ Programa integrado de extracción de sondeos marinos |
| **IRD** | Ice rafted debris/ detritos transportados por hielo |
| **ISCE** | Ice sheet collapse events/ Eventos de colapso de los casquetes polares |
| **ISOW** | Iceland-Scotland overflow waters/ Aguas profundas que sobrepasan el promontorio entre Islandia y Escocia |
| **ITCZ** | Intertropical Convergence zone/ Zona de convergencia intertropical |
| **ka** | thousands of years ago/ hace … miles de años |
| **kyr** | thousands of years/ miles de años |

| | |
|---|---|
| **LC** | Labrador current/ Corriente del Labrador |
| **LGM** | Last glacial maximum/ Último máximo glacial |
| **LNADW** | Lower North Atlantic Deep Water/ Aguas Noratlánticas profundas inferiores |
| **LR04** | benthic d18O stack (Lisiecki and Raymo, 2005) |
| **LSW** | Labrador Sea waters/ Aguas profundas del Labrador |
| **Ma** | Millions of years ago/ hace … millones de años |
| **MARGO** | Multiproxy Approach for the Reconstruction of the Glacial Ocean surface/ Reconstrucción de la superficie oceánica durante los periodos glaciales a partir de varios herramientas paleoclimáticas |
| **MAT** | Modern analog technique/ Método de análogos modernos |
| **MBE** | Mid-Brunhes event/ Evento localizado en la mitad del cron Brunhes |
| **mcd** | Meters of composite depth/ Metros de la composición hecha con todos los testigos |
| **MIS** | Marine Isotope stage/ Estadio isotópico marino |
| **MPT** | Mid-Pleistocene transition/ Transición del Pleistoceno medio |
| **NAC** | North Atlantic Current/ Corriente Noratlántica |
| **NADW** | North Atlantic Deep Water/ Aguas Noratlánticas profundas |
| **NAO** | North Atlantic Oscillation/ Oscilación del Atlántico Norte |
| **NC** | Norwegian Current/ Corriente de Noruega |
| **NGS** | Norwegian-Greenland Sea/ Mar de Noruega-Groenlandia |
| **ODP** | Ocean Drilling program/ Programa de extracción de sondeos marinos |
| **PF** | Polar front/ Frente Polar |
| **SST** | Sea Surface Temperature/ Temperatura superficial del mar |
| **UNADW** | Upper North Atlantic Deep Water/ Aguas Noratlánticas profundas superiores |
| **psu** | Practical salinity unit/ Unidad práctica de salinidad |

# A. II. FOTOGRAFÍAS DE MICROSCOPIO ELECTRÓNICO

A continuación se muestra una selección de fotografías de microscopio electrónico de barrido de las principales especies de foraminíferos planctónicos que forman parte de las asociaciones estudiadas en esta Tesis. También hemos seleccionado unas fotografías de las especies de foraminíferos bentónicos utilizadas para los análisis de isótopos estables, y fotografías de algunos radiolarios, ostrácodos y espículas que se hallaron en las muestras.

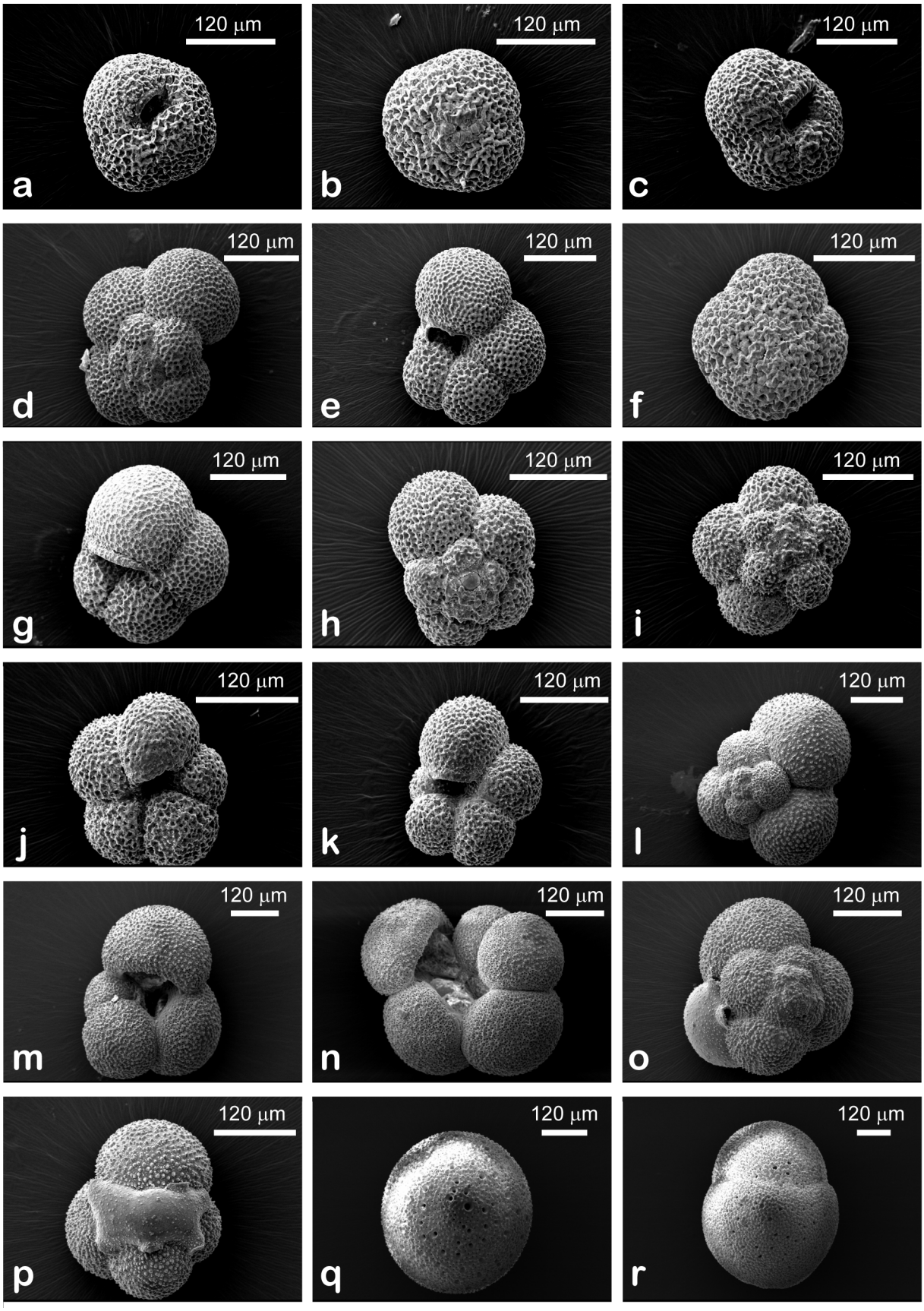


Lámina 1. *Neogloboquadrina pachyderma* sin (a, b y c), *Neogloboquadrina pachyderma* dex (d, e, f y g), *Turborotalita quinqueloba* (h, i, j y k), *Globigerina bulloides* (l, m y n), *Globigerinita glutinada* (o y p), *Orbulina universa* (q y r).

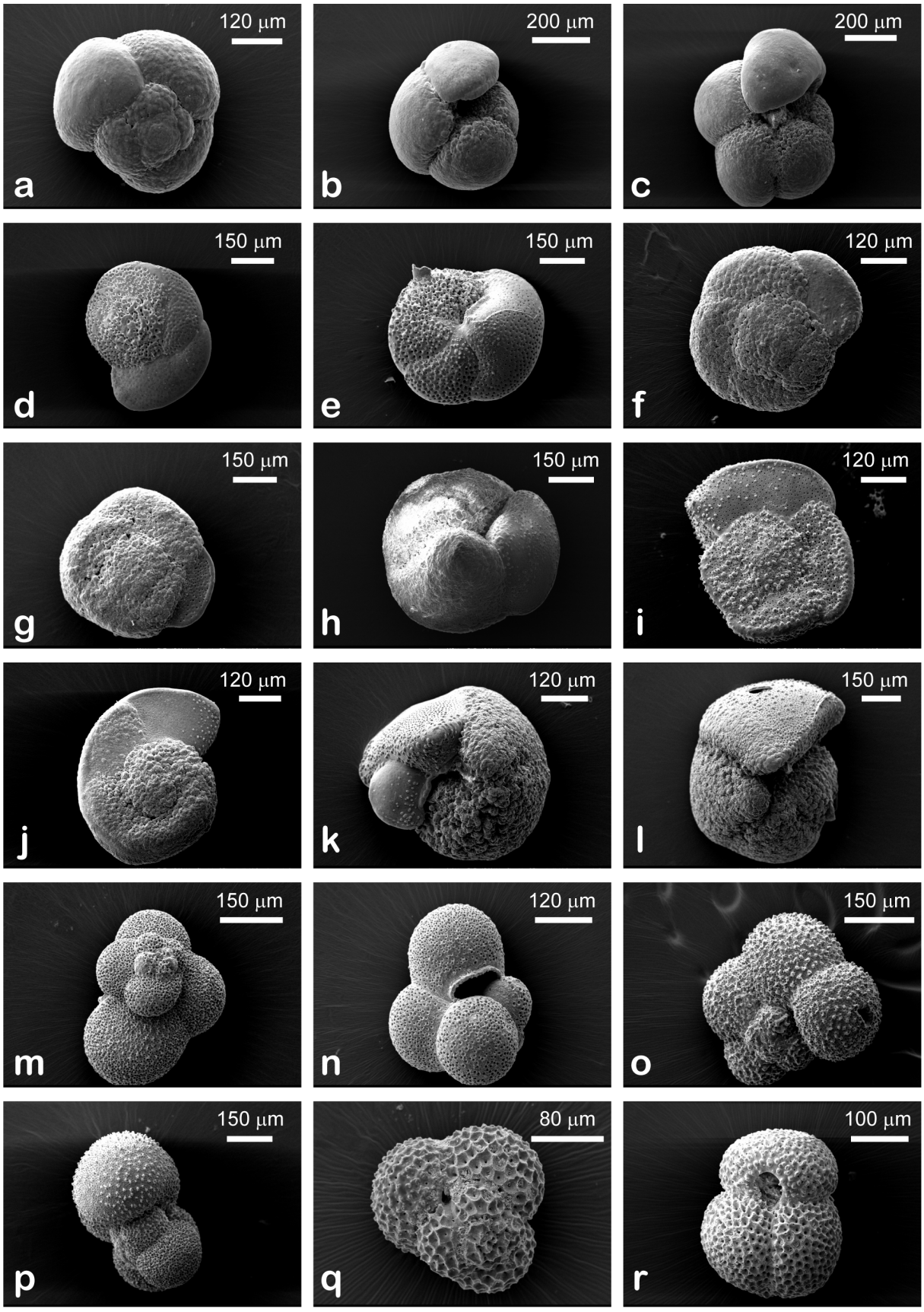


Lámina 2. *Globorotalia inflata* (a, b y c), *Globorotalia hirsuta* (d y e), *Globorotalia crassaformis-crotonensis* (f, g, h, i, y l), *Globorotalia truncatulinoides* (j y k), *Beela digitata* (m y n), *Globigerinella siphonifera* (o y p), *Globigeriniodes ruber* (q y r).

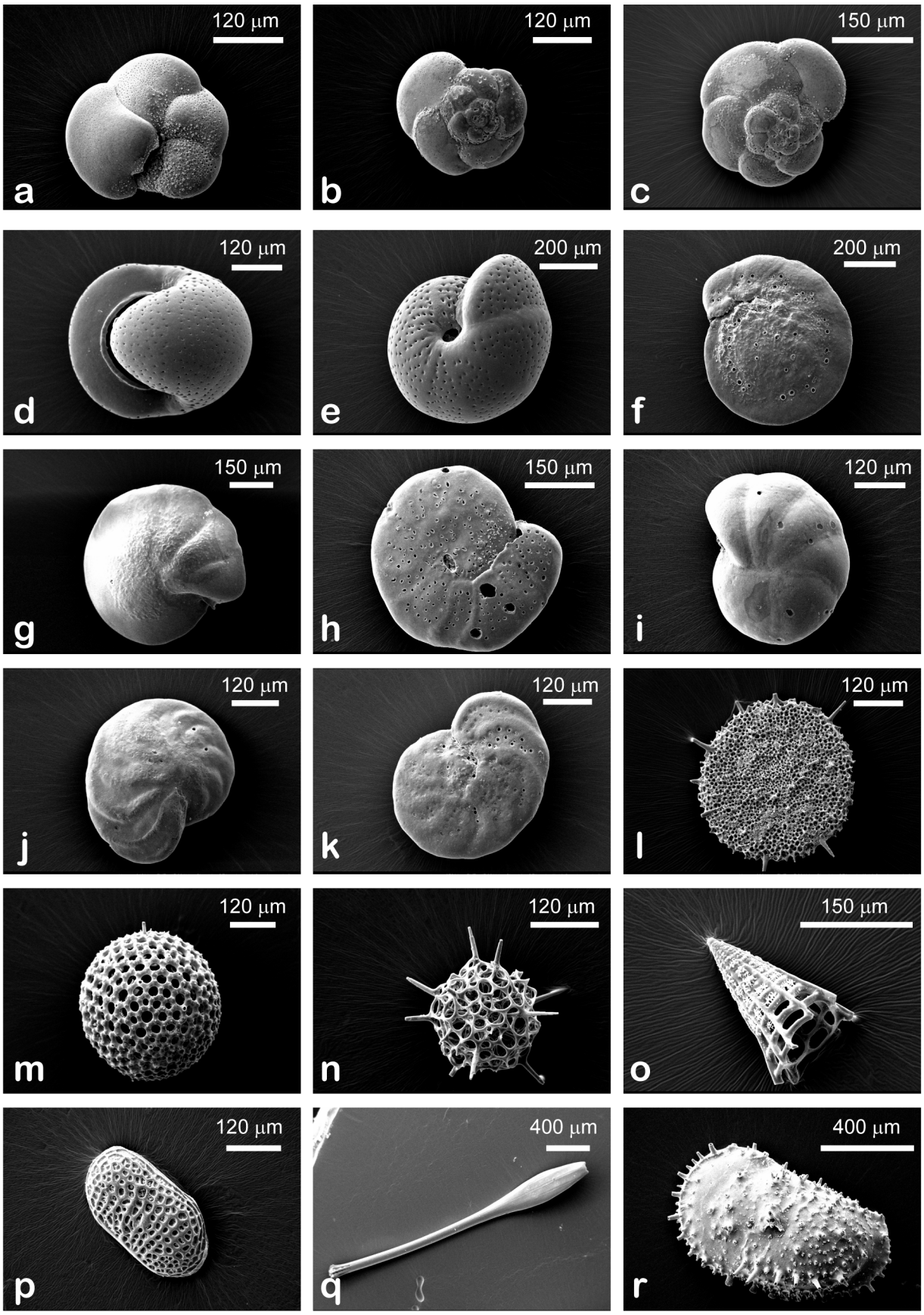


Lámina 3. *Globorotalia scitula* (a, b y c), *Melonis pompilioides* (d y e), *Cibicidoides pachyderma* (f y g), *Cibicidoides sp.* (h e i), *Cibicidoides wuellerstorfi* (j y k), radiolarios (l, m, n y o), ostrácodos (p y r) y espícula de equinodermo (q).

# A. III. PROTOCOLO DE LIMPIEZA PARA ELEMENTOS TRAZA

(Modificado del protocolo del GRC-GM-UB de Enero de 2006)

**Antes de empezar**

→ Asegurarse de que hay suficiente:

mezcla de ácido cítrico+$NH_4$

NaOH 0,1M

$HNO_3$ 0,001M

$HNO_3$ ultrapuro al 1% (sólo para la disolución)

Tubos limpios (sólo para la disolución

→ Poner a calentar el baño del reductivo porque tarda 1,5 h o más. El baño del oxidativo hay que encenderlo al final del reductivo.

→ Poner un vial vacío como prueba en blanco para detectar posibles contaminaciones.

→ Poner dentro de la campana de flujo laminar las pipetas, los botes para el agua y el $HNO_3$, el vaso de precipitados para residuos y los viales cerrados. Limpiar las puntas de las pipetas: 2 veces con $HNO_3$ y 3 con agua ultrapura (MQ). Igualmente hay que limpiar la punta de pipeta entre muestra y muestra en las extracciones para no contaminar.

→ No coger nunca los reactivos de la botella, echarlos a un bote más pequeño para evitar contaminarlo todo con las pipetas. Los reactivos para la limpieza se preparan con agua MQ.

## 1. LIMPIEZA DE ARCILLAS

1- Limpiar la punta de la pipeta pequeña y echar 30-40 µl de agua MQ en cada vial y ponerlos 30" al ultrasonidos. No hace falta cerrar los viales al ultrasonicar, mientras se esté dentro de la campana de flujo laminar.

2- Echar agua MQ hasta completar cada vial, esperar a que decanten los foraminíferos, dando pequeños golpecitos, y retirar el sobrante de agua con la pipeta de 1000 (ponerla a ~750 µl). Hacerlo de 3 en 3 para que no decanten también las arcillas. Repetir 3 veces en total.

4- Echar metanol hasta 0,4 µl de la marca del vial y poner al ultrasonidos 30". Después retirar el metanol. Repetir otra vez y después llenar los viales de agua MQ (para limpiar el metanol), dejar que decanten los foraminíferos y retirar el sobrenadante.

→Si se cree que las muestras pudieran tener alta contaminación arcillosa, repetir los pasos 1 y 2 más veces.

## 2. REDUCTIVO

1- Cambiar la punta de pipeta de 1000 y limpiarla. Pasar los viales a la campana específica para compuestos de amoniaco, y poner agua y $HNO_3$ nuevo en los botecitos de limpieza.
2- Mezclar el ác.cítrico+NH4 (2000 µl) con la hidracina (500 µl) y agitar un poco la mezcla.
3- Echar 100 µl de la mezcla en cada vial y poner el cierre de seguridad.
4- Meter al baño caliente 16 min ultrasonicando 5" cada 2 min. (Poner el cronómetro a 2 min 7 veces e ir apuntando en una tabla para asegurarse de que se hace 7 veces). Poner a calentar un poco de agua MQ en un vaso de precipitados.
5- Apagar el baño del reductivo, encender el baño del oxidativo y sacar los viales. Abrirlos con cuidado porque a veces están presurizados y puede saltar, y rellenar rápidamente con agua MQ vial y tapa para parar la reacción, después extraer el agua sobrante con la pipeta. Se limpian 2 veces más con agua MQ.
6- Echar 400 µl de agua MQ caliente, dejarla 5 min y luego retirarla. Hacerlo otra vez.
7- Echar agua MQ fría en vial y tapa y retirarla.

## 3. OXIDATIVO

1- Cambiar la punta de pipeta de 1000 y limpiarla. Pasar los viales a la campana de flujo laminar, tirar el líquido del vaso de residuos, para no inhalar $NH_3$ y poner agua y $HNO_3$ nuevos en los botecitos.
2- Mezclar 10 ml de NaOH con 100 µl de $H_2O_2$ y agitar un poco.
3- Poner 250 µl de la mezcla en cada vial, cerrarlos con el cierre de seguridad y poner en el baño caliente 5 min. A la mitad del tiempo sacar los viales y dar unos golpes contra la encimera para evitar que se formen burbujas (sujetar los viales con las palmas de las manos o con la tablita de plástico). Al final poner al ultrasonidos 15". Repetir y apagar el baño.
4- Sacar los viales, abrirlos y rellenar con agua MQ vial y tapa. Dar golpecitos para que decanten los foraminíferos (porque suelen formarse burbujas) y extraer el agua sobrenadante con la pipeta. Repetir 2 veces más.

## 4. WEAK ACID LEACHING

1- Echar 250 µl de HNO3 0,001 M en cada vial y poner 30" al ultrasonidos.
2- Echar agua MQ hasta rellenar los viales y después de esperar a que decanten los foraminíferos retirar el sobrenadante. Repetir 3-4 veces más.
3- Eliminar el máximo de agua con la pipeta pequeña, para que solamente queden foraminíferos en el vial. Cerrarlos y guardar los viales hasta que se haga la disolución.

## 5. DISOLUCIÓN

**→ Sólo se hace el día anterior al análisis en el ICP-MS.**

→ Hacer una lista con las muestras y el código asignado a cada una.

1- Echar 400 µl de $HNO_3$ 1% (ultrapuro)+ Rh en cada vial. Hacerlo en grupos de 8.

2- Poner las muestras en el baño de ultrasonidos 15" para facilitar la disolución o más si fuera necesario, dando golpecitos para evitar que los fragmentos de foraminíferos se queden en burbujas.

3- Agitar los viales y después ponerlos en grupos de 8 en la microcentrífuga 5 min a 6000rpm.

4- Transferir 370 µl de muestra en un tubo limpio de 14 ml usando una pipeta y añadir 2630 µl de $HNO_3$+Rh. Agitar con el vortex para homogeneizar.

## PREPARACIÓN DE REACTIVOS

**Reactivos del reductivo** (ácido cítrico+ $NH_4$)

→ Trabajar dentro de la campana específica para amoniaco.

1. Pesar 5,25 g de ácido cítrico en un vaso de precipitados
2. Añadir 100 ml de $NH_4$ (30%)
3. Pon a calentar el vaso de precipitados con el ácido cítrico y un mezclador magnético a 40-50 ºC.
4. Transferir la mezcla a un bote de plástico limpio y meterlo al frigorífico.

**Reactivos del oxidativo**

1. $H_2O_2$ al 30% w/v. (mantenerlo en la nevera).
2. Pesar 4 g de NaOH 0,1M (Aristar grade) y mezclarlo con un litro de agua MQ.

**Weak acid leaching**

El $HNO_3$ 0,001M se prepara mezclando 69,4 µl de $HNO_3$ (65%) con agua MQ hasta completar un litro (o 37,4 µl $HNO_3$ (65%) con agua MQ hasta completar medio litro).

**Disolución**

El $HNO_3$ 1% ultrapuro Aristar grade se prepara diluyendo el $HNO_3$ 5% ultrapuro Aristar grade a 1/5 con agua MQ.

# A. IV. FACTOR LOADINGS

En este anexo se detalla la lista completa de los factor loadings obtenidos a partir del análisis factorial de las abundancias de foraminíferos planctónicos. Se han resaltado los valores más altos de cada factor, en los factores 1 y 2 por encima de 0,7 y el en factor 3 por encima de 0,5. Al final del todo se indica la varianza explicada por cada factor.

| age (ka) | Factor loadings | | |
|---|---|---|---|
| | Factor 1 | Factor 2 | Factor 3 |
| 407.26 | 0.8941 | 0.1542 | 0.12761 |
| 407.72 | 0.9270 | 0.2263 | 0.08536 |
| 408.17 | 0.9735 | 0.0750 | 0.09499 |
| 408.63 | 0.9204 | 0.2404 | 0.04265 |
| 409.08 | 0.9235 | 0.1663 | 0.14230 |
| 409.54 | 0.9441 | 0.1727 | 0.10888 |
| 410.00 | 0.9167 | 0.2800 | 0.15054 |
| 410.45 | 0.8970 | 0.3202 | 0.11506 |
| 410.91 | 0.9066 | 0.3100 | 0.19517 |
| 411.36 | 0.9218 | 0.2536 | 0.20230 |
| 411.82 | 0.9185 | 0.2914 | 0.18529 |
| 412.28 | 0.8129 | 0.5490 | 0.09188 |
| 413.06 | 0.9530 | 0.2300 | 0.02679 |
| 413.84 | 0.9808 | 0.0456 | -0.01660 |
| 414.61 | 0.9385 | 0.0693 | 0.29934 |
| 415.39 | 0.9162 | -0.0172 | 0.30033 |
| 416.17 | 0.9167 | 0.1407 | 0.29323 |
| 416.95 | 0.9315 | 0.1790 | 0.17588 |
| 417.73 | 0.9462 | 0.0617 | 0.22462 |
| 418.32 | 0.9697 | 0.1891 | 0.07124 |
| 419.09 | 0.9751 | 0.0192 | 0.11703 |
| 419.87 | 0.9195 | 0.1524 | 0.28333 |
| 420.65 | 0.9748 | 0.1114 | -0.00602 |
| 421.43 | 0.9485 | 0.1352 | 0.09214 |
| 422.21 | 0.9604 | 0.2158 | 0.11305 |
| 422.99 | 0.9477 | 0.2480 | 0.16055 |
| 423.77 | 0.9351 | 0.2527 | 0.21913 |
| 424.55 | 0.9507 | 0.2394 | 0.09671 |

| age (ka) | Factor loadings | | |
|---|---|---|---|
| | Factor 1 | Factor 2 | Factor 3 |
| 425.33 | 0.9203 | 0.2892 | 0.20382 |
| 426.11 | 0.8832 | 0.2959 | 0.32978 |
| 426.89 | 0.8414 | 0.4014 | 0.22844 |
| 427.66 | 0.7794 | 0.4644 | 0.21303 |
| 428.44 | 0.5472 | 0.7044 | 0.26533 |
| 430.83 | 0.3830 | 0.8746 | 0.25735 |
| 433.21 | 0.1865 | 0.9702 | -0.00133 |
| 435.60 | 0.1987 | 0.9557 | 0.19154 |
| 437.98 | 0.1961 | 0.9278 | 0.29999 |
| 440.36 | 0.2923 | 0.8285 | 0.44659 |
| 441.85 | 0.4153 | 0.7931 | 0.42286 |
| 444.24 | 0.3959 | 0.7856 | 0.41600 |
| 446.62 | 0.5611 | 0.7020 | 0.41354 |
| 449.00 | 0.3504 | 0.8669 | 0.32725 |
| 451.39 | 0.4286 | 0.7951 | 0.39964 |
| 453.77 | 0.6438 | 0.5812 | 0.43307 |
| 456.16 | 0.2331 | 0.9663 | 0.04849 |
| 458.17 | 0.1453 | 0.9803 | 0.00908 |
| 459.68 | 0.2713 | 0.9438 | 0.07755 |
| 461.70 | 0.3700 | 0.9011 | 0.02472 |
| 463.71 | 0.2620 | 0.9510 | -0.12510 |
| 465.73 | 0.4202 | 0.9009 | 0.03681 |
| 467.74 | 0.7172 | 0.6793 | -0.09244 |
| 468.72 | 0.8273 | 0.5405 | -0.04374 |
| 469.69 | 0.8746 | 0.4429 | -0.08024 |
| 470.67 | 0.8346 | 0.5008 | -0.09706 |
| 471.65 | 0.8633 | 0.4734 | -0.06771 |
| 472.62 | 0.8684 | 0.4515 | 0.12501 |

| age (ka) | Factor loadings | | |
|---|---|---|---|
| | Factor 1 | Factor 2 | Factor 3 |
| 473.60 | 0.5696 | 0.7976 | -0.04805 |
| 474.58 | 0.6386 | 0.7544 | 0.08271 |
| 475.24 | 0.8446 | 0.5113 | 0.09228 |
| 475.90 | 0.8887 | 0.4331 | 0.06603 |
| 476.57 | 0.8757 | 0.4379 | 0.01036 |
| 477.23 | 0.8828 | 0.4320 | 0.11812 |
| 477.90 | 0.8166 | 0.5504 | -0.02956 |
| 478.56 | 0.4346 | 0.8910 | 0.09412 |
| 479.41 | 0.3134 | 0.9449 | -0.02633 |
| 480.05 | 0.4000 | 0.9121 | 0.04076 |
| 480.90 | 0.5366 | 0.8218 | -0.08856 |
| 481.75 | 0.6229 | 0.7586 | 0.06948 |
| 482.60 | 0.5681 | 0.7712 | 0.09229 |
| 483.45 | 0.4655 | 0.8729 | 0.08066 |
| 484.30 | 0.5049 | 0.7993 | 0.08652 |
| 485.15 | 0.3165 | 0.9326 | 0.14456 |
| 486.00 | 0.2761 | 0.8965 | 0.29883 |
| 486.85 | 0.2932 | 0.9026 | 0.28034 |
| 487.70 | 0.3038 | 0.9347 | 0.05426 |
| 488.56 | 0.7616 | 0.6094 | 0.14950 |
| 489.59 | 0.8738 | 0.4547 | 0.07356 |
| 490.63 | 0.9066 | 0.2965 | 0.24255 |
| 491.66 | 0.9151 | 0.3480 | 0.10858 |
| 492.70 | 0.8915 | 0.3683 | 0.17829 |
| 493.73 | 0.9057 | 0.3939 | 0.07121 |
| 494.77 | 0.8874 | 0.4116 | 0.12390 |
| 495.81 | 0.8758 | 0.4402 | 0.14577 |
| 496.84 | 0.8675 | 0.4265 | 0.04052 |
| 497.62 | 0.8737 | 0.4024 | 0.20481 |
| 498.65 | 0.8826 | 0.3639 | 0.22415 |
| 499.69 | 0.8812 | 0.3610 | 0.25166 |
| 500.72 | 0.8650 | 0.4021 | 0.28336 |
| 501.76 | 0.8621 | 0.4533 | 0.18971 |
| 502.80 | 0.8686 | 0.4129 | 0.13465 |
| 503.83 | 0.8752 | 0.4208 | 0.06369 |
| 504.87 | 0.8666 | 0.4302 | 0.17820 |
| 505.90 | 0.8165 | 0.4524 | 0.26771 |
| 506.94 | 0.7871 | 0.5209 | 0.25065 |
| 507.98 | 0.8205 | 0.4739 | 0.22057 |
| 508.79 | 0.7991 | 0.4983 | 0.30199 |
| 509.37 | 0.8228 | 0.5103 | 0.21074 |
| 510.25 | 0.8507 | 0.4022 | 0.24291 |
| 510.54 | 0.8933 | 0.3758 | 0.17139 |

| age (ka) | Factor loadings | | |
|---|---|---|---|
| | Factor 1 | Factor 2 | Factor 3 |
| 511.13 | 0.8668 | 0.3840 | 0.20491 |
| 511.71 | 0.8968 | 0.3999 | 0.02040 |
| 512.30 | 0.8143 | 0.3620 | 0.20155 |
| 512.89 | 0.8928 | 0.3614 | 0.21956 |
| 513.32 | 0.8845 | 0.3391 | 0.24386 |
| 513.91 | 0.9290 | 0.2332 | 0.06707 |
| 514.50 | 0.8972 | 0.2683 | 0.20310 |
| 515.08 | 0.9098 | 0.2992 | 0.15288 |
| 515.67 | 0.8906 | 0.2909 | 0.29864 |
| 516.25 | 0.8874 | 0.2213 | 0.37034 |
| 516.84 | 0.9098 | 0.1172 | 0.34604 |
| 517.42 | 0.8934 | 0.2172 | 0.33966 |
| 518.01 | 0.9369 | 0.0362 | 0.28601 |
| 518.60 | 0.9243 | 0.2416 | 0.25256 |
| 519.18 | 0.9227 | -0.0067 | 0.34005 |
| 519.77 | 0.8875 | 0.2254 | 0.39668 |
| 520.35 | 0.8923 | 0.1043 | 0.40039 |
| 520.94 | 0.9172 | 0.1709 | 0.32148 |
| 521.52 | 0.9339 | 0.1124 | 0.31599 |
| 522.11 | 0.8956 | 0.2330 | 0.37077 |
| 522.82 | 0.8785 | 0.3394 | 0.28824 |
| 523.64 | 0.8990 | 0.3724 | 0.18096 |
| 524.47 | 0.9070 | 0.2541 | 0.32227 |
| 525.09 | 0.8876 | 0.3384 | 0.29088 |
| 525.91 | 0.8339 | 0.3514 | 0.40178 |
| 526.74 | 0.8539 | 0.3795 | 0.31930 |
| 527.57 | 0.8300 | 0.4055 | 0.35842 |
| 528.39 | 0.7860 | 0.4902 | 0.35296 |
| 529.22 | 0.6866 | 0.5791 | 0.38462 |
| 530.04 | 0.5996 | 0.6858 | 0.19504 |
| 530.87 | 0.4569 | 0.7959 | 0.33885 |
| 531.82 | 0.2508 | 0.8382 | 0.47120 |
| 532.88 | 0.1162 | 0.7956 | 0.59156 |
| 533.94 | 0.0966 | 0.7910 | 0.59107 |
| 535.00 | 0.2428 | 0.6759 | 0.67655 |
| 536.07 | 0.4287 | 0.7194 | 0.53036 |
| 537.13 | 0.3442 | 0.6461 | 0.65581 |
| 538.19 | 0.4509 | 0.6717 | 0.57557 |
| 539.10 | 0.4222 | 0.5560 | 0.68721 |
| 540.02 | 0.5152 | 0.5963 | 0.59911 |
| 540.93 | 0.3855 | 0.6713 | 0.59679 |
| 541.84 | 0.3365 | 0.7736 | 0.52889 |
| 542.75 | 0.2466 | 0.7522 | 0.60462 |

| age (ka) | Factor loadings | | |
|---|---|---|---|
| | Factor 1 | Factor 2 | Factor 3 |
| 543.66 | 0.2391 | 0.7834 | 0.55716 |
| 544.57 | 0.1979 | 0.8297 | 0.51958 |
| 545.48 | 0.3188 | 0.7640 | 0.55530 |
| 546.39 | 0.2945 | 0.7449 | 0.59501 |
| 547.30 | 0.1454 | 0.8805 | 0.44307 |
| 548.21 | 0.1182 | 0.9169 | 0.36563 |
| 549.12 | 0.3613 | 0.8120 | 0.45224 |
| 549.65 | 0.3921 | 0.7401 | 0.53393 |
| 550.25 | 0.6642 | 0.4652 | 0.50112 |
| 550.86 | 0.5317 | 0.6805 | 0.42717 |
| 551.46 | 0.4297 | 0.7136 | 0.54976 |
| 552.06 | 0.5261 | 0.6019 | 0.57579 |
| 552.67 | 0.7049 | 0.4659 | 0.47801 |
| 553.27 | 0.8055 | 0.4492 | 0.36260 |
| 553.87 | 0.8181 | 0.4857 | 0.25348 |
| 555.61 | 0.7446 | 0.6266 | 0.19807 |
| 557.35 | 0.5039 | 0.8526 | 0.12734 |
| 558.87 | 0.5823 | 0.6969 | 0.35709 |
| 560.18 | 0.4579 | 0.8610 | 0.19311 |
| 561.49 | 0.2932 | 0.9220 | 0.23036 |
| 562.80 | 0.3193 | 0.8150 | 0.44022 |
| 563.78 | 0.7040 | 0.3870 | 0.56720 |
| 565.09 | 0.8299 | 0.3136 | 0.42054 |
| 566.58 | 0.7292 | 0.2480 | 0.54300 |
| 568.25 | 0.7852 | 0.2647 | 0.46593 |
| 569.92 | 0.8108 | 0.1712 | 0.51458 |
| 571.60 | 0.7945 | 0.2609 | 0.44005 |
| 573.27 | 0.7559 | 0.1915 | 0.57182 |
| 574.94 | 0.7852 | 0.3262 | 0.51742 |
| 576.61 | 0.7758 | 0.2459 | 0.55818 |
| 578.13 | 0.7759 | 0.3649 | 0.43824 |
| 579.49 | 0.7366 | 0.3012 | 0.57097 |
| 580.85 | 0.6815 | 0.4304 | 0.56108 |
| 582.21 | 0.3915 | 0.8448 | 0.34085 |
| 582.93 | 0.5280 | 0.6998 | 0.46046 |
| 583.64 | 0.7566 | 0.5542 | 0.32641 |
| 584.35 | 0.5986 | 0.6497 | 0.44776 |
| 585.06 | 0.8017 | 0.4234 | 0.37542 |
| 585.78 | 0.8840 | 0.1306 | 0.37729 |
| 586.49 | 0.8839 | 0.1546 | 0.35977 |
| 587.02 | 0.8758 | 0.2473 | 0.30900 |
| 587.74 | 0.9456 | 0.1879 | 0.18387 |
| 588.45 | 0.9382 | 0.2234 | 0.20509 |

| age (ka) | Factor loadings | | |
|---|---|---|---|
| | Factor 1 | Factor 2 | Factor 3 |
| 589.16 | 0.8592 | 0.3869 | 0.27857 |
| 589.88 | 0.8463 | 0.3657 | 0.33414 |
| 590.59 | 0.4760 | 0.5944 | 0.60851 |
| 591.30 | 0.5366 | 0.4149 | 0.70708 |
| 592.14 | 0.6324 | 0.3270 | 0.68324 |
| 592.98 | 0.6941 | 0.2601 | 0.62215 |
| 593.82 | 0.7907 | 0.1605 | 0.58819 |
| 594.67 | 0.7598 | 0.3341 | 0.52244 |
| 595.51 | 0.6042 | 0.6325 | 0.42702 |
| 596.35 | 0.3704 | 0.8399 | 0.35256 |
| 597.19 | 0.2093 | 0.8286 | 0.51164 |
| 598.32 | 0.5745 | 0.6588 | 0.46878 |
| 599.44 | 0.6643 | 0.6100 | 0.37802 |
| 600.57 | 0.8299 | 0.4397 | 0.26491 |
| 601.69 | 0.7934 | 0.4716 | 0.30653 |
| 602.82 | 0.7586 | 0.6316 | 0.11543 |
| 603.66 | 0.8173 | 0.4940 | 0.26667 |
| 604.79 | 0.8872 | 0.3943 | 0.20860 |
| 605.91 | 0.8749 | 0.4353 | 0.18544 |
| 607.04 | 0.9246 | 0.3280 | 0.11193 |
| 608.17 | 0.9185 | 0.3449 | 0.13634 |
| 609.29 | 0.9406 | 0.2846 | 0.06810 |
| 610.42 | 0.9175 | 0.3297 | 0.16093 |
| 611.54 | 0.9506 | 0.2153 | 0.11004 |
| 612.67 | 0.9221 | 0.2209 | 0.20310 |
| 613.80 | 0.9368 | 0.1214 | 0.22162 |
| 614.92 | 0.9021 | 0.2522 | 0.15746 |
| 616.05 | 0.9634 | 0.1862 | -0.02390 |
| 617.18 | 0.8461 | 0.4047 | 0.22545 |
| 618.30 | 0.8439 | 0.3775 | 0.13245 |
| 619.43 | 0.8437 | 0.3836 | 0.17748 |
| 620.56 | 0.8633 | 0.3562 | -0.03844 |
| 621.68 | 0.8791 | 0.4192 | 0.14861 |
| 622.81 | 0.8970 | 0.3673 | 0.11857 |
| 623.94 | 0.8555 | 0.4452 | 0.23451 |
| 624.78 | 0.7860 | 0.5610 | 0.19206 |
| 625.91 | 0.6439 | 0.6578 | 0.38441 |
| 627.03 | 0.5777 | 0.7255 | 0.31657 |
| 628.03 | 0.5163 | 0.7009 | 0.43709 |
| 628.91 | 0.3875 | 0.7619 | 0.48034 |
| 629.78 | 0.1697 | 0.7491 | 0.61810 |
| 630.65 | 0.1788 | 0.6832 | 0.69574 |
| 631.53 | 0.1905 | 0.6979 | 0.67286 |

| age (ka) | Factor loadings | | |
|---|---|---|---|
| | Factor 1 | Factor 2 | Factor 3 |
| 633.11 | 0.1546 | 0.7021 | 0.68845 |
| 635.39 | 0.1097 | 0.7108 | 0.69104 |
| 637.68 | 0.1598 | 0.8266 | 0.50684 |
| 639.97 | 0.1070 | 0.8609 | 0.48090 |
| 642.26 | 0.1913 | 0.8638 | 0.42256 |
| 644.54 | 0.1045 | 0.9104 | 0.36240 |
| 646.83 | 0.1813 | 0.9798 | 0.03211 |
| 649.12 | 0.1307 | 0.9892 | 0.02145 |
| 651.40 | 0.1570 | 0.9840 | 0.05256 |
| 653.69 | 0.2601 | 0.9262 | 0.06096 |
| 655.41 | 0.5367 | 0.7597 | 0.32280 |
| 657.34 | 0.4398 | 0.7594 | 0.40482 |
| 658.91 | 0.4467 | 0.7955 | 0.38549 |
| 660.49 | 0.5405 | 0.5525 | 0.58212 |
| 662.06 | 0.6713 | 0.4842 | 0.49403 |
| 663.63 | 0.2421 | 0.8832 | 0.34435 |
| 665.21 | 0.2244 | 0.9549 | 0.16012 |
| 666.78 | 0.4033 | 0.8950 | 0.13709 |
| 668.36 | 0.2599 | 0.9620 | 0.04388 |
| 669.93 | 0.3296 | 0.9223 | 0.18773 |
| 671.50 | 0.3752 | 0.9209 | 0.03909 |
| 672.69 | 0.4005 | 0.9021 | 0.14464 |
| 673.30 | 0.6190 | 0.6982 | 0.35157 |
| 674.10 | 0.8225 | 0.5368 | 0.10111 |
| 674.91 | 0.7821 | 0.5219 | 0.30247 |
| 675.72 | 0.8091 | 0.5613 | 0.14580 |
| 676.52 | 0.6137 | 0.7302 | 0.27945 |
| 677.33 | 0.5934 | 0.7839 | 0.07720 |
| 678.37 | 0.6404 | 0.7356 | 0.15156 |
| 679.42 | 0.7524 | 0.5435 | 0.32586 |
| 680.46 | 0.6941 | 0.6358 | 0.30869 |
| 681.70 | 0.6370 | 0.7046 | 0.19448 |
| 683.14 | 0.6361 | 0.6588 | 0.32042 |
| 684.58 | 0.3885 | 0.8283 | 0.31693 |
| 686.01 | 0.5585 | 0.7237 | 0.35301 |
| 687.45 | 0.2830 | 0.8080 | 0.47797 |
| 688.88 | 0.4474 | 0.7787 | 0.43410 |
| 690.32 | 0.5380 | 0.7345 | 0.33042 |
| 691.75 | 0.5379 | 0.7540 | 0.29945 |
| 693.19 | 0.5646 | 0.7477 | 0.28645 |
| 694.13 | 0.6622 | 0.7041 | 0.04308 |
| 694.84 | 0.7735 | 0.5318 | 0.12666 |
| 695.78 | 0.7425 | 0.6507 | 0.09214 |

| age (ka) | Factor loadings | | |
|---|---|---|---|
| | Factor 1 | Factor 2 | Factor 3 |
| 696.72 | 0.7150 | 0.6550 | 0.05936 |
| 697.66 | 0.7284 | 0.6614 | 0.01876 |
| 698.61 | 0.7712 | 0.6159 | 0.06748 |
| 699.55 | 0.8185 | 0.5355 | -0.00480 |
| 700.37 | 0.8557 | 0.4517 | 0.05797 |
| 701.32 | 0.8536 | 0.4477 | 0.07145 |
| 702.26 | 0.8166 | 0.5026 | 0.18511 |
| 703.20 | 0.9156 | 0.3523 | 0.03351 |
| 704.14 | 0.8956 | 0.3071 | 0.07244 |
| 705.09 | 0.9194 | 0.3584 | 0.01399 |
| 706.03 | 0.9391 | 0.2963 | -0.10646 |
| 706.97 | 0.9204 | 0.3690 | 0.02997 |
| 707.91 | 0.9179 | 0.3717 | 0.04336 |
| 708.86 | 0.8919 | 0.4102 | 0.13595 |
| 709.80 | 0.8836 | 0.3939 | 0.17661 |
| 710.74 | 0.8319 | 0.4261 | 0.18341 |
| 711.69 | 0.8226 | 0.4593 | 0.18118 |
| 712.39 | 0.8252 | 0.4604 | 0.19911 |
| 713.33 | 0.8121 | 0.5198 | 0.10803 |
| 714.28 | 0.8034 | 0.4663 | 0.21628 |
| 715.22 | 0.5263 | 0.7794 | 0.19260 |
| 716.16 | 0.4599 | 0.7651 | 0.35169 |
| 717.06 | 0.0971 | 0.9882 | -0.10705 |
| 717.96 | 0.5044 | 0.8277 | 0.17892 |
| 718.85 | 0.3469 | 0.9285 | 0.00776 |
| 719.75 | 0.3544 | 0.9109 | -0.02040 |
| 720.65 | 0.0611 | 0.9920 | -0.09576 |
| 721.54 | 0.2193 | 0.9713 | -0.01693 |
| 722.44 | 0.2790 | 0.9497 | -0.05391 |
| 723.34 | 0.5856 | 0.7877 | -0.02413 |
| 724.23 | 0.7268 | 0.6507 | 0.06885 |
| 726.00 | 0.7785 | 0.5654 | 0.23032 |
| 727.76 | 0.8092 | 0.5468 | 0.20211 |
| 729.53 | 0.7134 | 0.6606 | 0.13409 |
| 731.30 | 0.6681 | 0.6843 | 0.19162 |
| 733.06 | 0.7634 | 0.5969 | 0.15291 |
| 734.39 | 0.7132 | 0.6435 | 0.16572 |
| 736.15 | 0.7762 | 0.5579 | 0.26364 |
| 737.92 | 0.6708 | 0.6618 | 0.29119 |
| 739.93 | 0.3382 | 0.8976 | 0.23017 |
| 742.19 | 0.1412 | 0.9780 | 0.07361 |
| 744.04 | 0.1424 | 0.9834 | 0.03746 |
| 745.47 | 0.2999 | 0.9257 | 0.06690 |

| age (ka) | Factor loadings | | |
|---|---|---|---|
| | Factor 1 | Factor 2 | Factor 3 |
| 746.90 | 0.3098 | 0.9345 | 0.13699 |
| 748.33 | 0.2810 | 0.9383 | 0.19259 |
| 749.76 | 0.2907 | 0.9269 | 0.22542 |
| 751.19 | 0.3486 | 0.8879 | 0.20732 |
| 752.62 | 0.3033 | 0.8831 | 0.29818 |
| 754.05 | 0.5519 | 0.7224 | 0.07068 |
| 755.48 | 0.5952 | 0.7007 | 0.07805 |
| 757.55 | 0.5066 | 0.8275 | 0.12907 |
| 759.62 | 0.1118 | 0.9583 | 0.22535 |
| 761.69 | 0.5855 | 0.6556 | 0.42610 |
| 762.81 | 0.7329 | 0.4987 | 0.24609 |
| 763.93 | 0.8697 | 0.3822 | 0.25691 |
| 764.76 | 0.7778 | 0.4649 | 0.37094 |
| 765.88 | 0.3522 | 0.8731 | 0.32496 |
| 767.00 | 0.5014 | 0.6838 | 0.49085 |
| 768.11 | 0.4982 | 0.5848 | 0.58784 |
| 769.22 | 0.6128 | 0.5016 | 0.60473 |
| 770.33 | 0.7393 | 0.4508 | 0.49222 |
| 771.44 | 0.2684 | 0.9266 | 0.16957 |
| 772.55 | 0.3245 | 0.8955 | 0.29393 |
| 773.31 | 0.4276 | 0.8637 | 0.05648 |
| 774.06 | 0.5698 | 0.7577 | -0.05324 |
| 774.82 | 0.6040 | 0.7311 | -0.01079 |
| 775.57 | 0.7383 | 0.6156 | 0.09301 |
| 776.33 | 0.7741 | 0.5257 | 0.11120 |
| 777.09 | 0.8482 | 0.4596 | 0.11145 |
| 777.84 | 0.8412 | 0.4288 | -0.12084 |
| 778.60 | 0.8172 | 0.4206 | 0.21504 |
| 779.35 | 0.7788 | 0.4642 | -0.03965 |
| 780.11 | 0.8672 | 0.4154 | 0.04863 |
| 780.86 | 0.8272 | 0.4453 | -0.11369 |
| **Explained variance** | 49.071 | 37.346 | 9.631 |